
Dissertation zur Erlangung des Doktorgrades
der Fakultät für Chemie und Pharmazie
der Ludwig-Maximilians-Universität München

**Development of Ultrasound Contrast Agents
for Targeted Drug and Gene Delivery**

Steliyan Tinkov

aus

Lovech, Bulgarien

2009

Erklärung

Diese Dissertation wurde im Sinne von § 13 Abs. 3 der Promotionsordnung vom 29. Januar 1998 von Herrn Prof. Dr. Gerhard Winter betreut.

Ehrenwörtliche Versicherung

Diese Dissertation wurde selbstständig, ohne unerlaubte Hilfe erarbeitet.

München, am 01. Juni 2009

.....
(Steliyan Tinkov)

Dissertation eingereicht am 18. Juni 2009

1. Gutachter Prof. Dr. Gerhard Winter

2. Gutachter PD Dr. Conrad Coester

Mündliche Prüfung am 13. Juli 2009

For my parents.

For Mina.

For my friends.

Acknowledgements

The present doctor thesis was only possible thanks to the cooperation and support of my supervisors, colleagues, relatives, and friends. Foremost, I would like to express my sincere gratitude to my advisor Prof. Dr. Gerhard Winter for the many valuable advices and for putting lots of negotiation effort. Special thanks to my supervisor PD Dr. Conrad Coester who motivated and supported me not only through subject-specific but also in many personal conversations. I would like to express my acknowledgements also to PD Dr. Raffi Bekerdjian for the fruitful cooperation with him and for making together with Prof. Winter my Ph.D. study possible. In this connection special thanks go to the German Academic Exchange Service for granting me the funding for the first year of the study. I am grateful to all my advisors for giving me the free hand to decide in many occasions.

I express my gratitude also to the colleagues from the team of Prof. Dr. Ernst Wagner – Dr. Martin Mayer and Mr. Alexander Philipp for supporting me during many unlucky experiments and I am glad that they were indeed successful at the end.

Furthermore, I am indebted to Dr. Stephan Zahler from the team of Prof. Dr. Angelika Vollmar for introducing me into the fluorescent staining and confocal laser scanning microscopy as well as for his active support.

I am also much obliged to Dr. Lars Allmendinger from the group of Prof. Dr. Klaus Wanner for the much patience during the long NMR analyses.

I am also much obliged to my colleagues Mr. Timo Lebold and Mr. Peter Schwaderer from the team of Prof. Dr. Christoph Bräuchle for their ideas and support in many experiments.

Sincere thanks to my colleagues and friends from our small club “BubbleLab” Mr. Klaus Freitag, Mr. Stephan Schultes, and Mr. Sebastian Fuchs for the nice time together and for the inspiring discussions in the hope that this would last over our professional career, too.

I would like to thank also all my friends and colleagues for helping me in the work as well as to get familiar with the Bavarian culture and traditions.

I also owe a sincere debt of gratitude to my parents who were every time at my side. I am also much obliged to my former spouse for being with me during these difficult times.

TABLE OF CONTENTS

| | |
|---|-----------|
| <i>I. CHAPTER: General introduction</i> | 14 |
| 1. Abstract | 14 |
| 2. Microbubble agents – a general overview | 15 |
| 3. Microbubble behavior in ultrasonic field | 17 |
| 4. Microbubbles as targeted drug carriers | 18 |
| 5. Advanced formulation design of phospholipid microbubbles | 23 |
| <i>II. CHAPTER: Formulation and characterization of model microbubbles</i> | 32 |
| 1. Abstract | 32 |
| 2. Introduction | 33 |
| 3. Materials and Methods | 38 |
| 3.1. Reagents | 38 |
| 3.2. Production of liposome precursors and model microbubbles..... | 38 |
| 3.2.1. Production of liposome precursors..... | 38 |
| 3.2.2. Production of model MBs | 38 |
| 3.3. Pre-formulation studies on model microbubbles..... | 39 |
| 3.3.1. Effects of agitation time | 39 |
| 3.3.2. Effect of liposome viscosity..... | 39 |
| 3.3.3. Effect of tube fill volume | 39 |
| 3.3.4. Effect of tube shape..... | 40 |
| 3.4. Characterization of microbubbles | 40 |
| 3.4.1. Size distribution measurements..... | 40 |
| 3.4.2. Determination of MB Zeta potential | 42 |
| 3.4.3. Determination of MB concentration | 42 |
| 4. Results and Discussion | 43 |
| 4.1. Pre-formulation studies on model microbubbles..... | 43 |
| 4.1.1. Effect of agitation time | 43 |
| 4.1.2. Effect of liposome viscosity..... | 45 |
| 4.1.3. Effect of tube fill volume | 47 |
| 4.1.4. Effect of tube shape..... | 48 |
| 4.2. Characterization of microbubbles | 48 |
| 4.2.1. Size distribution measurements..... | 48 |
| 4.2.2. Determination of MB Zeta potential | 56 |
| 4.2.3. Determination of MB concentration | 56 |
| 5. Summary | 57 |

| | |
|---|-----------|
| III. CHAPTER: <i>In-vitro</i> studies on the acoustic destructibility of microbubbles..... | 60 |
| 1. Abstract..... | 60 |
| 2. Introduction | 61 |
| 3. Materials and methods..... | 63 |
| 3.1. Reagents | 63 |
| 3.2. <i>In-vitro</i> experimental setup | 63 |
| 3.3. Establishing the <i>in-vitro</i> model | 65 |
| 3.4. Acoustic destructibility studies | 66 |
| 4. Results and Discussion | 67 |
| 4.1. Establishing the <i>in-vitro</i> model | 67 |
| 4.2. Acoustic destructibility studies | 68 |
| 5. Summary | 70 |
| IV. CHAPTER: <i>Ultrasound targeted tumor therapy</i> | 72 |
| 1. Abstract | 72 |
| 2. Introduction | 73 |
| 3. Materials and Methods | 80 |
| 3.1. Reagents | 80 |
| 3.2. Pre-formulation studies on doxorubicin-loaded liposomes and microbubbles..... | 81 |
| 3.2.1. Differential scanning calorimetry studies | 81 |
| 3.2.2. Effect of US homogenization of liposomes on the MB yield | 82 |
| 3.2.3. Effect of third phospholipid compounds | 82 |
| 3.2.4. Effect of agitation time on the DOX loading in MBs | 83 |
| 3.2.5. Optimal formulation procedures for DOX-loaded liposome precursors and MBs..... | 83 |
| 3.3. Characterization of doxorubicin-loaded liposomes | 84 |
| 3.3.1. Size distribution and Zeta potential..... | 84 |
| 3.3.2. Measuring the DOX concentration | 84 |
| 3.3.3. Association of DOX with liposomes..... | 85 |
| 3.3.4. Electrolyte-induced liposomal leakage of DOX | 85 |
| 3.3.5. Chemical stability of DOX during the production of liposomes..... | 86 |
| 3.3.6. Photochemical stability of DOX | 86 |
| 3.4. Pre-formulation studies on doxorubicin-loaded microemulsions and acoustically active lipospheres | 87 |
| 3.4.1. Partition equilibrium of DOX-base between triacetin and water | 87 |
| 3.4.2. Optimal formulation procedures for DOX-loaded microemulsions and AALs | 88 |
| 3.5. Characterization of doxorubicin-loaded microemulsions..... | 88 |
| 3.5.1. Particle size distribution and colloidal stability of DOX-loaded microemulsions | 88 |
| 3.6. Characterization of doxorubicin-loaded microbubbles and acoustically active lipospheres | 89 |
| 3.6.1. Structure analysis of DOX-loaded MBs and AALs | 89 |
| 3.6.2. Particle size distribution..... | 89 |

| | |
|---|-----------|
| 3.6.3. Particle concentration..... | 89 |
| 3.6.4. Effectiveness of DOX loading into MBs and AALs..... | 89 |
| 3.6.5. <i>In-vitro</i> acoustic destructibility of DOX-loaded MBs and AALs..... | 90 |
| 3.6.6. <i>In-vivo</i> evaluation of the acoustic properties of DOX-loaded MBs..... | 90 |
| 3.6.7. <i>In-vivo</i> / <i>in-vitro</i> acoustic destructibility correlation..... | 91 |
| 3.7. Therapeutic evaluation of doxorubicin-loaded microbubbles..... | 91 |
| 3.7.1. Intracellular distribution of DOX after treatment with DOX-loaded MBs..... | 91 |
| 3.7.2. <i>In-vitro</i> evaluation of the anti-proliferative efficacy of DOX-loaded MBs..... | 92 |
| 3.7.3. <i>In-vivo</i> evaluation of the targeting efficacy of DOX-loaded MBs..... | 93 |
| 4. Results and Discussion | 94 |
| 4.1. Pre-formulation studies on doxorubicin-loaded anionic liposomes and microbubbles..... | 94 |
| 4.1.1. Differential scanning calorimetry studies..... | 94 |
| 4.1.2. Effect of US homogenization of liposomes on the MB yield..... | 101 |
| 4.1.3. Effect of third phospholipid compounds..... | 101 |
| 4.1.4. Effect of agitation time on the DOX encapsulation in MBs..... | 104 |
| 4.1.5. Optimal formulation procedure for DOX-loaded liposome precursors and MBs..... | 105 |
| 4.2. Characterization of doxorubicin-loaded liposomes..... | 106 |
| 4.2.1. Size distribution and Zeta potential..... | 106 |
| 4.2.2. Measuring the DOX concentration..... | 107 |
| 4.2.3. Association of DOX with liposomes..... | 107 |
| 4.2.4. Electrolyte-induced liposomal leakage of DOX..... | 107 |
| 4.2.5. Chemical stability of DOX during the production of liposomes..... | 110 |
| 4.2.6. Photochemical stability of DOX..... | 110 |
| 4.3. Pre-formulation studies on doxorubicin-loaded microemulsions and acoustically active lipospheres | |
| 112 | |
| 4.3.1. Partition equilibrium of DOX-base between triacetin and water..... | 113 |
| 4.3.2. Optimal formulation procedures for DOX-loaded microemulsions and AALs..... | 115 |
| 4.4. Characterization of doxorubicin-loaded microemulsions..... | 116 |
| 4.4.1. Particle size distribution and colloidal stability of DOX-loaded microemulsions..... | 116 |
| 4.5. Characterization of doxorubicin-loaded microbubbles and acoustically active lipospheres..... | 117 |
| 4.5.1. Structure analysis of DOX-loaded MBs and AALs..... | 117 |
| 4.5.2. Particle size distribution..... | 117 |
| 4.5.3. Particle concentration..... | 118 |
| 4.5.4. Effectiveness of DOX loading into MBs and AALs..... | 118 |
| 4.5.5. <i>In-vitro</i> acoustic destructibility of DOX-loaded MBs and AALs..... | 119 |
| 4.5.6. <i>In-vivo</i> evaluation of the acoustic properties of DOX-loaded MBs..... | 121 |
| 4.5.7. <i>In-vivo</i> / <i>in-vitro</i> acoustic destructibility correlation..... | 122 |
| 4.6. Therapeutic evaluation of doxorubicin-loaded microbubbles..... | 123 |
| 4.6.1. Intracellular distribution of DOX after treatment with DOX-loaded MBs..... | 123 |
| 4.6.2. <i>In-vitro</i> evaluation of the anti-proliferative efficacy of DOX-loaded MBs..... | 125 |
| 4.6.3. <i>In-vivo</i> evaluation of the targeting efficacy of DOX-loaded MBs..... | 127 |

| | |
|---|------------|
| 5. Summary and outlook | 130 |
| V. CHAPTER: Ultrasound targeted gene therapy | 132 |
| 1. Abstract | 132 |
| 2. Introduction | 134 |
| 2.1. Amphiphilic conjugates of polyethylenimine | 137 |
| 2.2. Microbubble-mediated gene therapy..... | 138 |
| 2.3. Gene delivery by secondary carrier-associated microbubbles..... | 140 |
| 3. Materials and Methods | 147 |
| 3.1. Reagents | 147 |
| 3.2. Synthesis of branched polyethylenimine palmitate (bPEI-PA) conjugates | 148 |
| 3.2.1. Chemical structure analysis of bPEI-PA..... | 149 |
| 3.3. Characterization of bPEI-PA..... | 150 |
| 3.3.1. Particle size distribution of bPEI and bPEI-PA in polar and non-polar solvents | 150 |
| 3.4. Formulation and characterization of polycationic liposomes with bPEI-PA | 150 |
| 3.4.1. Mixing behavior of DPPC and DPPE | 150 |
| 3.4.2. Effect of glycerol on the colloidal stability of DPPC / DPPE liposomes | 151 |
| 3.4.3. Mixing behavior of bPEI-PA with DPPC / DPPE bilayers | 151 |
| 3.4.4. Determination of bPEI-PA buffer capacity | 152 |
| 3.4.5. Zeta potential of polycationic liposomes with bPEI-PA | 152 |
| 3.5. Studies on the loading of bPEI-PA liposomes with pDNA | 153 |
| 3.5.1. Complexation capacity of bPEI-PA liposomes for pDNA..... | 153 |
| 3.5.2. Effect of pH on the polycationic liposome size | 154 |
| 3.5.3. Polycationic liposome size according to bPEI molecular weight, PA substitution, and loading with pDNA | 154 |
| 3.6. Formulation and characterization of polyplex-associated MBs, loaded with pDNA | 154 |
| 3.6.1. Effect of electrolytes on the MB production and liposome aggregation..... | 154 |
| 3.6.2. Optimal formulation for polyplex-associated MBs for <i>in-vivo</i> studies | 155 |
| 3.6.3. Structure analysis of polyplex-associated MBs..... | 156 |
| 3.6.4. Protection of pDNA against enzymatic degradation | 157 |
| 3.6.5. Effective loading of pDNA in polycationic liposomes and in polyplex-associated MBs | 158 |
| 3.7. Comparative <i>in-vitro</i> transfection / cell viability studies with pDNA-loaded polycationic liposomes and polyplex-associated microbubbles | 159 |
| 4. Results and Discussion | 160 |
| 4.1. Synthesis of branched polyethylenimine palmitate (bPEI-PA) conjugates | 160 |
| 4.1.1. Chemical structure analysis of bPEI-PA..... | 161 |
| 4.2. Characterization of bPEI-PA..... | 162 |
| 4.2.1. Particle size distribution of bPEI and bPEI-PA in polar and non-polar solvents | 162 |
| 4.3. Formulation and characterization of polycationic liposomes with bPEI-PA | 166 |
| 4.3.1. Mixing behavior of DPPC and DPPE | 167 |

| | |
|--|-------------------|
| 4.3.2. Effect of glycerol on the colloidal stability of DPPC / DPPE liposomes | 170 |
| 4.3.3. Mixing behavior of bPEI-PA with DPPE / DPPC bilayers | 174 |
| 4.3.4. Determination of bPEI-PA buffer capacity | 175 |
| 4.3.5. Zeta potential of polycationic liposomes with bPEI-PA | 176 |
| 4.4. Studies on the loading of bPEI-PA liposomes with pDNA | 179 |
| 4.4.1. Complexation capacity of bPEI-PA liposomes for pDNA | 179 |
| 4.4.2. Effect of pH on the polycationic liposome size | 180 |
| 4.4.3. Polycationic liposome size according to bPEI molecular weight, PA substitution, and loading with pDNA | 182 |
| 4.5. Formulation and characterization of polyplex-associated MBs, loaded with pDNA | 186 |
| 4.5.1. Effect of electrolytes on the MB production and liposome aggregation | 186 |
| 4.5.2. Optimal formulation for polyplex-associated MBs for <i>in-vivo</i> studies | 189 |
| 4.5.3. Structure analysis of polyplex-associated MBs | 190 |
| 4.5.4. Protection of pDNA against enzymatic degradation | 191 |
| 4.5.5. Effective encapsulation of pDNA in polycationic liposomes and in polyplex-associated MBs | 193 |
| 4.6. Comparative <i>in-vitro</i> transfection / cell viability studies with pDNA-loaded polycationic liposomes and polyplex-associated microbubbles | 194 |
| 4.6.1. The effect of bPEI molecular weight | 194 |
| 4.6.2. The effect of conjugation with PA | 195 |
| 4.6.3. The effect of phospholipid | 196 |
| 4.6.4. The effect of US-mediated destruction of MBs | 198 |
| 5. Summary and outlook | 200 |
| <i>VI. Chapter: General summary of the thesis</i> | <i>204</i> |
| <i>References:</i> | <i>210</i> |
| <i>Curriculum Vitae</i> | <i>228</i> |

I. CHAPTER: General introduction

1. Abstract

Today, ultrasound (US) applications in medicine are so extensive that one cannot imagine routine clinical practice without them. US applications provide non-invasive, cost-efficient and well-developed modalities for imaging and diagnostics. In addition, several therapeutic approaches involving US have gained public acceptance and compliance. For example, high-intensity focused US (HIFU) is used to ablate solid tumors and tissue regions, and lithotripter shockwaves are used to destroy kidney stones.

The introducing of the first microbubble US contrast agents (MBs) has brought a great improvement in US diagnostics. Until the 1990's, they were mainly used for right heart opacification and cardiac shunt diagnostics. This approach was limited due to MBs' low stability and large size, making them unable to pass pulmonary capillaries after intravenous injection. Developing stable and sufficiently small gas filled MBs allowed systemic circulation of an effective US contrast agent after intravenous injection, thus opening a wide range of new diagnostic applications. More recently, such MBs have evolved into a promising carrier for therapeutic substances. This work will focus on the aspects of pharmaceutical developing of MB carriers for site specific tumor and gene therapy.

Keywords: Ultrasound, microbubble contrast agents, sonoporation, capillary fenestration, rational formulation design;

Abbreviations: AAL – acoustically active lipospheres, US – ultrasound, MB – microbubble, UTMD – ultrasound-targeted microbubble destruction, HSA – human serum albumin, pDNA – plasmid DNA, siRNA – small interfering RNA;

2. Microbubble agents – a general overview

MBs are gas-filled colloidal particles, with a size range of 1-8 μm . Their structure comprises a gas core which is wrapped in a more or less flexible shell of protein, surfactant, or polymer. Currently, MBs are marketed as contrast agents for ultrasound (US) diagnostics and imaging. Their introduction into clinical practice led to the development of more sensitive imaging techniques both in cardiology and radiology, including subharmonic and multi-pulse imaging, pulse inversion and harmonic power Doppler [1]. Recently, MBs are anticipated to find further uses in therapy as efficient and safe targeted deliverers of drugs and genes.

Forty years ago, Gramiak and Shah (1968) [2] reported that agitated saline enhanced the US echo signal in the human ascending aorta and cardiac chambers. Since this first breakthrough, three generations of acoustically-active US contrast agents have been developed (Table 1).

First generation MB products were simple air bubbles. Since they lacked a stabilizing shell, they were stable for only a few seconds in circulation and would not pass capillaries due to their large size. Therefore, first generation MBs could not reach the left heart if injected intravenously, and left ventricular opacification could only be achieved by direct injection into the left ventricular cavity. A stabilized form of such airbubbles was approved and marketed by Schering AG as Echovist[®], still being used for cardiac shunt diagnostics.

The *second generation* MBs was stabilized by a shell of protein, polymer or surfactant, and had a smaller size distribution (transpulmonary MBs). Thus, they were able to pass through the lungs and reach the left heart and other organs after intravenous application. However, the second generation MBs had instable gas cores consisting of air and dissolved in blood within less than five minutes.

In *third generation* MBs, the air core was replaced by gases that were only sparingly soluble in blood and physiologically inert. This improvement prolonged the half-life of MBs to more than fifteen minutes.

The development of more stable MB agents made possible them to reach any US accessible and blood perfused organ. This and some specific physical characteristics of MBs broadened the scope of their applications beyond US imaging and encouraged the development of US-targeted drug delivery. Today, studying the potential use of MBs in gene and drug delivery is the focus of many research groups worldwide [3].

| MB agent | Marketing Authorization Holder | Presentation | Core material | Shell material |
|--|--|---|---|--|
| <i>First Generation Vascular Agents</i> | | | | |
| Echovist ^{® 3)} | Schering AG, Germany | D-galactose microparticles for reconstitution | Air | None |
| <i>Second Generation Vascular Agents (transpulmonary MBs)</i> | | | | |
| Levovist ^{® 2)} | Schering AG, Germany | D-galactose microparticles for reconstitution | Air | PA |
| Albunex ^{® 3)} | Molecular Biosystems, USA | Aqueous MB suspension | Air | HSA |
| Quantison ^{® 3)} | Quadrant Ltd, UK | Spray-dried powder | Air | HSA |
| <i>Third Generation Vascular Agents</i> | | | | |
| Optison ^{® 1),2)} | GE Healthcare, USA | Aqueous MB suspension | C ₃ F ₈ | HSA |
| EchoGen ^{® 3)} | Sonus Pharmaceuticals Ltd., USA | Phase shift colloid emulsion | C ₅ F ₁₂ | Surfactant: PEG-telomer B |
| SonoVue ^{® 1),2)} | Bracco International B.V., The Netherlands | Lyophilized powder | SF ₆ | Phospholipid composition: DSPC / DPPG / PA |
| Definity ^{® 1),2)} (in the EU: Luminity [®]) | Bristol-Myers Squibb Medical Imaging, USA | Aqueous phospholipid solution for agitation | C ₃ F ₈ | Phospholipid composition DPPC / DPPA / MPEG 5000-DPPE |
| Imagent ^{® 1),2)} | Alliance Pharm. Corp., USA | Spray-dried powder | C ₆ F ₁₄ / Nitrogen | Phospholipid: DMPC |
| CardioSphere ^{® 4)} | Point Biomed. Corp., USA | Lyophilized powder | Nitrogen | Polymer-based bilayer (biSphere [™]): PLGA / HSA |
| <i>Third Generation Liver Specific Agents</i> | | | | |
| BR-14 ⁴⁾ | Bracco Research SA, Switzerland | n.a. | C ₄ F ₁₀ | Phospholipid composition |
| Sonazoid ^{™ 4)} | GE Healthcare, USA | Dry powder | C ₄ F ₁₀ | Hydrogenated egg phosphatidylserine |
| SonoVist ^{® 4)} | Schering AG, Germany | n.a. | SF ₆ | PCA |
| <i>Third Generation Agents for Research Purposes</i> | | | | |
| PESDA | Porter et al. (1997) [4] | n.a. | C ₄ F ₁₀ | HSA |
| Quantifuxian | Chi et al. (2003) [5] | n.a. | C ₃ F ₈ | HSA |

Table 1: Classification and constitution of MB products. ¹⁾ Licensed for clinical use by FDA; ²⁾ Licensed for clinical use by EMEA; ³⁾ No longer commercially available or development suspended, ⁴⁾ Under development. PLGA – polylactide-co-glycolide; PCA – polycyanoacrylate; HSA – human serum albumin; DPPC – dipalmitoyl phosphatidylcholine; DPPA – dipalmitoyl phosphoric acid; DPPG – dipalmitoyl phosphatidylglycerol; MPEG 5000-DPPE – polyethyleneglycol 5000-dipalmitoyl phosphatidylethanolamine; DMPC – dimyristoyl phosphatidylcholine; DSPC – distearoyl phosphatidylcholine; PA – palmitic acid [6-8]; n.a. – not available.

3. Microbubble behavior in ultrasonic field

There is a very intensive interaction between MBs and diagnostic US (Figure 1). When exposed to US with lower intensity MBs perform a symmetric volume contractions and expansions (linear oscillations). At increasing US intensity, the oscillations are accompanied by bubble shape deformations (non-linear oscillations), and at reaching of a certain intensity limit – cavitation threshold, the oscillating MB is fragmented or “burst” by US to smaller gas artifacts and shell fragments.

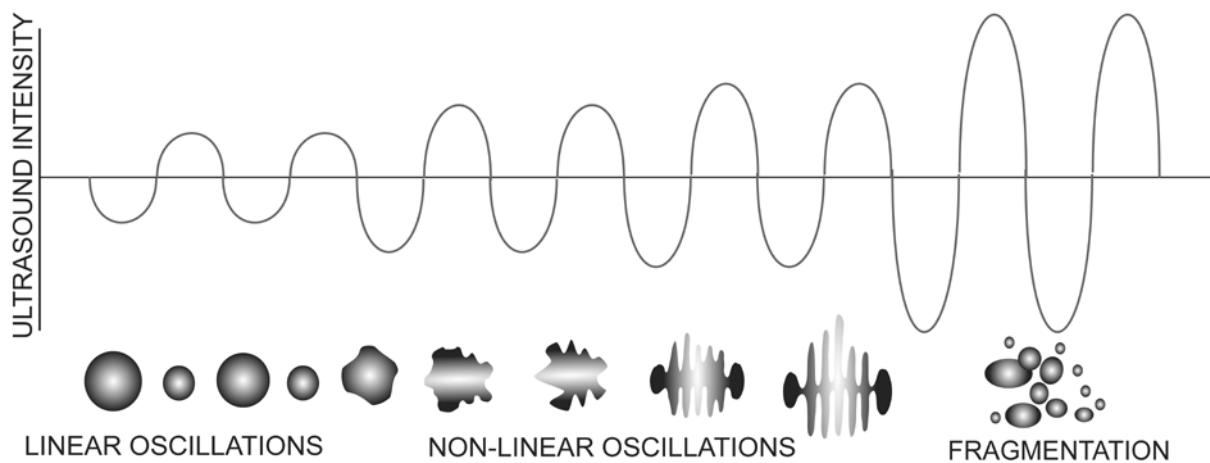


Figure 1: MB oscillation and fragmentation (“bursting”) in dependence of the US intensity.

The higher acoustic response of MBs compared to blood and most body tissues can be explained by their differing acoustic impedances. At moderate acoustic pressures the acoustic impedance (Z) is linearly dependent from the specific density of the propagation medium (ρ , [g/cm³]) and the respective sound velocity (c , [m/s]) according to Equation 1 [9].

$$Z = \rho \cdot c$$

Equation 1

While the acoustic impedance of most tissues lies in the range $1.5\text{-}8.0 \times 10^6$ kg/m²s, it is about five orders of magnitude lower for gases (4.0×10^1 kg/m²s) [10, 11]. The greatly higher acoustic responsiveness of MBs, compared to blood and tissues, allows specifically addressing them by diagnostic US with a minimal burden to the organism [12, 13].

The cavitation threshold and the MB half-life in an US field depend mainly on the US frequency and MB diameter, but also on the physico-chemical properties of the MB shell,

drug-loading, *etc.* On their turn, these factors are decisive for the magnitude of non-thermal mechanic *in-situ* effects of cavitation and accordingly for the permeabilization of biological structures. For example, MBs with soft shells such as phospholipid monolayers follow a specific pattern of destruction, during which the flexible membrane expands and reseals again, accompanied by gradually shedding out of submicron lipid associates in the order of liposomes to micelles [14]. The mechanic effects of soft-shelled MBs on capillaries and cells is therefore mostly considered rather moderate and safe [15].

On the other hand, MBs with robust shells made of protein or polymeric material are rather weak oscillators and are mostly fragmented by “sonic cracking”, where the gas explosively escapes the shell. Therefore, the mechanic effects of sonic cracking to cells and tissues are more intensive compared to soft-shelled MBs [16].

Another class of MBs – acoustically active lipospheres (AALs), comprises an additional oil layer between the gas core and the outermost surfactant monolayer. The acoustic fragmentation of AALs has been explained by May et al. (2001) [17]. Depending on their diameter and US parameters, AALs may undergo one-step collapse fragmentation producing a set of smaller fragments, or continuously pinch off small shell fragments and eventually shed out a large fragment, containing the main fraction of shell material.

The fragmentation behavior of US contrast agents is an important factor for their contrasting activity, therapeutic efficacy, and biological safety with regard to the US intensity, necessary to achieve MB bursting and drug release.

4. Microbubbles as targeted drug carriers

It is known that exposure to US may improve cellular uptake of polynucleotides [18-21], proteins [18], and small-molecule drugs [19]. Cavitation has been found to be responsible for this effect. However, the high US energy levels required to induce gas cavitation in organisms bears a high risk of acoustic damage and are clinically impractical.

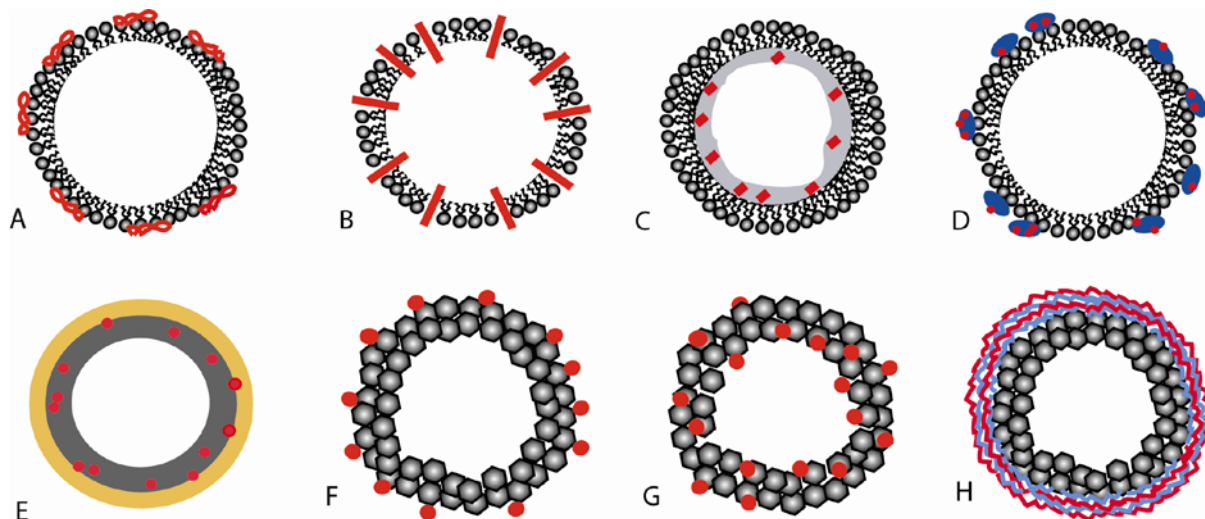


Figure 2: MB structure classes and drug-load localizations (in red). A: Attachment to the outer shell surface; B: Intercalation between monolayer phospholipids; C: Incorporation in an oil layer (acoustically active lipospheres, AALs); D: Complexes with smaller particles (secondary carriers, in blue); E: Physical encapsulation in a polymer layer (grey) and coating with biocompatible material (yellow); F: Surface loading of protein-shelled MBs; G: Entire shell volume loading of protein MBs; H: Layer-by-layer loaded protein-shelled MBs. The negatively charged DNA is represented in blue, and the polycationic polymer – in red.

MBs offer a different approach to facilitate the US triggered drug uptake. They respond to the US field of their resonance frequency by oscillation. At higher US energies, high amplitude oscillations cause MB destruction. If such MBs have been loaded with a drug or gene vector, *ultrasound targeted microbubble destruction* (UTMD) can be used to locally deliver and release the transported substance. Because MBs act as cavitation nuclei, they lower the required US energy to safe intensity levels, mandated by the FDA [20, 21].

On the cellular- and tissue-level several additional effects, associated with high amplitude oscillations, have been described that mediate the drug transport into cells. In the near vicinity of oscillating MBs cell membranes may show sonopores [22-24] which could be due to several MB phenomena including microstream swirling [25, 26], micro-jetting [27], and the formation of hydrodynamic shock waves [28, 29]. Some authors also suggest a significant role of free radical stress on cells [30-32], others however doubt their contribution [30, 31]. The auxiliary impact of enhanced ion-channel conductance has also been proposed as a possible mechanism [32].

Sonopores may range in size from 30-100 nm up to a few micrometers [33] (Figure 3A to D). They have a transient character and actively reseal by an endogenous vesicle-based healing response [33] with the aid of Ca^{2+} [34] and ATP [35] after several seconds [36] or

minutes [37]. It is strongly suggested that bioactive substances, such as proteins, plasmids and siRNA can permeate the cytosol through these membrane pores (Table 2).

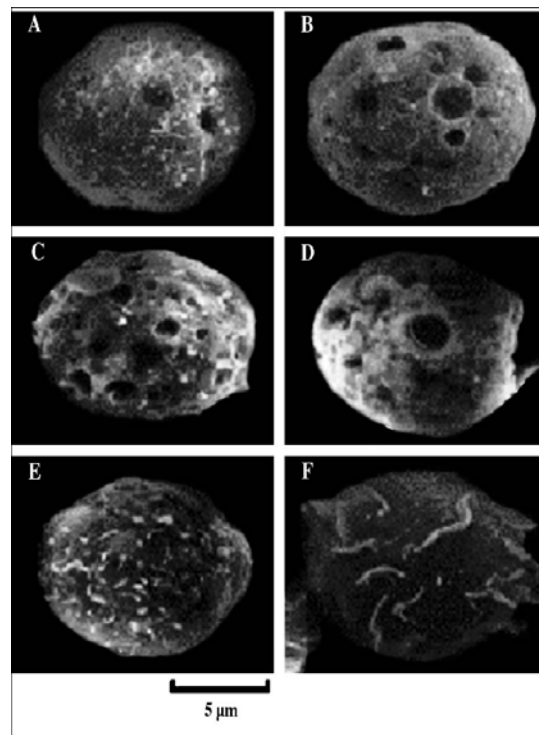


Figure 3: Scanning electron microscopic images of HL-60 cells exposed to US in the presence of MBs (A to D), irradiated with US alone (F) or untreated (E). From Liu et al. (2006)¹ [38].

The development of pores is limited to the cell membrane and most reports indicate that it does not affect the nucleus [33] apparently because the highly viscous cytoplasm prevents direct perturbations of it. However, Duvshani-Eshet et al. (2006a,b) [39, 40] recently reported that nuclear uptake of rhodamine-labeled pDNA by UTMD in cell cultures is possible.

In addition to the effects on a cellular level, UTMD has also effects on the microvasculature. It has been shown that UTMD transiently increases capillary permeability by putting micron-range pores in the endothelium. These endothelial gaps allow the transportation of colloidal particles towards the tissue interstitium.

The UMTD mediated transport through blood vessels is limited through the thickness of the vessel wall. In small vessels such as arteriole and venule small molecules and macromolecules but no colloidal particles can be transferred out of the vessel bed [41]. Permeabilization of the blood-brain barrier and transportation of small polar molecules, macromolecules, and colloidal particles is also possible using MBs [48-50].

¹ Reprinted, with permission, from the Journal of Controlled Release, Volume 114 ©2006 by Elsevier Ltd.

| Biological barrier | Size/molecular weight of molecules/particles transported by UTMD | Examples |
|--|---|--|
| Cell membrane | 2-3 MDa [33] | Polar macromolecules, micelles, polyplexes, or viruses [42] |
| Capillary endothelium (vessel diameter < 7 μm [43]) | 6-8 μm | Small- and macromolecules [44], colloidal nanoparticles sized approx. 100 [45], 200 and 500 nm, and cells [46, 47] |
| Vessel wall (vessel diameter approx. 55 μm) | approx. 9 nm | Polar macromolecules [41] |
| Blood-brain barrier (BBB) | approx. 100 nm | Small polar molecules [48], polar macromolecules (pDNA) [49], colloidal particles (liposomes) [50] |

Table 2: Transfer of molecules and particles across biological barriers using UTMD. Approx. – approximately.

The experience in using MBs as contrast agents helped pave the way for their use in the therapeutic research. Extensive studies have established the MB safety profile [51], and guidelines for the use of contrast enhanced US have been recommended [13, 52]. Furthermore, several recent diagnostic devices *e.g.* Sonos 5500, Philips Medical Systems, USA are appropriately equipped and can be directly applied for UTMD-assisted drug delivery. Additionally, there are established methods for the small and large scale production of MBs.

In the past years, the trends in the MB-mediated drug and gene delivery have diverged from the development of US contrast agents in many aspects. Diverse MB structure types have been specifically developed to accommodate molecules with various molecular weights and physico-chemical properties (Figure 2).

According to the particular MB structure classes, the thickness and shell volumes of MBs can vary broadly (Table 3).

| MB structure class | Shell thickness |
|--|--|
| Phospholipid-MBs | 2 – 3 nm [53] |
| Microcapsules (emulsification method) | 50 – 200 nm [15] |
| HSA-shelled MBs (probe-type sonication method) | 200 – 300 nm [54] |
| AALs | 500 – 1000 nm (triacetin layer), 300 – 700 nm (soy-bean oil layer) [17] |

Table 3: Shell thickness of the main MB structure classes. AALs – acoustically active lipospheres; HSA – human serum albumin.

Compared to phospholipid-MBs, microcapsules, AALs, and protein-shelled MBs possess larger shell volumes and can potentially embed higher drug loads. On the other side, a greater shell thickness can impair the acoustic properties of such MBs.

Drug molecules can be associated with the MB shell by means of electrostatic or hydrophobic interactions, van-der-Waals forces or merely by physical encapsulation (Table 4). For instance, charged hydrophilic macromolecules like DNA and RNA can be directly charge-coupled to the outer MB surface (Figure 2 A), whereas amphiphilic molecules can penetrate into the monolayer (Figure 2 B). Highly hydrophobic molecules like paclitaxel can be included in a layer of thick oil to form acoustically-active lipospheres (AALs, Figure 2 C). Alternatively, the payload can be associated with smaller particles which are in turn attached to the MB (Figure 2 D). Drug molecules can also be encapsulated into shells of biodegradable polymer (Figure 2 E, in grey), and the obtained hollow microcapsules can be coated with a biocompatible material, such as gelatin (in yellow) to inhibit systemic elimination. In Figure 2 F and G, the drug is complexed to adhesive serum albumin molecules, forming the shell. According to the formulation processes, the drug can be either surface attached or included in the albumin shell.

Albumin-shelled as well as phospholipid-shelled MBs can be efficiently loaded using the layer-by-layer approach (Figure 2 H). According to it layers of negatively charged DNA and polycationic polymer such as poly-L-lysine are consecutively laid over the pre-formed MBs.

| MB structure class | Attaching forces | Drug molecule properties | Examples |
|---|---|---|--|
| Phospholipid-MBs (Figure 2 A and B) | Electrostatic and/or hydrophobic interactions | Electrostatically charged small- and macromolecules, small amphiphilic and lipophilic molecules | Dexamethasone dipalmitoyl ester [55], pDNA [56, 57] protein [58, 59] |
| Acoustically-active lipospheres (AALs, Figure 2 C) | Hydrophobic interactions | Small lipophilic molecules | Paclitaxel [60-62], resveratrol [60] |
| Double-emulsified microcapsules (Figure 2 E) | Physical encapsulation | Hydrophilic small- and macromolecules | pDNA [61], doxorubicin [62] |
| Secondary-carrier MB (Figure 2 D), coupled with liposomes [63], nanoparticles [64], viruses [65], polyplexes [66, 67], lipoplexes [71-73] | Mostly electrostatic interactions | Electrostatically charged macromolecules | pDNA [69-72] |
| Protein-shelled MB (Figure 2 F) | Diverse non-covalent interactions | Hydrophilic small- and macromolecules | pDNA [68-70] |

Table 4: Drug and gene carrier potentials of various MB structure classes.

One further approach – the MB formulation concept of phase shift colloid emulsions, was originally implemented in the diagnostic product EchoGen® (Table 1) and advanced by Rapoport et al. (2007) [68]. The authors designed a sophisticated microemulsion system of perfluoropentane, stabilized by biodegradable block copolymer surfactants and loaded with doxorubicin. Under heating to physiological temperatures or mild sonication a droplet-to-bubble phase shift proceeded, resulting in the *in-situ* formation of stable drug-loaded MBs.

5. Advanced formulation design of phospholipid microbubbles

MBs are complex structures, where numerous physico-chemical parameters and interactions play a crucial role in order to provide an adequate MB stability along with a sufficient acoustic backscatter activity and destructibility. Together with the complexation interactions between drug molecules and MB shell, there are interactions between gas core and surrounding medium, as well as processes within the MB shell taking place. From this reason, an in-depth formulation design is needed towards an advanced MB product.

In a phospholipid-shelled MB the gas core is surrounded by a flexible, but stable layer of amphiphilic molecules which may also embed an effective drug payload. The crucial role of shell and core gas for an optimal MB stability can be illustrated by the following example. A shell-free air MB with initial diameter of 2 μm in water at 37 $^{\circ}\text{C}$ is theoretically predicted to fully dissolve within 25 ms. A bubble of the same size, but consisting of octafluoropropane is predicted to dissolve within 400 ms [69]. In contrast, third generation MBs such as Definity®, possessing a stabilizing phospholipid-shell, have a circulation half-life of over 15 minutes.

Shell-free air bubbles dissolve nearly instantaneously due to the effect of surface tension and hydrostatic blood pressure. The pressure difference across the bubble surface ΔP is given by the Laplace equation [70]:

$$\Delta P = P_b - P_a = \frac{2\sigma}{r}$$

Equation 2

where P_b is the pressure inside the bubble, P_a is the hydrostatic pressure outside the bubble, σ is the surface tension, and r is the bubble radius. The high surface curvature in the MB size range of 1 μm to 5 μm renders a significant pressure drop of *e.g.* 1 bar for a bubble with a

diameter of 2 μm . This pressure difference drives gas into the surrounding medium and causes the bubbles' rapid dissolving.

MB shell contributes two major stabilizing components – a resistance to gas escape from the core and a reduction of the surface tension, as modeled in the modified Epstein-Plesset equation [71, 72] (Equation 3).

$$-\frac{dr}{dt} = \frac{L}{r/D_w + R_{shell}} \left(\frac{1 + 2\sigma_{shell}/P_a r - f}{1 + 3\sigma_{shell}/4P_a r} \right)$$

Equation 3

where dr/dt is the time-resolved reduction of MB radius after gas loss; L is the Ostwald's coefficient; D_w – gas diffusion coefficient in water; R_{shell} – shell resistance to gas permeation; σ_{shell} is the shell surface tension, and f is the ratio of core gas concentration in the medium vs. the gas concentration at saturation. The Epstein-Plesset model assumes a perfectly spherical form of the MB and neglects shell deformation effects like folding and buckling throughout the gas escape.

Following from above, one possible way to increase the bubble lifespan is by implementing poorly soluble core gases such as SF_6 or perfluorinated hydrocarbons rather than nitrogen or air. By using poorly water soluble gases the gas permeation resistance into water ($L^{-1}D_w^{-1}$) can be increased in several orders of magnitude compared to air [73, 74]. This concept has been employed in the development of third generation US contrast agents such as SonoVue[®] (Bracco International, B.V., The Netherlands) and Definity[®] (Bristol-Myers Squibb Medical Imaging, USA).

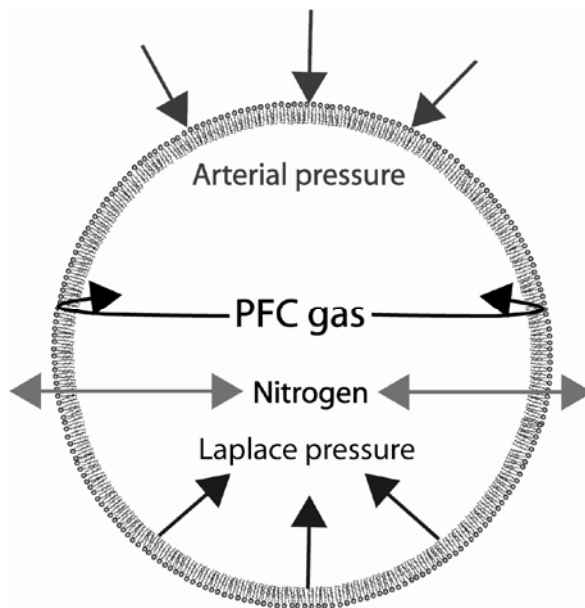


Figure 4: Osmotically stabilized MB. There is an osmotic equilibrium between the water-soluble gases inside the MB and in the blood, whereas the water-insoluble perfluorocarbon (PFC) remains inside the shell.

The blood plasma contains physiological amounts of dissolved gases of low molecular weight such as nitrogen, oxygen, and carbon dioxide. Considering a gas core composed of perfluoropropane and surrounded by physiological gases, dissolved in the blood plasma (mainly nitrogen and oxygen), there is an osmotic gradient directed into the bubble where the blood-gases concentration is zero. While the phospholipid shell and the surrounding aqueous medium widely prevent inside-out perfluorocarbon permeation, the shell still can be passed in the opposite direction by the small blood gas molecules. Consequently, when MBs containing only perfluorocarbon are introduced into the blood, they increase in size by taking up blood gases. The bubbles swell until the partial pressures of blood gases inside them equal the ambient concentrations, and the partial pressure of perfluorocarbon counterbalances the combined Laplace and blood pressure [74]. These equilibrium observations support the development of osmotically stabilized MBs (Figure 4). Schutt et al. (2003) [75] have previously published a detailed review on the principles of gas-exchange and osmotic stabilization of MBs. The ingenious designing concept of osmotically stabilized MBs has found application in Imagent[®] (Alliance Pharm. Corp., USA).

One further MB stabilizing factor – the shell resistance to gas permeation, is considered negligible for gases with low molecular weight [73, 74, 76], though it is greatly enhanced for high molecular weight gases like the perfluorocarbons. For example, the shell resistance for perfluorobutane compared to air is estimated to be approximately 1,400 times higher [77]. The shell resistance to gas permeation depends on the rate of monolayer condensation on an

exponential manner [78]. Since the phospholipid condensation state also depends on the temperature, the shell phospholipids should have a phase-transition temperature (T_m) above the physiological body temperature of 37 °C [14] and persist in condensed phase state at physiological conditions. For the same reason – maintaining the condensed phospholipid packaging, a MB formulation cannot include unsaturated phospholipids with extensive conformational freedom, since they would destroy the dense monolayer order [79].

According to the Epstein-Plesset theory, the second major component of MB stability contributed by the phospholipid shell is the reduction of surface tension. In homological orders of saturated symmetric diacyl phosphatidylcholines the equilibrium surface tension on the air / water surface was extremely sensitive to phospholipid chain length, decreasing by more than an order of magnitude for each methylene group added [80]. Their values varied from 9.8 mN/m (for $n = 6$) through 4.0 mN/m (for $n = 12$) [80] down to 1.3 mN/m (for $n = 16$) [81].

Beneath surface tension hydrophobic chain length plays a role for the MB shell permeation resistance to gases either [80, 84, 86, 90, 91]. The exponential relationship between shell resistance and phospholipid acyl chain length has been first predicted by the energy barrier model [82, 83] (Equation 4)

$$R_{shell} = R_0 \exp\left(\frac{E(n)}{BT}\right)$$

Equation 4

where R_0 is a frequency constant, $E(n)$ is the activation energy that depends on the number of carbon atoms per phospholipid acyl chain, B is the Boltzmann universal gas constant, and T is the temperature.

Later on, it has been experimentally proven that the cohesive energy between n -alkyl chains increases linearly with the addition of each methylene group [84] which renders reasonable an exponential increase of the shell resistance to monolayer gas permeation. On the other hand, the increase of acyl chain length raises the shell viscosity which results in more robust and less echogeneous MBs [85].

Recently, semi-synthetic phospholipids are generally preferred in the designing of MBs because of their non-animal origin and the favorable acoustic properties of phospholipid monolayers. Presently there is also a broad range of phospholipids with a variety of

hydrophobic chain lengths and electrostatic charges that are commercially available. In aqueous surroundings the phospholipid MB shell presents a flexible, thin monolayer film with the hydrophobic tails facing the gas core and the headgroups coming into contact with the medium. The stability of the shell monolayer is provided by its highly condensed structure of saturated fatty acid tails.

Including certain shell excipients, such as PEGylated phospholipids, can sterically stabilize MBs and delay their blood elimination. This advantageous effect has been implemented in the design of Definity[®] (Bristol-Myers Squibb Medical Imaging, USA). However, the bulky PEGylated headgroups possess a large positive intrinsic curvature which may be unadvantageous for the MB geometry and can disturb shell integrity as will be demonstrated below.

Recent research by Kim et al. (2003) [85] and Borden et al. (2006a) [86] disproved the prevailing opinion of phospholipid MB shell as a homogeneous structure. Now the phospholipid monolayer is realized to be a complex, multiphase structure of ordered (condensed) and disordered (liquid) domains. This lateral phase separation within the monolayer sheet results from the imperfect miscibility of certain shell components, for example, single-chain PEGylated emulsifiers and double-chain phospholipids.

On the one hand, the coexistence of liquid and condensed phospholipid phase states confers the MB shell physical flexibility and stability. On the other, it has been demonstrated that phase heterogeneity dictates MB properties including the localization of targeting ligands, protective brush moieties, and drug loading. Phase heterogeneity may thus have negative consequences on the formulation quality. According to several studies, it is possible to confine the effects of lateral phase separation by adjusting the shell composition and manufacturing parameters [86].

Two factors are decisive for the miscibility in phospholipid systems – the intrinsic miscibility of phospholipid components and the possible influence of the drug on it. The prevailing effect results from the phospholipid acyl tails, but the structure and physico-chemical properties of the headgroup may also have an influence on the miscibility.

In binary mixtures saturated phospholipids with the same headgroup and various acyl chains possess different miscibilities. Nearly ideal mixing was observed between phospholipids with a chain length difference of up to two carbon atoms [87]. Imperfect lateral miscibility or a complete immiscibility in condensed state was demonstrated for chain length differences of four and more carbon atoms [87-89].

Lateral phase immiscibility can occur even in chain-uniform mixed phospholipid monolayers if the headgroups of phospholipid components possess distinct differences in terms of their physical size, state of hydration, and possible conformational flexibility. Phase separation has been observed *e.g.* in chain-uniform binary monolayers of DPPC and DPPI [90]. To minimize lateral phase separation and optimize the MB shell stability, the shell should preferably consist of phospholipid species with equal fatty-acid residues and close phase-transition temperatures.

Abundant surface electrostatic charges can also disturb the formation and stability of the MB monolayer shell by causing lateral electrostatic repulsions within the monolayer [67]. The repulsing between charged headgroups can overcome the associative hydrophobic forces between acyl chains on a concentration dependent manner and disrupt the shell monolayer.

The lyotropic phase behavior of phospholipids is their important characteristic, determined mainly by their molecular geometry *i.e.* the ratio between the areas of head group and acyl chains. Phospholipid geometry determines the average intrinsic curvature ($C_{0,ave}$) of its lyotropic phase. At $C_{0,ave} \sim 0$ phospholipid molecules have a roughly “cylindrical” geometry and tend to form lamellar phase structures as in the case of DPPC and DPPG. Intrinsic curvatures smaller than zero indicate that head-group area is smaller than the acyl-chain area. The stable lyotropic phase for such phospholipids *e.g.* DPPE is bended towards the aqueous phase. Phospholipids with sterically “bulky” hydrophobic headgroups such as PEGylated phospholipids, possess a positive $C_{0,ave}$ and tend to curve towards the acyl-chain region, thus forming micellar structures.

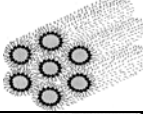
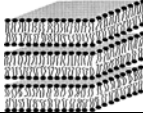
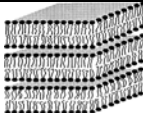
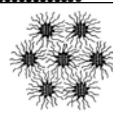
| Phospholipid | Electrostatic charge | Hydrogen bonding | Lyotropic phase at room temperature | |
|--------------|------------------------------|--------------------------------|---|---|
| DPPE | Zwitterionic | Donor: 2 Acceptor: 1 | Inverse hexagonal phase (H_{II}) [91] |  |
| DPPC | Zwitterionic | Non-bonding | Lamellar gel phase (L_a) [91, 92] |  |
| DPPG | One negative charge (pH > 4) | Donor: 2 Acceptor: 2 | Lamellar gel phase (L_a) [91] |  |
| DPPE-PEG2000 | One negative charge | Donor: 1 Acceptor: multiple | Micellar phase |  |

Table 5: Some important characteristics of phospholipids, used in following pre-formulation studies.

Following in this thesis, several phospholipids have been focused on in order to reveal their complexation potential for doxorubicin, their ability to produce sufficiently stable liposomal formulations, and to form MBs with an appropriate stability, size, and loading capacity.

The selected range of phospholipid candidates includes DPPC, DPPG, and DPPE, and DPPE-PEG2000 (Table 5). Rather strong lateral cohesion forces exist between DPPC molecules. Hence, this phospholipid is able to form mechanically stable mono- and bilayers [93]. Concerning its head-group hydration, DPPC interacts weakly with the external aqueous phase [93].

DPPE is another zwitterionic phospholipid, thus its properties differ much from DPPC. Its headgroup possesses a primary amine residue, allowing hydrogen-bond formation. Therefore, the hydration of DPPE is much more pronounced compared to DPPC [93, 94]. On the other hand, the molecular geometry of DPPE is governed by its small headgroup. Therefore DPPE forms in water an inverted hexagonal H_{II} phase which causes lacking colloidal stability and sedimentation of aqueous DPPE dispersions.

DPPG is an acidic phospholipid, existing above a pH of 4 in its anionic form [95]. At physiological pH and in the presence of sodium DPPC obtains the lamellar phase like DPPC [96].

At last in this chapter, focus will be put on the mid-term stability of MBs in aqueous media. In contrast to albumin- and polymer-shelled MBs, phospholipid MBs does not provide over long shelf-life in the range of months or years. For this reason, all of the approved phospholipid MB products are formulated as vials for activation by either reconstitution (SonoVue[®], Imagent[®], Sonazoid[®]) or by mechanical agitation (Definity[®]).

When stored at rest, MBs form in aqueous media highly hydrated microfoam colloidal systems, denoted in the literature as wet foam, microfoam, or “kugelschaum”. One surprising quality of near-sized MBs is that in microfoams they order almost perfectly in 3D and form quasi-crystalline structures. In the crystalline microfoam the MBs mainly have a three-dimensional organization in body centered cubic, face centered cubic, or hexagonal close-packed crystalline structures [97, 98].

The colloidal state of microfoams is metastable and mainly depends on their hydration since the microfoam remains wet up to a height h , reversely depending on the MB diameter d and straightly depending on the square of the capillary length l_0 according to Equation 5:

$$h \approx \frac{l_0^2}{d}$$

Equation 5

On its side the capillary length l_0 can be expressed by the following equation:

$$l_0^2 = \frac{\gamma}{\rho g}$$

Equation 6

where ρ is the density of the medium, γ is the surface tension, and g is the gravitational acceleration. Due to the action of gravitational forces microfoam dehydration affects on the first place the top layers which are mostly occupied by bubbles of the upper size range. For this reason, MBs of size above 10 μm should be considered as an unstable fraction of the “native” MB suspension.

In summary, the MB stability after the activation of the precursor vial depends on several pharmaceutical factors in a complex interplay. The medium density plays together with the gravitation a negative role for the stability of the microfoam. In contrast, the capillary length is rendered greater and the microfoam wet layer is thicker provided the surface tension is lower and the MB diameter is smaller.

The complicated physico-chemical interactions between gas core, phospholipid monolayer, drug, and surrounding medium dictate the formulation design of soft-shelled MBs. An advanced MB structure design is supposed to assure MB pharmaceutical quality, sustainable *in-vivo* behavior, echogenicity, and an adequate therapeutic effect.

II. CHAPTER: Formulation and characterization of model microbubbles

1. Abstract

Originally developed as contrast agents for ultrasound diagnostics, in the past years, microbubbles (MBs) have made an unusual way from the patient's bedside back to the researcher's laboratory, since their potential as carriers for drugs, nucleotides, and proteins has been discovered. Today, numerous MB structures have been designed for the purposes of targeted drug delivery.

The present thesis work is focused on the formulation of drug and gene-loaded MBs with soft phospholipid shells. Thereby, drug and gene-loaded liposome formulations are used as precursors for the production of MBs by high-speed mechanical agitation together with the MB core gas.

The following chapter provides some insights on the validation of mechanical agitation for production of MBs with optimal pharmaceutical properties. The influence of several process factors such as the agitation time, tube fill volume, and tube shape, will be studied and discussed.

Furthermore, validation and selection of appropriate methods will be put on MB particle size distribution, Zeta potential, and concentration.

Keywords: Phospholipid microbubbles, production, quality control, process control, particle sizing;

Abbreviations: LCMP – liposomal-controlled microbubble production, MB – microbubble;

2. Introduction

In the past decades microbubbles (MBs) have gained wide clinical applications as well tolerated contrast agents for the ultrasound diagnostics. Recently, they have made an unusual way from the clinical practice back to the research laboratory, since their potential as specific drug and gene-carriers for targeted therapy has been discovered. Drug-loaded MBs provide the unique ability to outline the site of disease and to achieve drug targeting in a single needle prick.

The present dissertation work focuses on the formulation of phospholipid-shelled MBs by mechanical high speed agitation. Thereby, a pre-filled sterile vial containing liquid phase and MB core gas is agitated on its length-axis for a definite time and with an exact frequency using a mechanical device. For the first time mechanical agitation has been implemented on a commercial scale by Bristol-Myers Squibb Medical Imaging, Inc. with the diagnostic US contrast product Definity[®]. In this case, the precursor vial comprises an aqueous phospholipid dispersion and octafluoropropane gas. Immediately prior to the drug administration the vial is activated by agitation for 45 s at 4,500 oscillations/min using VialMix[®] (Bristol-Myers Squibb Medical Imaging, Inc., North Billerica, USA). The produced concentrated MB dispersion is then diluted with physiological medium and administered mostly by intravenous infusion or bolus injection.

Mechanical agitation is a comfortable one-step method for MB production which is appropriate for the *in-situ* production of drug-loaded MBs [56] and acoustically active lipospheres [99]. It requires a two-step formulation process, whereby initially a precursor liposomal formulation is created using a conventional method such as thin-film hydration, phase inversion, or ethanol injection. Next, the liposomal dispersion is placed into vials, and the remaining head-space of the vial is filled with a suitable gas which will form the MB cores upon agitation. Liposome precursors may be additionally stabilized by spray-drying or freeze-drying. Shortly prior to the administration the vial is activated by high-speed agitation.

After the vial activation the resulting MB dispersion is mainly stable for a couple of hours, therefore MBs have to be produced at the patient's bedside.

MBs can be drug-loaded by means of two approaches – loading of pre-formed MBs by incubation with the active drug, or by loading of the liposome precursors which are then transformed into drug-loaded MBs. Many authors prefer the first approach of drug-loading pre-formed MBs [64, 66, 102] which is yet complicated and barely practicable on a large scale and in the clinical practice.

On the contrary, drug-loading of precursor liposomes offers a better applicable and elegant approach, having the advantage to provide a ready precursor formulation for one-step production of drug-loaded MBs in a single vial [55, 56, 58].

The present work proposes a method to control the formulation properties of drug-loaded MBs such as size, particle yield, and encapsulation efficiency by manipulating the formulation properties of the precursor liposomes which will be referred to as *liposomal-controlled microbubble production* (LCMP) approach. In the following chapter an optimal setup for MB production by mechanical agitation will be established, without yet considering the aspect of drug loading which will be addressed in later chapters. Furthermore, appropriate methods for characterization of MBs *e.g.* in their concentration and particle size distribution will be selected. The effects of various formulation factors such as the volume ratio of gas to liposomal dispersion, the agitation time, *etc.* on the formulation properties will be observed and discussed. Following, an attempt will be made to establish a theory about the mechanism of MB formation under high mechanical shear.

One further aspect in this chapter will be the characterization of MBs in their particle size, Zeta potential, and concentration. These pharmaceutical properties play an important role for the *in-vivo* applicability of drug-loaded MB formulations and must therefore be accurately determined. For example, the particle size distribution in MB formulations is decisive for their therapeutic effectiveness and clinical safety, since large gas bubbles are not only very rapidly cleared from the circulation [100], but may also cause embolism and ischemic stroke. On its turn, Zeta potential of MBs can influence their microcirculation behavior and capillary retention [101].

Various approaches for particle sizing and Zeta potential measuring will be following compared and the most suitable method will be selected as well as the optimal setup parameters for its application.

Unfortunately, recent research literature still lacks studies on method applicability, validation, and application comparisons for the characterization of such complex systems as the MBs. Most difficulties of MB characterization are related to their intricate light scattering features, the phenomenon of buoyancy *i.e.* the size dependent flotation in upright direction, and their sensitivity to pressure fluctuations and shear stress.

Many particle sizing approaches such as the dynamic light scattering and the laser diffraction are based on the correlation between light scattering pattern and particle size. Depending on the ratio between particle diameter and light wavelength the light scattering has been described by the theories of Rayleigh, Mie, and Fraunhofer. Roughly, the light scattering

theories of Rayleigh and Fraunhofer describe the scattering from particles which are either much smaller (about a factor of 10) or much larger (about a factor of 50) than the light wavelength. MBs are typically sized between 1 μm and 3-5 μm and are considered under the scattering theory of Mie [102], since their size is comparable to the wavelength range used by the most particle sizing instruments – 400-600 nm. The equations of Mie are complex and require an imaginary number, comprising of two material specific parameters: the refractive index and the absorption index which must be known in order to derive the particle size from the intensity of scattered light.

Several literature works have dealt with light scattering by MBs with regard to accurately determining of their particle size. The refractive index of pure water is 1.333 and lies above the values for MB core gases such as nitrogen and air which are about 1.000. Commonly, the refractive index of dispersed media lies above the refractive index of the dispersant as in the case of liposomes (1.440) or proteins (1.450). Compared to droplet dispersions, MBs scatter at the angle region from 40° to 110° , rather than at 120° to 180° with regard to the axis of light beam. Therefore, light scattering characteristics for MBs strongly differ from other known dispersion systems such as suspensions or emulsions, even if they have exactly the same size [103].

The light scattering by MBs is even more complicated by the existing multiple order light refractions within a single particle. In the simplified model of a shell-free gas bubble the light scattering is distorted by reflections and internal refractions of first, second, or higher orders [104]. Another factor, playing role in the theoretical modeling, is the presence of MB shell which possesses an intrinsic refractive index of roughly 1.20 for proteins and 1.10 for lipids [105], and contributes to the overall refraction and absorption.

Optical sizing methods typically consider the particle shape as spherical which in many cases evolves significant deviations from the real particle size. Bubbles sized under 100 μm are considered spherical [106] and thus no stereological conversions are necessary due to their shape [107].

All this exemplifies the need of properly established optical models for MBs and even for MB formulations with different shell constitutions which are based on empirical relations rather than on complex mathematical models. For the first time, laser diffraction for MBs has been established in approximation for coated spheres based on modifications of the Mie theory [108] and applied later for coated gas bubbles [109]. It has been shown that there is a monotonic relationship between the bubble size and the scattered light intensity [110]. Further

in this chapter, an optical model will be proposed for laser diffraction particle sizing of phospholipid-shelled perfluorocarbon MBs.

One further problematic issue on the particle sizing and Zeta potential measuring of MBs is their buoyancy. The effective net force F , [N] exerted on a MB surrounded by liquid, can be expressed as the sum of the buoyant force and the gravitational force:

$$F = mg - \rho Vg$$

Equation 7

where m is the mass of the MB, [g], g is the gravitational acceleration, [m/s^2], ρ is the density of the liquid, [g/l], and V is the volume of the liquid, displaced by the object [cm^3]. However, it has to be taken into account that soft-shelled MBs are compressible objects and their volume V as well as the resulting buoyant force decrease when the hydrostatic pressure increases in accordance with the particle position on the z-axis.

The rising velocity of MBs in a diluted dispersion is further determined by the viscosity of the surrounding medium which can be roughly described on the theoretical basis of the Stokes' law (Equation 8) [111].

$$V = \frac{gd^2}{18\nu}$$

Equation 8

where V is the rising velocity of the MB, [m/s], g is the gravitational acceleration, [m/s^2], d is the MB diameter, [m], and ν is the kinematic viscosity the dispersant medium, [m^2/s]. On Figure 5 the graphic plot according to this equation is represented.

The effect of buoyancy may significantly influence particle sizing and determination of Zeta potential depending on the particular measurement method. For this reason, one of the criteria for selection of methods for MB characterization will be the independence from buoyancy.

In order to thoroughly characterize one MB dispersion, especially with regard to newly developed formulations, particles of all size classes must be compassed in the sampling. The effect of buoyancy turns MB sampling intricate since shortly after dilution of the freshly prepared concentrated MB dispersion large MBs float on the liquid surface and disrupt.

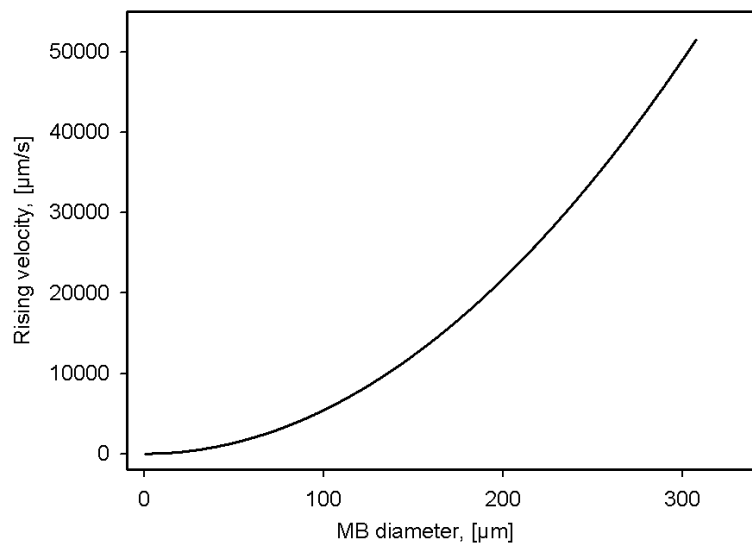


Figure 5: Mathematical calculation of the MB rising velocity according to the particle diameter based on the Stokes' law. The buoying speed exponentially increases with the MB size.

According to Figure 5, a MB with a diameter of 100 μm in diluted aqueous medium rises with a velocity of 5.5 mm/s and is exposed on the liquid surface quickly after the dilution of the MB dispersion. As seen from Equation 5, p.30 the stability of wet MB foams decreases with increasing MB size, thus on the air / water interface larger MBs are quickly dehydrated and degraded. Therefore, although larger MB fractions are mostly present in the undiluted MB dispersion they are undetectable with the most particle sizing methods which require exhaustive. On the other hand, since dilution precedes every clinical application of MBs, large-sized bubbles will be degraded in the vial, too. Nevertheless, since large bubbles may be clinically harmful their analysis requires special attention. One further criterion for selection of particle sizing methods will be therefore the detection of large bubble fractions in MB dispersions.

Particle size and concentration measurements using electrical zone sensing were performed in cooperation with Mr. Raffi Bekeredjian, MD from the Internal Medicine III, Ruprecht-Karls-University – Heidelberg, Germany and with Mr. Stefan Zahler, Ph.D. from Department of Pharmacy, Pharmaceutical Biology at the Ludwig-Maximilians-University – Munich, Germany. The author expresses his acknowledgements to Mr. Michael Pohl, Ph.D., Vice President Scientific Marketing at Horiba Instruments, Inc., Irvine, USA for the peer-reviewing of this chapter.

3. Materials and Methods

3.1. Reagents

| Substance | Abbreviation | Purchased from |
|---|--------------|---|
| Dipalmitoyl phosphatidylcholine | DPPC | Lipoid AG, Ludwigshafen, Germany |
| Dipalmitoyl phosphatidylglycerol sodium | DPPG | Lipoid AG, Ludwigshafen, Germany |
| Chloroform, HPLC-grade | --- | Sigma-Aldrich GmbH, Munich, Germany |
| Octafluoropropane | --- | Sauerstoffwerk Friedrich Guttroff GmbH, Wertheim, Germany |
| 1,2,3-Propanetriol, water free | Glycerol | Sigma-Aldrich GmbH, Munich, Germany |

3.2. Production of liposome precursors and model microbubbles

3.2.1. Production of liposome precursors

Liposomes were formulated as intermediate product, and were following used to produce MBs by mechanical agitation. The thin-film hydration method was applied as described below. Briefly, dipalmitoyl phosphatidylcholine (DPPC) and dipalmitoyl phosphatidylglycerol sodium (DPPG) were dissolved under heating in HPLC-grade chloroform. After removing the organic solvent for 60 min at 65 °C under vacuum using a Büchi Rotavapor R-114 (Büchi Labortechnik GmbH, Essen, Germany), the phospholipid blend was hydrated with highly purified electrolyte-free water (Purelab Plus[®], USF Elga Ionpure GmbH, Germany) to produce large multilamellar liposomes. Accordingly, the liposomes were shortly processed with low-frequency horn-type US homogenizer (Branson Sonifier[®], Branson Ultrasonics Corp., USA) to produce small unilamellar vessels. The final total phospholipid concentration was 5 mM (3.68 mg/ml). The concentration of DPPC was 80 mol% of the total phospholipid, corresponding to 4 mM or 2.94 mg/ml, and that of DPPG – 20 mol%, corresponding to 1 mM or 0.75 mg/ml.

3.2.2. Production of model MBs

The prepared small unilamellar anionic liposomes were placed in 2 ml safe-lock tubes (Eppendorf AG, Hamburg, Germany), cap space was filled with octafluoropropane gas and agitated at 4,500 oscillations / minute using a mechanical agitator

CapMix™ (3M Deutschland GmbH, Neuss, Germany). With exception to experiments where the agitation time was varied, tubes were agitated for 20 s at room temperature.

3.3. Pre-formulation studies on model microbubbles

3.3.1. Effects of agitation time

Microbubbles were produced by mechanical agitation, as the length of agitation (agitation time) was varied from 0 s to 60 s with an increment of 20 s. Immediately after agitation the tube temperature was measured by immersing a sensor (Ama-digit ad 15th, Amarell GmbH, Kreuzwertheim, Germany) into the liquid phase. Simultaneously, the air temperature under the CapMix™ protective hood was measured in order to eliminate the influence of device heating on the tube temperature. Air temperature increase was then subtracted from the tube temperature.

Accordingly, the MB size distribution was determined by laser diffraction using Partica LA-950 (Horiba Ltd., Kyoto, Japan). MB concentration was determined by PAMAS SVSS-C (PAMAS GmbH, Rutesheim, Germany). All measurements were carried out in triplicate.

3.3.2. Effect of liposome viscosity

Liposomal precursor formulations were prepared as described above, whereby the aqueous phase was adjusted with glycerol from 0 mass% to 30 mass% with an increment of 5 mass%. The viscosity of liposomal formulations was determined by rheometry using Physica MCR (Anton Paar GmbH, Graz, Austria) at a constant shear of 2 Pa and a torsional moment of 61.4 μNm . Tubes were agitated for 20 s. Temperature in the tube was measured with an immersed sensor (Ama-digit ad 15th, Amarell GmbH, Kreuzwertheim, Germany). MB concentration was determined in freshly prepared samples by light blockage using PAMAS SVSS-C (PAMAS GmbH, Rutesheim, Germany). MB size distribution was determined by laser diffraction using Partica LA-950 (Horiba Ltd., Kyoto, Japan).

3.3.3. Effect of tube fill volume

Tube fill volume will be defined here as the per cent ratio between the volume of liquid phase and the total volume of the tube container. Tube fill volume was varied from 10% to 50% of the total tube volume of 2 ml. Polypropylene tubes with U-shaped bottom (Eppendorf AG, Hamburg, Germany) were used in this study. Filled tube containers were agitated for 20 s and the MB concentration was measured in the freshly prepared samples by light blockage using PAMAS SVSS-C (PAMAS GmbH, Rutesheim, Germany). MB size distribution was

determined by laser diffraction using Partica LA-950 (Horiba Ltd., Kyoto, Japan). Samples were prepared and measurements were carried out in triplicate ($m = 3$, $n = 3$).

3.3.4. Effect of tube shape

Containers with constant volumes of 2 ml and different bottom geometry were tested in order to evaluate the influence of agitation dynamics, determined by the container geometry, on the MB size distribution and concentration at constant agitation speed and time. Polypropylene tubes having V-shaped and U-shaped bottoms (Eppendorf AG, Hamburg, Germany), as well as glass vials with F-shaped bottom (VWR International GmbH, Darmstadt, Germany) were tested.

Particle concentration was determined by light blockage using PAMAS SVSS-C (PAMAS GmbH, Rutesheim, Germany). Particle size distribution was determined by laser diffraction using Partica LA-950 (Horiba Ltd., Kyoto, Japan).

3.4. Characterization of microbubbles

3.4.1. Size distribution measurements

Five instrumental methods for particle sizing were compared in their applicability for characterization of MB samples. The methods included laser diffraction, dynamic light scattering, light blockage, and electrical zone sensing.

Laser diffraction measurements were performed using Partica LA-950 (Horiba Ltd., Kyoto, Japan), equipped with a blue LED laser source, operating at a wavelength of 405 nm, and a red laser source, operating at 650 nm. The measurement range of the device was from 40 nm up to 3 mm. The laser diffractometer was equipped with quartz cuvettes with volumes of 15 ml and 10 ml and a magnetic stirring facility. Optical model was produced and data processing was carried out using the software Horiba LA950 v.5.00. The iteration value was set to 15 for all measurements. MB formulations were sampled immediately prior to measurements by addition of 20-100 μ l undiluted freshly prepared MB dispersion into the dilution medium – highly purified water, under continuous stirring.

Optical method parameters – refractive index and absorption index, were established based on the approach of Kinoshita et al. (2001) [112]. Briefly, the detected intensity of scattered light (s) was mathematically transformed into particle size distribution and back again into estimated light intensity distribution (s^*). The conformity of s and s^* was automatically calculated by the application software as the cosine of the value of the angle between

them ($\cos\theta$). When the optimal refractive index has been selected, the most accurate particle size distribution has been obtained and then it was expected that s^* would be completely the same or very close to s and $\cos\theta$ would trend to zero.

In order to determine an appropriate refractive index range for MB sizing, three identical MB samples were measured by laser diffraction. Rough measurement data for each sample was recalculated using various refractive index values ranging from 0.300 to 3.000 with an increment of 0.300 for both blue and red laser sources, while keeping the absorption index at zero. Values of $\cos\theta$, as well as number-weighted median particle sizes, were calculated by the application software for each value of the refractive index. Accordingly, $\cos\theta$ and median particle size were graphically plotted against the refractive index. Refractive index values, corresponding to the minimum values of $\cos\theta$, were selected as appropriate for MB particle sizing and implemented in the optical model. In the application software Horiba LA950 v.5.00, $\cos\theta$ is referred to as *chi-square* (χ^2).

The same procedure was followed in order to determine appropriate values for the MB absorption index which was varied in the range from 0.0100 to 0.1000 with an increment of 0.0100, while keeping the refractive index at the previously selected optimum value.

For verification MB particle size data, obtained with the established optical model, was compared with data, obtained from electrical zone sensing and light blockage measurements.

Alternatively, particle size in MB formulations was determined by dynamic light scattering in the range from 0.001 nm to 5,000 nm using right-angle and backscatter approaches. Zetamaster S (Malvern Instruments Ltd., Worcestershire, UK) was utilized for the right-angle approach, while Zetasizer Nanoseries Nano-ZS (Malvern Instruments Ltd., Worcestershire, UK) was used for backscatter measurements. MB concentration was adjusted to about 1×10^4 MB/ml for right angle measurements and to about 1×10^7 MB/ml for backscatter measurements. The refractive index for MBs was set to 0.90, and the absorption index – to 0.01, according to the established optical model. The refractive index for the dispersant was set to 1.333, corresponding to water. The Zetasizer device was equipped with a laser source operating at 405 nm wavelength.

MB size distribution was determined by light blockage in the size range between 800 nm and 200 μm in diluted samples using PAMAS SVSS-C (PAMAS GmbH, Rutesheim, Germany) equipped with a syringe sampling pump and a stirring facility. Samples for measurements were prepared by dilution of 20 μl of the freshly prepared MB sample in highly-purified degassed water until the particle count decreased to less than 2×10^5 MB/ml. Portions of 1 ml were drawn in triplicate from the diluted sample for analysis. The bubble size distribution in

the range from 800 nm to 200 μm as well as the MB concentration were determined simultaneously.

The syringe pump speed was varied from 2 ml/min to 20 ml/min in order to assess the influence of pressure stress on the measured MB size.

As an alternative to the optical methods, measurements with electrical zone sensing were performed using MultisizerTM 3 Coulter counter (Beckman Coulter, Inc., Fullerton, USA) equipped with a stirring facility. Aperture current was set to 800 μA and volumes of 100 μl were metered. Samples were measured at concentrations of about 10^6 MB/ml after dilution with Isoton II.

3.4.2. Determination of MB Zeta potential

Zeta potential of MB formulations was determined by electrophoretic light scattering using Zetasizer Nanoseries Nano-ZS (Malvern Instruments Ltd., Worcestershire, UK). During the measurements the dielectric constant (τ) was set to 78.48 (pure water at 25 °C). The optical parameters – refractive index and absorption index, for MBs were set to correspondingly 0.90 and 0.01. The applied voltage value was set to 50 V and the monomodal analysis model was used. MB concentration was adjusted to about 1×10^5 MB/ml. Prior to measurements MB size was determined by laser diffraction using Partica LA-950 (Horiba Ltd., Kyoto, Japan). Measurements were carried out in triplicate for each sample. Data was processed using Dispersing Technology Software v.5.10 (Malvern Instruments Ltd., Worcestershire, UK).

3.4.3. Determination of MB concentration

MB concentration measurements in the size range from 800 nm to 200 μm were performed by light blockage using PAMAS SVSS-C (PAMAS GmbH, Rutesheim, Germany). The particle concentration in samples was kept below the maximum measurable particle concentration of 2×10^5 MB/ml. Portions of 1 ml were automatically drawn by a syringe pump from the diluted MB dispersion with a pace of 5 ml/min.

Alternatively, the MB concentration was determined by electrical zone sensing using MultisizerTM 3 Coulter counter (Beckman Coulter, Inc., Fullerton, USA) after dilution with Isoton II.

4. Results and Discussion

4.1. Pre-formulation studies on model microbubbles

4.1.1. Effect of agitation time

According to the results of this study, the net energetic effect of mechanical agitation is exothermic and depends rather linearly from the agitation time (Figure 6, dashed line). The temperature of the liquid phase increased from $24.31\text{ }^{\circ}\text{C} \pm 1.75\text{ }^{\circ}\text{C}$ to $46.57\text{ }^{\circ}\text{C} \pm 3.04\text{ }^{\circ}\text{C}$ within 60 s of agitation. The tube temperature was not significantly influenced by the device heating since the air temperature under the protective hood only raised by $2.08\text{ }^{\circ}\text{C} \pm 0.87\text{ }^{\circ}\text{C}$. Interestingly, the MB concentration increased during the first 20 s of agitation, followed by a steep 3-fold decline after 40 s to 60 s. The influence of tube temperature on the MB yield can be attributed to the transition state of the shell phospholipids. MB shell is much more stable when the phospholipid exists in condensed gel state. The phase-transition temperature of the used DPPC / DPPG mixture is $41.55\text{ }^{\circ}\text{C} \pm 0.11\text{ }^{\circ}\text{C}$ (refer to Table 10, p.98) which was approached after 40 s of agitation. The resulting phase shift from condensed gel to liquid-crystalline phase state apparently destabilized the monolayer shell and led to degradation of MBs.

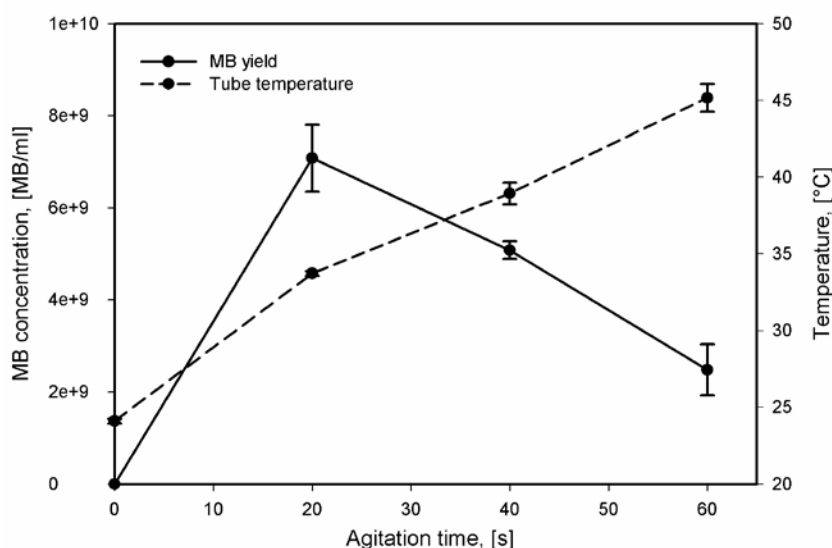


Figure 6: Effect of agitation time on the tube temperature and MB yield ($n = 3$). Tube temperature increased proportionally to the agitation time, while MB concentration reached a maximum at 20 s and steeply decreased, when the melting temperature of the shell phospholipid was reached.

However, the effect of MB degradation cannot be explained only by the temperature increase, since in follow-up studies MB dispersions, incubated for over 90 min at 60 °C under static conditions, showed only a moderate concentration decrease of about 17.5%. Apparently, the observed phenomenon can only be explained under consideration of the combined effect of temperature and shear stress.

A significant effect of the agitation time on the MB particle size distribution was also demonstrated, as shown on Figure 7. Initially, a single broad peak between 260 nm and about 10.1 μm was present in MB samples 20 s after agitation start. Longer agitation of 40 s resulted in a peak sharpening and narrowing to size values between about 800 nm and 5.8 μm . Furthermore, a second small peak was formed between 34 μm and 77 μm . At 60 s agitation, the large-sized peak gained intensity and broadened between about 23 μm and 153 μm .

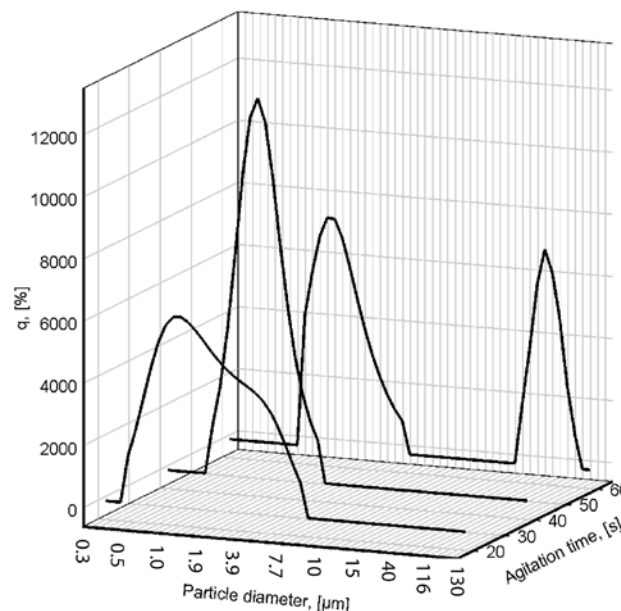


Figure 7: Surface-weighted MB particle size distribution as a function of the agitation time.

Microscopic observations revealed that during the first five to ten seconds of agitation the MB dispersion is rather “immature” and inhomogeneous, comprising micrometer- to millimeter-sized agglomerates of small and large bubbles and phospholipid (data not shown). Later on, after 20-30 s the phospholipid aggregates and large “primary” bubbles were sheared and a homogeneous MB dispersion was formed.

Obviously, the optimal MB size distribution was obtained 40 s after agitation start. However, this was accompanied by an about 1.5-fold decrease of MB concentration after 40 s agitation compared to 20 s. These results suggest that with regard to each particular drug-loaded

formulation, the optimal agitation time should be sought between 20 s and 40 s under consideration of the two factors – MB size distribution and yield.

4.1.2. Effect of liposome viscosity

Liposome viscosity increased almost linearly from 1.5 Pa.s to about 3 Pa.s upon increasing glycerol concentration. The influence of liposome viscosity on the production of MBs by mechanical agitation revealed complex trends both in the devolution of the tube temperature curve, as in the MB concentration.

By increasing the viscosity in the above range two maxima were observed in the tube temperature curve after 20 s of agitation (Figure 8, solid line). Initially, addition of 5 mass% to 10 mass% glycerol led to a small but reproducible tube temperature increase of about 2 °C compared to glycerol-free samples. Interestingly, the moderate temperature increase was accompanied by an over 2-fold increase of MB concentration (Figure 8, dashed line).

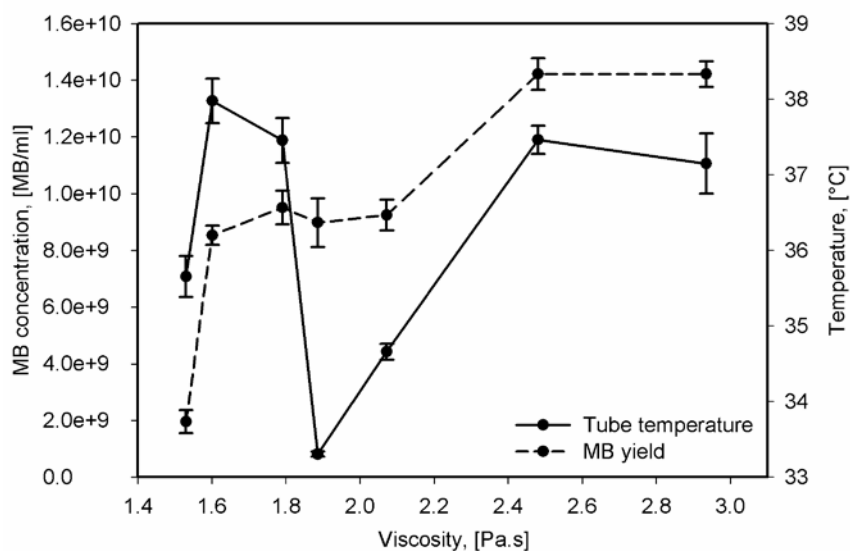


Figure 8: Effect of liposome viscosity (at $\tau = 2$ Pa) on the tube temperature and the MB yield at agitation time 20 s ($n = 3$). Dashed line represents the tube temperature after agitation for 20 s. Solid line represents the MB concentration in freshly prepared samples.

Further increase of viscosity resulted in an unexpected drop of tube heating of over 5 °C together with an insignificant decrease of MB concentration. Tube heating rate rose back to about 37 °C upon reaching a viscosity of 2.73 Pa.s. In general, a viscosity increase of 1.405 ± 0.054 Pa.s raised the MB yield about 10-fold. This was despite the enhanced tube

heating during agitation, since the gel-to-liquid phase transition of shell phospholipids – $41.55 \text{ }^\circ\text{C} \pm 0.11 \text{ }^\circ\text{C}$, had not yet been reached.

Apparently, glycerol had some more specific effects on the system rather than simply increasing the viscosity, since the non-linear character of both the temperature curve and the MB concentration curve did not correspond to the linearity of the viscosity increase at growing glycerol concentration.

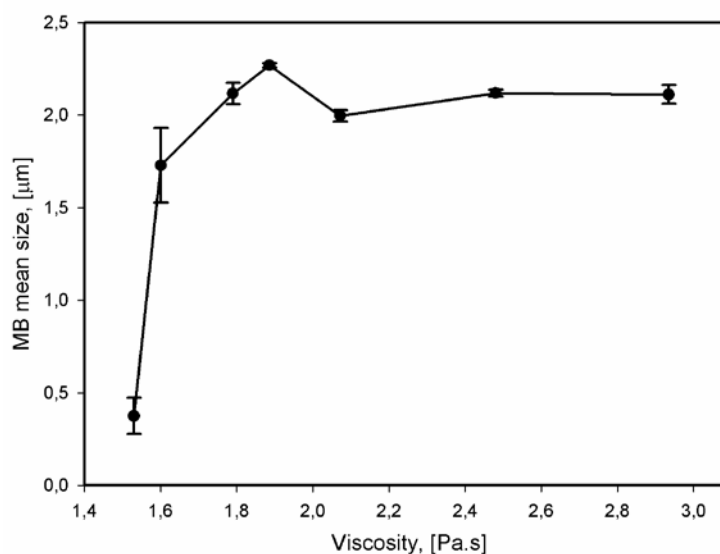


Figure 9: Effect of viscosity (at $\tau = 2 \text{ Pa}$ and $25 \text{ }^\circ\text{C}$) on the MB mean size according to number-weighted particle size data.

Furthermore, viscosity had significant influence on the MB size distribution, yet this effect was only pronounced between 0 mol% and 5 mol% (Figure 9), in which range the viscosity increase was only 0.07 Pa.s . Thus, apparently this is also due to interactions between the phospholipids and glycerol, rather than an effect, caused by the viscosity.

Generally, addition of 5 mass% to 10 mass% of glycerol resulted in a sharpening and narrowing of the main MB peak between 500 nm and $7 \text{ }\mu\text{m}$. On surface area-weighted diagrams, the emerging of a second peak between $50 \text{ }\mu\text{m}$ and $100 \text{ }\mu\text{m}$ was observed at glycerol concentrations above 10 mass%.

4.1.3. Effect of tube fill volume

The proportion between the volume of liposomal dispersion and the total volume of the tube container was denoted here as tube fill volume. It had a moderate, but significant influence on the MB yield (Figure 10), and a more pronounced effect on the MB size distribution. Generally, with increasing the tube fill volume from 10% to 50% of the total tube volume the MB concentration decreased approximately two times, as maximum yield was achieved at 20% tube fill volume.

Along with this, the fraction of large MBs in the size range of several hundred micrometers steeply increased. In surface area-weighted size diagrams only the MB peak between about 500 nm and about 6 μm was present at fill volumes of 10% and 20%. At 30% tube fill volume the size peak between about 60 μm and about 100 μm appeared, while further increase to 40% and 50% of the tube volume resulted in the emerging of smearing peaks from about 200 μm to about 600 μm .

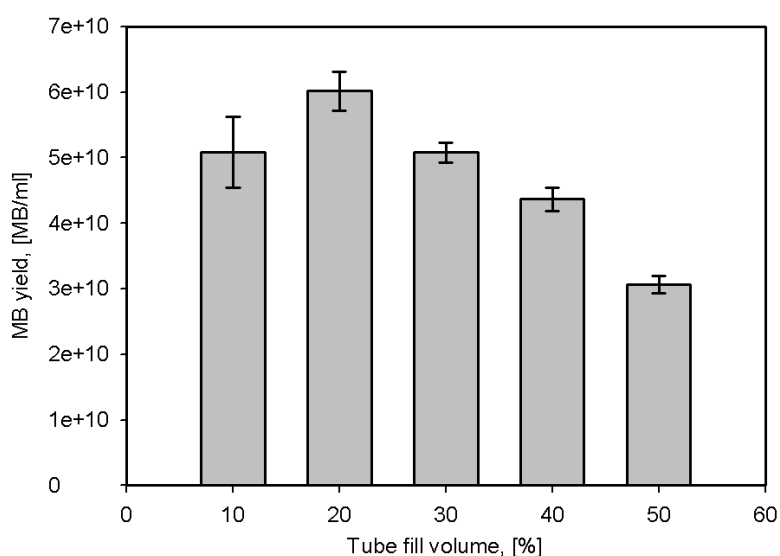


Figure 10: Effect of tube fill volume on the MB yield ($m = 3$, $n = 3$) after agitation for 20 s. Maximal MB yield was achieved, when 400 μl liquid phase – liposome precursor dispersion, were filled in the tubes, having a total volume of 2,000 μl (20% tube fill volume).

The observed effects can be explained with the downgraded mixing kinetics of gas and liquid, if the cap space is too small to allow adequate bouncing of the liquid phase during agitation. At higher tube fill volumes of *e.g.* 50% a large part of the gas phase is absorbed into the liquid phase. Because of the MB formation, the dynamic viscosity of the liquid phase grows about

300-fold (data not shown). Therefore, the fluid dynamics in the tube are hindered and no sufficient shear forces can result.

This is an appropriate explanation for the reduced fraction of small MBs since at higher tube fill volumes more shell material is employed in larger bubbles.

4.1.4. Effect of tube shape

Tube geometry had a moderate effect on the MB formulation. No difference could be found between size distribution and concentration of MBs, produced in F-bottom and U-bottom tubes. When V-bottom tubes were used, there was a significant increase of MB size and a large-sized bubble peak between 60 μm and 120 μm emerged. Once again this effect could be attributed to the unadvantageous fluid dynamics during agitation, caused by the narrow V-shaped tube bottom.

4.2. Characterization of microbubbles

4.2.1. Size distribution measurements

MB optical parameters – absorption index and refractive index, are additive values, resulting from the interplay of gas core and MB shell. The light scattering pattern by MBs is rather complex and influenced by high-order refraction, reflection, and light absorption events.

Optimal refraction- and absorption indices for phospholipid-shelled MBs were established by plotting the $\cos\theta$ function at various refractive index values (Figure 11). On the refractive index scale from 0.3 to 3.0 the value of $\cos\theta$ varied from 0.2100 ± 0.0500 to 8.7960 ± 0.8000 . The number-weighted median particle size varied correspondingly from $0.2070 \mu\text{m} \pm 0.0200 \mu\text{m}$ to $0.8330 \mu\text{m} \pm 0.0500 \mu\text{m}$ (Figure 12). The plot of $\cos\theta$ revealed two minima at refractive index values from 0.600 to 0.900 and from 2.700 to 3.000, corresponding to median particle sizes of about $0.80 \mu\text{m} \pm 0.08 \mu\text{m}$.

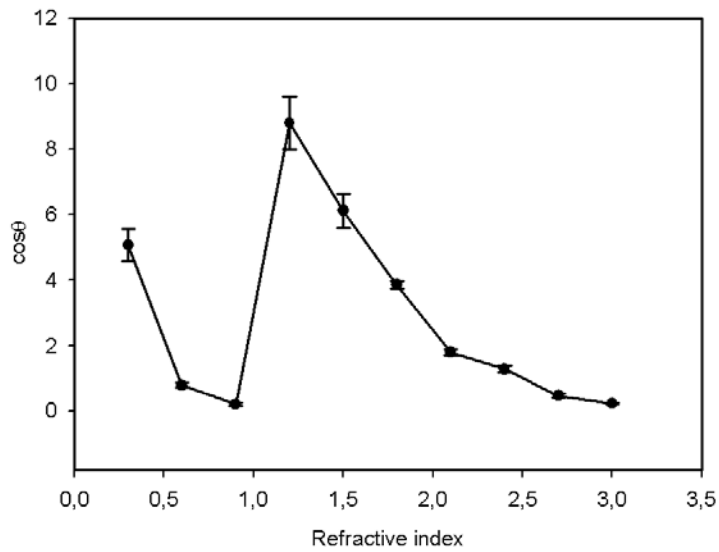


Figure 11: Graphical plot of the value $\cos\theta$ at refractive index-values, ranging from 0.300 to 3.000. The minimum $\cos\theta$ value of 0.21 corresponded to the correct refractive index of 0.90.

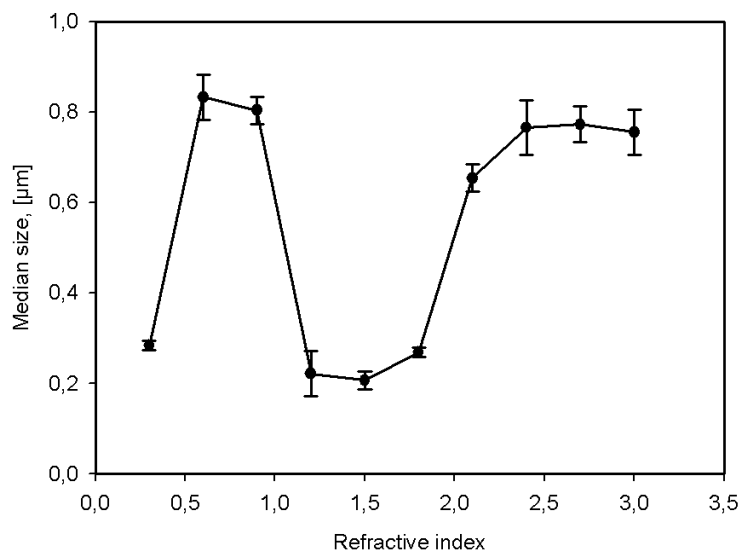


Figure 12: Graphical plot of the value median particle size in number-weighted size distributions at refractive index-values, ranging from 0.300 to 3.000. The selected refractive index value of 0.90 corresponded to a median MB size of about 0.800 μm which was consistent with referent measurements by light blockage.

Since the refractive index of MB gas cores is about 1.000 values between 0.900-0.950 were rendered suitable for MB size measurements. MB particle size, corresponding to this value was further confirmed by electrical zone sensing and light blockage measurements.

The effect of absorption index on $\cos\theta$ and median particle size is shown on Figure 13. Interestingly, varying of absorption index in the range between 0.01 and 0.10 resulted in no

change of $\cos\theta$. Nevertheless, a deviation of about 200 nm was observed in the median particle size in this range.

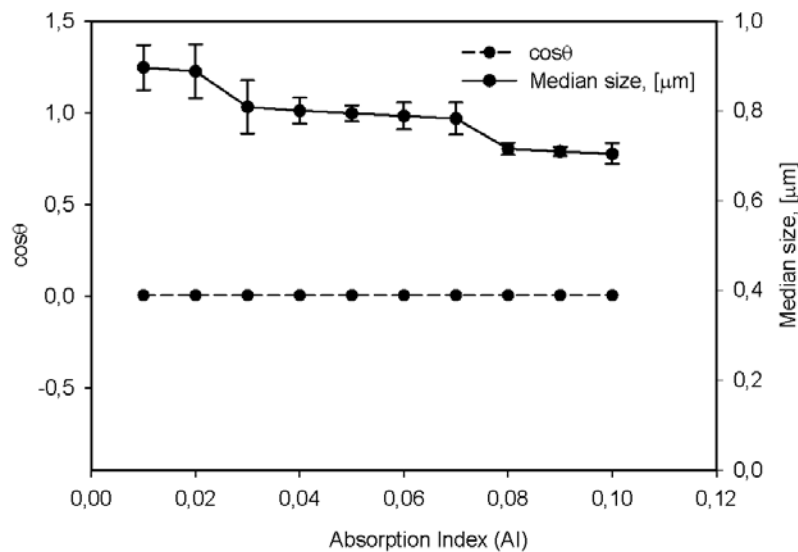


Figure 13: Graphical plot of the value $\cos\theta$ at absorption index-values, ranging from 0.01 to 0.10 (dashed line) and a refractive index of 0.95. Next to that, the change of median particle size in number-weighted size distributions is represented (solid line).

Taking a look on the surface-weighted MB size distribution at refractive indices in the above range, peak form and size range variations were even more pronounced. At refractive index values below 1.000 they mainly affected the MB peak between 0.8 μm and 6.0 μm , whereby the larger-sized peak between 60.0 μm and 100.0 μm remained mostly unchanged. Higher values of the refractive index completely distorted the size distribution.

Based on these findings, the values of refractive index and absorption index for MBs were correspondingly set to 0.90 and 0.01.

Comparisons between number-weighted data provided by laser diffraction with light blockage and by electrical zone sensing proved that the established optical model successfully represents the MB particle size in the size region between about 0.8 μm and 10 μm . This finding rendered as a proof of concept for the applicability of the own optical model.

Another important issue regarding particle sizing of MBs is the data weighting approach and how to interpretate the size distribution data.

The original particle size data, produced by laser diffraction, is the volume-weighted distribution, represented as a dashed-line plot on Figure 14. When weighing size distribution according to the particle volume, large particles are overstated in their intensity. However, the payload-carrying MB compartment is not their entire volume, but the MB shell, since over 90% of MB volume comprises of gas. In the case of phospholipid MBs, the MB shell is only a

few nanometers thick and therefore its volume can be approximated to the MB surface. Therefore, in several recent publications [113] the MB loading is represented as a ratio of the loaded mass per surface area in [$\text{pg}/\mu\text{m}^2$].

Therefore, the surface area-weighted particle size distribution (Figure 14, dotted line) is apparently the most purposeful mode to display the size distribution of drug-loaded MBs, while the volume-weighted size distribution can be considered as a quality method, when large MBs need to be observed. The surface-area weighted distribution can provide an approximate estimation about the percent amount of MBs smaller than $10\ \mu\text{m}$ and the percent payload amount, carried by them. As it is known, MBs greater than $10\ \mu\text{m}$ are liable to be more rapidly eliminated by the narrow capillary vasculature of the lungs and the spleen.

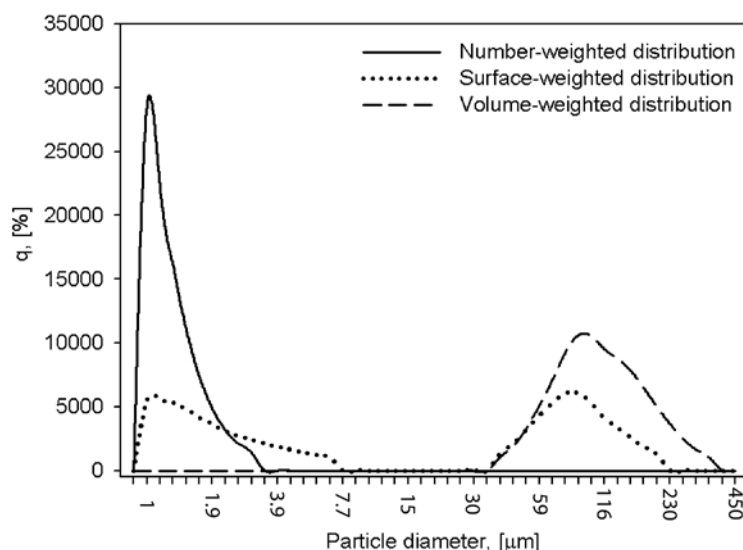


Figure 14: Particle size distribution in a whole freshly-prepared MB formulation, represented in number-weighted (solid line), surface area-weighted (dotted line), and volume-weighted (dashed line) modes. The value q , [%] on the y-axis represents the percentage of particles with a certain size in the measured sample.

The number-weighted size distribution can be either mathematically derived from the volume-weighted distribution. In this mode, smaller sized particles are displayed with the greatest peak intensity, while larger particles are ignored. Therefore, the number-weighted size distribution is less purposeful in the characterization of MB size distribution.

The sampling of undiluted MB dispersion directly into the measurement cuvette under continuous stirring allowed to measure larger bubbles in the range over $50\ \mu\text{m}$ which are not detectable after dilution.

Another light scattering method – dynamic light scattering which is less frequently used in accordance to MBs [68, 114, 115] has been either assessed for particle sizing of MBs. The dynamic light scattering derives particle size information from the time-dependent fluctuations in the intensity of scattered light due to the random Brownian motion of the particles. Thereby, the mathematical conversion is based on the Stokes' law. Its measuring range embraces the entire nanometer range and the lower micrometer range up to about 3-6 μm . Similarly to the laser diffraction, particles' refractive and absorption indices are needed for measurements in certain particle sizes.

Two different setups of dynamic light scattering were tested: the right angle scattering, where the laser beam and the detector are positioned at a 90° angle, and the backscattering approach, where laser source and detector embrace an angle of 173° . While the right angle scattering setup was limited concerning concentrated and turbid samples, the backscattering setup was applicable with highly concentrated MB dispersions. However, both approaches suffered serious reproducibility problems as well by measuring of different samples as during consecutive measurements of a single sample over a certain time span. Apparently, the measurements were disturbed by upright particle movement due to buoyancy which overlapped the random Brownian movement. Furthermore, the typical MB size distribution lies on the upper end of the size scale of dynamic light scattering. For these reasons, dynamic light scattering was considered inappropriate as a method to determine MB particle size.

Light blockage is a particle counting method which operates independently from the particles' optical parameters refractive and absorption index. According to it, particles flow one at a time through a narrow region of uniform light illumination and their light shades are detected. The method is applicable for simultaneously particle counting and sizing in the range from 0.8 μm to 200 μm .

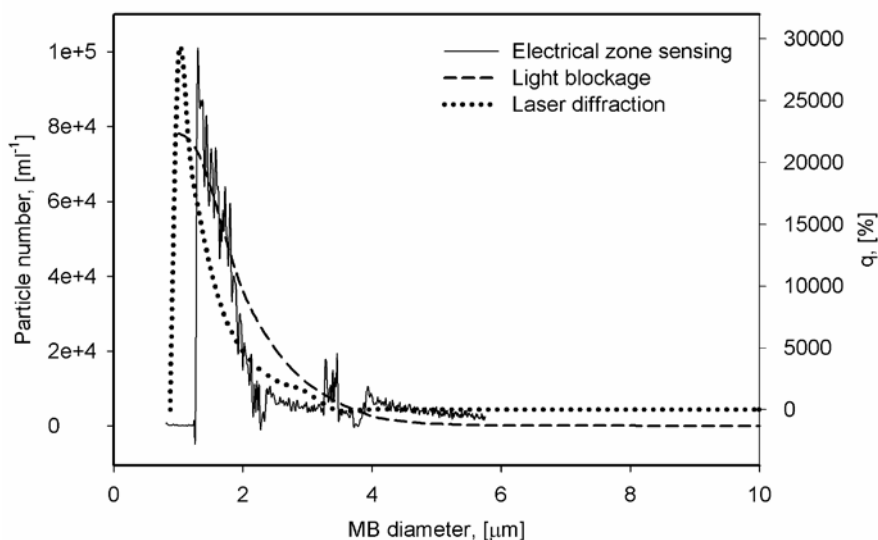


Figure 15: Number-weighted particle size distribution of MB dispersions, obtained by light blockage (dashed line), electrical zone sensing (solid line), and laser diffraction (dotted line). MB formulation comprised 80 mol% DPPC and 20 mol% DPPG.

The particle size data, originating from light blockage measurements, is number-weighted and is therefore less useful to determine the drug-load mass distribution than the surface-weighted data (Figure 15, dashed line). Furthermore, since the size region below 800 nm is out of the method range, the MB size peak cannot be represented completely. Recent particle counting devices, implementing both the concepts of light blockage and single particle light scattering, such as Accusizer 780A (NICOMP Particle Sizing Systems, Santa Barbara, USA) can overcome these limitations in the nanometer region [116].

One further limitation of light blockage as particle sizing method for MBs is the exhaustive sample dilution necessary for measurements. As stated above, due to their rapid buoyancy and low stability at the water-air interface larger MBs were undetectable by this method.

Another setup complication was revealed by varying the speed of the sampling syringe pump from 2 ml/min to 20 ml/min. Since MBs are sensitive to pressure changes a shift in the measured upper MB size from 5 μm to about 3 μm was detected during measurements of the same sample. With increasing syringing pace the MB size decreased continuously corresponding to the increased hydrostatic pressure within the measuring cell.

An effect of decreasing of MB concentration was observed under continuous stirring of diluted MB dispersions. The particle concentration decreased by $32.1\% \pm 1.51\%$ during stirring at 100 rpm for 20 min.

For these reasons conditions for MB size measurements should be selected very consciously, avoiding excessive shear forces and pressure stress, and the measurements ought to be carried out immediately after sampling.

Electrical zone sensing is a non-optical method for particle sizing and counting which has been most widely applied in the literature for characterization of MB formulations [59, 117, 118]. It allows particles to be counted and sized on the basis of the impedance change in an electromagnetic field when a particle passes through an aperture, positioned between two electrodes. The size capacity of the method ranges between 0.4 μm and 1.0 μm when using an aperture of 1 μm and from 1.0 to about 30 μm when using an aperture of 50 μm . In the case of MBs, only the larger aperture of 50 μm is applicable which limits the sizing range to the micrometer range (Figure 15, solid line). Occurring aperture clogging through larger bubbles makes measurements in the nanometer range impossible. Important advantages of electrical zone sensing are the independency from buoyancy effects and the stirring option. However, little is yet known about the electric resistance of shelled MBs. This renders the precise calibration of Coulter counters complicated.

| Method | Size range, [μm] | Measured peaks, [μm] | Drawbacks | Advantages |
|--------------------------|-------------------------------|---|--|---|
| Light blockage | 1-200 | 1-6 (95%) | <ul style="list-style-type: none"> Limited in the nanometer range High dilutions required | <ul style="list-style-type: none"> Particle counting Stirring option |
| Dynamic light scattering | Right angle | 0.3-3 (90%) | <ul style="list-style-type: none"> Limited in the micrometer range | <ul style="list-style-type: none"> Broad measuring range in the nanometer region |
| | Backscatter | 0.001-3 0.085 (10%) 0.68 (85%) 4.59 (5%) | <ul style="list-style-type: none"> Lacking reproducibility due to buoyancy | <ul style="list-style-type: none"> Backscatter approach: broad concentration range |
| Electrical zone sensing | 1 μm aperture | Not applicable | <ul style="list-style-type: none"> Capillary clogging | <ul style="list-style-type: none"> Particle counting |
| | 50 μm aperture | 1-4 (97%) | <ul style="list-style-type: none"> Limitations in the nanometer range | <ul style="list-style-type: none"> Stirring option |
| Laser diffraction | | | <ul style="list-style-type: none"> Broad measuring range No exhaustive dilutions required Independent of buoyancy effects | <ul style="list-style-type: none"> Stirring option |
| | | 0.04-3,000 | <ul style="list-style-type: none"> Optical model required | |

Table 6: Particle size characterization of phospholipid MBs, consisting of 80 mol% DPPC and 20 mol% DPPG – a comparison of alternative measurement methods.

In comparison, from the tested particle sizing methods laser diffraction appears to be the most suitable approach, since it covers both the nanometer and micrometer size ranges, and is not affected by MB buoyancy (Table 1). However, because of the complex light scattering characteristics of MBs, an arbitrary method such as electrical zone sensing or light blockage should be used to prove the reliability of measurement data. Particle size data, obtained using these three methods for characterization of model MBs comprising 80 mol% DPPC and 20 mol% DPPG, is represented in Figure 15. Measured MB peak from 0.8 μm to 4.10 μm appeared on the bottom limit of the measurement range of light blockage. The peak, obtained using electrical zone sensing, slightly deviated and emerged between 1.18 μm and 2.97 μm . Compared to the above standard methods, laser diffraction delivered a MB size peak, ranging from 1.005 μm to 2.976 μm . The above comparison was a proof of the concept that laser diffraction in combination with the properly established optical model provides reliable particle size data for phospholipid-shelled MBs. Based on the comparison between advantages and drawbacks of the evaluated particle sizing methods (Table), laser diffraction was established as standard method further on in this thesis.

4.2.2. Determination of MB Zeta potential

Zeta potential is an important characteristic of a MB formulation and provides information on its colloidal stability, biological characteristics, and drug-loading capacity. For example, anionic MBs are longer retained in the myocardium and in the lungs compared to neutral MBs [101]. The charge-coupling of *e.g.* pDNA to cationic MBs is dependent on the Zeta potential, too [57, 117, 118].

Electrophoretic light scattering is the most commonly used method to determine the Zeta potential of MBs [119]. Charged particles are brought to oscillation by means of alternating electric field. Laser scattering, caused by the moving particles, is then measured and the particle mobility is determined. The electrophoretic mobility is then mathematically converted to Zeta potential.

Because Zeta potential measurements are based on directed particle movements, they can be influenced by MB buoyancy. According to the present study, the influence of buoyancy on Zeta potential measurements was size dependent. Repeated measurements in MB samples with narrow size distribution of between 0.8 μm and about 4.0 μm revealed no shift of the measured Zeta potential within a time span of 40 min, but a gradual decrease of the count rate from about 500 kcps to about 200 kcps. On the contrary, Zeta potential in samples comprising larger MBs, sized between 30 μm and 60 μm could not be determined with a satisfactory reproducibility. This was attributed to their more rapid buoyancy which caused a gradual shift of measured Zeta potential from $-43.2 \text{ mV} \pm 3.75 \text{ mV}$ to $-29.8 \text{ mV} \pm 4.12 \text{ mV}$. Therefore, in further studies the Zeta potential of liposomes will be determined instead of that of MBs under the assumption that these two values are similar or identical.

4.2.3. Determination of MB concentration

MB concentration was reliably determined both by electrical zone sensing and by light blockage. In the case of light blockage, the upper measurement concentration limit for MBs was about 2×10^5 MB/ml, corresponding with manufacturer's specifications. Above this concentration, measured particle counts were significantly lower than expected values, based on the dilution coefficients. This effect can be explained with the overlapping of particle shades within the illuminated region of counting, whereby two or more particles are detected as a single larger particle. A similar effect of detection co-incidence could also be observed in measurements with electrical zone sensing in the concentration range of about $1\text{-}2 \times 10^5$ MB/ml.

5. Summary

Although mechanical agitation as a method to produce MBs is well-known for a long time, its basics have not yet been discussed in the literature. Therefore, one purpose of the studies in this chapter was to arrange the basic process parameters for MB production, using model phospholipid MBs without considering the impact of drug load. Several intriguing effects of such process parameters as agitation time, tube fill volume, and tube geometry on the MB size distribution and MB yield have been demonstrated. Based on this, an attempt was made to describe the mechanism of MB formation under high mechanical shear.

There seems to be an analogy between the dispersing processes during high-shear mechanical agitation and horn-type ultrasound emulsification, yet by aid of some approximation. Similarly to the shear forces during high-speed agitation, intensive shear – acoustic streaming emerges around the sonication horn-type, too. Nonetheless, in the case of mechanical agitation there is no evidence of occurring cavitation, as during horn-type homogenization.

A model of the mechanic processes, occurring during US horn-type emulsification has been described by Li et al. (1978) [120, 121]. According to it, the dispersing of the oil phase in the water phase takes place in two stages. Instability of the oil / water interface results in the entrapment of large “primary” droplets into the aqueous phase. Following, the “primary” droplets are broken down to smaller “final” droplets of various sizes which is the origin of the emulsion polydispersity.

During mechanical agitation the contact interface between liquid phase and gas phase is rapidly enhanced by the dispersing of gas into the aqueous phase. The enhanced gas-liquid interface is stabilized by phospholipid monolayers, emerging from the “unzipping” of liposome bilayers. By analogy, large “primary” bubbles are formed during the first 5-10 s of agitation as described in *4.1.1 Effect of agitation time*, p.43.

In the context of *4.1.3 Effect of tube fill volume*, p.47 the second step of the MB formation – breaking down of large “primary” bubbles was apparently inhibited by the insufficient free tube volume at tube fill volumes of 40-50%. Therefore, the “primary” bubbles could be still observed in these samples.

During the mechanical agitation, equilibrium appears to exist between liposomes and MBs, since liposomes are degraded to form MBs and MBs can be degraded back to liposomes. Within the vial, mechanical shear forces and temperature increase are apparently the two main physical factors, governing the equilibrium.

For the first time the temperature increase in the tube due to the exothermic character of mechanical agitation has been disclosed as the correlation link between agitation time and MB

yield. Furthermore, it was possible to steer the equilibrium between MBs and liposomes as well as the MB size by manipulating several properties of the precursor liposome formulations, agitation process parameters, *etc.* This approach rendered a novel effective strategy for formulation development of drug-loaded MBs which has been named *liposomal-controlled microbubble production (LCMP)*.

The effect of liposome viscosity on MB size and yield has been revealed in this chapter, too. However, it was difficult to discuss on the observed effects since there seemed to be an additional effect of glycerol, used as thickening agent, on the phospholipids.

One further aim of the studies in this chapter was to select appropriate methods for particle sizing, determination of Zeta potential, and MB concentration. Candidate particle sizing methods embraced laser diffraction, dynamic light scattering, light blockage, and electrical zone sensing. Laser diffraction in combination with a properly established optical model for MBs was chosen as standard MB sizing approach, based on its broad size range, sampling manner, allowing the detection of large bubbles, and independency of buoyancy effects. The applicability of the own optical model was scrutinized by comparison with data, established by electrical zone sensing and light blockage measurements.

Zeta potential measurements with MBs did not always deliver a satisfactory reproducibility depending on the MB size and intensity of buoyancy effects. Therefore, only precursor liposome formulations were characterized in their charge under the assumption that Zeta potential of the resulting MBs is close to its value.

Measurements of MB concentration were possible by both approaches tested – electrical zone sensing and light blockage.

The studies under this chapter revealed the most important process parameters for MB production by mechanical agitation and for MB characterization. These will be applied by analogy in formulation studies on drug and gene-loaded MBs further in this work.

III. CHAPTER: *In-vitro* studies on the acoustic destructibility of microbubbles

1. Abstract

Microbubble contrast agents (MBs) in combination with diagnostic ultrasound (US) have recently become a very promising approach for specific drug and gene targeting. Numerous MB structure designs have been adapted to carry and deliver genes and drug molecules with different physico-chemical properties. Drug-loaded MBs can be administered by intravenous infusion or injection and reach even distant tissues and organs. On the target site they can be visualized by well tolerated diagnostic US and aid the localizations of tissue lesions, tumors, *etc.* Accordingly, the drug can be released from the MB carriers by increasing the US intensity and “bursting” the MBs.

The acoustic destructibility is one of the most important MB features, especially for those, having polymeric, albumin, or oil shells. Nevertheless, loading of MBs with drugs and genes may also have an influence on the acoustic properties and destructibility of MBs. In the present work, an improved, near *physiological conditions acoustic transmission line* (PCATL) *in-vitro* model will be described for fast pre-clinical screening of MB formulations.

The PCATL model will be used to demonstrate the differences in the destructibility of MBs with various sizes and give an empirical proof of the theory of Apfel and Holland (1989). Following, the destructibility of MBs will be examined at various US frequencies and intensities.

In the next *IV. CHAPTER: Ultrasound targeted tumor therapy* the PCATL model will be applied to evaluate the acoustic destructibility of doxorubicin-loaded phospholipid MBs and doxorubicin-loaded acoustically-active lipospheres in order to select the better candidate for *in-vivo* clinical studies.

Keywords: microbubbles, ultrasound, acoustic destructibility, *in-vitro* modeling;

Abbreviations: PCATL – (near) physiological conditions acoustic transmission line, MB – microbubble; US – ultrasound;

2. Introduction

Ultrasound mediated destruction of microbubbles (MBs) has become a promising tool for site specific drug and gene delivery. One of the most important properties of drug-loaded MBs is their destructibility by ultrasound (US). Therefore, the aim of this study was to establish an improved *in-vitro* model that allows evaluation of the kinetics of US-mediated MB destruction at near physiological conditions.

With respect to the development of new drug-loaded MB formulations, the acoustic destructibility is an issue of great importance as it is influenced not only by the type of phospholipid, but even more by the physico-chemical properties and amount of the drug, loaded to MBs.

Numerous *in-vitro* approaches for characterization of the backscatter efficacy, oscillation behavior, and fragmentation onset have been described in the literature (Table 7). Most *in-vitro* models are based on the detection of acoustic backscatter signals or high-speed microscopy in order to monitor the oscillation of single bubble or a population of MBs. Furthermore, many authors implement facilities for near physiological conditioning of their *in-vitro* setups *e.g.* pressurizing, temperature adjusting, embedding MBs in physiological media and/or blood vessel mimicking capillaries, tissue-mimicking, *etc.*

The aim of this study was to develop an *in-vitro* model to assess the US destructibility of various MB formulations at near physiological conditions. In addition, the potential influence of drug-loading was investigated using the newly developed *in-vitro* model.

| Author | Medium | Detection | Near physiological conditioning | Experimental MB type | Commercial standard |
|--------------------------------|---|---------------------------|--|--|---|
| Unger et al. (1998) [122] | Degassed water | Echo-backscatter | Pressurizing at 0, 80, or 150 mmHg | soy-bean oil | Aerosomes MRX-113, (ImaRx, Tucson, USA) |
| | Saline | Echo-backscatter | Blood-vessel simulation | AALs | |
| Moran et al. (2000) [123] | Sterile water (Definity [®] and Optison [®]), or 5% dextrose solution (Sonazoid [®]) | Echo-backscatter | Tissue-mimicking material | Definity [®] (Bristol-Myers Squibb, USA), Sonazoid [®] (GE Healthcare, USA), Optison [®] (GE Healthcare, USA) | none |
| Lazewatsky et al. (1999) [124] | Blood or saline | Backscatter visual signal | Circulation, pressurizing at 110 mmHg, conditioning at 37 °C | Definity [®] (Bristol-Myers Squibb, USA) | none |
| Marsh et al. (2002) [125] | Phosphate buffer | Acoustic microscopy | Circulation | Liquid perfluorocarbon nanoparticles | none |
| Hoff et al. (1998) [126] | Isoton II | Echo-backscatter | Pressurizing at 120 mmHg | Sonazoid [®] (GE Healthcare, USA) | none |
| Caskey et al. (2007) [127] | 0.75% agarose gel phantom | High-speed microscopy | none | Phospholipid-monolayer shelled MBs | none |
| Caskey et al. (2006) [128] | n.a. | High-speed microscopy | Artificial capillary tubes | Phospholipid-monolayer shelled MBs | none |
| Lum et al. (2005) [64] | n.a. | Fluorescence microscopy | Cellulose capillary tubes | Fluorescent nanobeads-associated phospholipid MBs | none |

Table 7: Previously described *in-vitro* models for characterizing of MB acoustic properties. AALs – acoustically active lipospheres; n.a. – not available;

The *in-vitro* model was designed in cooperation with Mr. Ralf Hiermaier from the University workshop for fine mechanics at the Ludwig-Maximilians-University – Munich, Germany and build by himself.

3. Materials and methods

3.1. Reagents

| Substance | Abbreviation | Purchased from |
|---|--------------|---|
| Bovine serum albumin | --- | Sigma-Aldrich GmbH, Munich, Germany |
| Dipalmitoyl phosphatidylcholine | DPPC | Lipoid AG, Ludwigshafen, Germany |
| Dipalmitoyl phosphatidylglycerol sodium | DPPG | Lipoid AG, Ludwigshafen, Germany |
| Dulbecco's phosphate-buffered saline | --- | Sigma-Aldrich GmbH, Munich, Germany |
| Chloroform, HPLC-grade | --- | Sigma-Aldrich GmbH, Munich, Germany |
| Octafluoropropane | --- | Sauerstoffwerk Friedrich Guttroff GmbH, Wertheim, Germany |
| 1,2,3-Propanetriol, water free | Glycerol | Sigma-Aldrich GmbH, Munich, Germany |

3.2. *In-vitro* experimental setup

The experimental setup represents an improved, near physiological conditions acoustic transmission line (PCATL) model, based on the work of Lazewatsky et al. (1999) [124].

The *in-vitro* model comprised a closed circulating system of silicone Tygon[®] tubings (Figure 16) driven by a programmable peristaltic pump (Ismatec[®] IPC 8, Ismatec SA, Switzerland).

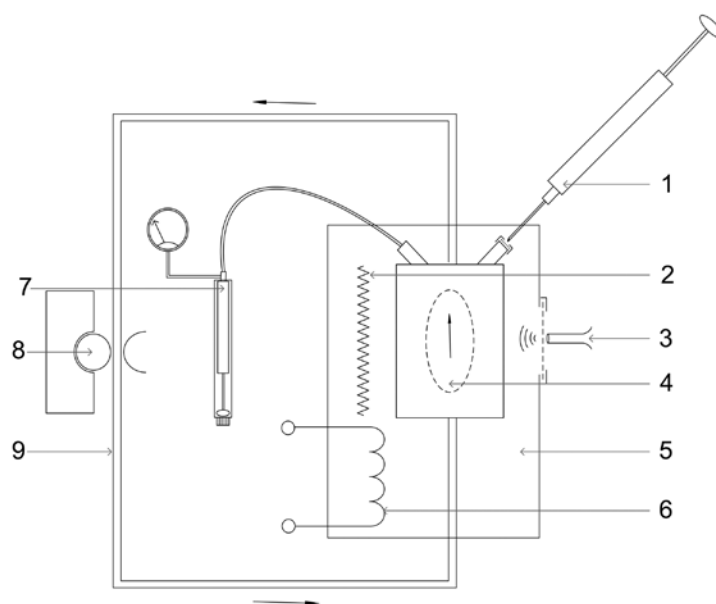


Figure 16: Main experimental setup scheme: 1. Sample input / output syringe; 2. Acoustic absorbing plate; 3. Sonotrode (sonication probe); 4. Sonication membrane window; 5. Water bath; 6. Immersion heater; 7. Pressure input (110 mm Hg); 8. Gastric pump; 9. Tygon[®] tubing; The arrows represent the flow direction of the medium.

The interaction between MBs and US took place in a membrane flow-cell where the MBs were pumped through in an upright direction (Figure 17, C and D). The flow-cell was provided with a self-sealing septum that allows collecting samples for measurements (Figure 17, A). Another port served to adjust the pressure in the system (Figure 17, B).

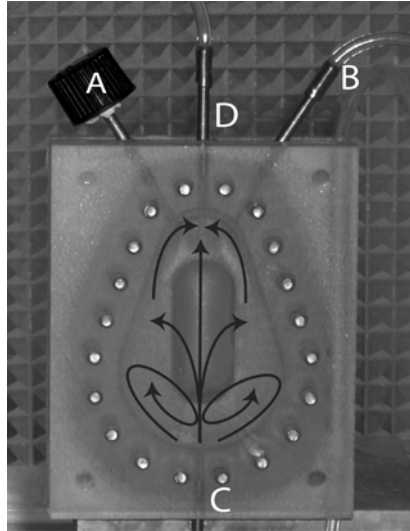


Figure 17: Membrane flow-cell of the *in-vitro* model. A: Input / output septum gap; B: Pressure input port; C: and D: Circulation inlet- and outlet-ports. Black arrows represent the proposed MB flow-through pattern in the cell.

The membrane flow-cell encompassed an egg-shaped inner compartment with a volume of 4.5-4.8 ml and an oval membrane window where the US beam was applied. The distance between the front and rear membrane of the flow-cell window was 8-10 mm at working conditions.

The setup allowed certain physiological conditions such as blood pressure and body temperature to be mimicked. The pressure in the system was adjusted to 110 mmHg by the aid of a gauge-controlled syringe and a manometer. In all experiments the temperature was conditioned at 37 °C using a circulating water bath.

The flow-cell was mounted in the water bath with a slide mechanism, allowing the distance between the sonotrode and the membrane window to be precisely adjusted.

The US beam was produced by a technical US source Sonitron-2000 (RichMar Corp., Chattanooga, USA) equipped with 3 mm and 5 mm sonication probes. The sonication probe was installed on a membrane window in the wall of the water bath.

3.3. Establishing the *in-vitro* model

The PCATL model was validated in order to determine the optimal operation conditions and to assure reproducibility of results.

A series of blank measurements was performed with circulating MBs without applying US in order to assess the pace of MB decay through shear stress, pressure, and tube squeezing by the peristaltic pump. Additionally, the sampling syringe was calibrated by repeatedly drawing 100 μ l portions of water and determining their weight ($n = 30$).

Generally in this manuscript, the US intensity is expressed through the overall energy output at the tip of the sonication probe, called output intensity, [W/cm^2]. However, due to the specific conditions in the flow-cell, distribution of the US field and its attenuation, the peak-negative acoustic pressure, [MPa] was measured directly in the flow cell under working conditions. A 250 μ m fiber-optic probe hydrophone (FOPH 2000, RP Acoustics, Germany), equipped with an 810 nm infra-red laser source was used. In this manner the optimal focal distance of the sonication probe and the peak-negative acoustic pressure in the flow-cell under working conditions were determined.

The flow conditions and the potential occurrence of dead volume compartments within the membrane cell were observed by injecting aqueous solutions of methylene blue into the circulation and pursuing their admixing with the medium.

Finally, the flow rate through the membrane cell was optimized by determining the MB decay upon exposure to US with a frequency of 1 MHz and an intensity of 4 W/cm^2 during varying the flow rate from 1 ml/min to 10 ml/min.

Compared to previous similar *in-vitro* models the PCATL model was optimized in the following aspects:

- a) For the first time a particle-counting method is involved to simultaneously monitor MB concentration and size distribution during sonication;
- b) The optimized flow-cell shape minimizes the appearance of dead volume compartments;
- c) The model fulfills a number of physiological conditioning parameters such as temperature, hydrostatic pressure, ionic strength, and medium viscosity.

3.4. Acoustic destructibility studies

The studies were directed towards investigation of the acoustic destructibility of MBs depending on the US frequency and intensity. Unloaded model phospholipid-shelled MBs were prepared according to the thin-film hydration method. Briefly, 80 mol% DPPC and 20 mol% DPPG at a total concentration of 5 mM were blended in HPLC-grade chloroform. The organic solvent was eliminated under vacuum at 65 °C for 60 min using a Büchi Rotavapor R-114 (Büchi Labortechnik GmbH, Essen, Germany). The phospholipid film was hydrated with highly-purified water (Purelab Plus[®], USF Elga Ionpure GmbH, Germany). The resulting liposome formulation was aliquoted in amounts of 400 µl into 2 ml round bottom safe-lock tubes (Eppendorf AG, Hamburg, Germany) and covered with octafluoropropane gas. The liposomal dispersion was mechanically agitated for 20 s using a CapMix[™] (3M Deutschland GmbH, Neuss, Germany).

MBs were mounted into 1.2 µm filtered 5% w/w bovine serum albumin solution in Dulbecco's phosphate-buffered saline, imitating blood plasma in viscosity, ionic strength, and pH.

Prior to each experiment the flow-cell of the PCATL model was filled with medium and conditioned to 37 °C. The background particle concentration in the medium was measured. The freshly prepared MB suspensions were introduced into the running PCATL model by a calibrated 1 ml syringe through the septum gap. After the distribution of MBs in the entire setup volume, the pressure was adjusted to 110 mmHg and a sample of 100 µl was drawn through the septum, indicating the starting MB concentration. The drawn volume was replaced with medium in order to prevent pressure loss. US was applied and the above procedure was repeated. The collected sample was diluted in 40 ml particle free deionized water (Purelab Plus[®], USF Elga Ionpure GmbH, Germany) and MBs size distribution and concentration were measured with light blockage using PAMAS SVSS-C (PAMAS GmbH, Rutesheim, Germany). The procedures of sampling and measuring were repeated after each sonication frame.

MBs were exposed to US with a lower frequency of 1 MHz, and a higher frequency of 3 MHz at a constant US intensity of 4 W/cm². This was in order to ascertain whether there is a dependency of MB destructibility from the MB size as known from the theory of Apfel et al. (1991) [129] and Holland et al. (1989) [130].

In the second study, MBs were exposed to US with a frequency of 3 MHz and output intensity, increasing from 1 W/cm² to 4 W/cm² in order to characterize the correlation of MB

destructibility and US intensity. In both experiments, MBs were exposed to six sonication frames of 10 s at a duty cycle of 50% using a 5 mm sonication probe.

In contrast to the *in-vitro* setup of Lazewatsky et al. (1999) [124] (Table 7), the implementation of whole blood into the PCATL model was impracticable due to the presence of formed blood elements which cannot be distinguished by the particle counting method used.

For both studies, collected data from five repeated measurements was averaged. The standard deviation was determined and the significance of the results was assessed by single factor variance analysis (ANOVA). Mathematical curve data fitting was performed using SigmaPlot[®], software version 9.0 (Systat Software, GmbH, Erkrath, Germany). The coefficient of determination R^2 for each sonication decay curve was calculated. The experimental data was fitted using a single exponent decay two parameter function (Equation 9), where a represents the *initial population coefficient*, b – the *decay coefficient*, and t – the sonication time. The MB half-life $t_{1/2}$ during US exposure was calculated using Equation 10.

$$y = a \cdot e^{-b \cdot t}$$

Equation 9

$$t_{1/2} = \frac{\ln(2)}{b}$$

Equation 10

4. Results and Discussion

4.1. Establishing the *in-vitro* model

The optimal flow rate through the membrane cell of the PCATL model was determined to be 4-5 ml/min (data not shown). Higher flow rates led to insufficient interaction of MBs with the US beam and therefore too slow destruction paces. A slower circulation caused MBs to buoy up and form a foam layer in the tubing, causing reduced reproducibility.

At optimum flow rate the minimum residence time for a MB in the membrane cell was calculated to be 1.5 s at a flow rate of 5 ml/min. Hence, a MB flowing through the membrane cell will be exposed to at least two US pulses when using a duty-cycle of 50%.

The standard deviation of the sampling syringe was considered acceptable ($\sigma = 1.7\%$) in a series of twenty repeats. The standard deviation of the PCATL model was derived from the measurement data. It was found to be $10.3\% \pm 3.2\%$.

The focal distance between the flow-cell and the sonication probe was measured to be approximately 15 mm. At this distance the measured peak-negative acoustic pressure in the flow-cell both for 1 MHz and 3 MHz and 100% duty cycle was 0.037 ± 0.008 MPa at 1 W/cm^2 and 0.131 ± 0.027 MPa at 4 W/cm^2 output intensity.

Compared to related circulation *in-vitro* setups [124, 131], the PCATL model possessed a membrane flow-cell with a specific egg-shape which provided optimized flow conditions (Figure 17, black arrows) and minimized compartments with low flow velocity (dead volume compartments). Dead volume compartments could accumulate MBs and substantially distort experimental results. Within the flow-cell MBs were pumped in an upright direction, approached into the broader bottom part of the cell and were slowed down. During their habitation in the bottom cell part MBs could interact with the US beam.

The upper flow-cell part was the most likely place for dead volume locations due to the affinity of MBs to float (buoyancy). Therefore, the outflow part was shaped so as to allow MBs to accelerate before leaving the cell.

4.2. Acoustic destructibility studies

According to the *in-vitro* studies, there was an apparent dependence of MB destructibility on the US frequency and intensity as well as on the MB diameter.

When US with a lower frequency of 1 MHz was applied, acoustic destructibility of MBs did not correlate with their diameter, resulting to half-lives of less than 50 s for MBs of any size (Figure 18, dashed line).

In contrast to that at a higher US frequency of 3 MHz MBs of sizes from $1.0 \mu\text{m}$ to $1.4 \mu\text{m}$ were burst 5.04 ± 3.42 -fold faster than MBs of sizes from $4.0 \mu\text{m}$ to $6.0 \mu\text{m}$ (Figure 18, solid line).

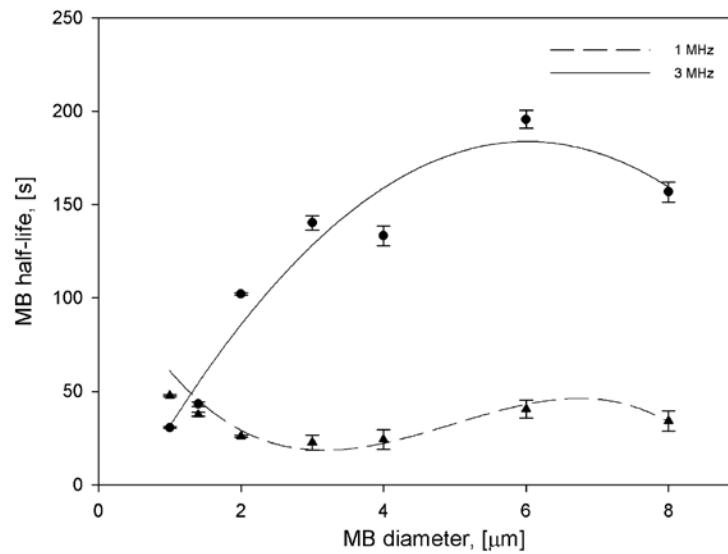


Figure 18: Half-life ($t_{1/2}$) of unloaded phospholipid-monolayer shelled MBs during exposure to US with an intensity of 4 W/cm^2 and frequencies of 1 MHz (dashed line) and 3 MHz (solid line).

Specific size-dependent destruction patterns for MBs at different US frequencies have been explained by different thresholds of transient cavitation which is required for MB destruction. This suggestion links the observed phenomenon to the analytical model established by Apfel et al. (1991) [129] and Holland et al. (1989) [130] (Figure 19) and recently related to SonoVue[®] by Greis et al. (2004) [132]. The authors proposed an approximate mathematical model, allowing for the calculation of acoustic pressure thresholds for transient cavitation over a variety of frequencies and MB diameters.

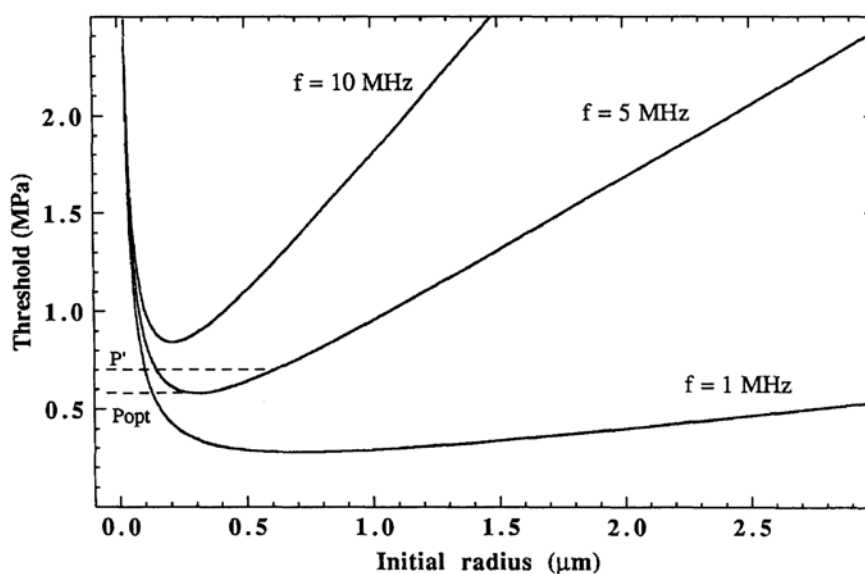


Figure 19: Computed plot of the cavitation threshold in water as a function of initial bubble radius for three frequencies of sonication: 1, 5, and 10 MHz. From: Apfel et al. (1991) [129].

In the context of the current study, MBs with larger diameters, exposed to ultrasound with a higher frequency (in this case 3 MHz), reach their bursting threshold at much higher peak-negative acoustic pressures than smaller MBs.

However, when exposed to US with a lower frequency (in this case 1 MHz) and the same output intensity, the influence of the MB size on the bursting threshold minimum decreases. As a consequence, at a frequency of 1 MHz both smaller and larger MBs are fragmented with a similar decay pace.

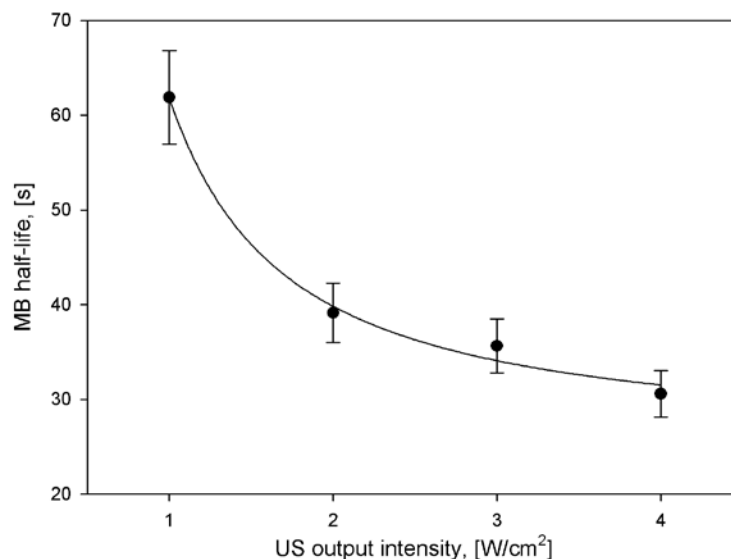


Figure 20: MB half-life during US exposure at a frequency of 3 MHz and an increasing intensity.

The dependence of the acoustic destructibility of unloaded MBs during US exposure at a frequency of 3 MHz and an intensity increasing from 1 W/cm² to 4 W/cm² is represented on Figure 20. Thereby, the MB life-time during US exposure decreases with 49.45% ± 2.73%, following a polynomial inverse second order equation ($R^2 = 0.9934$).

5. Summary

In recent years the knowledge about microbubbles (MBs) as targeted drug and gene-carriers grew rapidly. Since the relevance of this promising approach steadily increases and new drug-loaded formulations emerge on a pre-clinical stage, an accurate and fast screening method has

been necessary to characterize their acoustic destructibility. Expectably, any new drug-loaded MB formulation possesses different physico-chemical characteristics which affect MB acoustic characteristics such as echogenicity and destructibility.

In-vivo techniques are generally not suitable for high-throughput formulation screening. Therefore, near to physiologic conditions have to be imitated *in-vitro*, if clinically relevant data is to be obtained.

In this chapter, an improved *in-vitro* model was developed and tested for pre-clinical assessment of the acoustic destructibility of newly developed MB formulations, based on previous literature work. This tool combines many physical aspects of the *in-vivo* setup, such as flow conditions, pressurizing, temperature conditioning, and mounting of MBs in artificial blood plasma.

The near to *physiological conditions acoustic transmission line* (PCATL) *in-vitro* model proved as an useful tool for reproducible and reliable characterization of the MB acoustic destruction kinetics. Thus, it is possible to predict which drug-loaded MB formulations are appropriate candidates for further *in-vivo* evaluation, with regard to their sufficient acoustic destructibility.

In the above studies, MB acoustic destructibility of model unloaded phospholipid MBs was correlated to their diameter and an empirical evidence to the theory of Apfel and Holland [129, 130] was provided. According to it, at higher ultrasound frequencies MBs of smaller size are better destructible than larger ones. At lower frequencies no size-dependent difference could be observed.

Furthermore, MB destructibility was studied at various ultrasound intensities with no regard to the MB size. Thereby, MB destruction pace increased non-linearly with ultrasound intensity, following a polynomial inverse second order kinetics.

Further in this thesis, the PCATL *in-vitro* model will be implemented for characterization of doxorubicin-loaded MBs and acoustically active lipospheres, comprising an additional oil layer. The *in-vitro* data will be correlated with *in-vivo* studies and a correlation model will be established. The formulation with better acoustic properties – echogenicity and acoustic destructibility, will be selected for further *in-vivo* studies.

IV. CHAPTER: Ultrasound targeted tumor therapy

1. Abstract

In recent years drug targeting in the tumor therapy has become a rather challenging topic for the pharmaceutical research. The clinical treatment with many potent anti-tumor drugs *e.g.* the anthracyclines is time- and dose-limited by occurring severe adverse effects such as cardiotoxicity.

One promising recent approach for targeting solid tumors is the application of microbubble ultrasound contrast agents loaded with chemotherapeutic drugs. These novel drug delivery systems can release their active load in response to well tolerated diagnostic ultrasound. Microbubbles can be safely administered by intravenous injection or infusion. They are able to reach the even more distant tissues and organs such as the liver and the brain. Tumors can be precisely localized by diagnostic ultrasound since at low ultrasound intensities microbubbles act as contrasting agents. The site specific release of the active load can then be triggered by increasing the ultrasound intensity. Moreover, the energy, released from “bursting” microbubbles, opens small gaps in capillary walls and cell membranes and promotes the drug uptake and action.

In the present work a novel phospholipid microbubble carrier for doxorubicin has been developed and characterized. Doxorubicin-loaded phospholipid microbubbles rendered outstanding ultrasound contrasting properties comparable with the commercial agent SonoVue[®] (Bracco International B.V., The Netherlands). Furthermore, they demonstrated good acoustic destructibility by ultrasound. In combination with ultrasound the doxorubicin-carrying microbubbles demonstrated a 2.3-fold increase of the therapeutic activity compared to aqueous doxorubicin in cell cultures. In rat tumor models the doxorubicin-loaded microbubbles achieved an efficient tumor targeting by reaching an over 10-fold increased concentration of the drug in ultrasound-treated tumors compared to tumors which became doxorubicin-loaded microbubbles, but no ultrasound.

Keywords: drug targeting, tumor therapy, microbubbles, ultrasound, contrast agents;

Abbreviations: DOX – doxorubicin hydrochloride, AALs – acoustically active lipospheres, MBs – microbubbles; US - ultrasound; EPR – enhanced retention and permeability effect;

2. Introduction

One of the most promising therapeutic applications of the MB targeting is the drug and gene delivery to solid tumors. Recently, numerous research articles have dealt with this application of US contrast agents [68, 133-135], thus all of them being pursuing an adequate tumor targeting and minimum effects on healthy cells.

Anthracycline antibiotics are widely used anti-tumor agents with high treatment efficacy. Doxorubicin (DOX) is one of nowadays mostly used chemotherapeutics. In the form of aqueous solution it is indicated for the treatment of acute lymphoblastic leukemia, acute myeloblastic leukemia, neuroblastoma, soft tissue and bone sarcomas, breast carcinoma, ovarian carcinoma, *etc.* Liposomal DOX has been indicated for advanced ovarian cancer (Doxil[®], Ortho Biotech, Bridgewater, USA), advanced breast cancer, AIDS-related Kaposi's sarcoma, and multiple myeloma (Caelyx[®], SP Labo, N.V., Heist-op-den-Berg, Belgium). However, the broad therapeutic spectrum of DOX is accompanied by severe adverse effects like myelosuppression, cardiotoxicity, alopecia, gastro-intestinal ulceration, and hand-foot syndrome [136].

DOX anti-tumor activity is most directly attributed to its intercalation between nucleotide pairs [137], and / or to the inhibition of DNA topoisomerase II [138]. There is also a growing body of evidence of alternative action mechanisms which do not afford entering the cytoplasm [139], complexation to DNA [140], or inhibition of DNA synthesis [141]. To substantiate these phenomena, several interactions on the level of the cell membrane have been suggested in the literature [122-125]. For example, DOX was shown to increase membrane fluidity [142], to cause massive perturbations in phospholipid domains [143], and to inhibit several cardiolipin-dependent processes of energy conservation in mitochondria [144, 145]. These unspecific membrane interactions are currently considered the main cause for the adverse effects of DOX.

In addition to this, the pharmacokinetic behavior of DOX is rather complex, too. If used in stand-alone therapy, a typical injection dose of DOX is generally 60 mg/m² to 75 mg/m² of body surface area. About 62% of the applied dose binds to plasma proteins [146], while the free drug fraction rather freely distributes in blood and tissues (steady-state volume of distribution – 1.049 l) and is eliminated fast from the blood plasma (mean clearance – 73.7 l/h) [147]. A large portion of the administrated drug is retained mainly in the liver, the kidneys, and the spleen [148]. For these reasons, DOX circulates and is eliminated to a great

extend outside of the tumor which is approached only by a relatively small portion of the administered drug amount.

The unfavorable pharmacokinetic features together with the severe adverse effects of DOX are the arguments to look forward to modern strategies to direct drug distribution and therapeutic action to the tumor site. The need for targeting approaches guided recent research towards the development of particulate drug carriers for DOX such as liposomes, polymeric nanoparticles [149, 150], or covalent complexes with biodegradable polymers [151].

Up to now one of the best clinically established carriers for DOX are the PEGylated liposomes which are also marketed as Doxil[®], Caelyx[®], and Myocet[®] (Elan Pharmaceuticals, Princeton, NJ, USA). The encapsulation into liposomes fulfills several important clinical advantages for the application of DOX. It drastically decreases the mean clearance in humans (at least 250-fold) and the steady-state volume of distribution (60-fold) [152]. Furthermore, the susceptibility of cardiac events is at least three times reduced in patients, treated with liposomal DOX, compared to treatment with aqueous DOX [153]. However, because of their particulate nature, liposomes are prone to uptake by the reticulo-endothelial system and their retention in the liver is about 2-fold higher and roughly 3.5-fold longer than for the free drug [154].

In recent years there is a growing research interest at developing of strategies to direct DOX action to the disease site by means of tumor targeting. In solid tumors with fenestrated blood vessels nanoparticulate colloidal carriers can feature the *enhanced permeability and retention* (EPR) effect which results in a passive drug accumulation on the target site. For example, an about 3-fold higher drug uptake in tumors could be achieved in mouse xenograft models after administration of 10 mg/kg DOX as PEGylated liposomes (48 h after administration) compared to free DOX (3 h after administration) [154]. However, the EPR effect is a form of *passive targeting* and is limited in its therapeutic potential. In contrast, the *active targeting* approach through immunoliposomes [155, 156], pH-sensitive micelles [157], *etc.* can provide higher target concentrations and a better therapeutic efficacy.

Another effective approach to trigger the drug action at the target tumor site is by application of external energy in the form of *e.g.* temperature [158], magnetic fields [159], or diagnostic US [68, 133-135]. The targeting approach by means of diagnostic US and drug-loaded MBs gives several advantages, compared to other strategies. As first, it is possible to detect and visualize tumors and assess their replenishment with drug, since MBs act as contrasting agents. Furthermore, in combination with US MBs enhance the permeability of capillary walls and cell membranes and can improve the drug efficacy. At last, the drug release can be

precisely site targeted by focusing the US beam at the tumor. Rapoport et al. (2007) [68] designed a surfactant-stabilized perfluoropentane microemulsion, loaded with DOX. Burstein et al. (2006) [160] developed DOX-loaded hollow microcapsules with rigid polymeric shells. Finally, Treat et al. [50] co-administered Doxil[®] liposomes together with the US contrast agent Optison[®] (GE Healthcare, Oslo, Norway) and achieved therapeutically relevant administration through the blood-brain barrier in rats.

In the present work two novel acoustically active carrier candidates for DOX were developed and evaluated under *in-vitro* conditions in order to select the more appropriate formulation. The selected candidate was further launched into *in-vivo* studies.

The first carrier candidate comprised MBs with stable but surprisingly flexible phospholipid monolayer shell which was highly loaded with the active drug. Within the shell positively charged DOX molecules were electrostatically complexed to anionic phospholipid molecules. The complexation was further complemented by intercalation of DOX aglycon between the phospholipids (Figure 2 B, p.19) through hydrophobic forces.

The second candidate formulation comprised acoustically active lipospheres (AALs, Figure 2 C, p.19), possessing outermost phospholipid monolayer, covered by inner oil coat of glycerol triacetate (triacetin), and gas core. In this case DOX was dissolved in the triacetin layer.

The complex between DOX and negatively charged phospholipids has been well described and has found therapeutic applications on an experimental scale in the form of liposomal formulations [145-147]. Clinical studies revealed that DOX-loaded anionic liposomes have a similar anti-tumor activity compared to free DOX together with a substantially reduced cardiac toxicity, and at least no greater immunotoxicity [166-168]. In multidrug-resistant mice the therapeutic efficacy of the DOX-phospholipid complex was even superior to free DOX [161]. In terms of pharmacokinetics an about 4-fold increase of DOX half-life was achieved through encapsulation in anionic liposomes [148]. Anthracycline cardiotoxicity has been mainly related to the intervention of DOX into mitochondrial activity in heart due to the formation of a very stable complex with cardiolipin [144, 145, 162, 163]. According to Herman et al. (1983) [164] the complexation of DOX to the anionic phospholipid cardiolipin can totally prevent the occurrence of drug-induced cardiotoxicity in big animal models. Yet, it was a challenging task to combine the above benefits with the high targeting potential of MBs with regard to the fragility of phospholipid monolayers, especially when perturbed by intercalating molecules.

DOX molecule (Figure 21) consists of an anthraquinone aglycon moiety – adriamycinone, and a glycoside – daunosamine. At physiological pH of 7.4, about 96% of all DOX molecules in a solution bear one positive charge due to the protonation of the primary amine group on C_{3'} position in daunosamine, having a pK_a ranging from 7.2 to 8.6, according to different authors [173-176]. Another pK_a value of 9.6 corresponds to the phenol function in position C₁₁ of the aglycon [150]. The molecule of DOX has an amphiphilic character but its net polarity is rather high with an experimental octanol / water partition coefficient (at pH 7.4) between 0.45 and 1.85 according to different authors [180-182]. DOX molecule further provides over seven hydrogen-bond donor and twelve acceptor sites.

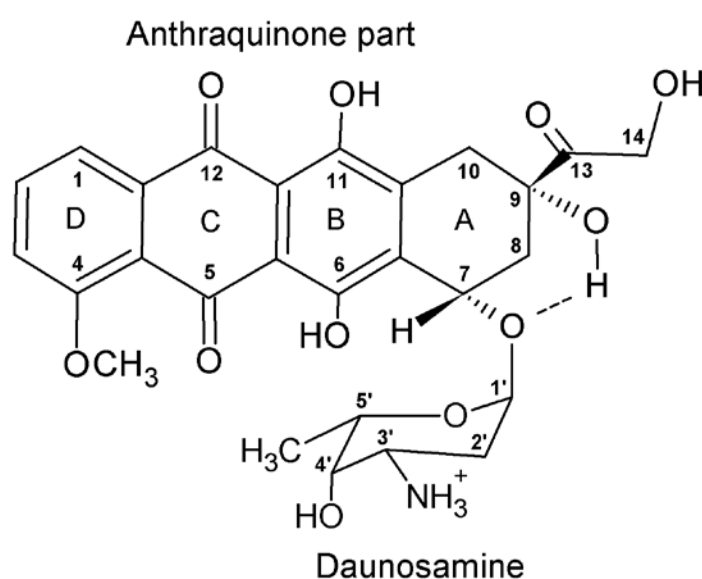


Figure 21: The chemical structure of DOX. Dashed line represents an intramolecular hydrogen bond.

DOX forms rather stable non-covalent complexes with various anionic phospholipids such as cardiolipin, phosphatidic acid, phosphatidylglycerol, and phosphatidylserine. The stoichiometric coefficients of complex binding roughly correspond to the phospholipid negative net charge being 1.8 mol DOX per mol cardiolipin, and 0.75 mol DOX per mol phosphatidylserine and phosphatidic acid [165]. Other authors have determined higher saturation coefficients of 2.4 mol DOX per mol phosphatidic acid, 1.5 equivalents for phosphatidylserine and phosphatidylglycerol, 1.3 equivalents per mol cardiolipin, and solely 0.02 equivalents per mol phosphatidylcholine [166].

Two complex structures have been suggested for the interactions between DOX and anionic phospholipids (Figure 22). In the first configuration an electrostatic interaction is involved in the association of the sugar moiety with the anionic phospholipid headgroup. Thereby, the

more lipophilic aglycon moiety intercalates into the lipophilic alkyl chain bilayer region (Figure 22 A) [166, 167]. According to several authors, the prevailing component of the interaction between DOX and anionic phospholipids appears to be the electrostatic attraction [178, 180-182], while according to others' opinion it is the hydrophobicity [168].

In the second complex configuration besides the electrostatic interaction the planar adriamycinone rings remain outside and may further interact with each other to form “stack” associates (Figure 22 B) [181, 186-188].

Furthermore, DOX possesses hydrogen-bond donor as well as acceptor sites. Therefore additional complexation interactions are expectable through hydrogen-bridges with hydrogen-bonding phospholipids such as DPPE and DPPG (Table 5, p.28). Indeed, literature data suggests that DPPE can enhance the binding of DOX to phospholipid bilayers better than other non-hydrogen bonding zwitterionic phospholipids [169].

Because of its weak lipophilicity, no significant interaction [165] or a very weak absorption [170] has been observed between DOX and the non-hydrogen bonding zwitterionic phospholipid DPPC.

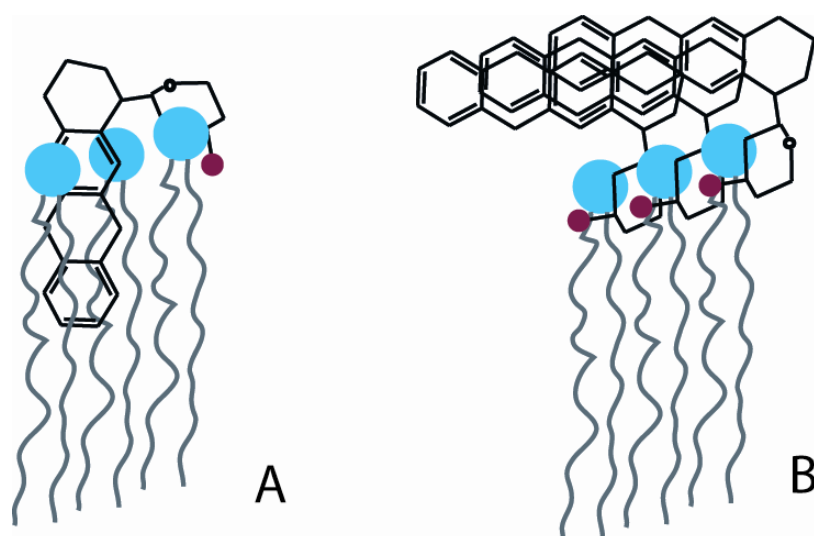


Figure 22: Configuration states of the complex between DOX and anionic phospholipids. A: Cationic daunosamine moiety is closely electrostatically bound to phospholipid anionic headgroups, while the hydrophobic aglycon penetrates the hydrophobic acyl chain region; B: Electrostatic complexation further persists, but aglycon moieties are detached from the monolayer and build “stack” aggregates. The centers of anionic charge are represented in blue and cationic charges – in red.

The present research work is focused on the formulation development of DOX-loaded liposomes which were used as intermediates for the production of DOX-loaded MBs through

mechanical high-speed agitation. The pharmaceutical properties of the liposome intermediates such as formulation constitution, particle size, *etc.* could be successfully used as steering levers to tune MB characteristics – a novel formulation approach called *liposomal-controlled microbubble production* (LCMP). According to this, the formulation properties of the precursor liposomes were varied and correlations with the properties of resulting MB formulations were studied.

Later in this chapter, various ratios between the amounts of excipients and DOX will be screened in order to establish optimal concentration ranges for the production of MBs. Following, the impact of further more specific formulation parameters such as the ionic strength, agitation time, filling volume of the agitated tube, *etc.* will be studied. The chemical stability of DOX in liposomal and in aqueous formulations will also be assessed.

Considering the second candidate formulation of DOX-loaded triacetin AALs, it presumably possesses a greater loading potential due to its extended shell volume compared to the thin MB monolayer shell (Table 3, p. 16). However, this US contrast agent structure class bears the concern of lacking acoustic echogenicity and / or destructibility.

In the next stage of development, the acoustic destructibility of the formulation candidates – DOX-loaded MBs and AALs will be compared using a properly build and improved *in-vitro* model which allows simulating close to physiological conditions [171]. The acoustic properties of the candidates will be further characterized *in-vivo* using rat's myocardium model, and for the first time an *in-vivo* / *in-vitro* correlation will be drawn. The anti-proliferative activity of the selected formulation will be firstly demonstrated in tumor cell cultures and following *in-vivo* in rat tumor models.

In the following work several studies were performed in cooperation. Fluorescence confocal laser scanning microscopy studies were carried out in cooperation with Mr. Stefan Zahler, Ph.D. from the Department of Pharmacy, Pharmaceutical Biology at the Ludwig-Maximilians-University – Munich, Germany. Studies involving measurements of peak-negative acoustic pressure in US fields were made together with Mr. Rainer Pecha, Ph.D. from the University of Stuttgart, Germany. Electron microscopy experiments were performed together with Mr. Markus Döblinger, Ph.D. from the Department of Chemistry, Physical Chemistry II at the Ludwig-Maximilians-University – Munich, Germany. Cell culture studies were carried out in cooperation with Mr. Martin Meyer, Ph.D. and Mr. Alexander Philipp from the Department of Pharmacy, Pharmaceutical Biology – Biotechnology, Ludwig-Maximilians-University – Munich. *In-vivo* clinical studies were performed in cooperation with Mr. Raffi Bekeredjian, MD, Ph.D. from the Internal Medicine III, Ruprecht-Karls-

University – Heidelberg, Germany. The research work was funded through a research grant by the NanoforLife initiative of the Federal Ministry of Education and Research, Germany in cooperation with Mr. Raffi Bekeredjian, MD, Ph.D.

3. Materials and Methods

3.1. Reagents

| Substance | Abbreviation | Purchased from |
|---|--------------|---|
| Acetonitril, HPLC-grade | --- | VWR International GmbH, Darmstadt, Germany |
| Calcium chloride, granulated, dehydrated | --- | Sigma-Aldrich GmbH, Munich, Germany |
| Chloroform, HPLC-grade | --- | Sigma-Aldrich GmbH, Munich, Germany |
| Cholesterol, $\geq 99\%$ | --- | Sigma-Aldrich GmbH, Munich, Germany |
| Concanavalin A-Alexa Fluor [®] 488 conjugate | --- | Invitrogen Molecular Probes [™] , Eugene, USA |
| 1,4-Diazabicyclo[2.2.2]octane | DABCO | Sigma-Aldrich GmbH, Munich, Germany |
| Dimethyl sulfoxide | DMSO | Sigma-Aldrich GmbH, Munich, Germany |
| (3-(4,5-Dimethylthiazol-2-yl)-2,5-diphenyltetrazolium bromide | MTT | Sigma-Aldrich GmbH, Munich, Germany |
| Dipalmitoyl phosphatidylcholine | DPPC | Lipoid AG, Ludwigshafen, Germany |
| Dipalmitoyl-phosphatidylethanolamine | DPPE | Lipoid AG, Ludwigshafen, Germany |
| Dipalmitoyl-phosphatidylethanolamine-polyethylenglycol-2000 | DPPE-PEG2000 | Avanti Polar Lipids, Alabaster, AL, USA |
| Dipalmitoyl phosphatidylglycerol | DPPG | Lipoid AG, Ludwigshafen, Germany |
| Dipalmitoyl phosphatidyltrimethylaminopropane | DPTAP | Avanti Polar Lipids, Alabaster, AL, USA |
| Disodium hydrogenphosphate, p.a. | --- | Sigma-Aldrich GmbH, Munich, Germany |
| Doxorubicin hydrochloride | DOX | Molekula Deutschland GmbH, Nienburg, Germany |
| Dulbecco's modified Eagle's medium, activated with 10% fetal calf serum | DMEM | Invitrogen Molecular Probes [™] , Eugene, USA |
| Ethylene diamine tetra-acetic acid | EDTA | Sigma-Aldrich GmbH, Munich, Germany |
| Glucose monohydrate, p.a. | Glucose | Sigma Aldrich GmbH, Munich, Germany |
| Glycerol triacetate, p.a. | Triacetin | Sigma-Aldrich GmbH, Munich, Germany |
| Hoechst 33342 | --- | Invitrogen Molecular Probes [™] , Eugene, USA |
| Hydrochloric acid, p.a., 1 M | --- | Sigma-Aldrich GmbH, Munich, Germany |
| Isopropanol, HPLC-grade | --- | Mallinckrodt-Baker B.V., Deventer, Holland |
| Methanol, HPLC-grade, water-free | --- | VWR International GmbH, Darmstadt, Germany |
| Octafluoropropane | --- | Sauerstoffwerk Friedrich Guttroff GmbH, Wertheim, Germany |
| Phosphorous acid, 85%, p.a. | --- | Sigma-Aldrich GmbH, Munich, Germany |
| Polyethyleneoxide-polypropyleneoxide block copolymer (Poloxamer 188) | Lutrol F68 | BASF SE, Ludwigshafen, Germany |
| Potassium hydroxide, p.a. | --- | Sigma Aldrich GmbH, Munich, Germany |

Continued from p. 80

| | | |
|--------------------------------------|--------------|--|
| Sodium chloride, p.a. | --- | Sigma-Aldrich GmbH, Munich, Germany |
| Sodium dodecyl sulfate, p.a. | --- | Sigma-Aldrich GmbH, Munich, Germany |
| Sodium dihydrogenphosphate, p.a. | --- | Sigma-Aldrich GmbH, Munich, Germany |
| SonoVue [®] | --- | Bracco International B.V., The Netherlands |
| Trypsin, 0.05% with tetrasodium EDTA | Trypsin/EDTA | Invitrogen Molecular Probes [™] , Eugene, USA |

3.2. Pre-formulation studies on doxorubicin-loaded liposomes and microbubbles

3.2.1. Differential scanning calorimetry studies

Differential scanning calorimetry (DSC) using a Mettler Toledo DSC821e (Mettler-Toledo GmbH, Giessen, Germany) was the leading analytical method in the pre-formulation studies.

Two groups of experiments were performed in this study. In the first group single phospholipids were screened for their binding affinity to DOX in order to select candidates which are able to mediate a complexation of DOX to the MB shell. For these experiments DOX concentration was set to 20 equivalent % (eq%) of the phospholipid concentration which was 100 mM. According to literature data, DPPC was expected to feature no relevant interaction with DOX.

In the second part of the study the selected phospholipid candidates which showed an interaction with DOX were blended at various concentration (from 10 mol% to 30 mol%) in binary mixtures together with DPPC. In a crosswise variation for each of the above cases the DOX concentration was changed from 0 eq% to 180 eq% of the concentration of DOX-binding phospholipid.

In order to prepare sample formulations, stock solutions of phospholipid compounds – DPPC, DPPG, and DPPE in HPLC-grade chloroform were prepared. The solutions were appropriately distributed in vials and the organic solvent was removed over 24 hours under nitrogen flow at room temperature using a Flowtherm II (Barkey GmbH, Leopoldshöhe, Germany). Solvent traces were eliminated in exsiccator under vacuum at room temperature over 24 hours. The obtained dried phospholipid blends were hydrated with low ionic strength phosphate buffered saline (ion concentration 5 mM) having a pH of 7.4 with and without addition of DOX. The hydration occurred at 75 °C under continuous shaking, light protection and nitrogen atmosphere. The total phospholipid concentration in all experiments was kept

high at 100 mM in order to detect even small changes in melting phase transitions. Prior to measurements samples were allowed to equilibrate for at least 12 hours at 4 °C in dark. Finally, liposome formulations in amounts of 30 µl were placed in 40 µl aluminum DSC pans and sealed. Three scanning runs in the temperature interval 20 °C to 85 °C at a heating rate of 5 °C/min were performed against air in triplicate for each formulation (n = 3, m = 3). Measured data was accordingly normalized against the sample weight and the phospholipid molar concentration.

Additionally, the colloidal condition of the formulations was macroscopically assessed and evaluated by scanning electron microscopy (SEM) using a JEOL 6500F (Jeol GmbH, Eching, Germany) equipped with an electron gun. The crystallinity of selected samples was examined with transition electron microscopy (TEM) using a JEOL 2011 electron microscope equipped with a tungsten cathode, operating at 200 kV.

3.2.2. Effect of US homogenization of liposomes on the MB yield

DOX-loaded liposomal formulations, comprising 80 mol% DPPC, 20 mol% DPPG, and 100 eq% DOX according to the amount of DPPG, were produced at a total phospholipids concentration of 3 mM.

The liposomes were subjected to US horn-type homogenization for different time intervals starting with 1 min up to 10 min using a Branson Sonifier[®] (Branson Ultrasonics Corp., USA) at a power output of 5 and a duty cycle of 50% using a 10 mm horn probe. The liposomes were placed in tubes, covered with octafluoropropane and agitated for 20 s using a CapMix[™] shaker (3M Deutschland GmbH, Neuss, Germany). MB concentration and size distribution were determined by light blockage using PAMAS SVSS-C (PAMAS GmbH, Rutesheim, Germany) after dilution with particle free water. Samples were compared in their MB concentration (MB yield).

3.2.3. Effect of third phospholipid compounds

Efforts were made to further improve the liposomes' colloidal stability and loading capacity through addition of small amounts of a third phospholipid component to the binary phospholipid mixture of bulk zwitterionic component (DPPC) and DOX-binding anionic phospholipid component, established through the DSC screening study above. Several phospholipids with widely varying properties were screened such as PEGylated (DPPE-PEG2000), cationic (DPTAP), non-bilayer (DPPE) phospholipids, and steroids (cholesterol). Liposomal intermediates were produced at a fixed proportion of 80% DPPC, 20 mol% DPPG, and 100 eq% DOX according to the amount of DPPG. The total phospholipid

concentration was kept constant at 3 mM. The concentration of the third-component phospholipid was varied from 0 mol% to 5 mol%, while the concentration of DPPC was correspondingly reduced.

Following, the liposomal size distribution and polydispersity were determined by dynamic light scattering Zetasizer Nanoseries Nano-ZS (Malvern Instruments Ltd., Worcestershire, UK). MB yield and size distribution were measured by light blockage using PAMAS SVSS-C (PAMAS GmbH, Rutesheim, Germany). Median liposome size, storage stability over 30 days, as well as median MB size and MB yield were compared and formulations with advantageous properties were selected for further development.

3.2.4. Effect of agitation time on the DOX loading in MBs

DOX-loaded liposomal formulations containing 3 mM total phospholipid of which 79 mol% DPPC, 20 mol% DPPG, and 1 mol% DPPE-PEG2000 were produced. Following, portions of 200 μ l liposomes were aliquoted in 2 ml Eppendorf tubes, covered with octafluoropropane gas, and agitated for different time intervals ranging from 10 s to 40 s with an increment of 10 s. In order to determine the amount of DOX encapsulated in MBs (C_{MB}), the procedure was followed, described under “3.6.4 Effectiveness of DOX loading into MBs and AALs”, p.89.

3.2.5. Optimal formulation procedures for DOX-loaded liposome precursors and MBs

According to the above pre-formulation research, the optimal process conditions for the production of DOX-loaded liposome precursors and MBs were identified. Liposomal precursors for the production of DOX-loaded MBs were produced via the thin-film hydration method. Briefly, per one milliliter liposomal formulation 1.74 mg DPPC, 0.45 mg DPPG, and 0.08 mg DPPE-PEG2000 were blended under heating at 60 °C in chloroform in a round bottom flask. The organic solvent was eliminated from the stock solution using a Büchi Rotavapor R-114 (Büchi Labortechnik GmbH, Essen, Germany) for 60 min at 60 °C. Next to that, a solution of 0.35 mg DOX, 0.003 mg EDTA and 50 mg glucose per milliliter liposomal formulation was prepared in highly-purified water (Purelab Plus[®], USF Elga Ionpure GmbH, Germany). The aqueous solution of DOX was brought in contact with the phospholipid thin-film and stirred under nitrogen and light protection for 60 min at 60 °C.

The liposomal precursor formulation was aliquoted at 400 μ l in 2 ml round bottom safe-lock tubes (Eppendorf AG, Hamburg, Germany) and covered with octafluoropropane gas. The liposomal dispersion was mechanically agitated at about 4,500 oscillations/minute for 20 s

using a CapMixTM (3M Deutschland GmbH, Neuss, Germany). For *in-vivo* administration MBs were diluted with octafluoropropane-saturated 5 mass% glucose in water.

3.3. Characterization of doxorubicin-loaded liposomes

3.3.1. Size distribution and Zeta potential

The size distribution and polydispersity of liposomes were determined by dynamic light scattering using a Zetasizer Nanoseries Nano-ZS (Malvern Instruments Ltd., Worcestershire, UK). Zeta potential of liposomal formulations was determined by electrophoretic light scattering using the same device.

During the measurements the dielectric constant (τ) was set to 78.48 (pure water at 25 °C). The optical parameters (refractive index and absorption index) for liposomes were set to correspondingly 1.450 and 0.01 [172]. Sample conductivity was kept below 0.01 mS/cm² during Zeta potential measurements.

3.3.2. Measuring the DOX concentration

DOX concentration and purity were determined using an ion-pair reversed-phase liquid chromatography method [173] using a C18 RP-HPLC column [Luna 5u C18(2) 100A, Phenomenex Ltd., Aschaffenburg, Germany]. The mobile phase consisted of 50 vol% acetonitril in highly purified electrolyte-free water, containing 1.44 g/l sodium dodecyl sulfate, p.a. and 1.125 g/l 85% phosphorous acid, p.a. A standard calibration curve was established ($n = 5$), where DOX concentration was represented as a function of the area under the DOX characteristic peak at 7.8 min retention time vs. the concentration of standard solutions.

The samples for measurement were prepared by dissolving 20 μ l liposomal dispersion in 1 ml solution of 7.5 vol% 1 M hydrochloric acid, p.a. in 92.5 vol% HPLC-grade isopropanol with a pH of 1.3.

Analysis was performed using a Merck-Hitachi LaChrom (Merck-Hitachi GmbH, Darmstadt, Germany) unit equipped with a binary pump model L-7100, an autosampler model L-7200, an interface model D-7000, and an L-7450 diode array detector. 10 μ l of each sample were injected into the column at a mobile phase flow rate of 1 ml/min. Time span of the HPLC measurement was 30 min.

The detection and quantification of DOX and products of its chemical decay were performed by measuring the UV-absorption at a wavelength of 254 nm.

The robustness of the HPLC method was scrutinized by the addition of various phospholipid amounts (both DPPC and DPPG) in the concentration range from 0.5 mg/ml to 5.0 mg/ml to a 0.5 mg/ml solution of DOX. The minimum signal-to-noise ratio was set to 3.

3.3.3. Association of DOX with liposomes

DOX-loaded anionic liposomes were prepared comprising a total phospholipid concentration of 3 mM of which 20 mol% were DPPG, 79 mol% DPPC, and 1 mol% DPPE-PEG2000. The amount of DOX corresponded to 100 eq% of the DPPG concentration. In whole liposome samples the total concentration of DOX (C_{tot}) was determined using RP-HPLC as described above. Following, DOX-loaded liposomes were subjected to freeze-thawing in order to destroy their colloidal structure and to separate the phospholipid from aqueous phase. The phospholipid was pelleted for 15 min at 14,000 rpm using a NeoLab 16/18 centrifuge (Hermle Labortechnik GmbH, Wehingen, Germany). The concentration of unassociated DOX (C_{free}) in the supernatant was then measured and the effective amount of DOX loaded to liposomes was calculated as a difference between C_{tot} and C_{free} .

3.3.4. Electrolyte-induced liposomal leakage of DOX

In order to assess the possibility of drug loss due to electrolyte-induced liposomal leakage, the influence of monovalent ions with various concentrations on the complexation of DOX to anionic liposomes was studied. Electrolytes have a shielding effect on the attractive electrostatic interactions between DOX and anionic phospholipids. Purpose of this study was to evaluate the robustness of DOX-binding prior to and after the complex formation with anionic phospholipids.

Two groups of experiments were conducted throughout this study. In the first experiment series the influence of ion concentration on the binding between DOX and anionic phospholipids was studied prior to the formation of the complex. Solutions of DOX were prepared in water and the ion concentration was adjusted with sodium chloride, *p.a.*, increasing from 0 mM to 100 mM ions. The solutions were used to produce DOX-loaded liposomes following the procedure described above (refer to “3.2.5 Optimal formulation procedures for DOX-loaded liposome precursors and MBs”, p.83). Accordingly, samples were freeze-thawed in order to precipitate the phospholipids and subjected to centrifugation at room temperature for 15 min at 14,000 rpm using the NeoLab 16/18 centrifuge (Hermle Labortechnik GmbH, Wehingen, Germany). The concentration of DOX was determined by HPLC in whole samples and in the supernatant as described in “3.3.2 Measuring the DOX concentration”, p.84.

In the second group of experiments the ability of increasing ion concentrations to dissociate the DOX-liposomal complex after its formation and cause liposome leakage was studied. Therefore, DOX-loaded liposomes were produced under electrolyte-free conditions and were subsequently brought in contact with electrolyte. The liposomes were incubated with sodium chloride in the same concentration range as above (from 0 mM to 100 mM ions) for 60 min at 37 °C under continuous shaking. The sample preparation was carried out as described above.

3.3.5. Chemical stability of DOX during the production of liposomes

During the formulation development of DOX-loaded liposomes and MBs the chemical stability of DOX was regularly scrutinized. If chemical decay of DOX occurred, its concentration, measured by HPLC, would decrease. Therefore, the concentration of DOX was determined in equal time intervals of 20 min during the phospholipid thin-film hydration at 60 °C over 60 min. Accordingly, DOX concentration was determined after a 5 minute US horn-type homogenization procedure using Branson Sonifier[®] (Branson Ultrasonics Corp., USA) equipped with a 10 mm sonication probe.

3.3.6. Photochemical stability of DOX

In a second group of experiments accelerated photostability tests on DOX-loaded liposomal formulations were conducted according to 1997 ICH Guidelines for photostability testing [174] using a Heraeus Ultratest Xenon light exposure unit (Original Hanau GmbH, Hanau, Germany). Aqueous solutions or liposomal dispersions of DOX with a concentration of 0.6 mM (0.350 mg/ml) were aliquoted in 5 ml portions in Schott 10 ml type I glass vials (Schott AG, St. Gallen, Switzerland), covered with octafluoropropane and flanged. The samples were accordingly exposed to light with an output intensity of 500 W/cm² for 72 hours. The concentration of DOX was determined four times in 24 hour intervals by RP-HPLC (refer to “3.3.2 *Measuring the DOX concentration*”, p. 84). The temperature was monitored using immersed sensors (Ama-digit ad 15th, Amarell GmbH, Kreuzwertheim, Germany) in both obscured and exposed vials containing liposomal and aqueous formulations. Accordingly, the concentration data was plotted against time and the half-life time of DOX in liposomal formulations and aqueous solutions was determined.

3.4. Pre-formulation studies on doxorubicin-loaded microemulsions and acoustically active lipospheres

The aim of the following pre-formulation studies was to develop an acoustically-active liposphere carrier for DOX. In order to increase the lipophilicity of DOX, the hydrochloride salt was chemically transformed into the DOX free base, where the primary amine group of daunosamine is not protonated. Therefore, DOX-base is more soluble in non-polar solvents [68] such as triacetin. Briefly, 50 mg DOX were dissolved in 50 ml methanol and dropwise titrated with a 1 mg/ml methanolic solution of potassium hydroxide until stoichiometric proportions of DOX and hydroxide ions were attained. The excess water resulting from the chemical neutralization was absorbed by granulated dehydrated calcium chloride.

Following, 10 ml triacetin was added to the solution and stirred overnight under light protection and nitrogen atmosphere. To obtain the triacetin solution of DOX-base, methanol was removed under vacuum at a temperature of 60 °C for 120 min, until a dark-red viscous solution of DOX-base in triacetin was obtained. The solution was allowed to equilibrate for 24 hours at 4 °C and the excess DOX-base along with the insoluble potassium chloride were removed by centrifugation. The effective concentration of DOX-base, dissolved in triacetin, was then determined by HPLC as described in “3.3 Characterization of doxorubicin-loaded liposomes”, p. 84.

3.4.1. Partition equilibrium of DOX-base between triacetin and water

Partition equilibrium of DOX-base between the lipophilic triacetin and aqueous phase was estimated by measuring the solute equilibrium concentrations in the aqueous phase at various pH values. Correspondingly, the apparent partition coefficient (P) was determined as the ratio between DOX concentrations in triacetin and in aqueous phase.

Partition equilibrium was obtained by continuous shaking of 2 ml DOX-base/triacetin solution and 2 ml Sørensen phosphate buffer for 24 hours at 4 °C. The concentration of DOX in the aqueous phase was measured by HPLC in time intervals of 3 hrs. Equilibrium was reached when the DOX concentration in water changed by no more than 5% over three hours. Phosphate buffers had a pH varying in the range from 5 to 9 with an increment of 0.5. The measured electric conductivity of all buffers used was 9-10 mS/cm² at 25 °C. Experiments were not performed above a pH of 9 due to the lacking DOX chemical stability at pH exceeding this value [175]. Prior to experiments, aqueous phase was saturated with triacetin by stirring with an excess of it over 24 hours at 4 °C. The concentration of DOX in both

aqueous and triacetin phases was determined by HPLC (refer to “3.3 Characterization of doxorubicin-loaded liposomes”, p. 84.).

3.4.2. Optimal formulation procedures for DOX-loaded microemulsions and AALs

In order to produce a phospholipid-stabilized microemulsion, DPPC, DPPG, and DPPE-PEG 2000 were blended in chloroform and the organic solvent was accordingly removed. 750 mg DOX-base solution in triacetin and 50 ml 10 mg/ml solution of Lutrol F68 and 30 µg/ml DOX in triacetin-saturated phosphate buffer with a pH of 8 were given to the phospholipid film. The mixture was then heated to 60 °C, and stirred for 60 min under light protection and nitrogen atmosphere.

The resulting coarse emulsion was divided in two portions which were further processed by homogenization using horn-type sonication (Branson Sonifier[®], Branson Ultrasonics Corp., USA) for 15 min at a power output of 12 and 50% duty cycle, or by high-pressure homogenization using a Gaulin homogenizer (APV Deutschland GmbH, Unna, Germany) by applying 1,300 bar in 20 run cycles.

DOX-loaded AALs were produced by mechanical agitation at 4,500 oscillations / minute for 20 s of 400 µl microemulsion with 1.6 ml octafluoropropane using the CapMix[™] mechanical agitator (3M Deutschland GmbH, Neuss, Germany).

3.5. Characterization of doxorubicin-loaded microemulsions

3.5.1. Particle size distribution and colloidal stability of DOX-loaded microemulsions

DOX-loaded triacetin microemulsions obtained by US horn-type homogenization and by high-pressure homogenization were stored for 30 days at 4 °C in dark. The particle size distribution in both samples was determined by dynamic light scattering (refer to “3.3 Characterization of doxorubicin-loaded liposomes”, p. 84) in 48 hours terms during the first two weeks and once weekly afterwards.

3.6. Characterization of doxorubicin-loaded microbubbles and acoustically active lipospheres

3.6.1. Structure analysis of DOX-loaded MBs and AALs

The structure and colloidal homogeneity of DOX-loaded MBs and AALs were characterized by confocal laser scanning microscopy (CLSM) using an inverted Zeiss LSM 510 (Carl Zeiss Microimaging, Göttingen, Germany). No additional fluorescent staining was necessary due to the intensive intrinsic DOX fluorescence emission at 570 nm following an excitation with 530 nm He-Neon laser light [176]. A pinhole of 118 μm was exerted with an oil-immersion objective producing optical stacks of about 225 μm thickness.

For sample preparation 20 μl freshly prepared suspension of DOX-loaded MBs or AALs was mounted in 1 ml 25 mg/ml solution of DABCO in a mixture of 80 vol% glycerol, p.a. and 20 vol% electrolyte-free water. The mounted sample was then introduced by a syringe into a thin-bottom Ibidi μ -slide IV (Ibidi GmbH, Munich, Germany) and imaged.

3.6.2. Particle size distribution

The particle size distribution in MB and AAL formulations was determined by laser diffraction using Partica LA-950 (Horiba Ltd., Kyoto, Japan) by means of the properly established optical model for MBs (refer to “*II. Ch. / 4.2.1 Size distribution measurements*”, p. 48). The MB refractive index was set to 0.90, and the absorption index – to 0.01. The value of $\cos\theta$ was kept below 0.1. The measured data was surface-area weighted.

3.6.3. Particle concentration

The concentration of DOX-loaded MBs was determined by light blockage using PAMAS SVSS-C (PAMAS GmbH, Rutesheim, Germany). Briefly, 20 μl of the freshly prepared MB sample were diluted with highly-purified degassed water until the particle count decreased to less than 2×10^5 MB/ml. Volumes of 1 ml were drawn in triplicate for analysis from the diluted sample. The bubble size distribution in the range of 800 nm to 200 μm as well as the MB concentration were determined simultaneously.

3.6.4. Effectiveness of DOX loading into MBs and AALs

In order to determine the amount of DOX associated with MBs, formulations were mildly centrifuged for 5 min at 1,000 rpm using a NeoLab 16/18 centrifuge (Hermle Labortechnik GmbH, Wehingen, Germany). The MBs formed a foam cake and were separated from the underlying liquid phase. Portions of the liquid fraction were collected by piercing through the

tube wall with a syringe needle and the concentration of residual DOX after MB production C_{res} was determined by HPLC (refer to “3.3.2 Measuring the DOX concentration”, p.84). The total DOX concentration C_{tot} was determined in whole liposome or microemulsion formulations. The effective loading of MBs C_{MB} was calculated as a difference between the total DOX concentration C_{tot} and C_{res} .

3.6.5. *In-vitro* acoustic destructibility of DOX-loaded MBs and AALs

The acoustic destructibility of DOX-loaded MBs and AALs was determined using the own improved near *physiological conditions acoustic transmission line* (PCATL) model, based on the work of Lazewatsky et al. (1999) [124] (refer to “III. Ch. / 3.2 *In-vitro* experimental setup”, p.63). MBs and AALs were exposed to US with a frequency of 1 MHz and an output intensity of 4 W/cm^2 using a Sonitron-2000 (RichMar Corp., Chattanooga, USA). Each sonication cycle comprised four frames of 30 s at a duty cycle of 50% using a 5 mm sonication probe. The decrease of particle concentration due to acoustic decay was measured by light blockage using a PAMAS SVSS-C (PAMAS GmbH, Rutesheim, Germany). The plotted experimental data was processed and fitted using SigmaPlot® 2004 software, v.9.0 (Systat Software GmbH, Erkrath, Germany).

3.6.6. *In-vivo* evaluation of the acoustic properties of DOX-loaded MBs

Acoustic backscatter efficacy (echogenicity) and destructibility of DOX-loaded MBs were tested in rat’s myocardium *in-vivo* model. A comparison was done between DOX-loaded MBs, DOX-loaded AALs, unloaded MBs, and the commercial standard SonoVue® (Bracco International, B.V., The Netherlands).

After test animals had been prepared, 1 ml of AAL and MB dispersions with concentrations of about $3\text{-}5 \times 10^7$ MB/ml were infused at a rate of 3 ml/hour. During the infusion, the left heart was visualized by diagnostic US (Sonos 5500, Philips Medical Systems, USA) having a frequency of 1.3 MHz and a mechanical index (MI) of 0.6. Following the visualization, the left heart was exposed to US bursting cycles with the same frequency and a higher MI of 1.6. A sequence of four bursting pulses was delivered every fourth diastolic cardiac cycle. It was triggered by the electrocardiographic R-wave with a delay of 80 ms after its peak.

Immediately prior and after every bursting sequence backscatter images were taken in order to calculate the rate of MB destructibility. Backscattered signal intensity was recorded immediately prior to the high-intensity US sequence (I_{bs}^*) and after it (I_{bs}). The MB *in-vivo* acoustic destructibility A , [%] was calculated according to Equation 11:

$$A \% = \left(1 - \frac{I_{bs}}{I_{bs}^*} \right) \times 100$$

Equation 11: Calculation of the *in-vivo* acoustic destructibility A , [%].

where A - *In-vivo* acoustic destructibility, [%]; I_{bs}^* - backscatter intensity before the bursting frame, [dB]; I_{bs} - backscatter intensity after the bursting frame, [dB].

3.6.7. *In-vivo* / *in-vitro* acoustic destructibility correlation

The properly formulated DOX-loaded MBs, DOX-loaded AALs, and unloaded MBs were ranked according to their sonication half-life $t_{1/2}$ which was determined *in-vitro* using the physiological conditions acoustic transmission line (PCATL) model. Next to that, the formulations were ranked with regard to their *in-vivo* acoustic destructibility, determined in the rat's myocardium model. The marketed US contrast agent SonoVue[®] was used as a standard.

The *in-vitro* data of MB and AAL formulations was ranked in the order of their decreasing half-life during sonication, corresponding to a better *in-vitro* acoustic destructibility. Accordingly, the data of *in-vivo* studies was ranked on the same manner with regard to the increasing MB *in-vivo* acoustic destructibility A , [%]. The *in-vivo* ranking coefficients were plotted vs. the *in-vitro* ranking coefficients and the coefficient of determination R^2 was calculated.

3.7. Therapeutic evaluation of doxorubicin-loaded microbubbles

3.7.1. Intracellular distribution of DOX after treatment with DOX-loaded MBs

295/KDR human kidney carcinoma cells were cultivated in Ibidi[®] μ -plate 96-well with thin bottom (Ibidi GmbH, Munich, Germany). The cells were treated with DOX aqueous solution and DOX-loaded MBs in combination with US. The final DOX concentration in all samples was $1.67 \mu\text{g} / 10^6$ cells. Samples, containing DOX-loaded MBs were treated with US at a frequency of 1 MHz, an intensity of 2 W/cm^2 , and a duty cycle of 100% for 15 s using a Sonitron-2000 (RichMar Corp., Chattanooga, USA), equipped with a 3 mm probe. US was applied by directly immersing the probe into the culture medium.

The cell cultures were incubated for 2 hours, followed by three washing steps with phosphate-buffered saline. The cells were fixed by incubation for 15 min with 3% formaldehyde. Cell

nucleus staining was made with Hoechst 33342 while cell membranes were dyed with Concanavalin A – Alexa Fluor[®] 488 conjugate, both according to manufacturer’s protocols. Three washing steps were carried out after each staining procedure. Finally, the cells were mounted in a 25 mg/ml solution of DABCO in 80 vol% glycerol and 20 vol% electrolyte-free water.

| Fluorescent dye | Excitation wavelength maximum, [nm] | Emission wavelength maximum, [nm] |
|---|-------------------------------------|-----------------------------------|
| Concanavalin A-Alexa Fluor [®] 488 conjugate | 495 | 519 |
| Hoechst 33342 | 350 | 461 |
| DOX | 530 | 570 |

Table 8: Excitation and emission wavelengths of fluorescent dyes and DOX used for fluorescence microscopy of cultured cells.

The cells were observed by fluorescence confocal laser-scanning microscopy using a Zeiss LSM 510 (Carl Zeiss Microimaging, Göttingen, Germany). A pinhole of 204 μm was exerted with a 63x oil-immersion objective producing optical slices of about 700 nm. The excitation and emission wavelengths used are represented in Table 8.

3.7.2. *In-vitro* evaluation of the anti-proliferative efficacy of DOX-loaded MBs

In the following experiment, the anti-proliferative activity of DOX-loaded MBs in cell cultures was compared with unloaded MBs, DOX-loaded and unloaded liposomes, as well as with aqueous DOX solutions. Furthermore, all setups were tested with and without application of US. The amount of DOX was kept constant at 70 ng/well in all samples. Blank measurements were done with DOX-untreated cells with and without application of US.

The therapeutic activity of DOX-loaded MBs was tested *in-vitro* on 293/KDR human kidney carcinoma cells. The decrease of cell viability was considered as a quantitative measure for the anti-tumor efficacy of DOX-loaded MBs.

Prior to the experiment, the adherent cells were treated with trypsin/EDTA solution and counted under microscope using the modified Neubauer chamber. Following, cell concentration was adjusted with DMEM medium and suspension was placed into 96-well plates (Greiner Bio-one GmbH, Frickenhausen, Germany) at an amount of 6×10^4 cells/well. A 3.5 cm thick gelatin gel tissue phantom was placed beneath the well plate in order to absorb US and to prevent standing waves.

Treatment medium in amount of 100 μl was added to 200 μl DMEM culture medium overlying the cell layer. The treatment medium contained either DOX-loaded or unloaded liposomes or MBs. In negative control samples phosphate-buffer saline was added, while DOX aqueous solution was added to positive control samples. In MB-treated samples the bubble-to-cell ratio was set to about 165.

Technical US was applied to US-treated samples using a Sonitron-2000 (RichMar Corp., Chattanooga, USA) equipped with a 3 mm probe by directly immersing the probe into the culture medium. According to preliminary studies US parameters were set to 1 MHz frequency, 1 W/cm^2 output intensity, 50% duty cycle, and a sonication time of 20 s. The peak-negative acoustic pressure, [MPa] in the wells was measured using a 250 μm fiber-optic probe hydrophone (FOPH 2000, RP Acoustics, Germany) [29]. Following, cell cultures were incubated for 24 hours at 37 °C and 5 vol% CO_2 .

Accordingly, the cell metabolic activity was assayed as previously described in the literature [177]. Briefly, 30 μl 5 mg/ml aqueous solution of MTT were given to each culture well and cells were incubated for 2 hours. The overlying culture medium was then aspirated and the cells were solubilized with 50 μl DMSO. The UV/Vis absorption of the cell produced purple formazan was measured using FluostarOmega plate reader (BMG Labtech GmbH, Offenburg, Germany) at a measurement wavelength of 590 nm and a reference wavelength of 630 nm. Cell viability was expressed as a percent ratio of the absorption of treated vs. untreated cell samples.

3.7.3. *In-vivo* evaluation of the targeting efficacy of DOX-loaded MBs

A double blinded study was performed in rat tumor model in order to evaluate the *in-vivo* targeting efficacy of DOX-loaded MBs. Each test animal was bearing two subcutaneously implanted pancreas xenograft tumors on each side of its back. Test animals were infused one dose unit of 400 μl MBs (corresponding to 140 μg DOX), diluted ad 1 ml with phosphate-buffered saline and administered over 20 min through the carotid artery. Simultaneously, one of the back-side tumors was treated with diagnostic US, while the tumor on the other side of animal's back became no US. The sonication mode was identical to that, used in “3.6.6 *In-vivo* evaluation of the acoustic properties of DOX-loaded MBs”, p. 90.

After the treatment test animals were sacrificed and the tumors were harvested along with the liver, the lungs, and the kidneys. The tumors and organs were homogenized using a defined volume of 92.5 vol% isopropanol acidified with 7.5 vol% 1 M hydrochloric acid. After 2 hours of incubation at 4 °C the insoluble tissue compounds were centrifuged at 14,000 rpm for 15 min using a NeoLab 16/18 centrifuge (Hermle Labortechnik GmbH, Wehingen,

Germany). The clear supernatant was collected and DOX was quantified by RP-HPLC using an Agilent 1100 Series unit (Agilent Technologies Deutschland GmbH, Böblingen, Germany) equipped with an UV-detector and a fluorescence detector model Spectra System FL 3000 (TSP Thermo Separation Products GmbH, Egelsbach, Germany). DOX was detected by its fluorescence at an excitation wavelength of 480 nm and an emission wavelength of 550 nm and by its UV-absorbance at 254 nm. The amount of DOX was quantified by the area under its characteristic fluorescence peak at 8.1 min retention time. Mobile phase and measurement setup were identical with the described under “3.3.2 *Measuring the DOX concentration*”, p.84.

4. Results and Discussion

4.1. Pre-formulation studies on doxorubicin-loaded anionic liposomes and microbubbles

4.1.1. Differential scanning calorimetry studies

During the following study two series of experiments were conducted. In the first series single phospholipids – DPPC, DPPE, and DPPG, were brought in contact with DOX at constant concentrations in order to assess the phospholipid complexation affinity to DOX and to select the most capable candidates. In the second part, binary phospholipid mixtures including DPPC and the selected DOX-binding phospholipid candidate were screened towards finding concentration ranges which are suitable for further development.

During the first experiment series, the found single phospholipid transitions in absence of DOX were in agreement with reported values [178, 179] and will not be further explained in detail.

Briefly, DPPC phase diagram revealed a broad pre-transition peak between 33 °C and 35 °C due to its tilted acyl chain packaging in gel state [180]. Furthermore, a sharp main transition peak of DPPC was observed at 41.5 °C. Upon addition of DOX the pre-transition endotherm was abolished and the main transition was moderately broadened and flattened, revealing a peak height decrease from 1.181 kW/mol to 0.879 kW/mol (Table 9), accompanied by a slight reproducible decrease of the gel to liquid-crystalline phase transition temperature (T_m) to 40.49 °C. Thereupon, the DPPC mean endotherm area slightly decreased from 31.451 kJ/mol to 30.538 kJ/mol.

| DOX | DPPC | | DPPE | | DPPG | |
|-----|------------------------|--------------------------|------------------------|--------------------------|------------------------|--------------------------|
| | Peak area, [kJ/mol] | Peak height, [kW/mol] | Peak area, [kJ/mol] | Peak height, [kW/mol] | Peak area, [kJ/mol] | Peak height, [kW/mol] |
| (-) | 31.451 ± 0.050 | 1.181 ± 0.013 | 30.472 ± 0.130 | 1.026 ± 0.006 | 41.001 ± 0.1162 | 1.174 ± 0.018 |
| (+) | 30.538 ± 0.092 | 0.879 ± 0.007 | 29.456 ± 0.063 | 0.715 ± 0.004 | 34.464 ± 0.042 | 0.529 ± 0.021 |

Table 9: Differential scanning calorimetry data on the phase transition behavior of various phospholipids alone and upon interaction with doxorubicin (n = 9). Numerical data established is closely compliant with previous work [179].

In the case of DPPE, the main transition peak was centered at 64.31 °C for the pure phospholipid and was slightly moved by less than 1 °C to 63.84 °C upon addition of DOX. The addition of DOX to DPPE caused similar moderate effects as in the case of DPPC – a slight peak area and peak height decrease and peak broadening.

The same thermotropic phenomena but much more pronounced were observed in the case of DPPG, too. For the pure DPPG the T_m was found at 39.84 °C and sank by 2.16 °C after addition of DOX, while the T_m depletions for DPPC and DPPE were only correspondingly 1.01 °C and 0.47 °C.

The reduction of peak height caused by DOX was 54.94% for DPPG vs. 30.31% for DPPE and 25.57% for DPPC. Regarding the peak area decrease upon addition of DOX, nearly the same progression was demonstrated by the three phospholipid candidates, too: 15.94% for DPPG, 3.33% for DPPE, and 2.90% for DPPC. Phospholipid-free DOX solutions, used as negative controls, showed no transition in the temperature range from 20 °C to 85 °C at the given concentration.

Based on the thermotropic modifications of the selected phospholipid candidates caused by their more or less intensive interaction with DOX, DPPG was selected as the phospholipid with the highest complexation affinity amongst them. These findings are also consistent with the calorimetric studies of Constantinides et al. (1986) [179], who found none or a very minor transition changes in the case of DPPC, but a remarkable effect of DOX over the behavior of DPPG. In the present study the phospholipid transition modifications in DOX-DPPC and DOX-DPPE systems were significant, apparently owing to the up to 17-fold higher DOX / phospholipid ratios and the 10-fold lower electrolyte concentrations used. Nevertheless, the substantial difference in the change of the thermotropic behavior of DPPG after complexation with DOX was still apparent compared to the slight alterations, demonstrated by the zwitterionic phospholipids DPPC and DPPE.

Numerous authors have also demonstrated the prevailing role of strong electrostatic interactions and the auxiliary contribution of hydrophobic forces in the formation of complexes between DOX and anionic phospholipids [166, 170, 181]. Since DOX is one of the most hydrophilic anthracyclines (octanol/water partition coefficient of 1.1 [182]) its complexation affinity to zwitterionic phospholipid layers *e.g.* DPPC is expectedly low as demonstrated above.

Interestingly, the affinity of DPPE to DOX was constantly higher than DPPC in spite of the large similarity of their chemical structures. This can be attributed either to the different lyotropic equilibrium phases (L_{α} for DPPC and H_{II} for DPPE) or to the ability of DPPE to form hydrogen bonds with DOX and therefore - a more stable complex than DPPC. Complementary CLSM data have shown that mixed DPPC-DPPE bilayers can indeed complex DOX to some extent (data not shown) which possibly occurs through the interplay of hydrogen bonding and hydrophobic interactions.

In the second experiment series the phase behavior in mixed bilayers comprising DPPC and DPPG were studied in a deeper detail upon titration with increasing amounts of DOX (Figure 23). In absence of DOX the thermotropic behavior of DPPC-DPPG at increasing DPPG concentrations in the range of 10 mol% to 30 mol% revealed an ideal mixing, as previously reported [183]. The pre-transition peak at 34.7 °C persisted until 20 mol% DPPG and was abolished at higher concentrations. At various molar ratios of DPPG the binary mixtures exhibited a single thermal transition in the range between the temperatures characteristic for the pure species. With increasing DPPG amount the peak height gradually diminished from 1.515 kW/mol to 0.838 kW/mol, and the main transition peak area also decreased from 37.128 kJ/mol to 29.192 kJ/mol.

Although DOX at a concentration of 20 eq% had little influence on DPPC, the addition of even 10 mol% DPPG strongly increased the effect of DOX on the phase transition. Even at relatively low DOX concentrations – between 0 eq% and 20 eq% according to the molar concentration of DPPG, the pre-transitional peak vanished apparently as a consequence of aglycon penetration between the phospholipid tails.

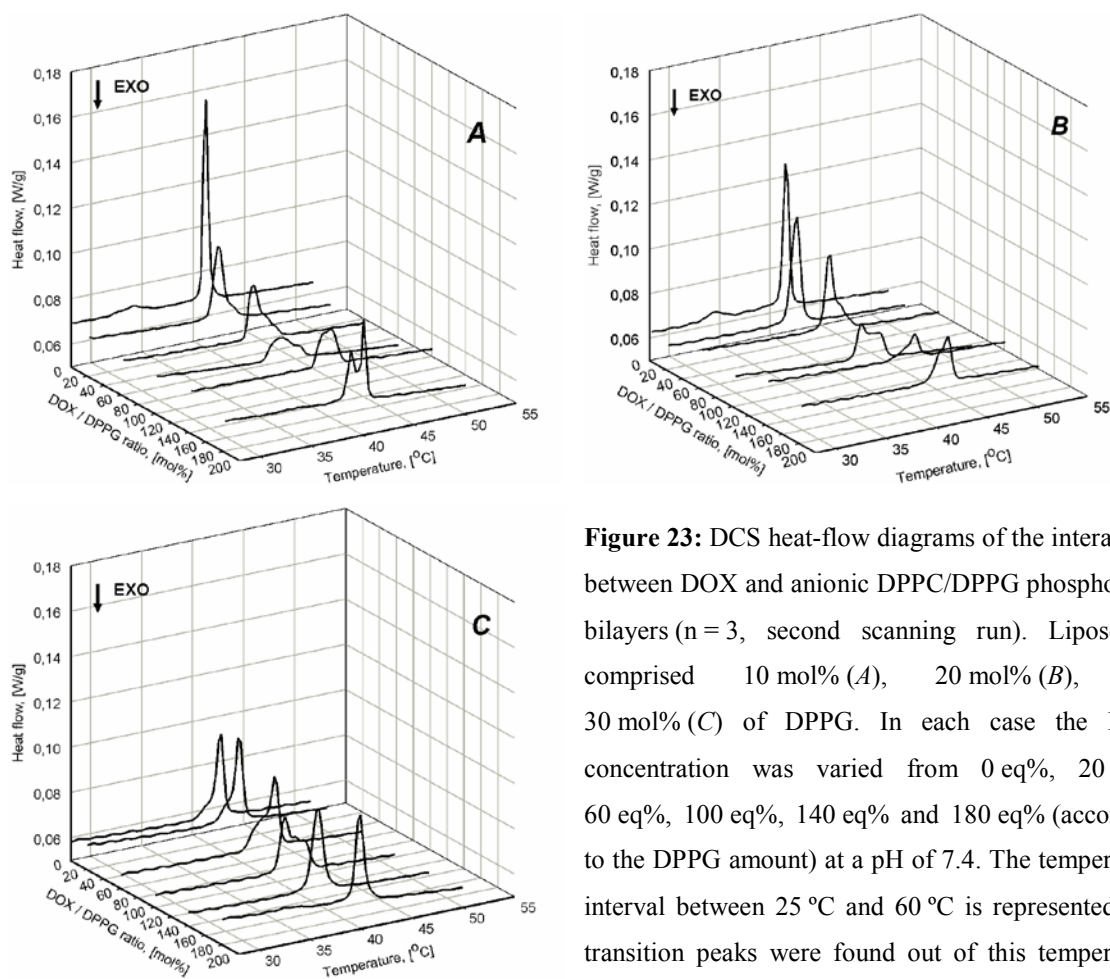


Figure 23: DCS heat-flow diagrams of the interaction between DOX and anionic DPPC/DPPG phospholipid bilayers ($n = 3$, second scanning run). Liposomes comprised 10 mol% (A), 20 mol% (B), and 30 mol% (C) of DPPG. In each case the DOX concentration was varied from 0 eq%, 20 eq%, 60 eq%, 100 eq%, 140 eq% and 180 eq% (according to the DPPG amount) at a pH of 7.4. The temperature interval between 25 °C and 60 °C is represented. No transition peaks were found out of this temperature span.

Under the same conditions, the main endotherm was broadened and T_m shifted down by 0.67 °C. At DOX concentrations above 100 eq% two overlapping peaks with a T_m difference of about 1 °C could be observed. The higher-melting peak appeared first as a shoulder when 60 eq% DOX were reached and became with increasing drug concentration a separate peak which finally became sharper and centered at about 42 °C. In summary, by raising of DOX concentration three major thermotropic phenomena could be observed:

- a small reproducible T_m shift towards lower temperatures at low DOX concentrations *e.g.* the shift from 41.52 °C (0 eq% DOX, 20 mol% DPPG) to 40.85 °C (20 eq% DOX, 20 mol% DPPG);
- a gradual decrease of mean transition peak intensity, mostly pronounced in samples with lower concentrations of DPPG *e.g.* in samples comprising 20 mol% DPPG the

mean peak area (peak 1 at 40.5 °C) decreased from 31.091 kW/mol (0 eq% DOX, 20 mol% DPPG) to zero (140 eq% DOX, 20 mol% DPPG);

- c) a gradual formation of a peak shoulder and a new higher-melting peak between 41.42 °C and 41.94 °C at higher DOX concentrations. This effect was the more pronounced, the higher the concentration of DPPG was.

| DOX, [eq%] | Peak 1 | | | Peak 2 | | |
|------------|--------------|---------------------|-----------------------|--------------|---------------------|-----------------------|
| | T_m [°C] | Peak area, [kJ/mol] | Peak height, [kW/mol] | T_m [°C] | Peak area, [kJ/mol] | Peak height, [kJ/mol] |
| 0 | 41.55 ± 0.11 | 31.091 ± 0.012 | 1.394 ± 0.020 | --- | --- | --- |
| 20 | 40.88 ± 0.05 | 33.772 ± 0.003 | 1.072 ± 0.002 | --- | --- | --- |
| 60 | 41.00 ± 0.08 | 27.553 ± 0.010 | 0.811 ± 0.001 | shoulder | --- | --- |
| 100 | 40.47 ± 0.13 | 14.366 ± 0.003 | 0.660 ± 0.005 | 41.50 ± 0.11 | 12.008 ± 0.001 | 0.526 ± 0.005 |
| 140 | shoulder | --- | --- | 41.42 ± 0.07 | 7.183 ± 0.011 | 0.551 ± 0.003 |
| 180 | --- | --- | --- | 41.94 ± 0.02 | 26.803 ± 0.007 | 6.023 ± 0.002 |

Table 10: Progression of multiple endotherms during titration with DOX of anionic phospholipid bilayers comprising 20 mol% DPPG and 80 mol% DPPC. At low DOX concentration a small T_m shift can be observed, followed by a gradual depletion of peak 1 height. Parallel to that a second higher-melting peak appeared and rose in height at DOX concentrations above 100 eq% ($n = 3$, $m = 3$).

Next to the phase transition perturbations in mixed anionic systems, DOX also altered the colloidal and lyotropic condition of liposomes. Small-angle X-ray scattering studies [166] indicated that DOX in the concentration range of 40 eq% to 80 eq% causes a bilayer reorganization of anionic liposomes into closely-packed multilamellar structures. In this concentration span DOX shows also small but definite fluidizing effects on phospholipid membranes [179] as observable from the peak broadening thermotropic phenomena.

At higher drug concentrations the appearance of high-melting peaks were correlated with the formation of a coarse crystalline phase (Figure 24), exclusion of the aqueous phase, and obliteration of the colloidal system. Surprisingly, although the stoichiometric proportions given by Goormaghtigh et al. (1980) [165] were exceeded, DOX was still bound beyond the concentration mark of 100 eq% (data not shown). Above this limit the concentration-dependent formation of crystalline phase could be related by its optical appearance with the differentiation of a high-melting peak in the thermogram. This finding substantiates the hypothesis that further binding of DOX above the electrostatic charge stoichiometry is possible due to hydrophobic and self-association interactions [166]. Apparently, the excessive

phospholipid complexation enhances phase crystallinity and is detrimental for the liposomes' colloidal state.

The macroscopic appearance of the crystalline aggregates was as micrometer to millimeter large dark-red particles, prone to sedimentation. A scanning electron microscopy (SEM) image revealed the various form and sharp-edged surface topography of the aggregates (Figure 24). Aggregate crystallinity was confirmed by transmission electron microscopy (TEM, data not shown). The formation of crystalline aggregates and colloidal collapse of the formulations can be explained by escalating formation of stacked aglycon associates [166], interdigitation of phospholipid acyl chains [184] or other unspecific interactions.

Dilution of the anionic phospholipid DPPG with zwitterionic phospholipids such as DPPC lowers the DOX binding ability of liposomes [169], but it also effectively inhibits the formation of crystalline aggregates as seen by the tendency of bilayers with a higher DPPG content to form more intensive high-melting peaks at lower DOX concentrations (Figure 23).

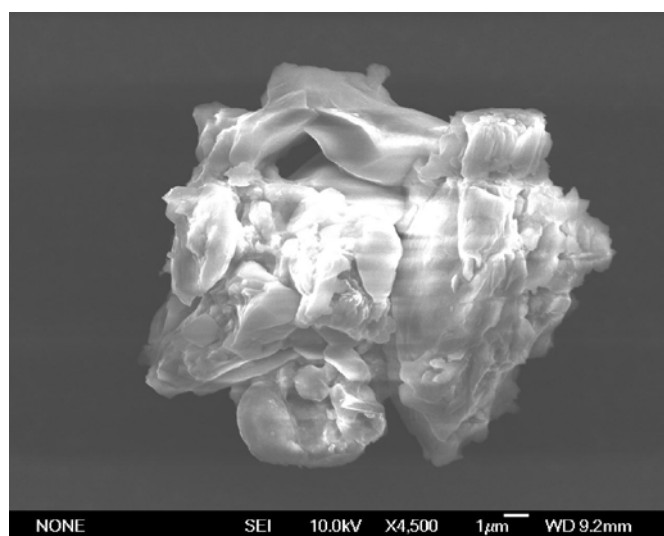


Figure 24: Scanning electron microscopy image of a condensed aggregate of DPPC/DPPG and DOX in formulations, containing 70 mol% DPPC, 30 mol% DPPG, and 140 eq% DOX.

The fluidizing effect of DOX on anionic phospholipid membranes, suggested in the literature [179], has been observed in the above thermograms (Figure 23) in terms of peak broadening and flattening. These peak shape changes can be numerically represented as the ratio between the peak width at half peak height ($W_{0.5}$) and the peak height (H). For example, in binary mixtures of 10 mol% DPPG and 90 mol% DPPC increasing DOX concentrations cause a continuous increase of the $W_{0.5}/H$ coefficient *i.e.* membrane fluidizing until 100 eq% of DOX are reached (Figure 25, solid line). Beyond this mark the membrane fluidity steeply

declines and crystalline complexes are bound in the final stage. Interestingly, the MB yield follows the same progression as represented by the dashed line plot. This finding together with several further examples later on corroborates the hypothesis that the phospholipid cooperativity is a major factor for the stability of MB shell. This opinion has already been maintained by other authors and witnessed by fluorescence microscopy [14, 79, 93].

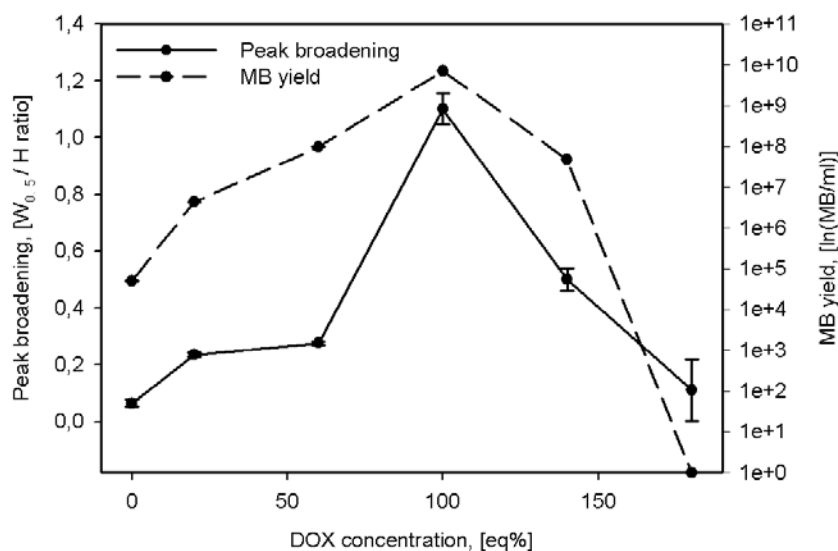


Figure 25: Transition peak flattening and broadening (solid line) of peak 1, appearing at about 41°C, in binary mixtures of 10 mol% DPPG and 90 mol% DPPC at DOX concentrations, increasing from 0 eq% to 180 eq% according to the concentration of DPPG. The dashed line represents the progression of MB yield produced upon mechanical agitation.

The key result of this study was the selection of suitable concentrations for the formulation of DOX-loaded liposomal MB precursors. The choice criteria for the optimum formulation range were: a) the highest molar ratio between DOX and total phospholipid (greatest loading amount of DOX); and b) the highest bilayer fluidity derived from the lowest height of the melting peak, arising below 41 °C (peak 1). The selected interval of 20 mol% DPPG and between 60 eq% and 100 eq% DOX satisfied both requirements, although a better membrane fluidity was existing under 10 mol% DPPG and 100 eq% DOX, yet the drug loading was then lower. Further on in this work, the range of 20 mol% DPPG and 60 eq% to 100 eq% DOX will be used as a milestone for further optimizations and development of DOX-loaded MBs.

4.1.2. Effect of US homogenization of liposomes on the MB yield

US homogenization of liposome intermediates for the production of DOX-loaded MBs in the time range from 0 min to 10 min had an unsteady effect on the MB particle yield (Figure 26).

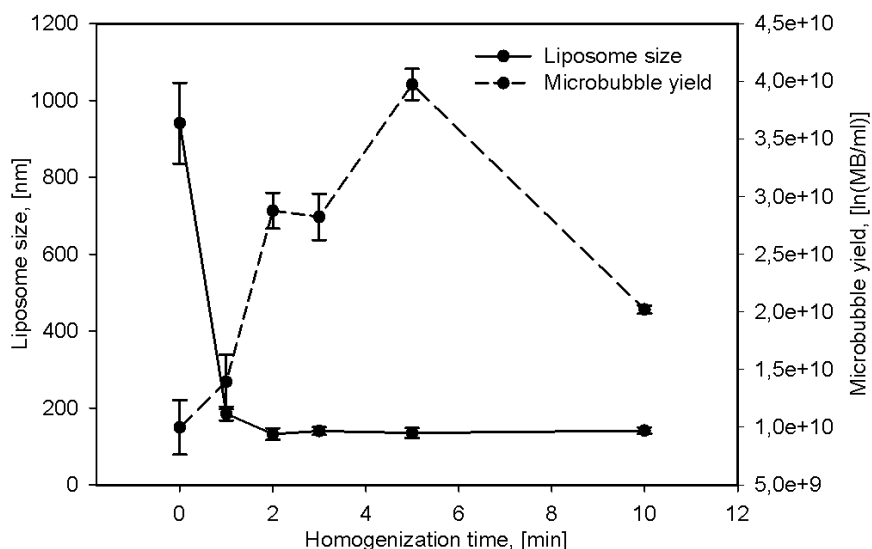


Figure 26: Progress of liposome size and MB yield during homogenization by US.

Rather short sonication times of 2 min caused a rapid 5-fold decrease of liposomal size down to about 150 nm with no significant change after further sonication (solid line). On the other hand, MB yield demonstrated an about 4-fold increase after five minutes US homogenization, followed by a steep 2-fold decrease (dashed line). However, the pattern of MB yield increase did not correlate with the progression of particle size reduction. The initial increase of MB concentration could be indeed explained with liposome size and / or viscosity effects. The following decrease of MB yield is apparently due to the loss of surface activity in samples, treated with US as observed by other authors [81]. In consequence, US horn-type homogenization for 3-5 minutes can be applied for improving the colloidal state of DOX-loaded anionic liposomes, yet with the concern of occurring chemical decay of the active drug.

4.1.3. Effect of third phospholipid compounds

In the following study DPPC-DPPG liposomal formulation were tuned by addition of minor amounts of third phospholipids in attempt to improve their pharmaceutical properties like liposomal size distribution, storage stability, MB yield, *etc.* Phospholipids with broadly

varying properties (Table 5, p. 28) such as PEGylated (DPPE-PEG2000), cationic (DPTAP), non-bilayer (DPPE) phospholipids and sterols (cholesterol) were applied.

The purpose of including PEGylated phospholipids such as DPPE-PEG2000 was to enforce the existing electrostatic repulsing interactions between liposomes by additional steric shielding and to improve their colloidal stability upon storage. Furthermore, the “bulky” PEG moieties increase the bilayer mean curvature (H), thus promoting the bending towards the acyl chain region, and expectedly favor the spontaneous formation of smaller liposomes [185, 186].

In the concentration range from 1 mol% to 2 mol% DPPE-PEG2000 the liposome size, measured in un-homogenized preparations, decreased from $2,800 \pm 330$ nm to 530 ± 83 nm (Figure 27). The polydispersity index (PDI) decreased from 1.000 to 0.382 ± 0.051 . This positive influence allowed eliminating the highly energetic step of US horn-type homogenization from the formulation procedure. Similar phenomenon of spontaneous small liposome formation upon addition of PEGylated phospholipids have been observed by Szleifer et al. (1998) [186]. In the denoted concentration interval of 1-2 mol% DPPE-PEG2000 the formation of MBs upon agitation was adequate with a yield of $2-4 \times 10^{10}$ MB/ml. As expected [187], a small increase (5-7 mV) of the negative liposomal Zeta potential was found in the above concentration range of DPPE-PEG2000, due to electrostatic shielding effects through the PEG-grafts.

With increasing the concentration of DPPE-PEG2000 to 5 mol% of the total phospholipid molar amount only a small reduction of liposome size followed. On the other side, the formation of MBs and their structural stability steeply decreased resulting in MB yields of between 1×10^5 MB/ml down to 1×10^2 MB/ml.

One possible hypothesis for the strongly diminished MB formation is given by the continuously increasing monolayer bending tension caused by the PEG-grafts. The same effect which decreases liposome size at lower surface PEG-graft densities apparently bends the MB shell monolayer towards increasingly smaller curvature radii which are no longer compatible with the MB geometry. This obviously leads to shell instability and MB degradation.

Due to their large positive intrinsic curvature and steric shielding properties PEGylated phospholipids contribute on a concentration-dependent manner two positive impacts to DOX-loaded liposomal formulations. These are first - the spontaneous formation of smaller liposomes with a narrower size distribution, and second - the prolonged colloidal storage stability from several hours to several weeks.

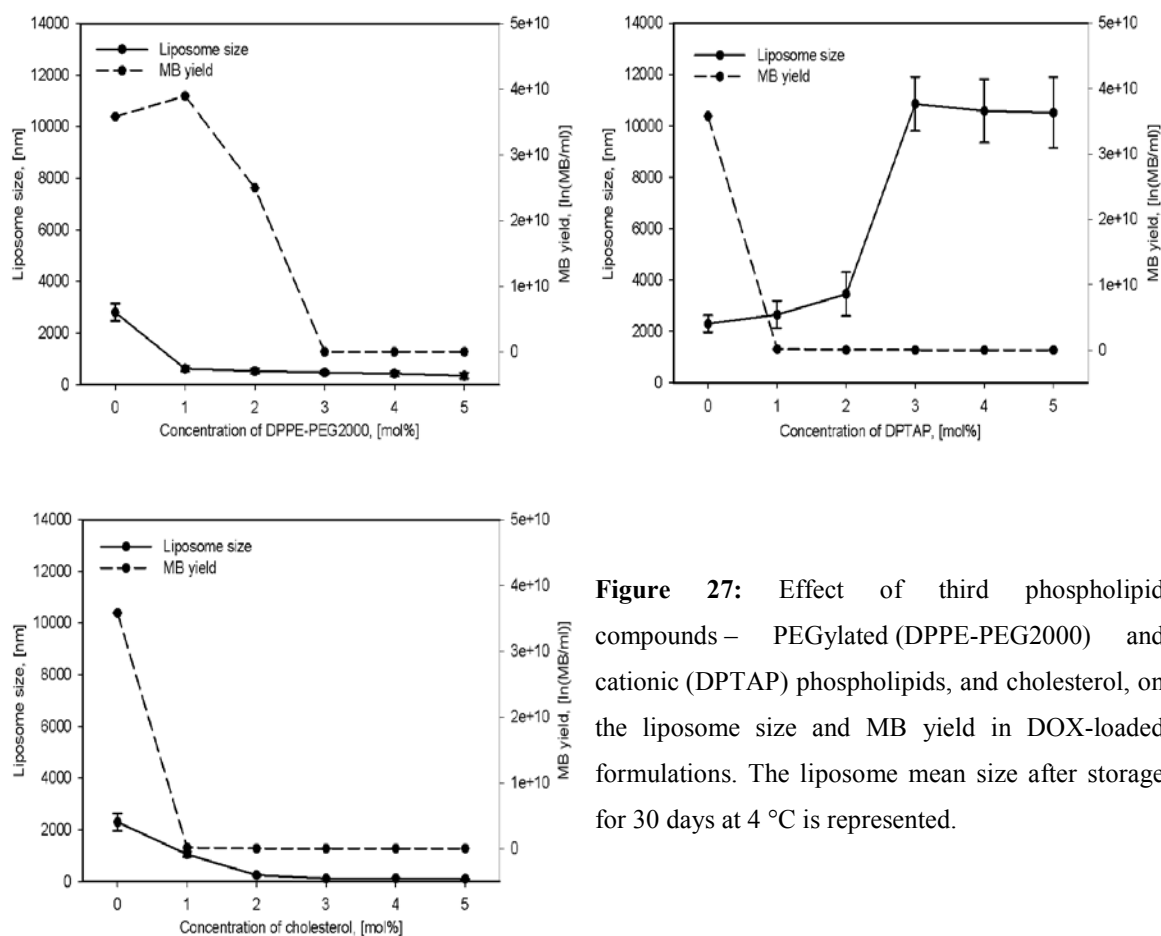


Figure 27: Effect of third phospholipid compounds – PEGylated (DPPE-PEG2000) and cationic (DPTAP) phospholipids, and cholesterol, on the liposome size and MB yield in DOX-loaded formulations. The liposome mean size after storage for 30 days at 4 °C is represented.

On a similar fashion cholesterol strongly hampered the formation of DOX-loaded MBs, although it improved the size distribution and colloidal stability of liposomes. In the concentration range of 3-5 mol% cholesterol completely prevented the formation of crystalline aggregated phase between DOX and phospholipids. Same amounts of cholesterol further preserved liposomal size to 120 ± 13.12 nm over a month during storage at 4 °C. However, cholesterol in above concentrations strongly hindered the MB formation and reduced MB yield by over 100-fold. On the cholesterol concentration scale its positive stabilization effects on liposomes commence equally with the negative effects on MB formation. Therefore, cholesterol-adjusted formulations can well be practicable for liposomal preparation, yet not for the production of MBs.

Including of non-bilayer hydrogen-bonding phospholipids such as DPPE [169] into anionic bilayers was done with the intension to enhance the combined electrostatic / hydrophobic complexation through hydrogen bonding between DOX and the free primary amine of DPPE headgroup. However, already small increments of DPPE in the order of 1-2 mol% strongly

increased the liposomal viscosity and raised the MB median size by over 3-fold. Higher DPPE concentrations led to the gelation of the formulations and made them useless for MB production.

An interesting formulation aspect offers the inclusion of small amounts of cationic phospholipids *e.g.* DPTAP into mixed anionic phospholipid blends and forming of so called *catanionic* bilayers [188]. Driven by electrostatic repulsions, cationic phospholipid molecules should distribute between the negative charges and increase the distances between them [189]. The larger distance between negative charges will expectantly reduce the possibility of forming stacked DOX associates due to the decreased probability of contact between aglycon moieties. On the contrary to our expectation, DPTAP had no positive impact on liposomal and MB formulations. Higher concentrations of DPTAP (3-5 mol%) even impaired the storage colloidal stability and caused a 5-6 fold increase of liposome mean size after 30 days at 4 °C. In summary, considering the pharmaceutical properties of both DOX-loaded liposomal and MB formulations, only the addition of small amounts of PEGylated phospholipids brought an advantageous impact and was accepted into the further formulation development.

4.1.4. Effect of agitation time on the DOX encapsulation in MBs

The effect of agitation time on unloaded MB formulations was discussed above under “II. Ch. / 4.1.1 *Effect of agitation time*” on p. 43. The general outcome of this study was that a steep decrease of MB concentration occurs after about 20 s agitation apparently due to the combined action of temperature increase and shear forces. This tendency was proven again by examining of DOX amount, associated to the MB fraction (C_{MB}) as function of the agitation time (Figure 28).

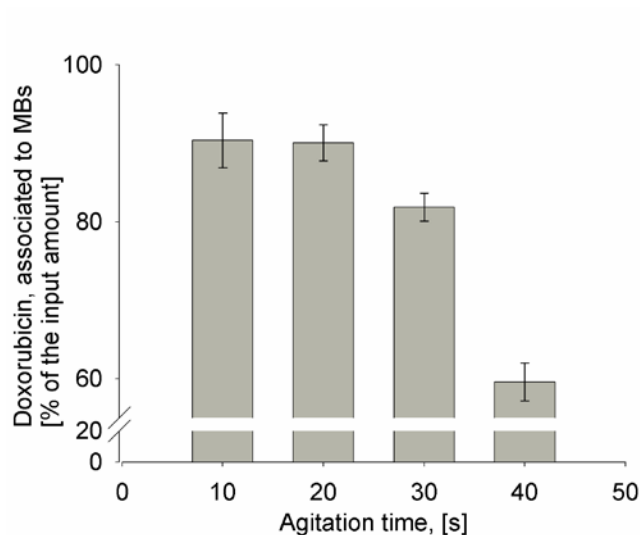


Figure 28: DOX amount, encapsulated in MBs in relation to various agitation times. As a result of temperature increase and shear forces, MB decay occurred after 20 s agitation. Therefore, DOX has been released from the MB fraction in the form of liposomes (n = 6).

After an agitation time of 20 s the amount of DOX, associated with MBs C_{MB} declined from approximately 95% to about 82% (after 30 s) and further to 59% after 40 s. Compared to Figure 6, p. 43 the reduction of C_{MB} (62% between the 20th and the 40th second) nearly quantitatively corresponds to the decrease of MB concentration (65.2% in the same time span). Therefore, the agitation time was set to 20 s in the standard formulation approach for DOX-loaded MBs.

Further formulation parameters such as tube fill volume and tube shape were adopted from “II. Ch. / 4.1 Pre-formulation studies on model microbubbles”, p. 43 without additional modifications.

4.1.5. Optimal formulation procedure for DOX-loaded liposome precursors and MBs

Based on the pre-formulation research the following standardized procedure was established. The resulting final concentrations of active drug and excipients in liposomal formulations for production of MBs are given in Table 11.

| Component | Molar concentration, [mM] | Mass concentration, [mg/ml] |
|--------------|---------------------------|-----------------------------|
| DOX | 0.60 | 0.35 |
| DPPC | 2.37 | 1.74 |
| DPPG | 0.60 | 0.45 |
| DPPE-PEG2000 | 0.03 | 0.08 |
| Glucose | 0.28 | 50.00 |
| EDTA | 0.01 | 0.003 |

Table 11: Constitution of “optimized” DOX-loaded liposomal formulations for the production of MBs by mechanical agitation.

Briefly, depending on the charge volume, appropriate amounts of DPPC, DPPG and DPPE-PEG2000 were dissolved in chloroform. Following, the organic solvent was removed and the phospholipid thin-film was allowed to dry under vacuum at a temperature of 60 °C for 60 min.

Accordingly, DOX, EDTA, and glucose were dissolved in highly purified electrolyte-free water (Purelab Plus[®], USF Elga Ionpure GmbH, Germany). The phospholipid film was hydrated with the DOX solution for 60 min under continuous stirring under light protection and nitrogen atmosphere. During the hydration the temperature was maintained above the gel-to liquid-crystalline phase transition temperature of the DOX / phospholipid complex (42 °C). Prior to characterization and further proceeding, the liposomes were allowed to equilibrate for at least 12 hours at 4 °C. The total molar concentration of phospholipid (PLT) in final liposomal formulations was 3 mM (2.27 mg/ml). The mass ratio of DOX to total phospholipid has been calculated to be 15.3%.

4.2. Characterization of doxorubicin-loaded liposomes

4.2.1. Size distribution and Zeta potential

In standard preparations according to Table 11 DOX-loaded liposomes had an average size of 530 ± 83 nm ($PdI = 0.382 \pm 0.051$) and a Zeta potential of -22.58 ± 0.56 mV at a medium conductivity of 0.0014 mS/cm².

The successful binding of DOX to anionic liposomes was also confirmed by the increase of their negative Zeta potential caused by the compensation of anionic charges by DOX. The Zeta potential of unloaded liposomes containing from 10 mol% to 50 mol% DPPG decreased rather linearly from -14.8 ± 0.20 mV to -38.4 ± 0.46 mV. After loading with 100 eq% DOX the Zeta potential in all samples increased by about 12.00 ± 0.75 mV to -27.45 ± 0.73 mV.

4.2.2. Measuring the DOX concentration

The characteristic peak of DOX appeared at a retention time of 7.82 ± 0.3 minutes (26.06% of the total elution time). The slope of the UV-spectrometric calibration line in the DOX concentration range from 0.5 $\mu\text{g/ml}$ to 100 $\mu\text{g/ml}$ was $13,952.670 \pm 350.563$ with an intercept of 1,372.91 AU ($R^2 = 0.9974$). The HPLC method was not significantly influenced by the presence of phospholipids in the studied concentration range. The recovery rate of DOX from liposome samples was $99.59 \pm 0.07\%$ ($C_m = 0.3486 \pm 0.0174$ mg/ml) after admixing of 20 μl liposomal dispersion with 1 ml acidified isopropanol.

4.2.3. Association of DOX with liposomes

In the described concentration range DOX showed a very high affinity to anionic phospholipid bilayers. The fraction of free DOX, found in liposomal preparations, was $2.76\% \pm 3.2\%$ of the total amount of drug used.

4.2.4. Electrolyte-induced liposomal leakage of DOX

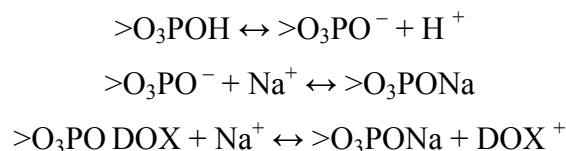
According to the literature, next to the weaker hydrophobic interaction, the major component of DOX complexation is the electrostatic attraction [165]. Increased electrolyte concentrations shield the Coulomb interactions between charges in an electrostatic complex which are separated by more than roughly a Debye screening length [190] (Equation 12).

$$\kappa^{-1} = \sqrt{\frac{\varepsilon_0 \varepsilon_r kT}{2N_A e^2 I}}$$

Equation 12: Debye length equation in an electrolyte solution or in a colloidal dispersion.

where I is the ionic strength of the electrolyte, ε_0 is the permittivity of free space, ε_r is the solvent's dielectric constant, k is the Boltzmann's constant, T is the absolute temperature in Kelvin, N_A is Avogadro's number, and e is the elementary charge. When increasing the ionic strength the Debye length *i.e.* the distance, over which significant ion charge separation can occur, decreases. Because of the shrinking Debye spheres opposite ion charges interact weaker and the electrostatic component between DOX and anionic phospholipid bilayer looses on magnitude.

On their turn the sodium cations also exert an effect on the ionization state of DPPG by binding and compensating negative charges [95]:



However, literature data indicates an association constant (K_a) of about 0.2 M^{-1} (by interpreting the surface potential) [95] or somewhat lower from 0.005 M^{-1} to 0.02 M^{-1} (by interpreting the surface pressure data) [191], for binding of Na^+ to phosphatidylglycerols. For comparison the association constants between anionic phospholipids (cardiolipin) and DOX are much greater and are in the order of 10^5 - 10^6 M^{-1} [192]. Apparently the salt-induced dissociation of the DOX-anionic bilayer complex is rather governed by Debye-shielding effects than by changing the phospholipid ionization state.

Experimental data revealed that the influence of increased ionic strength on DOX-anionic bilayer complex shows a strong dependency on whether the complex has already been formed or not. Prior to complex formation the effect of monovalent ion concentrations in the range of 0 mM to 100 mM almost completely inhibited the binding of DOX. Even at low ion concentrations of 10 mM DOX complexation was reduced from 87-90% to 21-28% of the total input amount (**Figure 29**). By increasing the ion concentration to 100 mM the amount of DOX, bound to liposomes, decreased gradually further to 7-9%.

The salt-induced dissociation of DOX-anionic phospholipid complex was far less pronounced when the electrolyte was added to the pre-formed complex. In this case small salt concentrations of 10-20 mM provoked the dissociation of only 7-13% of the total DOX amount used. The dissociation at 100 mM ion concentration reached 34-42% DOX.

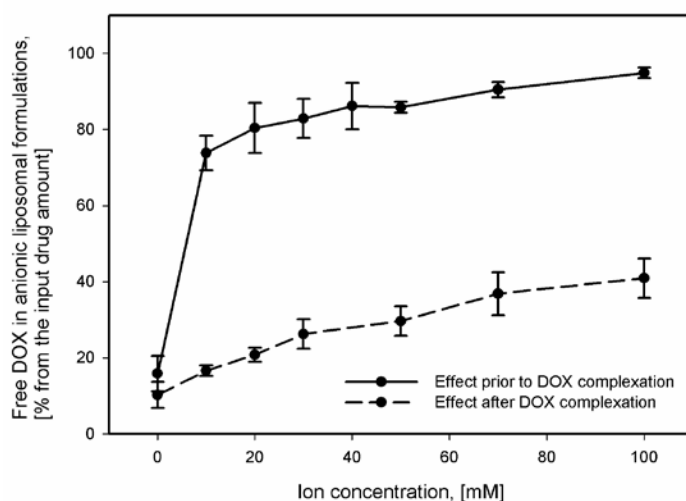


Figure 29: Electrolyte-induced leakage of DOX from anionic liposomes at increasing concentration of single-charged ions – sodium chloride, from 0 mM to 100 mM (n = 3). The concentration of free DOX in the supernatants is plotted as per cent according to the total DOX concentration in whole samples.

As found under “3.2.1 *Differential scanning calorimetry studies*” on p.81, the hydrophobic interactions of DOX with neutral phospholipids appear to be much weaker than the electrostatic attractions with anionic phospholipids. However, the present study allowed exerting the theory that electrostatic attractions only play an earlier role during the complex formation than hydrophobic interactions. Long-range electrostatic forces apparently attract the DOX molecules to such proximity where shorter-ranged hydrophobic interactions can occur.

This hypothesis has been implicated by the fact that shielding the electrostatic interactions by monovalent sodium cations prior to the complex formation results in almost total inhibition of the complexation (Figure 29, solid line). Apparently the hydrophobic attractions additionally stabilize the complex when the molecule is located in an approximate reach to the bilayer. This is supported by the fact that detaching of DOX upon electrolyte shielding of electrostatic attractions after the formation of the complex (Figure 29, dashed line) is about three times less pronounced than prior to that.

It appears that the electrostatic interaction is only a necessary prerequisite for the formation of DOX-phospholipid complex which further on is stabilized by hydrophobic interactions with the phospholipid acyl chains or / and the formation of stacked aglycon associates (Figure 22, p. 77). One indication for this event sequence is the fact that DOX interacts very scarcely with zwitterionic phospholipid layers of DPPC, where only hydrophobic interactions are possible. In contrast to that more lipophilic cationic anthracyclines such as pirarubicin [193] and N-trifluoroacetyladriamycin-14-valerate [179] are indeed able to form such complexes.

4.2.5. Chemical stability of DOX during the production of liposomes

In the early stages of formulation development the concentration loss of DOX due to chemical degradation during liposome production using the thin-film method with a following US-homogenization step was up to $10.4\% \pm 6.19\%$ of the input DOX amount. US homogenization alone had a great impact to the chemical decay making up about $4.8\% \pm 1.53\%$ of the total degradation rate.

After spontaneous formation of small liposomes was achieved by the addition of PEGylated phospholipids the highly energetic step of US horn-type homogenization was excluded from the processing lane (see “4.1.3 Effect of third phospholipid compounds”, p.101). Additional protection measures from air oxygen and light helped reduce DOX chemical decay to statistically insignificant values.

4.2.6. Photochemical stability of DOX

The photochemical degradation of DOX revealed a single exponential- to nearly linear order kinetics. Both aqueous and liposomal formulations showed significant concentration losses (correspondingly $27.16\% \pm 0.37\%$ and $12.81\% \pm 2.76\%$ according to the initial concentration) due to thermal effects in obscured samples (Figure 30 and Figure 31, solid lines). Interestingly, although the temperature, measured during the whole time range, in obscured samples of both liposomal and aqueous formulations did not deviate significantly ($25.94\text{ °C} \pm 3.21\text{ °C}$), liposomal DOX appeared to be more stable in absence of light.

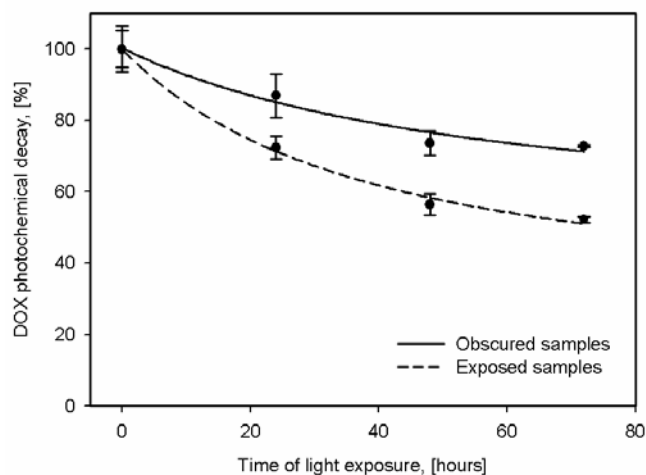


Figure 30: Photochemical stability of DOX in 0.6 mM aqueous solutions in obscured (solid line, $R^2 = 0.9738$) and light exposed samples (dashed line, $R^2 = 0.9975$), $n = 9$.

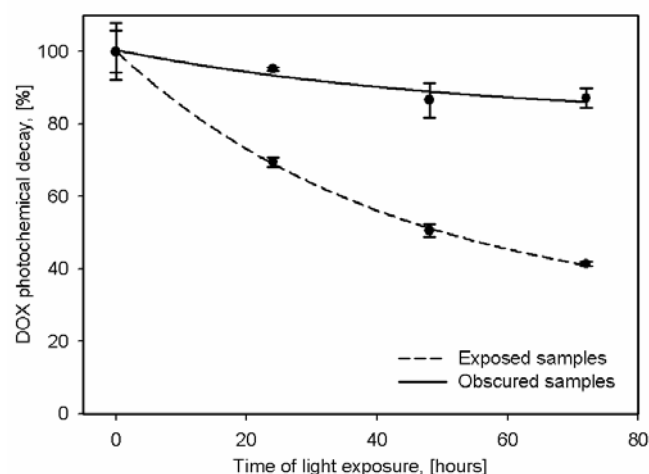


Figure 31: Photochemical stability of DOX in liposomal dispersions, containing 0.6 mM DOX and 3 mM total phospholipid concentration, in obscured (solid line, $R^2 = 0.9738$) and light exposed samples (dashed line, $R^2 = 0.9975$), $n = 9$.

The temperature difference between light exposed and obscured samples was moderate – $3.51 \% \pm 1.37 \%$. After 72 hrs exposure to light aqueous DOX solutions showed a total decay of $47.80 \% \pm 2.78 \%$, while in liposomal samples the DOX loss was higher – $58.59 \% \pm 1.97 \%$ (Figure 32). The half-life times of DOX are represented in Table 12.

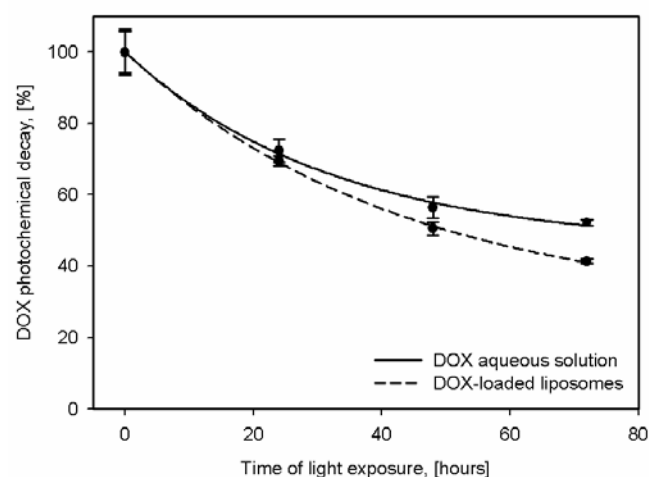


Figure 32: Comparison between the photochemical degradation of DOX in light-exposed aqueous solutions (solid line) and liposomal samples (dashed line).

However, if the more pronounced thermal decay be subtracted from the total degradation rate, liposomal formulations demonstrate a 2.22-fold lower photochemical stability than aqueous

solutions with 45.78% (in liposomes) vs. 20.64% (in solution) photochemical loss after 72 hrs.

| Formulation | Half-life (τ) of DOX, [hours] | |
|----------------------|--------------------------------------|-------------------------|
| | <i>Exposed samples</i> | <i>Obscured samples</i> |
| Aqueous solution | 22.38 \pm 1.13 | 29.18 \pm 1.28 |
| Liposomal dispersion | 29.87 \pm 2.01 | 37.26 \pm 1.21 |

Table 12: Half-life (τ) of DOX in aqueous solutions and in liposomal dispersions

The increased photochemical instability of DOX in liposomal formulations can be attributed mainly to their increased turbidity compared to aqueous solutions. Furthermore, the DOX stability is possibly influenced through the increased specific absorption constant when the aglycon persists in less polar medium between the phospholipid acyl chains [165].

In summary, in order to preserve the chemical stability of DOX, primary packages must be selected which provide an adequate light protection.

4.3. Pre-formulation studies on doxorubicin-loaded microemulsions and acoustically active lipospheres

The formulation strategy of DOX-loaded acoustically active lipospheres (AALs) was based on the production of foamable microemulsions, containing the active drug in their oil-phase. After mechanical agitation these drug-loaded microemulsions produce AALs, comprising DOX in the oil layer, covering the inner surface of the phospholipid monolayer (Figure 2, C, p.19). Drug-loaded AALs were first described by Unger et al. (1998) [122] in the case of paclitaxel. Several injectable oil excipients such as castor oil, soybean oil, or triacetin have been used to prepare drug-loaded AALs [194, 195]. Among them triacetin-containing AALs were found to provide the best acoustic destructibility, apparently because of its about four times lower viscosity of 28 cP vs. 110 cP in the case of soybean oil at 25 °C [194]. For this reason triacetin was preferred in the following pre-formulation studies.

During the pre-formulation development several main pharmaceutical challenges were addressed:

- a) colloidal stability of DOX-loaded microemulsions;
- b) retention of DOX in the lipophilic phase;
- c) ability of microemulsions to form AALs (foamability);
- d) US echogenicity and destructibility of AALs.

4.3.1. Partition equilibrium of DOX-base between triacetin and water

The distribution of DOX-base between the non-polar triacetin phase and the outer aqueous phase is a solubility- and pH-dependent process. Others than paclitaxel [122] which has a very high octanol / water partition coefficient of 99 and is barely soluble in water [122], DOX has a rather high water solubility and a low partition coefficient of 0.45 to 1.85 [180-182]. In addition, its molecule has an amphoteric character owing to the basic daunosamine primary amine group and the deprotonable phenol function of the aglycon. Depending on the pH DOX molecules are prone to self-association and formation of fiber-like aggregates [196], as well as to chemical degradation [175].

Triacetin is a rather non-polar medium with a dielectric constant of 6.2 which is over 10-fold lower than that of water – 78.48 (1 MHz, 25 °C). Because of its small molecule, triacetin is slightly soluble in water and has an equilibrium saturation concentration of 61.2 g/l (52.7 µl/ml) [197].

The above chemical parameters draw a rather challenging perspective for the formulation development which firstly needs to overcome the partitioning problems of DOX between triacetin and water.

The chemical transformation of DOX from its hydrochloride salt form into the free-base form (DOX-base) has increased its solubility in triacetin from undetectable concentrations to 4.37 ± 0.31 mg/ml (equilibrium saturation concentration at 4 °C). After the DOX-base / triacetin solution was brought in contact with aqueous phase, part of DOX migrated into it on a pH dependent manner.

The triacetin / water partition of DOX is an equilibrium process, depending on the lipophilicity values of DOX-base and triacetin, on the pH value in the aqueous phase, and on the DOX concentrations in both phases. The retention of DOX in the lipophilic phase was evaluated in terms of the apparent partition coefficient (P):

$$P \% = \frac{[DOX - NH_2]_{lip}}{[DOX - NH_2]_{aq} + [DOX - NH_3^+]_{aq}} \times 100$$

Equation 13

where $[DOX-NH_2]_{lip}$ is the molar concentration of DOX-base in the lipophilic phase while $[DOX-NH_2]_{aq}$ and $[DOX-NH_3^+]_{aq}$ are the concentrations of DOX-base and protonated DOX in the aqueous phase.

In the aqueous phase DOX-base is protonated on a pH-dependent manner and its concentration is reduced according to the equilibrium:



$$K_e = \frac{[\text{DOX-NH}_2][\text{H}^+]}{[\text{DOX-NH}_3^+]}$$

Equation 14

The theoretical plot of DOX ionization state [150] reveals a minimum protonation above a pH of 7. Between pH of 8 and 9 a maximum of 70% of all DOX molecules persist in uncharged form. Above a pH of 8 a steep increase of the deprotonated DOX species takes place.

As a result of its diffusion out of the triacetin phase and its protonation in the aqueous phase, DOX continuously migrates out of the AAL carriers which decreases their efficient loading. In order to ensure the stability of the loaded DOX amount, the control of pH and increasing the concentration of DOX-base are expectably effective levers for enhancing the retention of DOX in the lipophilic triacetin phase. The influence of surfactant / co-surfactant monolayer on the partition was not considered in this study.

At lower pH values between 5 and 7 nearly all DOX migrated from the non-polar triacetin into the aqueous phase (Figure 33, dashed line). Increasing the pH to 8.5 increased the concentration of DOX-base in the aqueous phase at the expense of the protonated DOX form which led to an increased retention in triacetin ($P = 45.43\% \pm 2.35\%$). Further increase up to a pH of 9 caused complications due to reduced solubility and precipitation of DOX.

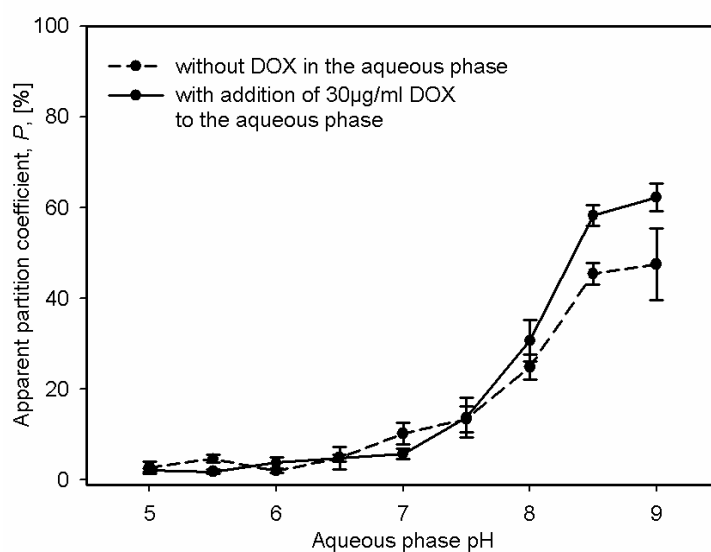


Figure 33: Experimental apparent partition coefficients of DOX between triacetin and aqueous buffers with various pH.

In a following study, DOX in a concentration of 30 µg/ml was added to the aqueous buffer in order to shift the above acid-base and diffusion equilibria towards the triacetin phase. As expected, the apparent partition coefficient at a pH of 8.5 has raised to 58.30% ± 2.31% (Figure 33, solid line) which value was accepted for further progress.

The above results were consistent with previous studies of Tewes et al. (2007) [150], who determined the apparent partition coefficients of DOX for two organic phases – methylene chloride ($P \sim 90-95\%$ at pH 8.5) and ethyl acetate ($P \sim 10-15\%$ at pH 8.5). Interestingly, these results do not correlate with the dielectric constants of these two solvents, being correspondingly 9.8 and 6.02. However, the influence of additional factors must be also taken into account such as the ionic strength, solute concentration, *etc.*

4.3.2. Optimal formulation procedures for DOX-loaded microemulsions and AALs

The resulting final concentrations of active drug and excipients in microemulsion and AAL formulations are given in Table 13 below.

| Component | Molar concentration, [mM] | Mass concentration, [mg/ml] |
|--|---------------------------|-----------------------------|
| DOX-base in triacetin | 0.121 | 0.065 |
| DOX in aqueous phase | 0.051 | 0.030 |
| DPPC | 4.63 | 3.40 |
| DPPG | 0.57 | 0.38 |
| DPPE-PEG2000 | 0.45 | 1.20 |
| Lutrol F68 | approx. 0.794 | 10 |
| Triacetin | --- | 15 |
| Triacetin-saturated phosphate buffer, pH 8.5 | | ad 50 ml |

Table 13: Final concentrations of DOX and excipients in standard formulations of DOX-loaded MBs.

In summary, according to the above calculated DOX partition, from the total amount of 0.172 mM DOX in the microemulsion, 41% (0.0705 mM or 35.814 $\mu\text{g/ml}$) were entrapped in the triacetin phase and 59% (0.1015 mM or 51.562 $\mu\text{g/ml}$) were situated in the outer aqueous phase.

4.4. Characterization of doxorubicin-loaded microemulsions

4.4.1. Particle size distribution and colloidal stability of DOX-loaded microemulsions

Directly after their production, both high-pressure homogenized and horn-type sonication homogenized microemulsions showed rather similar particle size distributions of correspondingly $102.0 \text{ nm} \pm 12.0 \text{ nm}$ and $114.7 \text{ nm} \pm 13.5 \text{ nm}$. The polydispersity index (PdI) of both formulations was correspondingly 0.276 and 0.312 ($n = 3$).

After storage for 14 days, DOX-loaded triacetin microemulsions, produced by horn-type sonication showed an over 2-fold increase of particle size (from $82.8 \pm 9.3 \text{ nm}$ to $175.3 \pm 31.5 \text{ nm}$) and resulted in coarse dispersions after 30 days. Within the first two weeks their polydispersity increased by about 2-fold from a PdI of 0.206 to 0.405, reaching the maximum value of 1.000 after 30 days.

In contrast, under the same storage conditions microemulsions, produced by high-pressure homogenization, showed no significant size increase over 30 days. Therefore, the high-pressure homogenization was chosen for a standard preparation method for microemulsions in order to prepare drug-loaded AALs.

4.5. Characterization of doxorubicin-loaded microbubbles and acoustically active lipospheres

4.5.1. Structure analysis of DOX-loaded MBs and AALs

CLSM microscopic images of DOX-loaded MBs (Figure 34, A) revealed their spherical shape with intensive fluorescence of the drug, included in the phospholipid shell. The DOX-bearing shell encompasses a dark core, comprising the octafluoropropane gas.

In the case of DOX-loaded AALs (Figure 34, B), the drug was also included into the surrounding shell which was thicker and its fluorescence often masked the dark core shadow.

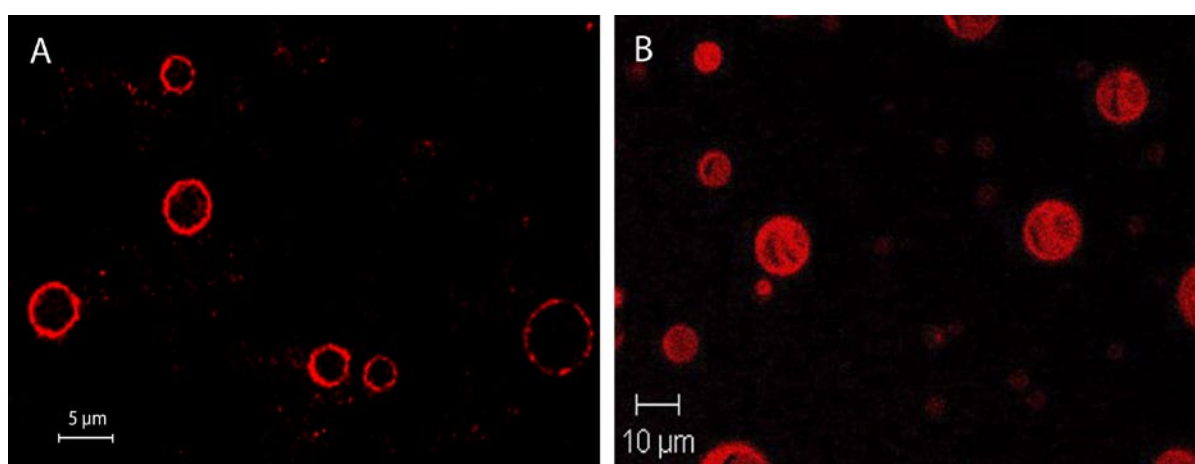


Figure 34: CLSM micrographs of DOX-loaded phospholipid MBs (A) and DOX-loaded AALs, containing triacetin (B). DOX (in red) is localized mainly in the anionic phospholipid MB shell and in the triacetin layer of AALs.

4.5.2. Particle size distribution

Concerning the formulation of DOX-loaded MBs and AALs in this work, the surface-weighted particle size distribution was considered most significant, especially with regard to the efficient loading (refer to “*II. Ch. / 4.1 Characterization of microbubbles*”, p. 43).

DOX-loaded MB formulations revealed a bimodal size distribution with a more intensive (~ 80%) peak between 800 nm and 4 μm with a mean size of $1.0165 \mu\text{m} \pm 0.0218 \mu\text{m}$. Another size peak with an intensity of about 20% smeared between 20 μm and 100 μm. In order to quantitatively determine the number of MBs, larger than 10 μm, additional particle size and counting measurements using light blockage accomplished covering the size range from 800 nm μm to 200 μm. According to them only between 0.06% and 0.40% of the total MBs number surpassed the size limit of 10 μm.

In the case of DOX-loaded AALs, the size distribution by laser diffraction also revealed a bimodal surface-weighted size distribution with a mean peak (~ 70% intensity) at $1.2036 \mu\text{m} \pm 0.1319 \mu\text{m}$ and a higher-sized peak (~ 30% intensity) between $30 \mu\text{m}$ and $110 \mu\text{m}$. Particle counting analysis revealed that between 0.98% and 1.22% of the overall AAL number are larger than $10 \mu\text{m}$.

4.5.3. Particle concentration

Particle concentration in freshly prepared samples of DOX-loaded MBs was $7.85 \pm 0.51 \times 10^9$ MB/ml. Compared to that, the average yield of DOX-loaded AAL was four decimal orders lower: $4.73 \pm 0.74 \times 10^5$ AAL/ml.

4.5.4. Effectiveness of DOX loading into MBs and AALs

Following, the effectively loaded amounts of DOX in phospholipid MBs and triacetin AALs will be outlined and the excipient burden of both formulations will be compared. *Excipient burden* will be defined as the mass ratio between the total formulation drug amount and the comprised excipients. *Effective loading amount* will be defined as the ratio between drug amount, encapsulated in MBs or AALs after their production, and the total drug amount in the formulation.

The experimentally determined effective DOX loading amounts of MBs and AALs are represented in Table 14. While in the case of MBs the larger part of the total drug amount was efficiently encapsulated in liposomes and consequently transferred into MBs, in AALs the encapsulation was not as effective. Since the DOX-base partitioning between triacetin and aqueous phase was rather unadvantageous only a small part of the entrapped amount was transferred into the AALs.

| | DOX-loaded MBs | DOX-loaded AALs |
|---|--|---|
| Total drug amount, [$\mu\text{g/ml}$] | 350 | 95 |
| Effective loaded amount, [% of the total drug amount] | 87.30 ± 2.78 | 22.53 ± 1.89 |
| Unbound DOX, [% of the total drug amount] | 10.65 ± 3.1 (~ 6% in residual liposomes and ~ 4.7% as free DOX) | 78.14 ± 2.73 (in form of free DOX or as residual triacetin droplets) |

Table 14: Phase distribution of DOX in optimal formulations of DOX-loaded MBs and DOX-loaded AALs.

The excipient burden of DOX-loaded AALs was about fifty times greater than for MBs. In the case of MBs the excipient burden was calculated to 6.49 and approximates the value of the

commercial DOX-loaded liposomes (Doxil[®], Ortho Biotech, Bridgewater, USA) having an excipient burden of 6.15. In the case of AALs, the excipient burden approached 312.51.

In summary, with regard to the loading efficiency phospholipid MBs were definitely more appropriate as targeted carriers for DOX than triacetin AALs. This can be mostly attributed to the low lipophilicity of DOX which made necessary complex formulation measures to be taken in order to retain the drug in the particles. Like in the case of paclitaxel [134] AALs might be appropriate carriers for more lipophilic anti-tumor drugs.

4.5.5. *In-vitro* acoustic destructibility of DOX-loaded MBs and AALs

The acoustic destructibility of DOX-loaded MBs and DOX-loaded AALs was compared with unloaded MBs and the commercial standard SonoVue[®] in order to select the better candidate formulation for further *in-vivo* studies. The corresponding single exponential decay curves of particle concentration vs. sonication time are represented on Figure 35.

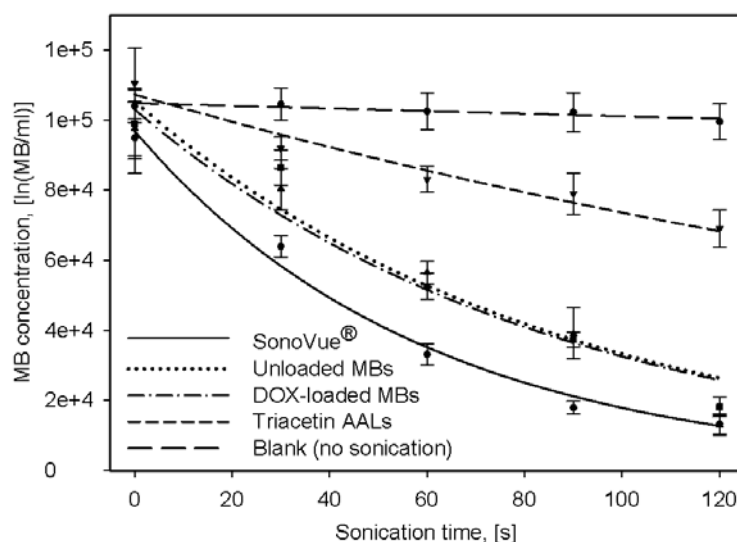


Figure 35: Ultrasound-mediated destruction of DOX-loaded MBs and AALs, compared to unloaded MBs and the commercial standard SonoVue[®].

After calculation of the sonication half-lives ($t_{1/2}$) for individual MB and AAL formulations (Table 15) they could be compared (Figure 36). The highest acoustic decay pace with a $t_{1/2}$ of about 41 s was shown for the commercial standard SonoVue[®]. In comparison to that, the decay of unloaded MBs ($t_{1/2} = 60.15$ s) and drug-loaded MBs ($t_{1/2} = 60.18$ s) was less rapid, having a small, but statistically significant difference to SonoVue[®] ($p < 0.0005$ for unloaded MBs and $p < 0.0001$ for DOX-loaded MBs). Interestingly, the difference between $t_{1/2}$

of unloaded and drug-loaded MBs was statistically insignificant ($p = 0.9893$). In this case, the presence of drug loading had no considerable effect on the MB acoustic destructibility.

| Formulation | R^2 | Initial population, a | Decay coefficient, b | Half-life, $t_{1/2}$, [s] |
|----------------------|--------|-------------------------|------------------------|----------------------------|
| Blank measurement | 0.8220 | $1.048 \times e^5$ | $3.622 \times e^{-4}$ | 1913 ± 0.9 |
| DOX-loaded AALs | 0.9605 | $1.073 \times e^5$ | $3.769 \times e^{-3}$ | 184.02 ± 3.12 |
| Unloaded MBs | 0.9363 | $1.030 \times e^5$ | $1.530 \times e^{-2}$ | 60.15 ± 2.63 |
| DOX-loaded MBs | 0.9450 | $1.053 \times e^5$ | $1.152 \times e^{-2}$ | 60.18 ± 1.32 |
| SonoVue [®] | 0.9894 | $9.693 \times e^4$ | $1.688 \times e^{-2}$ | 41.05 ± 1.83 |

Table 15: Coefficient of determination R^2 , decay function parameters, and half-life of different MB formulations during sonication at a frequency of 1 MHz and output intensity of 4 W/cm² (number of experiments, $n = 5$, number of measurements per experiment, $m = 3$).

In contrast, DOX-loaded AALs with $t_{1/2} = 184.02$ s were 4.5-fold less destructible than SonoVue[®], and 3.06-fold less destructible than DOX-loaded MBs which limited their applicability as potential drug-carrier candidates.

The loss of MBs due to stress factors in the *in-vitro* setup *e.g.* shear-stress, compression by the peristaltic pump, *etc.* was about a decimal order slower ($t_{1/2} = 1913$ s) than the slowest US-induced decay (those of triacetin AALs) and was considered negligible.

The observed slightly greater half-life of own DOX-loaded and unloaded MB formulations compared to SonoVue[®] might be explained with their different mean particle size maxima (2-3 μm for SonoVue[®] [132] and 0.9-1.0 μm for own formulations).

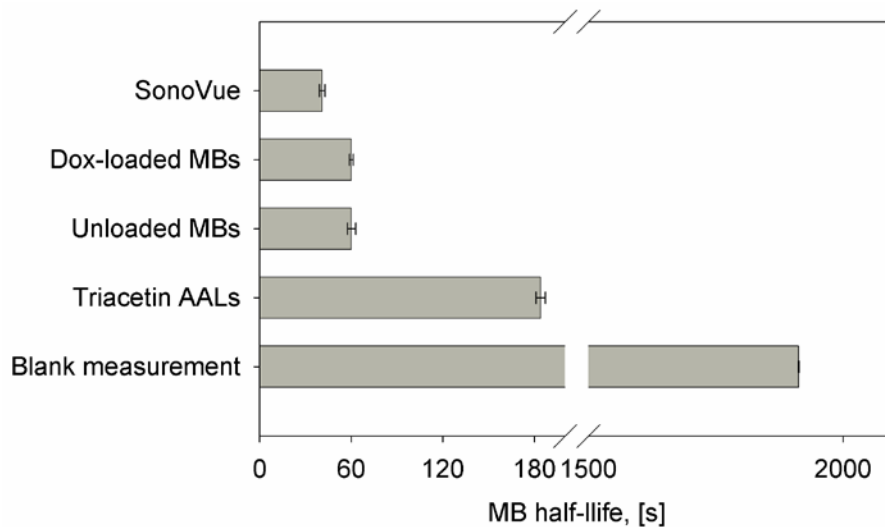


Figure 36: Half-life during US exposure of drug-loaded MBs compared to unloaded MBs, triacetin AALs and the commercial standard SonoVue®.

In conclusion, during the early formulation development and characterization of DOX-loaded phospholipid MBs and triacetin AALs, MB formulations obviously surpassed AALs with regard to their loading potential and acoustic destructibility. For this reason, DOX-loaded AALs were abolished from further studies.

4.5.6. *In-vivo* evaluation of the acoustic properties of DOX-loaded MBs

In rat's myocardium model DOX-loaded MBs produced a strong backscatter signal and allowed quantitative evaluation of the blood vessel replenishment (Figure 37).

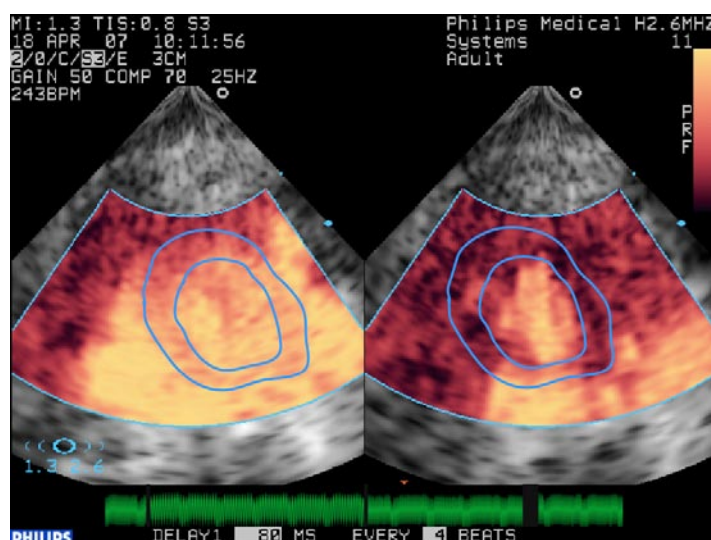


Figure 37: Backscattered signal contrasted image of rat's myocardium prior to MB destruction and immediately afterwards. The solid outline represents the approximate left myocardium margins.

DOX-loaded MBs possessed very good backscattering ability comparable to this of the commercial standard SonoVue® (Table 16). Their acoustic destructibility *in-vivo* was 1.75-fold higher than SonoVue® which correlated well with previous *in-vitro* results (refer to “4.5.5 *In-vitro* acoustic destructibility of DOX-loaded MBs and AALs”, p. 119).

| | SonoVue® | DOX-loaded MBs | DOX-loaded AALs | Unloaded MBs |
|-------------------------------|----------|----------------|-----------------|--------------|
| Opacification intensity, [dB] | 39.70 | 35.76 | 35.20 | 39.20 |
| Destructibility A, [%] | 40.74 | 70.01 | 58.85 | 63.73 |

Table 16: Opacification intensity, [dB] and acoustic destructibility A, [%] of DOX-loaded MBs compared to the marketed US contrast agent SonoVue[®].

4.5.7. *In-vivo* / *in-vitro* acoustic destructibility correlation

The acoustic destructibility data of *in-vitro* and *in-vivo* studies on DOX-loaded MBs, DOX-loaded AALs, unloaded MBs, and the marketed standard SonoVue[®] were ranked as shown on Table 17. The ranking coefficients ranged from 1 (best destructibility) to 4 (worst destructibility). In *in-vitro* studies the destructibility of DOX-loaded MBs did not significantly differ from that of unloaded MBs. Therefore, both formulations were ranked a coefficient of 2.

| Formulation | <i>In-vitro</i> acoustic destructibility half-life, [s] | <i>In-vitro</i> ranking | <i>In-vivo</i> acoustic destructibility, A, [%] | <i>In-vivo</i> ranking |
|----------------------|---|-------------------------|---|------------------------|
| SonoVue [®] | 41.05 ± 1.83 | 1 | 40.74 | 4 |
| DOX-loaded MBs | 60.18 ± 1.32 | 2 | 70.01 | 1 |
| DOX-loaded AALs | 184.02 ± 3.12 | 4 | 58.85 | 3 |
| Unloaded MBs | 60.15 ± 2.63 | 2 | 63.73 | 2 |

Table 17: Ranking of *in-vivo* and *in-vitro* acoustic destructibility data on DOX-loaded MBs and AALs, compared to unloaded MBs and the commercial standard SonoVue[®].

Within the properly formulated DOX-loaded MBs, DOX-loaded AALs, and unloaded MBs the ranking correlation was fulfilled with a coefficient of determination (R^2) of 0.7500 (Figure 38). SonoVue[®] deviated from own formulations and was therefore excluded from the correlation. Under physiologically close *in-vitro* conditions SonoVue[®] revealed the shortest half-life *i.e.* the highest acoustic destructibility, and was rendered a ranking coefficient of 1. In the animal model SonoVue[®] was the least destructible formulation and was ranked a coefficient of 4.

The difference of the acoustic behavior of SonoVue[®] under *in-vitro* and *in-vivo* conditions could be attributed to three major differences to the own formulations. Firstly, the mean size of SonoVue[®] is greater (2.5 μm) than that of the own MB and AAL formulations (1.2 μm). Furthermore, properly formulated MBs and AALs comprise gas cores of octafluoropropane, while in SonoVue[®] the gas is sulfur hexafluoride (SF_6). At last, the phospholipid composition of SonoVue[®] comprises a mixture of C16 (DPPG) and C18 phospholipids (DSPC) as well as single-chain surfactants (palmitic acid), while DOX-loaded MB shells consist solely of C16 phospholipids (DPPC, DPPG, and DPPE-PEG2000). The discrepancy could be possibly

overcome by employing a marketed standard which is closer to the tested formulations, e.g. Definity[®] (Bristol-Myers Squibb Medical Imaging, USA).

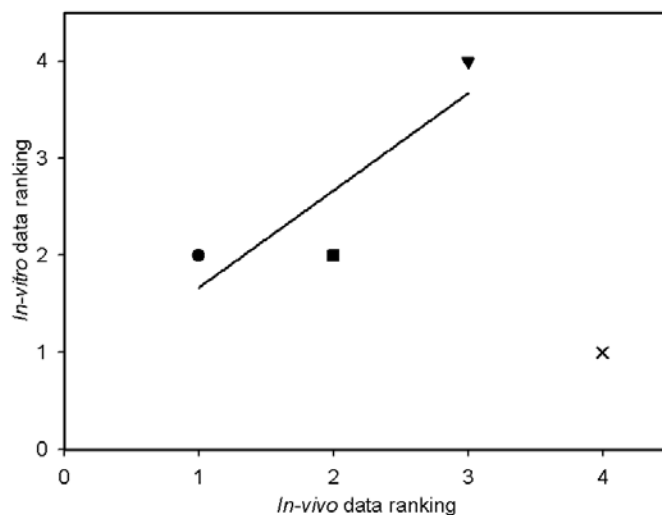


Figure 38: *In-vivo* / *in-vitro* ranking correlation between properly formulated DOX-loaded MBs (●), DOX-loaded AALs (▼), unloaded MBs (■), and the commercial standard SonoVue[®] (×).

Despite the deviating ranking data of SonoVue[®], the correlation between the properly developed DOX-loaded MBs, DOX-loaded AALs, and unloaded MBs was a substantial indication for the applicability of the physiological conditions acoustic transmission line (PCATL) *in-vitro* model as a useful tool for the early pre-clinical prediction of the *in-vivo* acoustic destructibility of newly established formulation candidates.

4.6. Therapeutic evaluation of doxorubicin-loaded microbubbles

4.6.1. Intracellular distribution of DOX after treatment with DOX-loaded MBs

The aim of the present study was to compare the intracellular uptake and partition of free aqueous DOX and DOX in complex with anionic phospholipids, as it is present in the MB shell. The complexation constant between DOX and anionic phospholipids is rather high in the order of $10^5 - 10^6 \text{ M}^{-1}$ [192] and is comparable to the DOX association constant with DNA – $2.4 \times 10^6 \text{ M}^{-1}$) [165]. Therefore, it could be presumed that in cells the complex of DOX with anionic phospholipids will have a less pronounced affinity to the nucleus than DOX in free form.

Mhawi et al. (2007) [198] observed the intracellular partition of DOX and demonstrated its localization in the nucleus, whereby the signal was concentrated at the nuclear periphery and on nucleoli. Furthermore, the authors suggested that DOX associates with the perinucleolar chromatin and the heterochromatin present near to the nuclear membrane.

In the present study similar results were observed with free DOX using comparable concentrations and incubation times as Mhawi et al. DOX was nearby thoroughly located in the cell nucleus as confirmed by the overlapping of DOX fluorescence and nuclear staining with Hoechst 33342 in 2D and 3D projections. Within the nucleus, DOX revealed a heterogeneous distribution, mostly near the nuclear membrane. At the middle of nuclei, numerous darker compartments were observed, corresponding apparently to the nucleoli.

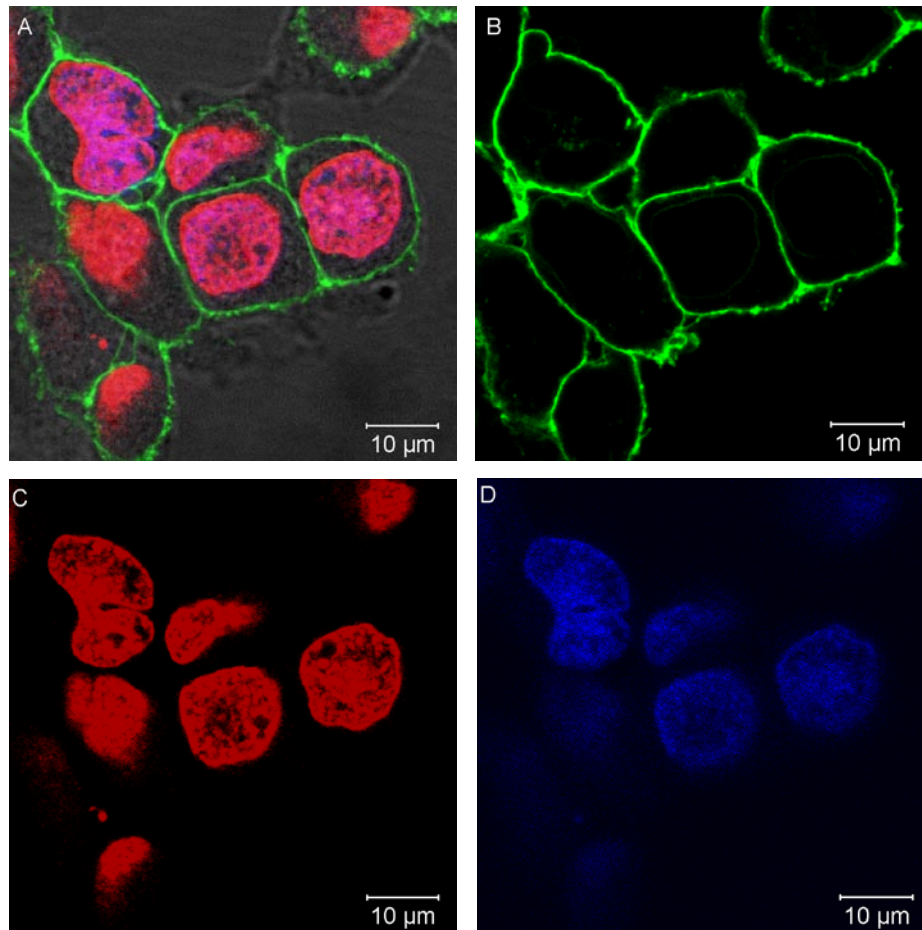


Figure 39: Confocal laser microscopy images of fluorescence labeled adherent cell cultures, treated with DOX-loaded MBs and US. A) Overlay image; B) Cell membrane staining; C) Intracellular partition of DOX; D) Nuclear staining.

Surprisingly, the DOX intracellular partition after application of DOX-loaded MBs and US (Figure 39) was not significantly differing from that of DOX in free form. The cell

membrane staining with Concanavalin A - Alexa Fluor[®] 488 conjugate (in green) allowed discriminating the cells' outlines. Cell nuclei were stained in blue with Hoechst 33342.

The intracellular partition of DOX (in red) in MB-treated cells coincided with the nuclear staining and no significant fluorescence was found in the cytosol.

These data also for the first time reveal the ability of DOX, complexed to anionic phospholipids, to enter the cell nucleus.

4.6.2. *In-vitro* evaluation of the anti-proliferative efficacy of DOX-loaded MBs

The purpose of this study was the proof of three concepts on human cell tumor cultures in an *in-vitro* model system:

- a) Does the complexation of DOX to anionic phospholipids inhibit its release and consequently its therapeutic efficacy?
- b) Do the DOX-loaded MBs provide a greater therapeutic activity than DOX alone or DOX-loaded liposomes?
- c) Provided there is an augmentation of the therapeutic activity through the interplay of US and DOX-loaded MBs, is this an additive or a synergistic interaction?

According to preliminary studies, applying US with a frequency of 1 MHz delivered a better efficacy than a higher frequency of 3 MHz. As expected, the cell viability also decreased with US intensity rising from 1 MHz to 4 MHz (data not shown). At the given US settings of 1 MHz frequency and 1 W/cm² output intensity the acoustic pressure, applied to the wells, was 0.283 ± 0.027 MPa without absorbing gel pad and sank to about 0.087 ± 0.32 MPa after the pad was laid under the well plate.

Experimental data revealed several comparisons, outlined in Figure 40. US alone did not have any effect on cell viability. Unloaded MBs in combination with US diminished cell viability to about $69.02\% \pm 5.93\%$ apparently because of cavitation effects. In the case of free DOX and DOX-loaded liposomes, the anti-tumor effect on cells was not affected by US and reduced cell viability in all cases to approximately 62-64%. The same impact was demonstrated also by DOX-loaded MBs without US. DOX-loaded MBs in combination with US produced a viability decrease down to $17.87\% \pm 1.95\%$.

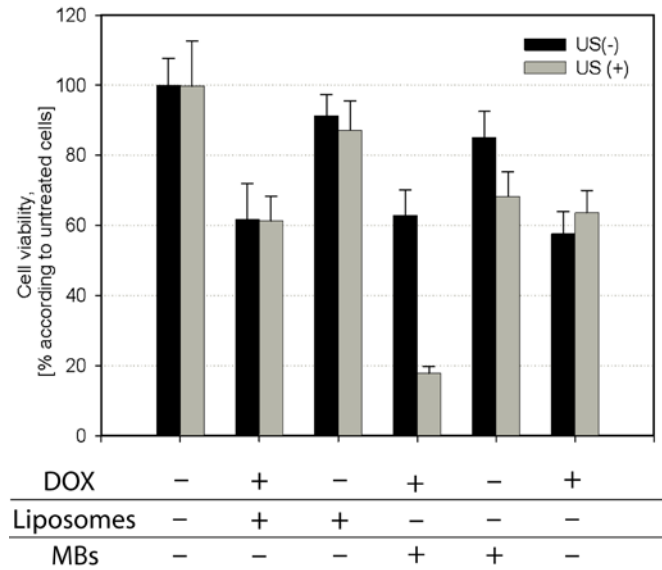


Figure 40: Metabolic activity in human tumor cell cultures, treated with aqueous, liposomal, and MBs-encapsulated DOX with or without application of US (n = 10).

In comparison, the combination of DOX-loaded MBs and US produced a 5.71 ± 1.48 fold reduction of cell viability (Figure 41). Free DOX produced only a moderate reduction (1.77 ± 0.46 fold) of cell viability. DOX-loaded liposomes had 1.68 ± 0.56 fold effectiveness and there was no statistically significant difference to free DOX. Nearby same activity as for DOX and DOX-loaded liposomes was found in the case of DOX-loaded MBs too (1.62 ± 0.43 fold), if they are not combined with US.

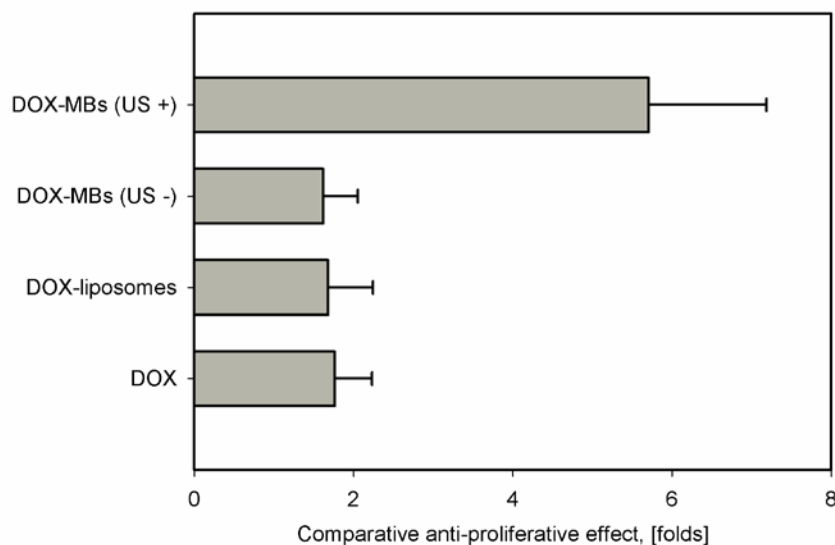


Figure 41: *In-vitro* anti-proliferative activity of DOX-loaded MBs with and without application of US compared to free DOX and DOX-loaded liposomes.

The obtained data indicated that there was no apparent reduction of DOX anti-tumor activity, resulting from its complexation to the anionic phospholipids. This was though expectable, regarding the high association constant (K_a) between cardiolipin and DOX ($1.6 \times 10^6 \text{ M}^{-1}$ at $25 \text{ }^\circ\text{C}$) which is comparable to K_a between DOX and DNA ($2.4 \times 10^6 \text{ M}^{-1}$) [165]. Therefore, a mass transfer competition of DOX between the anionic phospholipid and cell DNA and hence a reduced anti-proliferative efficacy were expectable.

Although unloaded MBs in combination with US possessed an intrinsic cell inhibition activity (1.49 ± 0.37 fold), the anti-proliferative effect of DOX-loaded MBs and US was about 1.75-fold greater than the additive inhibiting effect of aqueous DOX and unloaded MBs with US. Therefore, an about 150% mutual synergistic enhancement of DOX therapeutic activity has been achieved through its combination with US and MB carriers.

4.6.3. *In-vivo* evaluation of the targeting efficacy of DOX-loaded MBs

The ability of DOX-loaded MBs to specifically release and accumulate DOX in the target tumor site *in-vivo* after destruction with diagnostic US was evaluated. Briefly, rat models were implanted with two pancreas xenograft tumors on each back side. The test animals were infused intraarterially one dose unit of DOX-loaded MBs, comprising $140 \mu\text{g}$ active drug. Simultaneously, one of the back-side tumors was treated with diagnostic US in order to destroy MBs and to release DOX on the target site. The tumor on the other back-side became no US. Five minutes after the treatment the animals were sacrificed and the tumors were harvested along with the liver, the lungs, and the kidneys. The tumors and organs were homogenized and the amount of DOX was quantitatively determined by RP-HPLC with combined UV/Vis and fluorescence detection.

A total amount of $35.07\% \pm 5.14\%$ of the total injected dose of $140 \mu\text{g}$ DOX could be recovered from the analyzed tumors and organs. In sonicated tumors $7.65\% \pm 2.21\%$ of the injected DOX dose per gram tissue, [ID/g] were found, in contrast to $1.14\% \pm 1.02\%$ ID/g in tumors without US. Totally $23.59\% \pm 5.43\%$ ID/g of DOX were recovered from lungs, kidneys, and liver (spleen was not harvested). On the targeted tumor site a concentration of $10.15 \pm 2.96 \mu\text{g/g}$ DOX was achieved. Although DOX-loaded MBs have perfused US-negative tumors too, the drug concentration there was about 12-fold lower than in US-treated tumors ($p < 0.005$, Figure 42).

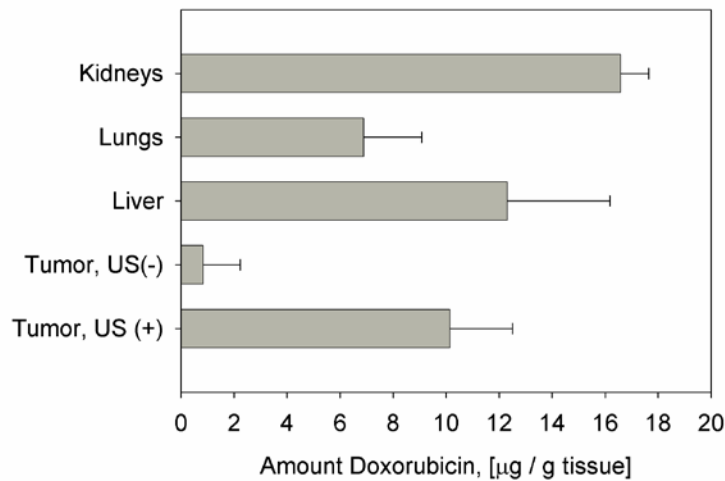


Figure 42: DOX distribution in US treated and untreated subcutaneous xenograft tumors in rats (n = 6). DOX concentrations in particle clearing organs such as kidneys, lungs, and liver are also represented. Average tumor weight was 194 mg to 511 mg.

In summary, DOX distribution could be effectively targeted towards the tumor site through US-triggered MB destruction. In tumors which became no US, DOX-loaded MBs promoted no significant drug release and accumulation. Thus, US has been proved as a necessary prerequisite for drug release and tissue accumulation from MBs. Upon interaction with diagnostic US, DOX-loaded MBs oscillate and are driven to fragmentation, if the US intensity surpasses their cavitation threshold. As a result of that, MB shell is fragmented [14]. The intensive mechanic effects of MB cavitation cause capillary fenestration and leakage of small MBs and shell debris into the interstitium, where they accumulate and exert their therapeutic effect.

Recently Tartis et al. (2008) [199] revealed that MBs demonstrate a specific pharmacokinetic profile different than that of liposomes. It was known that MBs can be actively taken up by phagocytosing cells such as monocytes, macrophages, Kupffer cells, *etc.* and captured in the organs of the reticulo-endothelial system – lung, spleen, and liver [200]. With regard to MBs, the spleen is one of the major clearing organs, since the typical MB diameter of 1-5 μm exceeds that of 200-500 nm narrow spleen channels [100, 201, 202]. Furthermore, a pronounced affinity to accumulation in the spleen and the liver could be expected from DOX-loaded MBs, since this is characteristic for the related anionic DOX liposomes [203]. Therefore, although the spleen was not considered for analysis in this study, a significant portion of DOX could be expected to be found there.

Similarly to the spleen, the lungs also have the property to size-specifically clear larger MBs which could be the reason the small portion of larger MBs, present in the formulations, to be retained there.

It is extremely difficult to make conclusions about the MB pharmacokinetics based only on this limited study, mainly because of the different distribution and uptake mechanisms of MBs and shell fragments. Nevertheless, next to its main goal, the above *in-vivo* study helped identify some of the important elimination sites for DOX-loaded MBs.

The obtained *in-vivo* and *in-vitro* data revealed the excellent acoustic properties of the novel DOX-loaded MBs, developed in this work, which were comparable with clinically recognized MB products (SonoVue[®]). Furthermore, the own DOX-loaded MBs possessed an over 3.2-fold increase of the therapeutic activity in cell cultures due to the synergistic action between DOX and US. The targeting efficacy of the combination of DOX-loaded MBs and diagnostic US was demonstrated *in-vivo* by the over 12-fold accumulation of DOX into US-treated tumors in comparison to tumors which became no US. These promising results give green light to further-going clinical studies which could demonstrate the therapeutic efficacy of this novel targeted tumor therapy by assessing the progression of tumor growth and the survival rate of animal models.

5. Summary and outlook

In the present chapter, two drug delivery systems for targeted tumor therapy which release their active load in response to US, have been developed and evaluated. Soft-shelled phospholipid MBs and triacetin AALs, having a more robust shell, were loaded with DOX and their acoustic destructibility was tested using an optimized *in-vitro* model. Since the acoustic properties and loading ability of DOX-loaded MBs exceeded these of the triacetin AALs, the development of phospholipid MBs was promoted into *in-vitro* tissue culture studies and accordingly into *in-vivo* studies.

Within the phospholipid monolayer-shelled MBs, the cationic doxorubicin (DOX) was complexed by electrostatic interactions to an anionic phospholipid – dipalmitoyl phosphatidylglycerol (DPPG). Furthermore, the complex was stabilized by additional hydrophobic attractions. In the case of DOX-loaded AALs the drug was turned more lipophilic by transforming its hydrochloride salt into free base. DOX was further included into the oil layer of glycerol triacetate (triacetin), comprising the AALs. Both candidates – DOX-loaded MBs and DOX-loaded AALs, were compared under *in-vitro* and *in-vivo* conditions and the more appropriate of them – the phospholipid MBs, was launched into clinical studies. DOX-loaded MBs were preferred rather than the triacetin AALs mainly for their much better echogenicity and acoustic destructibility, demonstrated *in-vitro* as well as *in-vivo*.

Anionic phospholipid MBs possessed superior loading potential for DOX reaching almost 90% of the total drug amount. The excipient burden, calculated on the basis of the mass concentrations of DOX and total phospholipid, was 6.49 which value approximates that of the commercially available DOX-loaded liposome product Doxil[®] (Ortho Biotech, Bridgewater, USA). The *in-vivo* US contrasting efficacy of DOX-loaded MBs was close to that of the commercial US contrast agent SonoVue[®] (Bracco International, B.V., The Netherlands) while their acoustic destructibility even surpassed the positive control by 175%.

In-vitro studies on the therapeutic efficacy of DOX-loaded MBs in tissue cultures revealed a 3.2-fold increase of therapeutic activity compared to free DOX and DOX liposomes (n = 10). *In-vivo* studies in subcutaneous xenograft tumor models in rats demonstrated an about 12-fold accumulation of DOX in US-treated tumors, compared to tumors which became DOX-loaded MBs but no US (n = 6, p < 0.005).

Further *in-vivo* studies in rat tumor models are foreseen in order to assess the therapeutic potential of DOX-loaded MBs by monitoring the pace of tumor growth. As a step forward, DOX-loaded MBs will be tested in large animal models.

In summary, DOX-loaded MBs brought at least three important advantages in comparison to current administration forms for this anti-tumor agent. Firstly, because of their backscattering properties DOX-loaded MBs can act as contrast agents and aid tumor visualization. Furthermore, DOX-loaded MBs provide specific drug targeting which can be externally controlled by the clinician. Furthermore, apparently because of the ability of MBs in combination with US to enhance the permeability of capillary endothelium and cell membranes, DOX-loaded MBs demonstrated an about 150% synergistic augmentation of the therapeutic efficacy *in-vitro* compared to free DOX and DOX-loaded liposomes. At last, MBs are generally considered blood-pool agents because of their size. Therefore, similarly to liposomes they obviously can reduce the distribution volume of DOX to that of blood plasma.

V. CHAPTER: Ultrasound targeted gene therapy

1. Abstract

Microbubbles (MBs) have become an established instrument as injectable contrast agents in diagnostic ultrasound (US) imaging. More recently, their potential as carriers for the targeted gene therapy has been revealed. After intravenous injection MBs can be destroyed by applying US, thus releasing their bioactive load directly at the target site. In the following work newly developed MB gene carriers will be presented, having phospholipid shells decorated with DNA-bearing polyplexes.

Polycationic amphiphilic conjugates (bPEI-PA) of palmitic acid (PA) and branched polyethylenimine (bPEI) were synthesized through covalent amide binding. Conjugates were synthesized using bPEI with various molecular weights of 1.8 kDa, 10 kDa, and 25 kDa. Furthermore, the conjugates were grafted with different amounts of PA. After purification, the successful conjugation of polyethylenimine and palmitic acid was confirmed by ^1H and ^{13}C NMR. The complexing capacity of bPEI-PA for plasmid DNA was demonstrated by an ethidium bromide fluorescence quenching assay and the optimal nitrogen-to-phosphorus ratio was determined for each conjugate.

In order to formulate MBs, polycationic liposome precursors were produced from C16-phospholipids (DPPC and DPPE) and bPEI-PA. The liposomes were loaded with plasmid DNA by incubation at room temperature. Following, they were placed into appropriate vials, covered with octafluoropropane gas and mechanically agitated at a high speed. The resulting polyplex-associated MBs were characterized in their particle size distribution (using laser diffraction), concentration (using light blockage) and structure (using confocal scanning laser microscopy). The anchoring of bPEI-PA conjugates into the MB shell and the successful loading of pDNA onto the MB surface were confirmed by fluorescence confocal laser scanning microscopy observations. Polyplex-loaded MBs had a size-distribution from 800 nm to 4 μm and concentration of approximately 7×10^9 MB/ml.

MB transfection efficacy upon exposure to US was demonstrated in comparison to polyplexes, polycationic liposomes on human tissue cultures using the luciferase assay. Additionally, cell metabolic activity after transfection was assayed. Comparative *in-vitro* studies on the polyplex transfection efficacies of bPEI-PA conjugates with various molecular weights and PA grafting ratios were carried out next. One candidate out of seven – bPEI 10 kDa, grafted with 12 PA molecules, showed appropriate transfection rates which were comparable to the positive standard bPEI 25 kDa, and superior cell viability.

The optimal candidate bPEI10-PA12 was used to produce polyplex-loaded MBs which were also tested on human cell cultures under exposure to US. However, no significant increase of transfection was observed which confirmed the findings of previous studies that colloidal particles such as the polyplexes cannot be transported across the cell membrane by means of sonoporation [33].

Keywords: gene therapy, drug targeting, polyplexes, ultrasound contrast;

Abbreviations: bPEI – branched polyethylenimine, PA – palmitic acid, RES – reticulo-endothelial system, SC – secondary carriers, scMBs – secondary-carrier associated microbubbles, UTMD – ultrasound-targeted microbubble destruction, US – ultrasound, PCL – polycationic liposomes, DPPC – dipalmitoyl phosphatidylcholine, DPPE – dipalmitoyl phosphatidylethanolamine;

2. Introduction

Initially, gene therapy had the purpose to treat inherited diseases by replacing defective genes with their normal copies. Nowadays the scope of potential applications has broadened to include also defeating of many “civilization diseases” like cancer and atherosclerosis.

Modern gene therapy puts several requirements on the development of gene delivery approaches which are on the first place supposed to achieve therapeutically relevant levels of gene expression, as well as to provide optimal spatial and temporal profiles of gene expression in the organism. Under *in-vitro* and *ex vivo* conditions gene transfection by means of physical, chemical and viral methods has become routine, however *in-vivo* implementations remain a hurdle. On its way to the nucleus, the genetic material encounters several specific physical and chemical barriers such as the digestion by serum nucleases, the capillary endothelium and the cell membrane, the endosomal degradation, and at last the nuclear membrane.

Various procedures have been established for the *in-vivo* gene transfer [204] which are ideally supposed to meet the following criteria:

- to carry and protect the genetic material from elimination by the *reticulo-endothelial system* (RES), degradation by serum nucleases, or endosomal degradation;
- to attain adequate cell transfection rates and a relevant therapeutic response;
- to enable site-specific gene delivery through targeting;
- to have an optimal safety profile including carrier agglomeration through serum proteins, immunological aspects, cytotoxicity, *etc.*

Despite the versatility of the nowadays known gene delivery approaches, only 2.4% from over 1,300 clinical trials conducted worldwide since 1989 have been moved into phase III, and to date no gene therapy product has been approved [205]. Although gene therapy holds the promise for ameliorating and curing diseases which are resistant to conventional treatments it is still limited by the lack of effective and safe gene carriers.

Up to now, the most effective and sustainable gene expression has been attained by using attenuated viruses that cannot replicate and cause diseases, but remain capable of delivering exogenous DNA into cells. Viral vectors, however, still bear considerable safety concerns because of the possibility of genetic mutations, immunogenic reactions and potential pathogenicity [206]. Furthermore, many viral vectors have only a limited capacity to envelop larger transgene molecules [207] and lack target specificity [56].

These drawbacks of viral vectors led to an increasing interest in developing nonviral gene carriers, such as gelatin nanoparticles, lipoplexes, and polyplexes [208]. The colloidal nonviral gene carriers are widely considered biologically safe compared to the efficient, but risky viral vectors. On the other side many nonviral carriers still lack targeting potential and transfection activity. Particularly the complexes of DNA with polycationic polymers – polyplexes, are currently considered the most effective nonviral gene carriers, approaching in some applications the activity of viral vectors.

About nine years ago Shohet et al. (2000) [209] demonstrated for the first time the outstanding targeting potential of a novel class of nonviral gene carriers – the *microbubbles* (MBs) which can be specifically targeted to target tissues and organs through external triggering by *diagnostic ultrasound* (US). This approach was denoted in the literature as *ultrasound-targeted microbubble destruction* (UTMD).

Numerous authors have shown the effective gene targeting and optimal *in-vivo* safety profile of MBs, obtaining a therapeutic effect over time periods as long as thirty days or more [73, 128, 227, 228]. As a further advantage the MBs enable the visualization of the target site as they backscatter diagnostic US and act as contrast agents. However, MBs are still limited in their loading capacity, since more than 80-90% of their volume comprises of gas (Table 18). Therefore, it is a challenge for the current research to find solutions to enhance the MB gene loading and / or to improve their *in-vivo* transfection efficacy.

| Author | Approximate amount of DNA loading, [pg/ μm^2] | MB type | Therapeutic/reporter transgene |
|----------------------------------|---|--|------------------------------------|
| Frenkel et al. (2002) [210] | 2.4 | PESDA | CMV-LacZ pDNA |
| Borden et al. (2007) [113] | 0.1 | PLL/DNA layer-by-layer phospholipid-MBs | SV40-Luc pDNA |
| Bekeredjian et al. (2003) [56] | 0.023 | DPPC/DPPE-based phospholipid-MBs | CMV-Luc pDNA |
| | 0.011 | HSA-shelled MBs | |
| Chen et al. (2003) [211] | 0.018 | DPPC/DPPE-based phospholipid-MBs | CMV-Luc pDNA |
| Chen et al. (2006) [212] | 0.004 | Lipofectamine 2000-associated DPPC/DPPE-based phospholipid-MBs | RIP-Luc and RIP-human insulin pDNA |
| Lentacker et al. (2006) [66] | 0.004 | Poly-allylamine hydrochloride/DNA layer-by-layer HSA MBs | SV40-Luc pDNA |
| Christiansen et al. (2003) [117] | 0.002 | DSPC/DPTAP-based cationic phospholipid-MBs | CMV-Luc pDNA |

Table 18: Amounts of DNA loaded on MBs by a number of research groups. The loaded amounts are represented as mass per MB surface area. PESDA – perfluorocarbon-exposed sonicated dextrose albumin MBs; LacZ – nuclear localized β -galactosidase; SV-40 – simian virus 40 promoter; CMV – cytomegalovirus promoter; RIP – rat insulin 1 promoter; Luc – luciferase coding plasmid; HSA – human serum albumin; DPPC – dipalmitoyl phosphatidylcholine; DSPC – distearoyl phosphatidylcholine; DPPE – dipalmitoyl phosphatidylethanolamine; DPTAP – dipalmitoyl phosphatidyltrimethylaminopropane; PLL – poly-L-lysine.

In the present work a promising novel concept was developed for the first time. It combines the targeting potential of US triggered gene delivery with MBs with the high loading and transfection efficacy of polyplexes. A novel MB construct of the structure class of *secondary-carrier associated MBs* (Figure 2 D, p. 19) was developed. Its phospholipid shell is decorated with DNA-loaded polyplexes, comprising an amphiphilic conjugate of polyethylenimine and palmitic acid. The polyethylenimine conjugate is able to bind and condense DNA and to protect it from serum degradation, as well as to mediate its cellular uptake and delivery into the cytosol and the nucleus. The polyplexes are anchored onto the MB shell due to the hydrophobic interaction between their palmitoyl residues and the phospholipid acyl chains of the shell monolayer. In this way the interplay of MBs and diagnostic US is responsible for the target site visualization, for the overcoming of the capillary endothelium, and for the site specific gene delivery. On their side, the polyplexes protect the gene material from serum degradation, and mediate the cell uptake on the endosomal pathway, as well as the endosomal escape and trafficking of DNA into the nucleus.

2.1. Amphiphilic conjugates of polyethylenimine

The polycationic polymer polyethylenimine (PEI) was originally introduced as gene transfection agent by the research group of Jean-Paul Behr [213] and represents one of the most significant excipient for polyplex compositions at the moment. Compared to other polycations, PEI has the distinct advantage of the highest positive charge density since every third atom in its structure is potentially protonable.

Like the most non-viral gene carriers PEI polyplexes have their optimal transfection efficacy when the particles present an overall net positive Zeta potential. This is provided by the excess of cationic charges through protonated PEI nitrogen atoms with respect to the anionic DNA phosphate groups and is expressed as the molar ratio of nitrogen to phosphor (*N/P ratio*).

Although the polyplex net cationic charge is assumed to be necessary for interactions with cell membranes [214, 215], it also poses problems when polyplexes are administered systemically. Cationic complexes are not only able to agglutinate erythrocytes [216], but also interact with many anionic blood proteins such as albumin [217]. Additionally, the positive charge of PEI/DNA complexes triggers their opsonization by the RES and leads to their rapid clearance from circulation within a few minutes. As a result polyplexes accumulate mainly in RES organs such as the liver, the spleen, and the lungs [218, 219].

As known, the ability of PEIs to condense DNA increases with their molecular weight within certain limits with an optimum between 5 kDa and 25 kDa [220]. However, especially high molecular weight PEIs are hardly biodegradable [221] which in turn increases their cytotoxicity and renders them dubious for repeated *in-vivo* application [222, 223]. In contrast, low-molecular weight PEIs possess a low cytotoxicity *in-vitro* [224], but mostly cease to condense DNA and form small polyplexes.

In order to improve the biodegradability of PEI-based vectors, attempts were made to bundle several PEI molecules with lower molecular weight (in the order of 600 to 10,000 Da) to larger structures which are yet biodegradable and less toxic, but possess a better ability to condense DNA. This have been done by either forming of biodegradable covalent bridges [221, 225] or by forming of non-covalent associates. These strategies increase the capability of low-molecular weight PEIs to condense DNA by bundling several small molecules into a larger associate and lower the polyplex cell toxicity since the associates are better biodegradable than the high-molecular weight PEI.

Recently, numerous authors have developed amphiphilic conjugates of low-molecular weight PEI which are able to form micelles and liposomes by either self-association or by co-

association with phospholipids. For the first time Yamazaki et al. (2000) [226] developed polycationic liposomes comprising cetylated branched PEI and demonstrated that they surmounted conventional cationic liposomes in terms of higher transfection activity and lower cytotoxicity. Further on, both water soluble and hydrophobic conjugates with cholesterol [236-238], palmitic acid [227], myristic acid [228], lauric acid [229], or cetyl alcohol [230] of linear and branched PEI (bPEI) were developed. In many studies, bundling of low-molecular weight PEIs into micellar or liposomal associates increased the transfection activity up to a factor of 400 [229] or lowered the *in-vitro* cytotoxicity down to 10-fold [231]. However, since the research data on amphiphilic PEI conjugates and polycationic liposomes is still insufficient, a broad scope to develop their potential as gene carriers is available.

2.2. Microbubble-mediated gene therapy

Gene transfer with MBs is widely considered safe and organ specific [3, 232]. Numerous *in-vitro* and *ex vivo* studies have shown that *ultrasound-targeted microbubble destruction* (UTMD) can enhance transfection rates from 10-fold [18] up to 3,000-fold [233] compared to naked plasmid DNA (pDNA). High transfection rates of approximately 1,000-fold over pDNA were measured with reporter genes under *in-vivo* conditions [234]. However, therapeutically relevant *in-vivo* transfection is more difficult to achieve.

Most *in-vivo* transfection studies focus on tissues and organs that have already been studied previously using US contrast imaging, including the heart [18, 56, 229, 254], the brain [48, 50], the kidneys [235, 236], the pancreas [212], skeletal muscles [127, 259-261], the liver [237, 238], and solid tumors [239]. Many experimental treatments were also directed against vascular dysfunctions, such as intimal hyperplasia or ischemia (Table 19). A rather intensive gene expression could be achieved *in-vivo* and even therapeutically relevant levels were reached [238]. However, in most applications the gene expression persisted for a relatively short time period of several days up to a month. In contrast to virus-mediated transfection, sonoporation with MBs is considered to deliver genetic material only to the cytoplasm where the plasmid copies are not replicated, and either vanish during cell proliferation or are fragmented by enzymes [42]. A greatly prolonged and specifically targeted transfection has been achieved through combining of adeno-associated viral vectors with phospholipid MBs [42, 65]. So far, expression levels and sustainability are still under investigation, and the clinical applicability of gene therapy with MBs has not yet been proven.

| Author | Target disease | MB / transgene | Animal model | Therapeutic effect | Duration |
|-------------------------------|----------------------------------|--|--------------|---|-----------|
| Porter et al. (2001) [240] | Carotid intimal hyperplasia | PESDA / synthetic antisense oligodeoxynucleotide | Pig | Significantly reduced stenosis formation | n.a. |
| Chen et al. (2006) [212] | Diabetes | Lipoplex-coupled MBs / RIP-hexokinase I pDNA | Rat | 30% decrease of serum glucose | ≥ 5 days |
| | | Lipoplex-coupled MBs / RIP-human insulin pDNA | | 20% decrease of serum glucose at day 5, 10% at day 10 | ≥ 10 days |
| Akowuah et al. (2005) [233] | Saphenous vein hyperplasia | BR-14 [®] / TIMP-3 pDNA (co-administration) | Pig | 60.5-65.6% enhancement of lumen area | ≥ 28 days |
| Korpanty et al. (2005) [241] | Myocardial ischemia | Lipoplex-coupled MBs / hVEGF ₁₆₅ pDNA | Rat | 33% increased capillary density, 86% increased alveolar density | 30 days |
| Leong-Poi et al. (2007) [118] | Skeletal muscle ischemia | Cationic phospholipid-MBs / hVEGF ₁₆₅ pDNA | Rat | Approximately 2-fold increase in normalized microvascular blood flow | 42 days |
| Zhigang et al. (2004) [242] | Myocardial ischemia | Quanfuxian / VEGF pDNA | Rat | 80% increase in capillary density | n.a. |
| Lan et al. (2003) [236] | Tubulo-intestinal renal fibrosis | Optison [®] / SMAD7-encoding pDNA (co-administration) | Rat | 85% reduced tubulointerstitial myofibroblast accumulation, 60 to 70% reduced collagen synthesis | ≥ 7 days |
| Sakakima et al. (2005) [237] | Hepato-cellular carcinoma | BR-14 [®] / IFN β pDNA (co-administered intratumoral injection) | Mice | 3 to 4 times reduced tumor growth | ≥ 42 days |
| Miao et al. (2005) [238] | Hemophilia | MBs / human Factor IX-encoding pDNA | Mice | 66-fold increase vs. naked pDNA, up to 63 ng/ml Factor IX (near therapeutic range) | n.a. |
| Negishi et al. (2008) [243] | None (model expression of GFP) | Phospholipid MBs / GFP-targeting siRNA | Mice | Gene silencing in the tibialis muscle after intradermal injection of 30 μ g siRNA | ≥ 21 days |

Table 19: *In-vivo* UTMD-mediated gene therapy for specific diseases and estimations of the therapeutic effects.

PESDA – perfluorocarbon-exposed sonicated dextrose albumin MBs; TIMP-3 – tissue inhibitor of metalloproteinase 3, hVEGF₁₆₅ – human vascular endothelial growth factor 165, RIP – rat insulin 1 promoter, SMAD7 – an intracellular key-mediator of signaling, IFN β - interferon beta, GFP – green fluorescent protein, siRNA – small interfering RNA; n.a. – not available.

In conclusion, several recent studies have demonstrated the therapeutic potential of MB-based gene therapy. However, the *in-vivo* application of UTMD still requires a greater understanding of the optimal US parameters, MB pharmacokinetics, and the applicability of the co-administration of genetic material and MBs compared to the gene-loading of MBs. The pharmaceutical formulation of disease-specific therapeutic MBs could make advanced clinical studies and product development possible.

2.3. Gene delivery by secondary carrier-associated microbubbles

About three years ago the idea of using drug-loaded nanoparticles, liposomes, or lipoplexes, associated with MBs, has been introduced by Lum et al. (2006) [64]. For the first time this particular hybrid class of MB carriers has been denoted as *secondary-carrier associated MBs* (scMBs) in several recent review articles [244, 245]. Secondary-carrier MBs are believed to have an increased loading capacity and to protect genetic material from degradation by serum enzymes.

The *secondary carriers* (SC) are usually nanometer-sized particles such as liposomes, solid nanoparticles, lipoplexes, polyplexes, *etc.*, decorating the outer MB surface and bearing the effective payload of *e.g.* oligonucleotides, siRNA, or pDNA. Previous research suggests that nanoparticles can hardly be introduced into the cytosol using sonoporation due to their large size (Table 2, p.21), but they can pass through the UTMD-perforated capillary endothelium. Therefore nanoparticulate SCs are supposed to possess an intrinsic transfection potential in order to further mediate the transfection on a cellular level.

The idea behind the concept of scMBs is to make use of the MB potential to produce capillary perforations and facilitate the extravasation of colloidal particles (Figure 43). After the intravenous application of scMBs they can be excited by low-intensity US (black solid lines) and back-scattered signal (grey dashed lines) can be detected, aiding the visualization of scMBs on the target site. A subsequent higher-intensity US pulse (red solid lines) destroys the MBs, thus releasing the SCs (red dots) and perforating capillary walls at the same time. Further on, SCs are promoted into tissue interstitium by the hydrodynamic blood pressure and get in contact with tissue cells. Due to their intrinsic transfection capacity, SCs can be taken up by the cells and deliver the genetic material into the cytosol and the nucleus. The intracellular SC trafficking and endosomal release may follow different pathways depending on the nature of the particular carrier.

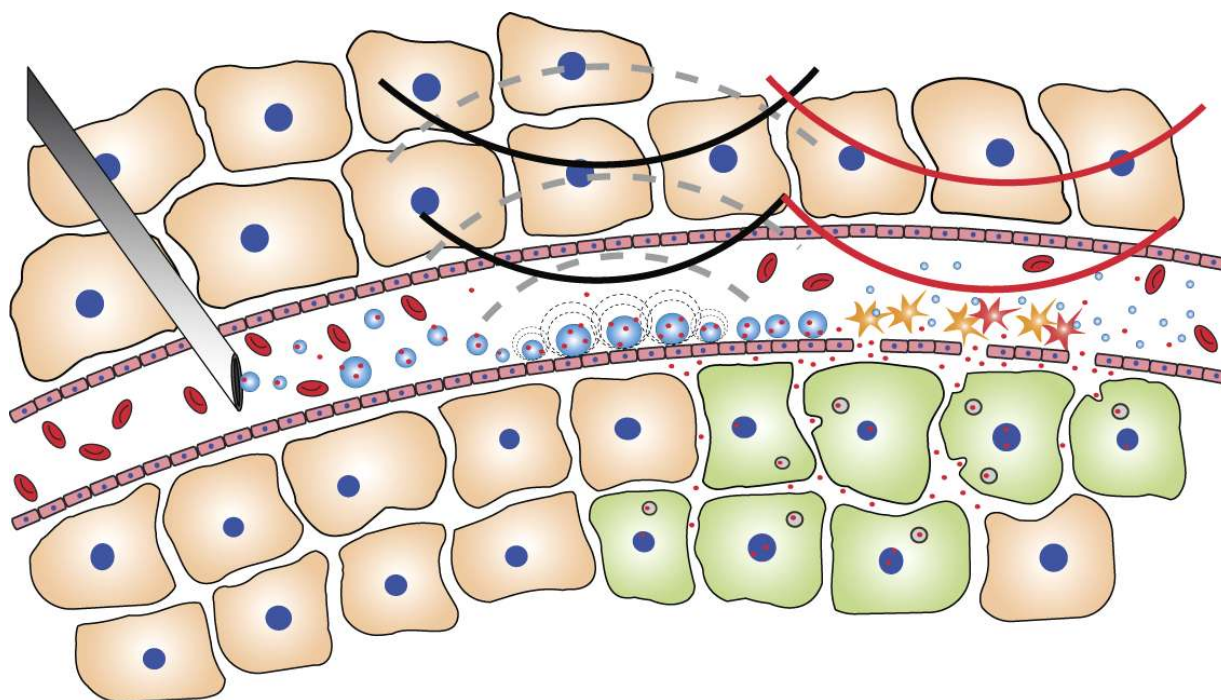


Figure 43: Mechanism of action of secondary carrier-associated MBs (scMBs). After their application, the MBs can be excited by low-intensity US (black solid lines) and visualized by their US backscattered signal (grey dashed lines). Following, they can be “burst” by high-intensity US (red solid lines), perforate capillary walls and simultaneously release the secondary carriers (red dots). Following, the nanoparticles penetrate the interstitium and can be taken up by tissue cells. Transfected cells are represented in green.

The *in-vivo* action mechanism of scMBs combines advantages of both MBs and nanoparticulate gene carriers. On the one hand, MBs are echogenic *i.e.* they act as US contrast agents and can be visualized on the target site using diagnostic US. Furthermore, the release of genetic material can be externally triggered and directed with high precision, allowing an effective site targeting. In addition to that, the utilization of SCs can increase the loading capacity of MBs. SCs can also protect the genetic material from serum degradation, facilitate its endosomal escape, and direct the gene transfer into the nucleus.

Up to now, several authors have described MB constructs, carrying several orders of magnitude smaller particles which can be denoted as scMBs. For the first time Lum (2006) [64] demonstrated the loading of phospholipid MBs with fluorescent latex nanobeads as model drug carriers. The authors showed the ability of the new construct to induce deposition of the model nanoparticles under *in-vitro* conditions. Kheirilomoom et al. (2007) [246] described phospholipid MBs associated with liposomes, loaded with a model fluorescent substance and studied their oscillation behavior during exposure to US using high-speed photography. Furthermore, the authors demonstrated that liposome-associated MBs can be focused on a cell culture monolayer and the fluorescent dye

can be internalized into the cells within the US field. All of the above strategies of direct loading of particles to pre-formed MBs exploit the linking either through avidin-biotin couples, or by neutravidin-biotin linkage. Although this is a very efficient approach, it bears concerns for *in-vivo* applications due to the significant immunogenicity of the avidin-biotin pair [247].

In their patent Schneider et al. (2007) [248] also described phospholipid MBs associated by electrostatic attractions with micelles or liposomes which may carry active drug substances.

A MB structure design, related to the scMBs, was implemented by Lentacker et al. (2006a and b) [249, 250] and Borden et al. (2007) [113] through layer-by-layer covering with poly-L-lysine and DNA of pre-formed albumin- or phospholipid-shelled MBs. Though this is in fact no nanoparticle loading on MBs, the biological mechanism of action of such MBs would be similar to scMBs since biologically active shell fragments are shed off during the MB destruction.

Lentacker et al. (2007) [251] thoroughly fulfilled the concept of scMBs by developing lipoplex-associated phospholipid MBs, loaded with plasmid DNA. The lipoplexes were loaded with gene material and possessed own transfection activity, demonstrated in cell cultures.

Several other authors like Korpanty et al. (2005) [241] and Chen et al. (2006) [212] combined phospholipid MBs with lipoplexes of Lipofectamine[®] (Invitrogen Molecular ProbesTM, Eugene, USA) and tested them in rat models. However, the authors did not provide evidence if the lipoplexes were physically attached to the MB shell.

In the present work, a novel hybrid gene vector comprising polyplex-associated scMBs has been developed for the first time. In this case, the polyplexes play the role of SCs, as they possess an intrinsic transfection activity and are able to condense and protect the DNA. While the MBs are responsible for the site specific targeting and the permeabilization of small blood vessels, the MB shell fragments mediate the further cellular uptake, the endosomal escape, and the gene transfection. The proposed MB structure design circumvents the *in-vivo* concerns related with the use of avidin-biotin complexes.

The polyplexes comprise an amphiphilic covalent conjugate of branched PEI with palmitic acid (bPEI-PA) and are associated to the MB shell through hydrophobic interactions between the PA residues and the phospholipid acyl chains in the shell monolayer.

Different branched PEIs with molecular weights of 1.8 kDa, 10 kDa, and 25 kDa were considered in this study. The bPEIs were covalently conjugated with various amounts of palmitic acid and the chemical structure of the bPEI-PA conjugates was characterized.

For the formulation of polycationic liposomes (PCL) comprising bPEI-PA, an established combination of two zwitterionic phospholipids – dipalmitoyl phosphatidylcholine (DPPC) and dipalmitoyl phosphatidylethanolamine (DPPE), was implemented. Since the colloidal stability of mixed bilayers of DPPC and DPPE was impaired by their net negative lyotropic curvature, formulation studies were performed to improve the stability of such liposomes. The miscibility of bPEI-PA and binary DPPC / DPPE mixtures was characterized and polycationic liposomes were formulated as precursors for the production of scMBs. The ability of the bPEI-PA / phospholipid liposomes to condense DNA and protect it from degradation by serum nucleases was further demonstrated. The bPEI-PA candidates, having different molecular weights and substitution rates with palmitic acid, were then screened for their capability to form small complexes with pDNA, as well as for their high transfection activity and low cytotoxicity. The most suitable candidate was used to formulate pDNA-loaded polyplex-associated scMBs. In prospective development, the optimal formulation of pDNA-loaded polyplex-associated MBs will be launched into *in-vivo* studies in order to prove their US backscattering ability, biocompatibility, transfection activity, and targeting potential.

A novel formulation strategy for MBs was also described in this work, called *liposomal-controlled microbubble production* (LCMP). It implicates the direct one step production of gene-loaded MBs through pre-formulation of liposomal intermediates, comprising both the necessary gene material and the excipients, covered with the core gas within a single vial. The MBs are produced by a short high-speed mechanical agitation and are immediately ready for administration.

The LCMP strategy involves the establishing of a relation between the pharmaceutical properties of the liposomal intermediates and the MBs, produced from them. This allows the tuning of the MB properties such as size, yield, loading, and stability, by manipulating the pharmaceutical features of the liposomal precursor formulations. The major advantage of this approach is that the resulting product allows a straightforward application on the patient's bed side in contrast to the loading of pre-formed MBs, bringing considerable complications such as MB instability, microbial contamination, *etc.*

The biological action mechanism of the bPEI-PA polyplex-loaded scMBs on the tissue level is identical with the other scMBs, described above (Figure 43, p.141). Nevertheless, on the cellular level the action of small polycationic liposomes and micelles, produced after the US-mediated “bursting” of the MB shell, is rather complex.

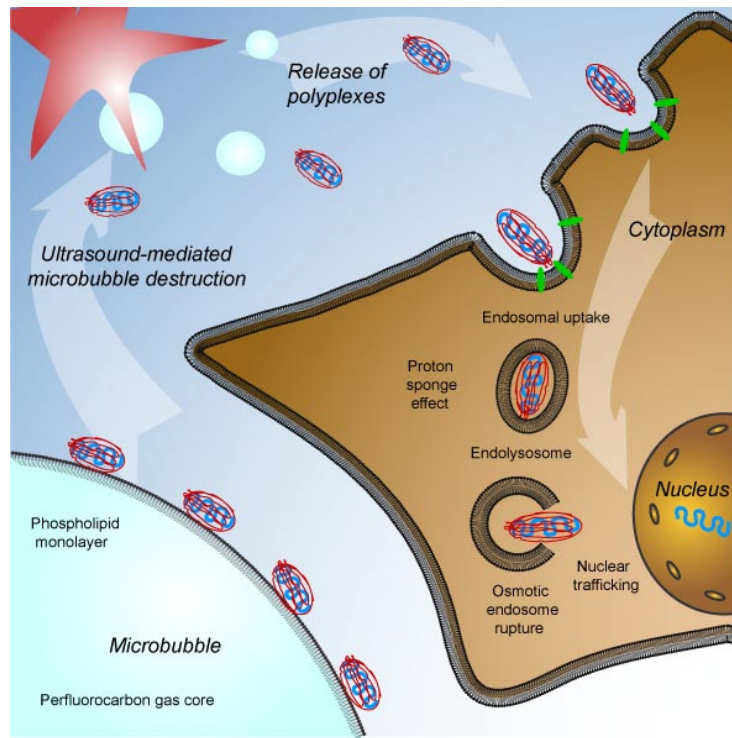


Figure 44: Endosomal uptake and delivery to the cell nucleus of secondary polyplex carriers, delivered by ultrasound-mediated MB destruction. Bottom left the surface of a scMB is represented which is decorated with polyplexes. The scMB is fragmented by US and the shell material in the form of DNA-loaded bPEI-PA / phospholipid liposomes is taken up by cells. In the cell, osmotic endosome degradation and polyplex release take place.

After the MBs are fragmented through diagnostic US, the shell monolayer rearranges and forms shell fragments which are apparently complexes of phospholipid, bPEI-PA, and DNA (Figure 44). A possible mechanism for the intracellular trafficking of such complexes was proposed by Sugiyama et al. (2004) [252]. The suggested pathway implies several similarities as well with the mechanisms of DNA release from lipoplexes [253] as with the endosomal escape of polyplexes [254].

Both polyplexes and lipoplexes are internalized into cells via the endosomal pathway, but within the cytosol they follow different mechanisms to escape the endosome. In the case of lipoplexes, comprising cationic phospholipids and DNA, a mechanism for endosomal release was proposed by Xu et al. (1996) [253]. On the basis of their studies, they proposed that the destabilization of endosomal membrane is induced by electrostatic attraction between anionic phospholipids (phosphatidylserine) of its outer layer and the cationic phospholipid, forming the lipoplexes. The flip-flop of anionic phospholipid within the endosomal membrane and towards the lipoplex neutralizes its positive charge and detaches the DNA which is then released through the fusion of the lipoplex and the surrounding endosomal membrane [255].

On the other hand, the escape from polyplexes between PEI and DNA follows a different mechanism. PEI has a number of amines which can be protonated over a broad pH range. Within the endolysosome, the pH usually approaches values of about 5 [256]. The high proton concentration is buffered by PEI resulting in protonation of about 45% of PEI nitrogen compared to approximately 20% protonation at a pH of 7.4 [257]. The proton excess induces an electrostatic gradient and an influx of chloride ions, followed by an increase of osmotic pressure in the endolysosome. The latter effect is compensated by an influx of water, leading to the degradation of the endosome. This so-called “*proton-sponge*” effect [258] causes the delivery of the intact polyplex into the cytosol. Furthermore, the PEI has the ability to accelerate the nuclear uptake of DNA, known in the literature as *nuclear trafficking* [259-261]. Recently, the hypothesis is being discussed that the PEI/DNA complexes, having a basic character, feature a similarity with several nuclear localizing signal peptides [252] which also contain numerous basic amino acids [262].

The intracellular transfer of polycationic liposomes, comprising DNA, amphiphilic PEI conjugates, and phospholipids, apparently combines characteristics which are specific for both lipoplexes and polyplexes. Similarly to lipoplexes and polyplexes DNA-encapsulating polycationic liposomes are taken up by the endosomal pathway. During the further intracellular trafficking the phospholipid is detached from the complex and remains in the cytosol. On its side the complex of PEI and DNA is preferentially transferred into the nucleus and processed towards gene expression [252]. It still needs to be clarified which of the two mechanisms – membrane fusion or “proton sponging” governs the endosomal escape after cellular uptake of polycationic liposomes. Nonetheless, since the gene transfer was successful not only in the presence of non-bilayer phospholipids such as DOPE [252], but also with liposomes, composed of bilayer-forming phospholipids [226, 230], the mechanism of osmotic endosome bursting apparently was claimed the prevailing role for the DNA release.

However, no *in-vivo* data is yet available in the literature and therefore no reliable conclusions are possible concerning the therapeutic effectiveness or possible biological concerns regarding the application of scMBs.

One possible challenge to scMBs is their integrity in terms of detaching of nanoparticles from the MB surface due to *e.g.* shear stress or electrolyte effects. The loss of SCs is even more likely during the visualization procedure when MBs perform intensive linear or non-linear oscillations, causing surface microstreaming effects accompanied by considerable shear stress for the MB surface.

Summarizing, the concept of the present research project aims on the establishing of polyplex-associated MBs, fulfilling the following advantages to related nonviral carriers:

- a) Site specific gene delivery through targeting by diagnostic US;
- b) Protection of the genetic material from digestion by serum nucleases through condensation to polyplexes;
- c) Facilitation of cellular uptake and endosomal escape through the osmotic endosome degradation;
- d) Promotion of nuclear delivery and expression of the genetic material through nuclear trafficking.

Further *in-vivo* studies are necessary in order to establish the therapeutic value and safety profile of the newly developed polyplex-loaded scMBs.

Within the following research work the chemical structure analysis of bPEI-PA conjugates was done in cooperation with Mr. Lars Allmendinger, Ph.D. from the Department of Pharmacy, Pharmaceutical Chemistry at the Ludwig-Maximilians-University – Munich, Germany. Gene transfection studies and agarose gel assays were carried out in cooperation with Mr. Martin Meyer, Ph.D. and Mr. Alexander Philipp from the Department of Pharmacy, Pharmaceutical Biology – Biotechnology, Ludwig-Maximilians-University – Munich. Confocal laser scanning microscopy imaging was done in co-work with Mr. Stefan Zahler, Ph.D from the Department of Pharmacy, Pharmaceutical Biology at the same university. Studies involving measurements of peak-negative acoustic pressure in US fields were made together with Mr. Rainer Pecha, Ph.D. from the University of Stuttgart, Germany. *In-vivo* clinical studies were performed in cooperation with Mr. Raffi Bekeredjian, MD, Ph.D. from the Internal Medicine III, Ruprecht-Karls-University – Heidelberg, Germany. The research work was funded through a research grant by the NanoforLife initiative of the Federal Ministry of Education and Research, Germany in cooperation with Mr. Raffi Bekeredjian, MD, Ph.D.

3. Materials and Methods

3.1. Reagents

| Substance | Abbreviation | Purchased from |
|---|--------------|--|
| Agarose, HEEO, ultra quality | Agarose | Carl Roth GmbH, Karlsruhe, Germany |
| Boric acid | --- | Sigma-Aldrich GmbH, Munich, Germany |
| Coumarine-6 [®] (laser grad, 98%) | --- | Acros Organix, Geel, Belgium |
| Chloroform, HPLC-grade | --- | Sigma-Aldrich GmbH, Munich, Germany |
| Chloroform, deuterated | --- | Euriso-Top SA, Gif sur Yvette, France |
| 1,4-Diazabicyclo[2.2.2]octane | DABCO | Sigma-Aldrich GmbH, Munich, Germany |
| (3-(4,5-Dimethylthiazol-2-yl)-2,5-diphenyltetrazolium bromide | MTT | Sigma-Aldrich GmbH, Munich, Germany |
| Dimethyl sulfoxide | DMSO | Sigma-Aldrich GmbH, Munich, Germany |
| Dipalmitoyl phosphatidylcholine | DPPC | Lipoid AG, Ludwigshafen, Germany |
| Dipalmitoyl phosphatidylethanolamine | DPPE | Lipoid AG, Ludwigshafen, Germany |
| DNase I, type IV from bovine pancreas | DNase I | Sigma-Aldrich GmbH, Munich, Germany |
| Dulbecco's modified Eagle's medium, activated with 10% fetal calf serum | DMEM | Invitrogen Molecular Probes [™] , Eugene, USA |
| Ethylene diamine tetra-acetic acid | EDTA | Sigma-Aldrich GmbH, Munich, Germany |
| Ethylene diamine tetra-acetic acid, trisodium salt | EDTA.3Na | Sigma-Aldrich GmbH, Munich, Germany |
| 1,2,3-Propanetriol, water free | Glycerol | Sigma-Aldrich GmbH, Munich, Germany |
| Ethidium bromide | --- | Invitrogen Molecular Probes [™] , Eugene, USA |
| 4-(2-hydroxyethyl)-1-piperazineethanesulfonic acid | HEPES | Sigma-Aldrich GmbH, Munich, Germany |
| Loading buffer for agarose gel electrophoresis | --- | Kindly provided by Martin Meyer, Ph.D., Department of Pharmacy, Pharmaceutical Biology – Biotechnology, Ludwig-Maximilians-University - Munich |
| Lysis buffer for cell cultures | --- | Cell signaling Technology, Inc, Danvers, USA |
| Magnesium chloride | --- | Merck-Schuchardt OHG, Hohenbrunn, Germany |
| N,N-dicyclohexylcarbodiimide | DCC | Sigma-Aldrich GmbH, Munich, Germany |
| Octafluoropropane | --- | Sauerstoffwerk Friedrich Guttroff GmbH, Wertheim, Germany |
| Palmitic acid, p.a. | PA | Sigma-Aldrich GmbH, Munich, Germany |
| Polyethylenimine, branched, 1.8 kDa | bPEI1.8 | Polysciences Europe GmbH, Eppelheim, Germany |
| Polyethylenimine, branched, 10 kDa | bPEI10 | Polysciences Europe GmbH, Eppelheim, Germany |
| Polyethylenimine, branched, 25 kDa | bPEI25 | Sigma-Aldrich GmbH, Munich, Germany |
| Potassium acetate | --- | Sigma-Aldrich GmbH, Munich, Germany |
| Propidium iodide | --- | MoBiTec GmbH, Göttingen, Germany |
| Pyridine | --- | Sigma-Aldrich GmbH, Munich, Germany |

Continued from p. 147

| | | |
|---|------------------------|---|
| Texas Red [®] sulfonyl chloride | Texas Red [®] | Invitrogen Molecular Probes [™] , Eugene, USA |
| Tris(hydroxymethyl)-aminomethan base | Tris base | Carl Roth GmbH, Karlsruhe, Germany |
| Trypan blue stain, 0.4 mass% in saline | Trypan blue | Invitrogen Molecular Probes [™] , Eugene, USA |
| Membrane tubing for dialysis, MW cut-off: 1 kDa | --- | Spectra/Por [®] , VWR International GmbH, Darmstadt, Germany |

3.2. Synthesis of branched polyethylenimine palmitate (bPEI-PA) conjugates

Covalent conjugates of branched PEI with molecular weights of 1.8 kDa, 10 kDa, and 25 kDa and palmitic acid (PA) were synthesized through pyridine-catalyzed nucleophilic substitution after chemical activation of PA with N,N-dicyclohexylcarbodiimide (DCC) (Figure 45). The molar degrees of substitution between number of PA residues and PEI monomer units per molecule were varied between 2 mol% and 50 mol%.

Branched PEI was dissolved in HPLC-grade chloroform at a concentration of 20 mg/ml and 500 μ l pyridine were added. Separately, the required amounts of PA and DCC were dissolved in chloroform and both solutions were mixed. The reaction mixture was stirred for 24 h at room temperature under nitrogen atmosphere and light protection.

The stoichiometric ratio between bPEI and PA in the final reaction mixture corresponded to the desired degree of substitution of the final product bPEI-PA plus an excess of 5 mol% PA. DCC was added in a 50% higher molar concentration than PA to ensure complete activation of the fatty acid. Conjugates of bPEI with a molecular weight of 1.8 kDa were synthesized with substitution rates of 2, 5, and 12 PA residues per bPEI molecule. Conjugates of bPEI with molecular weight 10 kDa were substituted with 10, 30, and 60 PA moieties. Branched PEI of 25 kDa was grafted with 10, 20, 30, 70, 100, and 200 PA moieties per molecule.

After the reaction time, the precipitated N,N-dicyclohexylurea was removed by filtration through a Schott filter, the product was concentrated under vacuum and purified by extensive dialysis in chloroform over a week using a recycled cellulose membrane dialysis tubing with a molecular weight cut-off of 1 kDa. Traces of water in the dialysis phase were absorbed with granulated water-free calcium chloride.

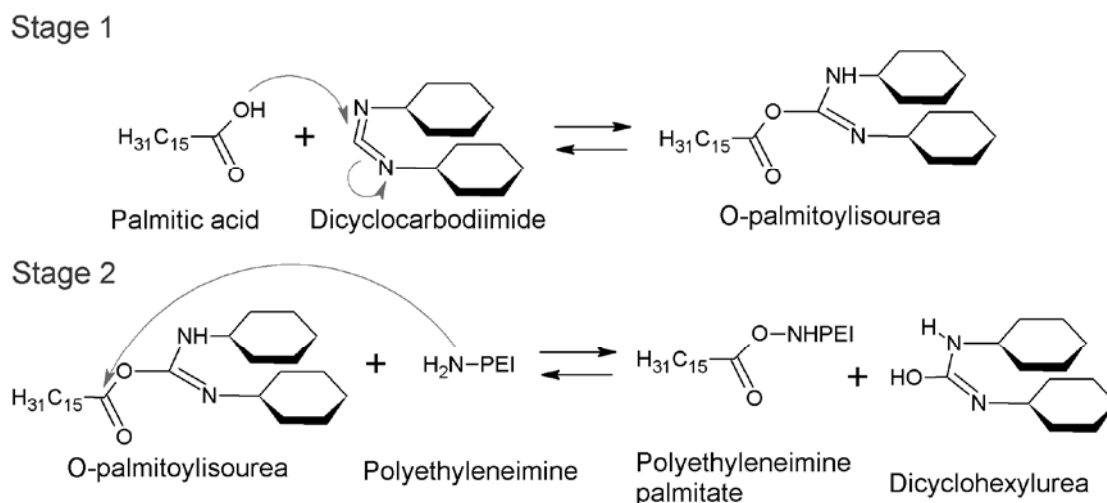


Figure 45: Chemical synthesis of amphiphilic bPEI-PA conjugates from branched polyethylenimine (bPEI) and palmitic acid (PA).

Following, the bPEI-PA solutions were adjusted with chloroform to a concentration of 25 mg/ml (0.581 M nitrogen concentration) based on the input amount of bPEI. The stock solutions were stored in dark at $-20\text{ }^{\circ}\text{C}$.

The approximate number of primary amine groups per conjugate molecule was calculated based on the polymerization degree of bPEI, the proportion of 33.33 mol% of primary vs. secondary, and tertiary amines [263], and on the number of PA grafts per conjugate molecule. The hydrophilic-lipophilic balance (HLB) for each conjugate was calculated according to the Griffin's method [264].

3.2.1. Chemical structure analysis of bPEI-PA

The chemical structure of the bPEI-PA conjugates was characterized by ^1H and ^{13}C NMR using a Jeol JNMR-GX400 (Jeol GmbH, Eching, Germany) operating at 400 MHz in order to prove the covalent bonding of PA to the backbone of bPEI and to determine the number of PA residues per bPEI molecule. Deuterated chloroform was employed as solvent. The approximate number of PA residues per molecule bPEI-PA was calculated as the ratio between the intensity of PA hydrogen and bPEI hydrogen in the ^1H NMR spectra.

3.3. Characterization of bPEI-PA

3.3.1. Particle size distribution of bPEI and bPEI-PA in polar and non-polar solvents

The particle size distribution of bPEI and of bPEI-PA conjugates was measured both in chloroform and in water by dynamic light scattering using Zetasizer Nanoseries Nano-ZS (Malvern Instruments Ltd., Worcestershire, UK). The concentration in all measured samples was adjusted to 25 mg/ml bPEI. For the production of aqueous bPEI-PA dispersions, the chloroform was eliminated from the stock solution using a Büchi Rotavapor R-114 (Büchi Labortechnik GmbH, Essen, Germany) for 60 min at 60 °C. Following, the bPEI-PA conjugate was hydrated with a medium, consisting of 30 mM HEPES, 1 mM EDTA, 15 mM sodium chloride, 50 vol% Glycerol, and highly-purified electrolyte free water (Purelab Plus[®], USF Elga Ionpure GmbH, Germany), having a pH between 4.8 and 5.0. After hydration, the dispersion was US homogenized for 60 s using a horn-type US homogenizer (Branson Sonifier[®], Branson Ultrasonics Corp., USA). The samples were allowed to equilibrate for at least 24 h at 4 °C in dark.

To prepare aqueous samples for measurements, 200 µl of the bPEI-PA dispersion or bPEI solution were diluted in electrolyte free water and the pH was controlled. The medium viscosity of samples for measurements (containing 7.7 vol% glycerol in water) was determined by falling ball viscosimetry using an Automated Micro Viscosimeter AMVn (Anton Paar GmbH, Ostfildern, Germany). The refractive index of the aqueous dispersant was set to 1.341, for chloroform – to 1.446, and for the bPEI-PA particles – to 1.450, with an absorption index of 0.01.

3.4. Formulation and characterization of polycationic liposomes with bPEI-PA

3.4.1. Mixing behavior of DPPC and DPPE

The mixing behavior between DPPC and DPPE in different proportions were studied by differential scanning calorimetry (DSC) using a Mettler Toledo DSC821e (Mettler-Toledo GmbH, Giessen, Germany). The molar ratio between DPPC and DPPE was varied from 100 mol% DPPC to 100 mol% DPPE with an increment of 25 mol% DPPE.

The phospholipids were separately dissolved in chloroform and mixed to achieve the desired proportions. Liposome dispersions with a total phospholipid concentration of 20 mM were

produced using the thin-film hydration method by hydrating the phospholipid film with highly purified water. Samples for measurements were prepared by placing 30 μl of the liposomal formulations in 40 μl aluminum DCS pans and sealing them. Samples were prepared in triplicate and three scanning runs were performed against air with each sample ($n = 9$). The scans were performed in a temperature range from 20 $^{\circ}\text{C}$ to 85 $^{\circ}\text{C}$ with a heating rate of 5 $^{\circ}\text{C}/\text{min}$. Between every heating and cooling segments an isotherm segment of two minutes was set. Measured data were accordingly normalized against the sample weight and phospholipid molar concentration.

3.4.2. Effect of glycerol on the colloidal stability of DPPC / DPPE liposomes

The influence of increasing amounts of glycerol on the colloidal stability and sedimentation of DPPC / DPPE liposomes was monitored over a week during storage at 4 $^{\circ}\text{C}$ in dark. Consequently, the miscibility of DPPC and DPPE at increasing glycerol concentration was monitored by differential scanning calorimetry (DSC).

Samples were prepared with 20 mol% DPPE and 80 mol% DPPC at a total concentration of 20 mM. The concentration of glycerol in the hydration medium varied from 0 vol%, to 100 vol% with an increment of 25 vol%, corresponding to 0 mol%, 7.6 mol%, 19.8 mol%, 42.5 mol%, and 100 mol% glycerol concentration. The conversion from vol% into mol% was made in order to simplify comparisons with the literature. Sample preparation, DSC measurements, and data weighing were carried out as described above under “3.4.1 *Mixing behavior of DPPC and DPPE*”. Samples were stored for 14 days in dark at 4 $^{\circ}\text{C}$ and the phase separation and formation of sedimentation layer was monitored.

3.4.3. Mixing behavior of bPEI-PA with DPPC / DPPE bilayers

Formulations of polycationic liposomes for analysis were prepared according to the thin-film method, whereby bPEI25-PA20 was blended together with the phospholipid and included into the thin-film. The bPEI25-PA20 / phospholipid blends were hydrated with 30 mM HEPES and, if necessary, adjusted with 0.5 N hydrochloric acid or 0.5 N sodium hydroxide to a pH of 7.

Samples contained a total phospholipid concentration of 20 mM, consisting of 20 mol% DPPE and 80 mol% DPPC and comprising bPEI25-PA20 at various nitrogen concentrations from 0 mM to 40 mM with an increment of 10 mM. The miscibility of bPEI25-PA20 with DPPC / DPPE bilayers was studied with DSC following the same measuring setup as described in “3.4.1 *Mixing behavior of DPPC and DPPE*”.

3.4.4. Determination of bPEI-PA buffer capacity

Sample preparation for titration measurements followed the same procedure as in “3.3.1 Particle size distribution of bPEI and bPEI-PA in polar and non-polar solvents”, p.162. Polycationic liposomes comprising 20 mol% DPPE and 80 mol% DPPC at a total phospholipid concentration of 5 mM, as well as bPEI25-PA20 at a nitrogen concentration of 190 mM were prepared. Samples for positive control were prepared with bPEI25 at the same nitrogen concentration as the PCL in highly purified water. Samples for negative control were prepared, comprising DPPC / DPPE liposomes with the same phospholipid constitution as the PCL, in water.

Titration was carried out using a Malvern Multi Purpose Titrator MPT-2, connected to a Zetasizer Nanoseries Nano-ZS (Malvern Instruments Ltd., Worcestershire, UK). Shifts in the pH were measured by potentiometry. Parallel to pH the Zeta potential was measured also during the titration. Titration excursions were carried out with 0.05 N hydrochloric acid from a pH of 7.5-7.8 down to 2.3.

The titration started from the existing pH value of the formulation and was left unadjusted. This was done in order to keep samples' conductivity low and to not influence Zeta potential measurements.

3.4.5. Zeta potential of polycationic liposomes with bPEI-PA

Three studies on the Zeta potential of polycationic liposomes were performed. The first study explored the influence of the substitution rate of bPEI25 with PA. Therefore, polycationic liposomes were produced comprising 20 mol% DPPE and 80 mol% DPPC at a total phospholipid concentration of 5 mM and a total nitrogen concentration of 20 mM. The formulations comprised bPEI25-PA with various substitution rates of PA per molecule bPEI25 ranging from 10 to 200. The pH value was buffered with 30 mM HEPES to 7.4. The Zeta potential was measured by electrophoretic light scattering using Zetasizer Nanoseries Nano-ZS (Malvern Instruments Ltd., Worcestershire, UK).

The aim of the second study was the determination of the effect of different bPEI-PA concentrations on the Zeta potential of polycationic liposomes at a constant pH, ionic strength and phospholipid concentration. Samples were prepared at a total phospholipid concentration of 3 mM and with an increasing concentration of bPEI25-PA20, corresponding to nitrogen concentrations ranging from 0 mM to 100 mM with an increment of 20 mM. The dispersant medium was highly-purified water buffered at a pH of 7 with 30 mM HEPES.

The third study examined the influence of pH excursions in the range of 7.5-7.8 down to 2.3 on the Zeta potential of PCL. The measurements were carried out simultaneously with the study under “3.4.4 Determination of bPEI-PA buffer capacity”, p.152, but will be discussed in this section.

For all Zeta potential measurements the dispersant dielectric constant was set to 78.5. The optical measurement settings were the same as used for size distribution measurements by dynamic light scattering. Sample conductivity during the titration was kept below 1.8 mS/cm².

3.5. Studies on the loading of bPEI-PA liposomes with pDNA

Various studies were performed in order to achieve small polyplex size distribution and an acceptable polydispersity by manipulating such formulation parameters as pH, electrolyte concentration, and the influence of triple-charged anions.

3.5.1. Complexation capacity of bPEI-PA liposomes for pDNA

The plasmid binding strength of the PEI-PA conjugates was assessed by exclusion of ethidium bromide of its complex with DNA [265]. Loading studies were performed with luciferase-encoding plasmid DNA bearing cytomegalovirus promoter (pCMV-LUC) and having a size of 7,040 base-pairs [266]. According to the chemical structure of DNA, two phosphorus atoms were assigned per base pair. The mass concentration of pDNA was determined using an automated spectrophotometer Eppendorf BioPhotometer (Eppendorf AG, Hamburg, Germany) at 260 nm wavelength. The molar concentration of DNA phosphorus was calculated based on an average molecular weight of 660 Da per DNA nucleotide pair.

Based on the average molecular weight of bPEIs, used for the synthesis of amphiphilic conjugates, an average number of 581 nitrogen atoms was assigned per molecule of bPEI25, 233 atoms per molecule of bPEI10, and 42 atoms per molecule of bPEI1.8. Accordingly, the nitrogen-to-phosphorus (N/P) ratios were calculated based on the molar concentration of bPEI and molar concentration of DNA phosphorus.

The fluorescence of 20 µg/ml solution of pDNA (corresponding to 60.61 µM DNA phosphorus) containing 400 ng/ml ethidium bromide in HEPES-buffeted glucose was initially measured and set to 100% ($\lambda_{\text{ex}} = 510 \text{ nm}$, $\lambda_{\text{em}} = 590 \text{ nm}$, slit width = 10 nm) using a Varian Cary Eclipse fluorescence spectrophotometer (Varian, Inc., Palo Alto, USA).

Liposome solutions with a nitrogen concentration of 1.5 mM and a phospholipid concentration of 3 mM were prepared with bPEI1.8 and its conjugates with 2 and 5 PA residues, bPEI10 and its conjugates with 12 and 30 PA residues, and with bPEI25 and its

conjugates with 10, 20, and 30 PA residues. Portions of 20 μ l PCL were added to 1 ml solution of pDNA, resulting in titration steps of 0.5 N/P.

Aliquots of bPEI-PA liposomes were added stepwise to the solution and the decrease of fluorescence was measured ($n = 3$) as indication for the interaction between complexing compound and nucleic acid.

3.5.2. Effect of pH on the polycationic liposome size

Polycationic liposomes were formulated containing 3 mM total phospholipid, of which 20 mol% were DPPE and 80 mol% DPPC, and bPEI25-PA20 at a nitrogen concentration of 20 mM. The liposomes were aliquoted in three portions and the pH was adjusted with 0.5 N hydrochloric acid to approximately 3.5, 5.5, and 8.5. The liposomes were loaded with pDNA under gentle vortexing and incubation at room temperature. DNA-loaded polyplex-liposomes were diluted to a proportion of 1:10 with electrolyte-free water and their particle size and polydispersity were determined by dynamic light scattering using Zetasizer Nanoseries Nano-ZS (Malvern Instruments Ltd., Worcestershire, UK).

3.5.3. Polycationic liposome size according to bPEI molecular weight, PA substitution, and loading with pDNA

Polycationic liposomes were produced via the thin-film hydration method as described above. The concentration of bPEI-PA nitrogen was kept constant at 20 mM, the final total phospholipid concentration was 3 mM. The pH was adjusted to 4.5-4.2 with 1 M hydrochloric acid, and the ion concentration was set to 30 mM by sodium chloride. The loading with pDNA was carried out at an N/P ratio of 10. Liposomes were prepared for measurements as described above. Particle size and polydispersity were determined by dynamic light scattering using Zetasizer Nanoseries Nano-ZS (Malvern Instruments Ltd., Worcestershire, UK).

3.6. Formulation and characterization of polyplex-associated MBs, loaded with pDNA

3.6.1. Effect of electrolytes on the MB production and liposome aggregation

Polycationic liposomes loaded with pDNA were produced as described above. The ion concentration was adjusted with sodium chloride and trisodium citrate, assuming a complete dissociation of salts to two moles ions for sodium chloride and four moles ions for trisodium citrate and an ion activity, linearly corresponding to the ion concentration. The ion

concentration was varied from 0 mM, 30 mM, 50 mM, 70 mM, and 100 mM. Accordingly, MBs were prepared by mechanical agitation at 4,500 oscillations / minute for 20 s of 400 μ l liposome dispersion with 1.6 ml octafluoropropane gas in a sealed tube. The MB concentration was determined by light blockage using a PAMAS SVSS-C (PAMAS GmbH, Rutesheim, Germany). MB size distribution was monitored by laser diffraction using a Partica LA-950 (Horiba Ltd., Kyoto, Japan). Particle size and polydispersity of polycationic liposomes were measured by dynamic light scattering using Zetasizer Nanoseries Nano-ZS (Malvern Instruments Ltd., Worcestershire, UK).

3.6.2. Optimal formulation for polyplex-associated MBs for *in-vivo* studies

The production of polycationic liposomes was performed according to the thin-film hydration method. The appropriate amounts of dipalmitoyl phosphatidylcholine (DPPC), dipalmitoyl phosphatidylethanolamine (DPPE), and bPEI-PA were blended under heating at 60 °C in HPLC-grade chloroform and the organic solvent was removed for 60 min at 65 °C under vacuum using a Büchi Rotavapor R-114 (Büchi Labortechnik GmbH, Essen, Germany). The bPEI-PA / phospholipid film was hydrated at gentle conditions at 50 °C under nitrogen protection, for 15-20 min. The medium for phospholipid hydration contained 30 mM HEPES, 1 mM EDTA, and 15 mM sodium chloride, dissolved in a mixture of 50 vol% water-free glycerol in highly-purified water (Purelab Plus[®], USF Elga Ionpure GmbH, Germany).

Accordingly, the raw phospholipid dispersion was shortly homogenized with low-frequency US using a horn-type homogenizer (Branson Sonifier[®], Branson Ultrasonics Corp., USA). The resulting clear yellow phospholipid dispersion was adjusted with 1 M hydrochloric acid to pH 4.5-4.2 and allowed to equilibrate at 4 °C in dark for at least 12 hours. Potentiometric pH measurements were performed as control prior and after the equilibration. The liposomes were stored at -4 °C at dark without any evident signs of aggregation and sedimentation over months.

In order to produce polyplex-associated MBs 160 μ l of 1 mg/ml solution of pDNA were added to 240 μ l polycationic liposomes in a 2 ml safe-lock tube (Eppendorf AG, Hamburg, Germany) and gently mixed with the pipette. The mixture was incubated for 15 min at room temperature, then covered with octafluoropropane and agitated for 20 s at 4,500 oscillations per minute using a mechanical agitator CapMixTM (3M Deutschland GmbH, Neuss, Germany). Prior to their application MBs were diluted with octafluoropropane-saturated 5 mass% solution of glucose in highly-purified water.

3.6.3. Structure analysis of polyplex-associated MBs

Fluorescence confocal scanning laser microscopy (CLSM) studies were performed using an inverted Zeiss LSM 510 (Carl Zeiss Microimaging, Göttingen, Germany) in order to confirm the loading of pDNA on the MBs and to examine the colloidal structure of the MB dispersion. A pinhole of 118 μm was exerted with an oil-immersion objective producing optical slices of about 225 μm thickness.

Microbubbles were double fluorescent labeled in order to localize the phospholipid, the bPEI-PA conjugates, and the pDNA. Phospholipids were labeled with the hydrophobic dye Coumarine-6[®] (Table 20, p.156) which emits light mostly when intercalated between the acyl chains, while it is practically quenched in water [267]. Coumarine-6[®] was included in the organic solution of bPEI-PA and phospholipids during the production of liposomes at a final concentration of 3 $\mu\text{g}/\text{ml}$.

In unloaded MB formulations the bPEI-PA conjugates were covalently labeled with TexasRed[®] sulfonyl chloride. The amino-reactive TexasRed[®] dye was incubated in chloroform solution with bPEI25-PA30 at a molar ratio, corresponding to about 150 dye molecules per molecule bPEI. Incubation was carried out for 24 hours at 4 °C in dark and under nitrogen protection. Following, the fluorescently labeled conjugate was purified from unbound dye by extensive dialysis in chloroform over two weeks at 4 °C in dark using a recycled cellulose dialysis tube with a molecular weight cut-off of 1 kDa. The TexasRed[®] labeled bPEI-PA conjugate was included in MB formulations as described in the standard formulation production.

| Fluorescent dye | Excitation wavelength maximum, [nm] | Emission wavelength maximum, [nm] |
|---|--|--------------------------------------|
| Coumarine-6 [®] | 420-450 | 490-520 |
| Propidium iodide (nucleic acid bound) | 535 | 617 |
| Texas Red [®] sulfonyl chloride | 596 | 615 |
| Concanavalin A- Alexa Fluor [®] 488 conjugate | 495 | 519 |
| Hoechst 33342 | 350 | 461 |

Table 20: Fluorescent dyes and their excitation and emission laser wavelengths, used here for fluorescent staining of polyplex-associated MBs.

In DNA-loaded MB formulations the TexasRed[®]-labeling was substituted by staining of pDNA with propidium iodide. To the freshly prepared MB 20 μg propidium iodide and 1 ml

highly-purified water were added. The MBs were accordingly incubated for 15 min at room temperature.

Prior to the microscopy, the labeled MBs were mounted in a medium, containing 2 mass% DABCO, 80 vol% water-free glycerol and 20 vol% water. The mounted sample was then introduced by a syringe into a thin-bottom Ibidi μ -slide IV (Ibidi GmbH, Munich, Germany) and observed.

3.6.4. Protection of pDNA against enzymatic degradation

The plasmid sensitivity to degradation by DNase I was evaluated using changes in plasmid migration on agarose gel electrophoresis. The DNase stress assay and the agarose gel assay were performed according to the protocols of Lentacker et al. (2006) [119] with some modifications. Briefly, polyplex-associated MBs loaded with pDNA were mixed with DNase I, type IV from bovine pancreas and incubated for 30 min at 37 °C under shaking using Eppendorf Thermomixer Comfort (Eppendorf AG, Hamburg, Germany). The final concentrations of DNase and pDNA during incubation were held constant in all samples at accordingly 200 U/L DNase activity and 198 μ g/ml pDNA. The concentration of bPEI25-PA30 nitrogen was varied from 3 mM, 6 mM, and 9 mM in order to produce N/P loading ratios of 5, 10, and 15. Furthermore, the samples contained magnesium chloride in a final concentration of 2.04 mM which is necessary for the activation of DNase I. The pH was maintained at 7.4 by addition of HEPES and potassium acetate at final concentrations of correspondingly 2 mM and 22 mM.

Seven setup combinations were prepared and tested. Firstly, the plasmid alone was used as positive control. MB dispersions were also incubated with DNase, inhibited in advance with EDTA.3Na in order to test its quenching activity on DNase. Furthermore, naked pDNA was incubated with DNase as a control of its digesting activity. As a negative control unloaded MBs were examined. At last, the DNA-loaded MBs were challenged with DNase at N/P loading ratios of 5, 10, and 15. After the incubation, the DNase I was quenched by the addition of 10 μ l 100 mM solution of EDTA.3Na. The pDNA was detached from its complex with bPEI-PA in order to examine whether it survived the challenging with DNase. Therefore, MBs were incubated with sodium chloride at a final concentration of 5 M at 50 °C for 30 min under shaking using Eppendorf Thermomixer Comfort (Eppendorf AG, Hamburg, Germany).

Agarose gel pads were prepared from 1 mass% agarose solution in tris / borate / EDTA buffer containing 10.8 g/l tris base, 5.5 g/l boric acid, and 0.58 g/l EDTA.3Na, and the 0.5 μ g/ml ethidium bromide were added to enable the visualization of DNA.

Accordingly, 50 μ l of each sample were mixed with 10 μ l loading buffer comprising 2.5 mg/ml bromophenol blue and 400 mg/ml sucrose in water, the samples were shortly vortexed, centrifuged, and loaded onto the agarose gel pad.

The samples were subjected to electrophoresis at 120 V for 80 min, and the pDNA was visualized under UV light prior to photography.

3.6.5. Effective loading of pDNA in polycationic liposomes and in polyplex-associated MBs

The partition of pDNA between free-form and polycationic liposomes was determined by a gel retention assay. The polycationic liposomes were loaded with pDNA at N/P ratios of 15, 13, 10, 7, 5, 3 and 1 and incubated for 15 min at room temperature. The samples were treated with loading buffer and subjected to agarose gel electrophoresis as described above. The intensity of fluorescence through leaked pDNA was evaluated using the software ImageJ v.1.41o (National Institute of Health, USA).

Accordingly, the binding of pDNA to polyplex-associated MBs was evaluated by fluorescence spectrometry. Freshly prepared samples of pDNA-loaded MBs were diluted with octafluoropropane-saturated 5 mass% glucose in highly-purified water. The bubbles were gently centrifuged for 5 min at 1,000 rpm using NeoLab 16/18 centrifuge (Hermle Labortechnik GmbH, Wehingen, Germany). Portions of the underlying liquid phase were drawn by piercing through the tube wall with a syringe needle. In order to detach pDNA from its complex with bPEI-PA the obtained samples were incubated with 5 M solution of sodium chloride at 50 °C for 30 min under continuous shaking using an Eppendorf Thermomixer Comfort (Eppendorf AG, Hamburg, Germany). Propidium iodide was added at a final concentration of 1 μ g/ml and the samples were centrifuged for 15 min at 14,000 rpm using a NeoLab 16/18 centrifuge (Hermle Labortechnik GmbH, Wehingen, Germany) in order to remove insoluble particles. The fluorescence of the pDNA / propidium iodide complex was determined using a Varian Cary Eclipse fluorescence spectrophotometer (Varian, Inc., Palo Alto, USA).

The fluorescence data was displayed in per cent according the fluorescence, obtained from whole pDNA-loaded liposomal formulations. The effective loading of polyplex-associated MBs was calculated by subtracting the amount of unbound pDNA from the total input amount of pDNA.

3.7. Comparative *in-vitro* transfection / cell viability studies with pDNA-loaded polycationic liposomes and polyplex-associated microbubbles

The transfection efficacy of pDNA-loaded polycationic liposomes and polyplex-associated MBs were examined in B16F10 human melanoma cell cultures and compared to polyplexes of bPEI with various molecular weight and naked plasmid.

The cells were treated with naked pDNA, bPEI polyplexes, bPEI-PA nanoparticles, as well as with polycationic liposomes and polyplex-associated MBs with US application. Thereby, various polycations and conjugates were tested also in the presence and absence of phospholipid. The candidates involved in this study, were bPEI1.8, bPEI1.8-PA2, bPEI1.8-PA5, bPEI10, bPEI10-PA12, bPEI10-PA30, as well as bPEI25 and its conjugates bPEI25-PA10, bPEI25-PA20, and bPEI25-PA30. The purposes of the current studies were to select the bPEI-PA candidate with the greatest transfection potential and to compare the transfection activities of bPEI25 as a positive control, and polyplex-associated MBs comprising it. Treatment with technical US was done using a Sonitron-2000 (RichMar Corp., Chattanooga, USA) equipped with a 3 mm probe by directly immersing the probe into the culture medium. According to preliminary studies US parameters were set to 1 MHz frequency, 1 W/cm² output intensity, 50% duty cycle and a sonication time of 20 s. The bubble-to-cell ratio was set to about 80. The peak-negative acoustic pressure, [MPa] in the wells was measured using a 250 µm fiber-optic probe hydrophone (FOPH 2000, RP Acoustics, Germany) [29].

Cell cultures were cultivated in T75 flasks in DMEM medium with 10% fetal calf serum at 37 °C in 5 vol% CO₂-enriched atmosphere. Prior to each experiment, the adherent cells were harvested with trypsin / EDTA solution. Dead cells were distinguished under microscope by staining with 0.4 mg/ml Trypan blue. Non-stained cells were counted using the modified Neubauer chamber. Cell concentration was adjusted with DMEM medium and suspension was placed into 96-well plates (Greiner Bio-one GmbH, Frickenhausen, Germany) with a final number of 6 x 10⁴ cells/well. Provided a treatment with US was carried out, a 3.5 cm thick gelatin gel tissue phantom was placed beneath the well plate in order to absorb US and prevent standing US waves.

After the transfection agent was added to the culture medium and eventually US treatment was applied, the cells were incubated for 24 hours. Accordingly, the overlying medium was removed and the adherent cells were solubilized with cell lysis buffer. The samples were analyzed using a luminometer Lumat LB 9507 (Berthold Technologies GmbH, Bad Wildbad,

Germany), whereby a solution of luciferin and ATP was automatically added to provide luminescence. The experimental data was represented as an average of $n = 8$.

The metabolic activity assay was carried out simultaneously to the gene reporter assay. 24 hours after transfection the metabolic activity of cells was determined by a methylthiazoletetrazolium (MTT) / thiazolyl blue assay as follows: 10 μ l of a 5 mg/ml solution of MTT in phosphate-buffered saline were added to each well. The cells were incubated for 2 hours at 37 °C, the medium was accordingly removed and 50 μ l of DMSO were added. The optical absorbance of thiazolyl blue, produced by cells, was measured at 590 nm (reference wavelength 630 nm) using a microplate reader (Fluostar Omega, BMG Labtech GmbH, Offenburg, Germany). The cell viability was expressed in percent against phosphate-buffered saline-treated control cells. The results are presented as means of $n = 15$.

4. Results and Discussion

4.1. Synthesis of branched polyethylenimine palmitate (bPEI-PA) conjugates

The synthesized conjugates of bPEI and PA appeared as yellowish to orange-red colored waxy substances. Lesser substituted conjugates were good soluble in organic solvents such as chloroform and isopropanol. In water they formed opalescent colloidal dispersions. Higher substituted bPEI-PA conjugates were poorly soluble in a series of organic solvents including isopropanol, chloroform, cyclohexane, acetonitril, acetone, and mixtures of them. The solubility in organic solvents was impaired by traces of water. Due to their scarce solubility the higher substituted conjugates bPEI1.8-PA12, bPEI10-PA60, bPEI25-PA70, bPEI25-PA10, and bPEI25-PA200 were excluded from following research.

The approximate calculated number of primary amine groups in bPEI 1.8 kDa was 14 mol/mol, for bPEI10 – 78 mol/mol, and for bPEI25 – 194 mol/mol bPEI. Consumption of primary amine groups through binding of amide groups with PA reduces the number of primary amines per bPEI molecule (Table 21). Generally, the bPEI-PA conjugates remain very hydrophilic with HLB-values in the range of O/W emulsifiers.

| Mr (bPEI), [kDa] | PA residues / PEI molecule | Hydrophilic-lipophilic balance ¹ | Mr (bPEI-PA), [kDa] | Approximate number of primary amine groups per bPEI molecule |
|------------------|----------------------------|---|---------------------|--|
|------------------|----------------------------|---|---------------------|--|

¹ According to the Griffin's method;

| | | | | |
|-----|----|-------|-------|-----|
| 1.8 | 2 | 15.57 | 2.31 | 12 |
| | 5 | 11.68 | 3.08 | 9 |
| 10 | 12 | 15.29 | 13.08 | 66 |
| | 30 | 11.30 | 17.69 | 48 |
| 25 | 10 | 18.14 | 27.56 | 184 |
| | 20 | 16.60 | 30.13 | 174 |
| | 30 | 15.29 | 32.69 | 164 |

Table 21: Basic characteristics of bPEI-PA conjugates.

4.1.1. Chemical structure analysis of bPEI-PA

Representative NMR spectra of the conjugate bPEI-PA are shown in Figure 46. In the ^1H NMR spectrum (Figure 46, A) following peaks were observed. The triplet at 0.78-0.83 ppm corresponds to the terminal $-\text{CH}_3$ groups of PA. The multiplet between 1.12 ppm and about 2.00 ppm corresponds to the $=\text{CH}_2$ protons of PA. The triplet at 2.3 ppm corresponds to the $=\text{CH}_2$ group of PA which is adjacent to the carbonyl moiety. The multiplet between 2.45 ppm and 2.70 ppm corresponds to the $=\text{CH}_2$, $=\text{NH}$, and $-\text{NH}_2$ protons of the bPEI. The amide protons were not detectable since they overlap this multiplet. The quartet at 3.5 ppm apparently matches the $=\text{CH}_2$ groups of bPEI which are located next to the amide nitrogen. These findings were well conformed with previous literature data [268, 269].

In the ^{13}C NMR spectrum (Figure 46, B) the amide moiety $-\text{CONH}-$ of the bPEI-PA conjugate was successfully identified, giving the proof of successful covalent grafting. The amide group was identified by the chemical shifting of the carbonyl peak in PA from 180.6 ppm to 173.8 in bPEI1.8-PA5 [270]. The multiplet between 52.16 ppm and 55.57 ppm corresponds $=\text{CH}_2$ groups of the bPEI. The multiple peaks between 22.8 ppm and about 35 ppm correspond to the $=\text{CH}_2$ groups of the PA moiety. The singlet at 14.14 ppm corresponds to the terminal $-\text{CH}_3$ of PA [227].

The NMR analysis was hampered by the polymeric nature of the conjugates. Polymeric molecules typically have short relaxations in NMR which leads to peak broadening and flattening. On the other hand, the signal intensity of amide carbons was rather weak compared to the rest of the molecule. Due to the strong peak broadening only bPEI-PA conjugates with lower molecular weight and higher substitution degree with PA have provided appropriate spectral data for analysis.

From the ^1H NMR-spectra of bPEI1.8-PA5 the approximate number of PA per bPEI-PA molecule was calculated to 5.6 which roughly corresponded to the stoichiometric amounts of reagents used in the synthesis.

4.2. Characterization of bPEI-PA

4.2.1. Particle size distribution of bPEI and bPEI-PA in polar and non-polar solvents

In order to determine the particle sizes of bPEI and bPEI-PA conjugates in molecular solutions and in colloidal dispersions, they were measured in non-polar solvents such as chloroform, and in polar solvents such as water.

The viscosity of the aqueous sample medium, containing 7.7 vol% glycerol in water, was 1.1203 ± 0.0103 cP at 25 °C and was applied in all measurements settings.

Comparing the particle size distribution of bPEI and bPEI-PA in non-polar solvents such as chloroform (dielectric constant, $\epsilon = 4.8$ at 20 °C) and in polar solvents such as water ($\epsilon = 78.48$ at 25 °C) revealed the strong affinity of bPEI-PA to self-associate in polar solvents, as might be presumed from their amphiphilic nature.

In chloroform, most bPEI-PA conjugates were well soluble depending on their PA substitution rate. Conjugates' solubility in a number of solvents was strongly impaired at high ratios between PA grafting and bPEI molecule weight as in the cases of bPEI1.8-PA12 and bPEI10-PA60. The solubility was further aggravated by traces of water in the solvent which presumably can deliver protons and/or hydrate the bPEI moiety and contribute to the molecule association.

Nevertheless, the particle size distribution in chloroform was comparable for bPEI10 and bPEI10-PA12 (Figure 47). Regarding the low polarity of the solvent, the molecular dispersion state of the solution was assumed and the measured particle sizes were attributed to the single molecules.

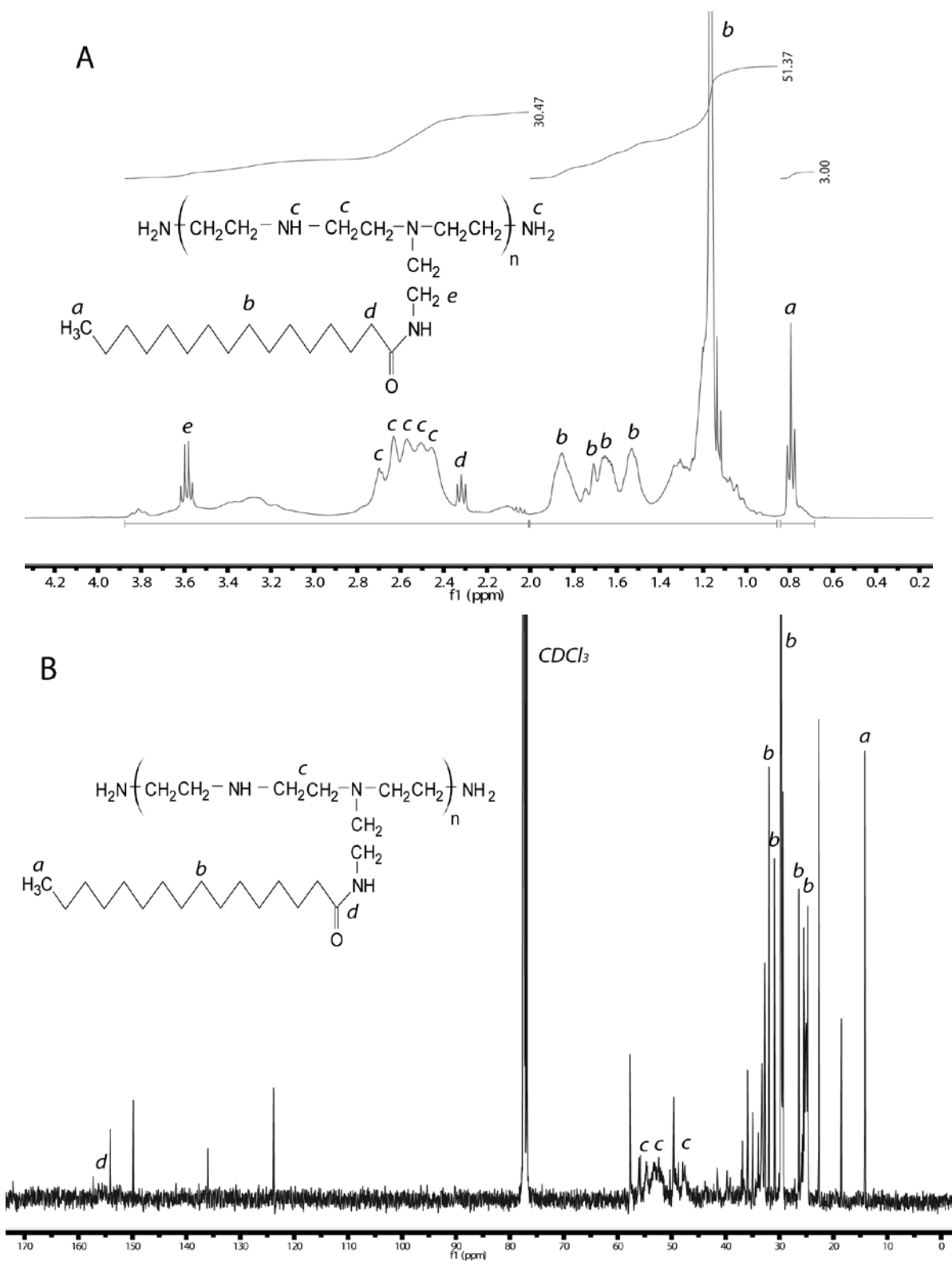


Figure 46: ^1H and ^{13}C NMR characterization for bPEI-PA synthesis, carried out on bPEI1.8-PA5 in deuterated chloroform. The polymerization degree of bPEI1.8 is 41.86, corresponding to 167.44 H from bPEI methylene units and 41.86 H from =NH units. Each of the five palmitic acid residues provides a single $-\text{CH}_3$ terminal group, 14 $=\text{CH}_2$ units, and a single amide moiety. A: Chemical structure and ^1H NMR spectrum of bPEI1.8-PA5; B: ^{13}C NMR spectrum of bPEI1.8-PA5. Explanations are given in the text.

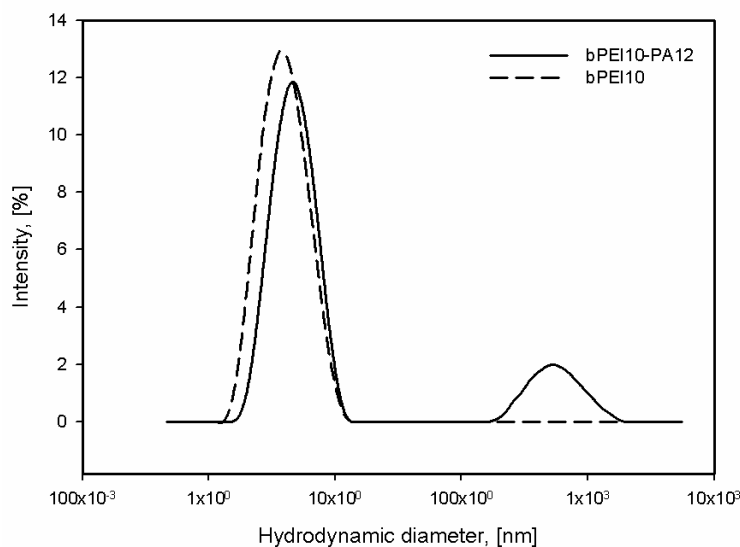


Figure 47: Size distribution of bPEI10 and bPEI10-PA12 measured by dynamic light scattering in chloroform solution. bPEI10 showed a monomodal distribution with peak maximum at 6.544 ± 0.08 nm. bPEI10-PA12 demonstrated a bimodal distribution with a mean peak at 7.675 ± 0.11 nm (82.6% intensity) and a smaller peak at 946.9 ± 65.7 nm (17.4% intensity). The polydispersity of bPEI10-PA12 was higher with a PDI of 0.261, while bPEI10 had a PDI of 0.150.

The average hydrodynamic diameter of bPEI10 molecules in chloroform was 6.544 ± 0.08 nm with a rather low PDI of 0.150. As expected, the grafting of PA residues led to a moderate but reproducible diameter increase of about 1.21 ± 0.06 nm. This was apparently due to an increase of molecule volume and/or due to altering the solvation state of bPEI-PA in chloroform. A second less intensive peak was observed with bPEI10-PA12 at about 950 nm, indicating the formation of molecule associates such as inverted micelles probably due to partially protonation and hydration of the polar bPEI10 moiety by traces of water.

In water, the particle size distribution of all bPEI-PA conjugates suggested a strong tendency to form particulate self-associates (Figure 48). Generally, the grafting of PA increased the particle size by several orders compared to non-grafted bPEI. On the other side, in the main case it lowered the polymer polydispersity.

Generally, the hydrodynamic diameters of non-conjugated bPEIs, measured in water, outweighed these, measured in chloroform, by about three- to five-fold. This can be attributed to the abundant hydration shell and polymer swelling in water.

The measured particle size of non-grafted bPEIs was nearly linearly dependent on their molecular weight. Furthermore, a rather high polydispersity, reaching a PDI of 1.00, was found in these samples. In low-substituted conjugates such as bPEI1.8-PA2, bPEI10-PA12,

and bPEI25-PA10 a steep decrease of PDI was observed which continuously grew up with increasing the substitution rate. This is most apparent in the case of bPEI25 and its conjugates on Figure 48. Even in highly substituted conjugates the PDI remained below this of the non-grafted polymer.

It can be hypothesized that the attaching of hydrophobic PA rests leads to the formation of thermodynamically stable associates such as micelles, cylinders, *etc.*, comprising a number of molecules. In this manner, bPEI-PA molecules with diverging sizes can be bundled to particles which sizes are dictated by the highest energetic loss and have therefore a lower polydispersity than the single molecules themselves.

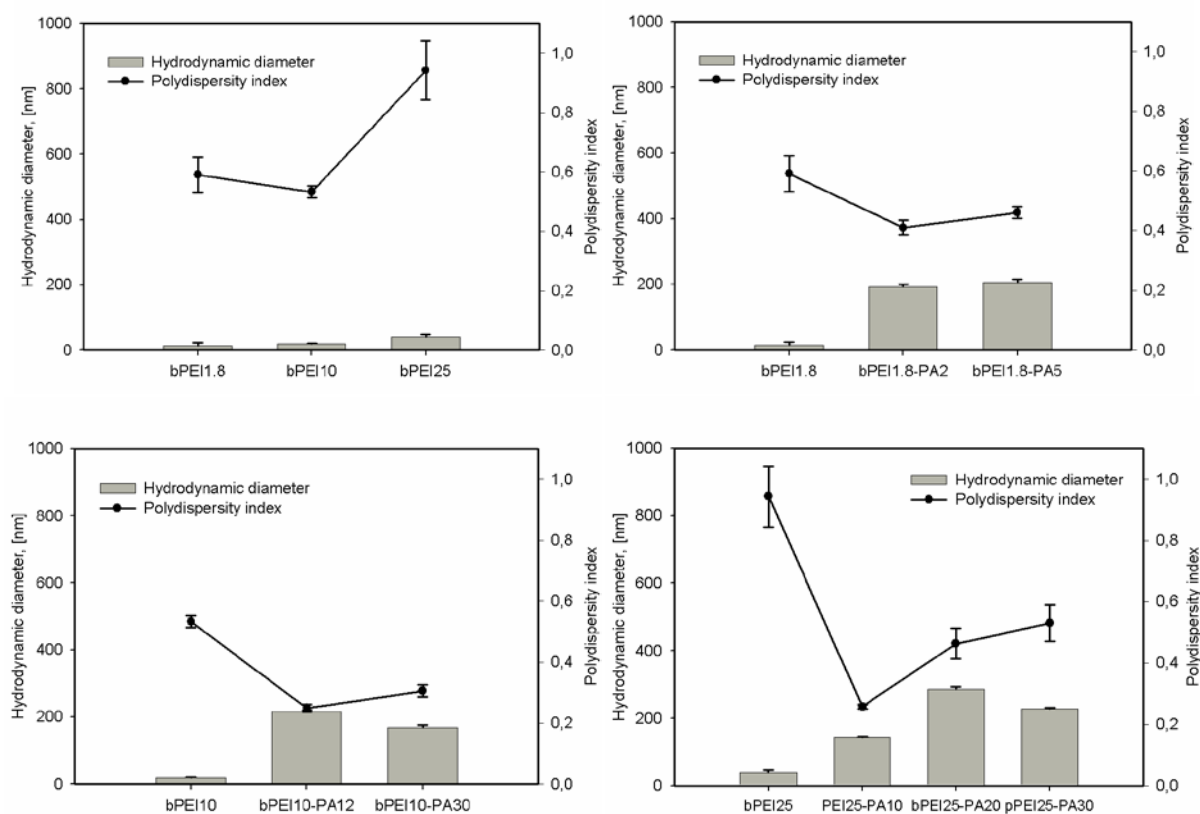


Figure 48: Hydrodynamic diameter and polydispersity index of bPEI with various molecular weights and their amphiphilic conjugates with various amounts of PA in water ($n = 3$).

In general, the particle size of the bPEI-PA associates increased together with the substitution rate up to a certain limit, where particle size slightly decreased. The smallest particle sizes combined (144.13 nm) with the lowest PDI (0.257) were achieved with bPEI25-PA10, corresponding to a hydrophilic-lipophilic balance (HLB) of 18.14. Less polar conjugates

having HLB values between 16.60 and 11.68 produced associates, sized between 200 nm and 290 nm.

4.3. Formulation and characterization of polycationic liposomes with bPEI-PA

In order to formulate polycationic liposomes as precursors for the production of polyplex-associated phospholipid MBs, the physico-chemical properties of the system have to be discussed. Based on this, the possible formulation problems can be identified, and a design concept can be elaborated.

The composition of the MB shell was based on zwitterionic phospholipids with an acyl chain length of 16 carbon atoms, corresponding to the palmitoyl residues of amphiphilic bPEI-PA lipopolymers. The non-covalent interactions, stabilizing the MB structure are the hydrophobic – between the bPEI-PA / DNA polyplexes and the phospholipid acyl chains, and prevailing electrostatic – between the bPEI-moiety and DNA. Additional interactions such as hydrogen bonding between phospholipids and bPEI-PA could also play a role in the MB organization.

Dipalmitoyl phosphatidylcholine (DPPC) has been well established in the literature as constituting component of the MB shell [59, 113]. However, DPPC alone cannot form MBs and needs a second phospholipid such as the DPPE. The combination of phosphatidylcholine and phosphatidylethanolamine was selected for its ability to form stable and narrow-sized MBs [58] and for its lack of electrostatic net charge at physiological pH.

As an initial formulation step, the miscibility between DPPC and DPPE was studied by means of their melting behavior. Accordingly, the miscibility of DPPC / DPPE binary mixtures with bPEI-PA was explored and concentration ranges were selected for further formulation research.

Precursor liposomes comprising DPPC and DPPE lacked colloidal stability and were prone to sedimentation which was one substantial formulation problem of this work. Therefore, next studies were directed towards improving the colloidal state of DPPC / DPPE liposomes by replacing water with hydrophilic solutes such as glycerol. Following research focused on the loading of bPEI-PA liposomes with pDNA and controlling the size and Zeta potential of liposomes, as well as obtaining appropriate MB yields upon agitation. This was done by handling formulation parameters such as the pH, ionic strength, N/P ratio, *etc.*

In the final pre-formulation stage, the developed MB formulations were tested in their ability to condense and protect DNA against enzymatic degradation, as well as in their *in-vitro* transfection activity and cytotoxicity.

In their works Naumann et al (2001a and b) [271, 272] and Foremal et al. (2003) [273] demonstrated that numerous amphiphilic lipopolymers can form two-dimensional gels when grafted on condensed phospholipid monolayers on the air-water surface. These monolayer-supported polymer networks were stabilized by two different types of associative interactions – hydrophobic association of the phospholipid acyl chains, and hydrogen bonding between adjacent hydrophilic polymer clusters on the top of the monolayer. Considering the abundant hydrogen bonding capacity of bPEI, this hypothesis should be considered when thinking about the organization of the bPEI-grafted MB shell.

4.3.1. Mixing behavior of DPPC and DPPE

The thermotropic behavior of pure DPPC and DPPE revealed symmetrical sharp peaks centered correspondingly at 41.5 °C and 64.31 °C (Figure 50). The mean transition peak temperature of the binary mixtures changed rather linearly ($R^2 = 0.9827$) between the melting temperatures of the single phospholipids.

The high ratios between peak half-height width ($W_{0.5}$) and peak height (H) of pure phospholipids were indicative for their high cooperativity [274, 275] (Figure 49). In mixed bilayers a pronounced peak broadening and flattening was observed which was indicative for decrease of cooperation and membrane fluidization. On the concentration scale this effect did not follow a symmetrical progression, but was more pronounced in the low-DPPE region.

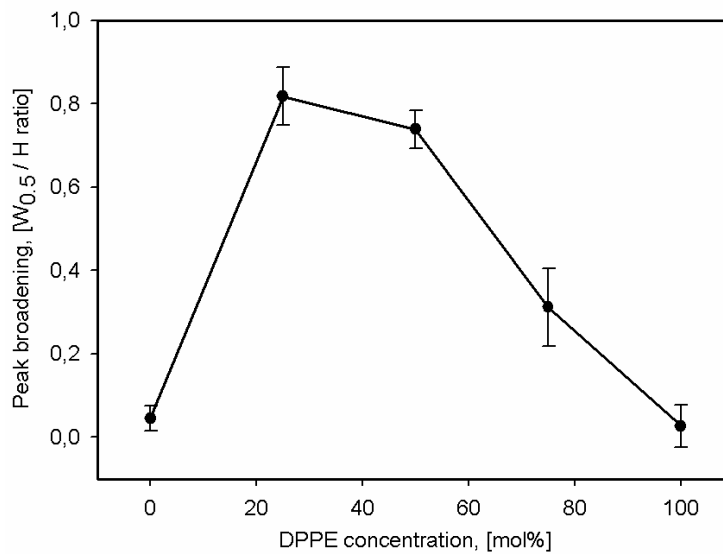


Figure 49: Transition peak flattening and broadening in binary mixtures of DPPC and DPPE, expressed as the ratio of peak width at half peak height ($W_{0.5}$) vs. peak height (H). The more pronounced peak broadening in the low-DPPE range indicates higher membrane fluidity and was beneficial for MB formulations with a high yield and an optimal size distribution.

The miscibility of phospholipid components constituting the MB shell is an important formulation parameter which determines the lateral shell homogeneity of the shell monolayer. Therefore, it was evaluated in the present study based on the melting behavior of mixtures comprising DPPC and DPPE.

In binary mixtures at various molar proportions DPPE and DPPC demonstrated an ideal miscibility in the liquid-crystalline phase, indicated by the appearance of a single transition endotherm (Figure 50). Miscibility limitations in the gel phase in the low-DPPE concentration region were indicated in DSC studies by Blume et al. (1974) [276].

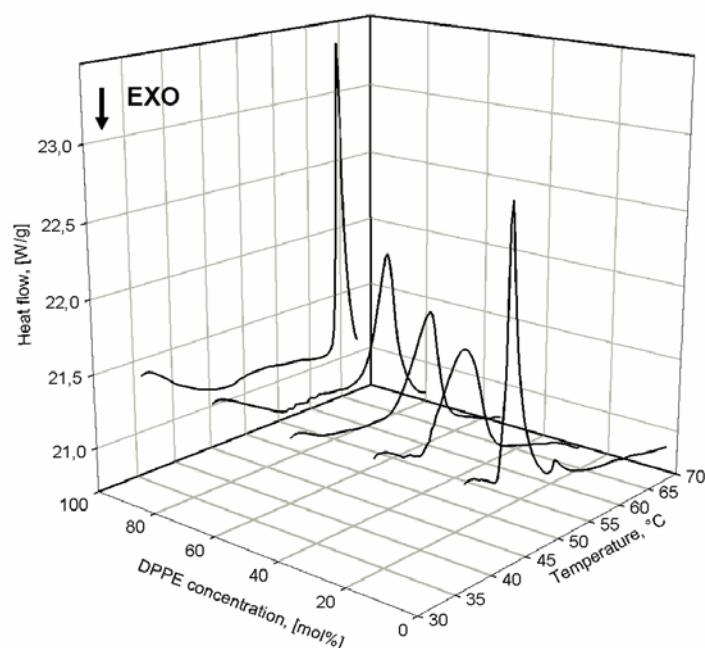


Figure 50: Phase shift diagrams of binary mixed phospholipid bilayers composed of DPPC and DPPE in various proportions in water. The concentration of DPPE increases from 0 mol% to 100 mol% with an increment of 25 mol%, while the total phospholipid concentration remains 20 mM ($n = 9$).

Due to the ideal miscibility of DPPC and DPPE, the identification of an optimal concentration region, based on this premise, was purposeless. However, macroscopic observations of the formulations during storage over a week in refrigerator showed that their colloidal stability decreases with rising DPPE concentration. Later experiments further revealed that liposomal precursors, containing 10-20 mol% DPPE at a total phospholipid concentration of 3 mM, produce the highest MB yields with an optimal size distribution. Higher molar ratios of DPPE led to an increase of the MB size, while DPPC and DPPE alone failed to produce MBs (data not shown).

Based on these observations, the concentration region of 10 mol% to 20 mol% DPPE in DPPC was selected for further development.

4.3.2. Effect of glycerol on the colloidal stability of DPPC / DPPE liposomes

The colloidal state of aqueous DPPE / DPPC dispersions is greatly impaired through the intrinsic negative curvature (towards the polar head group) of the DPPE molecules which is incompatible with the positive curvature in the outer bilayer leaflet of liposomes [277].

While DPPC molecules possess a “cylindrical” form and occupy the energetically most stable lamellar (L_{α}) lyotropic phase, those of DPPE are “cone-shaped” and adopt the inverted hexagonal (H_{II}) phase. The relatively high percentage of DPPE in liposomal formulations (20 mol% of the total phospholipid amount) apparently confers the mixed bilayer a net negative curvature [278]. The slow lyotropic transition, facilitated by the nearly to zero Zeta potential of liposomes, leads to their aggregation, coalescence, and sedimentation within several hours up to a day during storage of 3 mM dispersions at 4 °C.

Liposomal stability could be greatly increased by including bPEI-PA to the bilayer apparently due to electrostatic and steric repulsions. Nevertheless, the sterically large polar group of bPEI-PA could “unbend” the negative layer curvature caused by DPPE. Anyway, the liposome size could not be confined in the desired low nanometer range and a substantial increase of their size and polydispersity was observed on storage.

One possible opportunity to further stabilize the liposomal size and probably to increase the MB yield is posed by the replacing of water molecules from the hydration shell of the grafted phospholipid bilayer.

Glycerol has several important effects on phospholipid dispersions including viscosity increase, water substitution, decrease of solvent polarity and membrane relaxation and finally lowering of the surface tension. In the above engineered phospholipid system, DPPC is the component responsible for the high collateral cohesion [93], while DPPE possesses a higher hydration state [93, 279] and mediates therefore the interaction with the outer aqueous phase. While the methylated headgroup of DPPC is rather hydrophobic, DPPE intensively interacts with water mainly through hydrogen bonding [280]. However, glycerol has a greater hydrogen bonding capacity than water and can partially replace it from the hydrating shell of phospholipid headgroups [281]. Furthermore, since its molecule has an about 3.7-fold higher volume (109.6 \AA^3 [282]) compared to water (29.89 \AA^3 [283]), glycerol can enhance the hydration volume of phospholipid headgroups. Hence, it can increase the headgroup interfacial area [184, 281] which apparently can result in a positive bending effect, compensating the negative layer curvature due to DPPE.

Corresponding to its modulating effect on headgroup hydration, glycerol can relax phospholipid membranes by lowering the collateral adhesion between molecules. A relaxation

effect in the headgroup region in DPPC bilayers was reported by McDaniel et al. (1983) [281]. Furthermore, a relaxation in the acyl tail region could be explained through the lowering of dispersant polarity with increasing glycerol amount [282]. While pure water has a dielectric constant (τ) of 78.48 at 25 °C, for pure glycerol τ has a substantially lower value of 42.48 [284].

A further effect of glycerol is the reduction of the surface tension in aqueous systems which could be of major importance for the formation of MBs during mechanical agitation. At 50 mol% glycerol in water about 92% of the air-water interface area is occupied by glycerol molecules [285]. It is possible that the reduced surface pressure promotes the dislocation of phospholipid molecules onto the gas-liquid interface during agitation and shifts the existing equilibrium between liposomes and MBs towards the MB formation.

Another stabilizing contribution of glycerol in liposomal dispersions is the increase of their viscosity, limiting the Brownian motion, particle impact events, and therefore the probability for agglomeration and coalescence.

Several interesting effects were observed in the thermal transition behavior of DPPC / DPPE mixtures upon increasing the glycerol amount. In the range of lower glycerol concentrations from 0 mol% to 19.8 mol% glycerol (corresponding to 50 vol%) an significant increase of the melting peak temperature from about 45.2 °C to about 48.6 °C, followed by a steep drop to 42.5 °C when reaching 42.5 mol% glycerol (Figure 51, solid line) could be detected. Since under fully hydrated conditions the main phase transition characteristics of phospholipids are determined by their acyl chains [286] this effect can be mainly contributed to perturbations in the hydrophobic region.

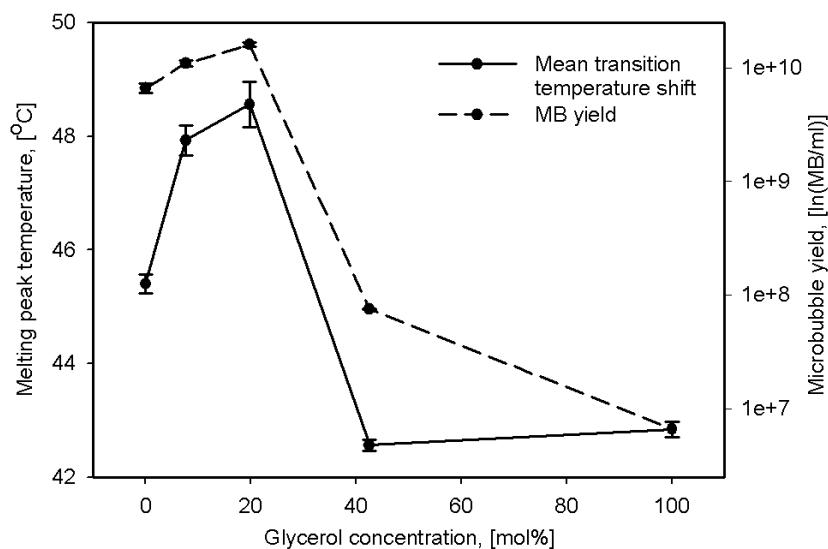


Figure 51: Influence of glycerol concentration on the melting temperature (T_m) of 80 mol% DPPC / 20 mol% DPPE with total phospholipid concentration 20 mM ($n = 9$).

In complementary follow-up experiments, implementing the same concentration range of glycerol, but at a phospholipid concentration of 5 mM which is suitable for the production of MBs, the progress of MB yield has been studied. Generally, the MB yield followed the progression of DSC events (Figure 51, dashed line). An about 5-fold increase of MB concentration was denoted upon addition of 19.8 mol% glycerol. When the amount of glycerol was further increased to 42.5 mol% the MB concentration dropped by about 10^4 -fold. Interestingly, 42.5 mol% is the lowest glycerol concentration at which a interdigitation peak differentiates from the broad mean transition at 44.2 °C and sharpens and migrates to 42.1 °C in water-free medium (Figure 52). The interdigitated state of phospholipid bilayers [184, 281] can be induced by small alcohols, drug molecules [287], *etc.* In interdigitated phospholipid bilayers, the acyl chains of the one bilayer sheet completely interpenetrate the hydrocarbon chains of the apposing monolayer. In this manner the terminal methyl groups of acyl chains are closely positioned to the phosphate groups of the opposite monolayer sheet and the bilayer sheets are fully “zipped”.

The glycerol induced interdigitation is typical for phosphatidylcholines at low water concentrations, yet the described main transition temperature shift has not yet been observed in pure DPPC [281, 288] and can apparently be denoted as a specific property of the binary mixture of DPPC and DPPE.

Finally, the melting thermograms in the concentration range up to 19.8 mol% (50 vol%) glycerol revealed a single transition peak for the binary phospholipid mixture, indicating that

no significant phase separation occurs due to the altered phospholipid hydration caused by glycerol.

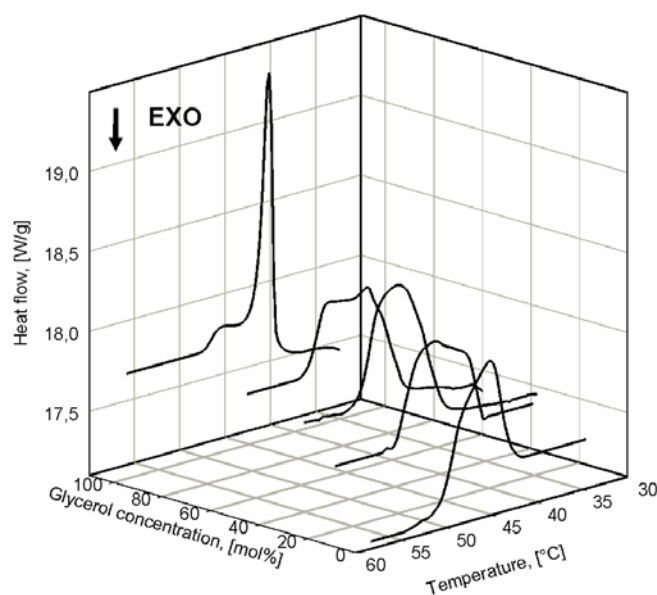


Figure 52: Phase transition diagrams of binary systems of 20 mol% DPPE and 80 mol% DPPC at a total phospholipid concentration of 20 mM and various concentrations of glycerol ranging through 0 mol%, 19.8 mol%, 42.5 mol%, and 100 mol% (curve of 7.6 mol% glycerol not shown for sake of clarity, $n = 9$).

One possible reason for that effect could be attributed to the onset of acyl chain interdigitation. Since the phospholipid bilayer needs to be “unzipped” in order to form the MB monolayer shell, the phospholipid condition in liposome intermediates need to combine a high lateral cohesion and collateral fluidity, together with a weak interaction between the bilayer sheets. The major effects of phospholipid interdigitation are the integration of the bilayer sheets and the enhancing of the lateral distance between phospholipid molecules.

Another hypothesis can be developed based on the increase of mean phase transition temperature. During the mechanic agitation of liposomes, temperature in glycerol free samples increases from about 25 °C to about 34 °C during the first 20 s, and may reach 45-50 °C after 60 s (see Figure 6, p.43). As the pace of temperature increase is viscosity dependent (yet, not linearly), the temperature during the agitation generally rises faster with increasing viscosity (see Figure 8, p.45). When tube temperature reaches the phospholipid melting temperature the lateral cohesion between molecules abruptly decreases upon phase transition from gel- to liquid-crystalline. Since the phospholipid monolayer is not stable in this phase state, the MB degradation apparently through shear forces surmounts the formation process, leading to low MB yields.

4.3.3. Mixing behavior of bPEI-PA with DPPE / DPPC bilayers

Following, the miscibility of bPEI-PA in binary mixtures of 20 mol% DPPE and 80 mol% DPPC was studied in the concentration range from 0 mM to 40 mM bPEI nitrogen with an increment of 10 mM.

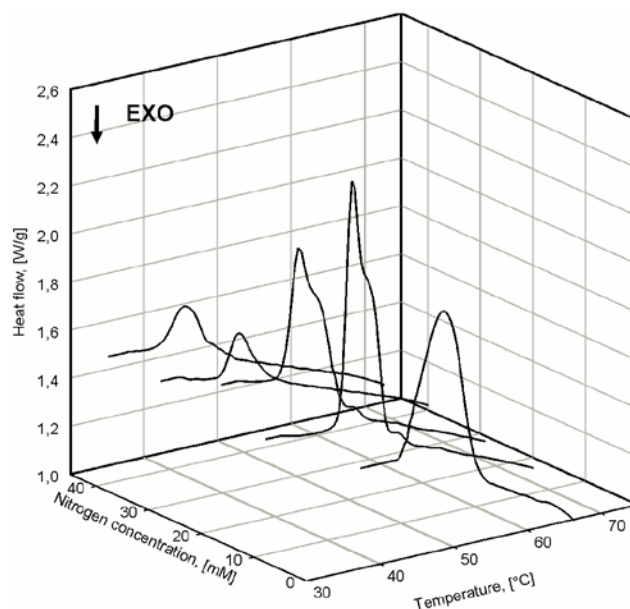


Figure 53: Phase shift diagrams of ternary mixed bilayers composed of 20 mol% DPPE, 80 mol% DPPC and various amounts of bPEI25-PA20 in water.

For the pure DPPE / DPPC mixture, the mean transition endotherm was broad and symmetrically centered at 45.31 °C. After addition of 17.2 μM bPEI25-PA20 (corresponding to 10 mM nitrogen and about 344.2 μM palmitic acid), the peak sharpened, shifted to about 43.3 °C and became a shoulder. Upon increasing the nitrogen concentration to 20 mM (corresponding to 34.4 μM) the peak retained its position and the shoulder, but became flatter and broader. Further increase of bPEI-PA concentration to 30 mM and 40 mM nitrogen depressed the transition to 42.1 °C and 41.3 °C, as well as led to further peak broadening and flattening.

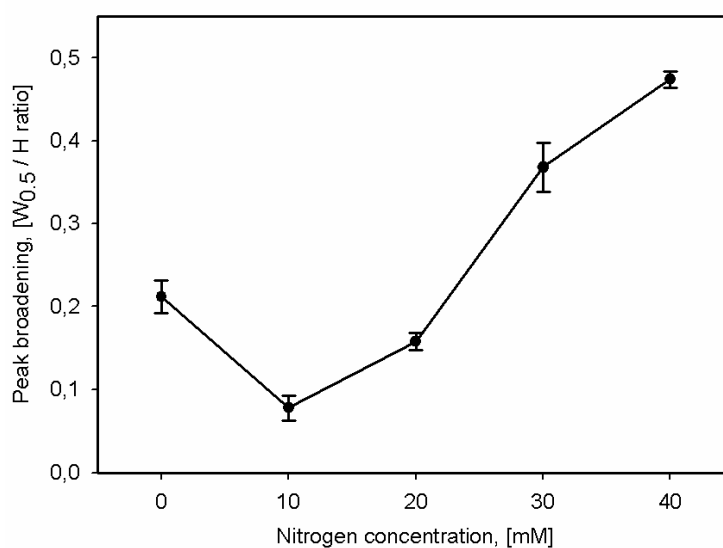


Figure 54: Transition peak flattening and broadening in ternary mixtures of 20 mol% DPPE, 80 mol% DPPC and bPEI25-PA20 in concentrations varying from 0 μ M to 68.8 μ M with an increment of 17.2 μ M. Peak broadening is expressed as the ratio between the peak width at half peak height ($W_{0.5}$) and the peak height (H).

As indicated by the progression of peak broadening, expressed as the ratio between the peak width at half height and the peak height, the addition of low amounts bPEI25-PA20 increases the membrane lateral order, while amounts of above 17.2 μ M bPEI25-PA20 (corresponding to 10 mM nitrogen) increase membrane fluidity.

Generally, the phospholipids demonstrated a good miscibility with bPEI-PA in all proportions. The occurring shouldering at nitrogen concentrations of 10 mM and 20 mM could be either due to a moderate phase separation, or because of the occurring of a second fluid crystalline phase of hydrogen-bridged bPEI-moieties above the phospholipid layer, as suggested in the literature for other systems of hydrogen-bonding lipopolymers and phospholipids [271-273, 289].

4.3.4. Determination of bPEI-PA buffer capacity

The buffering capacity of amphiphilic PEI conjugates has been demonstrated in previous studies [290-292] and has been confirmed for own bPEI-PA conjugates in PCL formulations. Similarly to the corresponding bPEI, the conjugates successfully buffered the pH range between 4 and 6.

The behavior of the negative control samples comprising water and DPPC / DPPE liposomes was identical. In the absence of buffering chemical moieties it revealed a rapid pH drop down to about 3 yet at as low proton concentrations as 0.67 mM. In spite of the obvious DPPE

protonation ability at pH beneath 4, demonstrated by Zeta potential studies below, no buffering effect has been observed in its case.

Generally, the substitution rate with PA showed a moderate influence on the buffering capacity. Compared to bPEI, amphiphilic conjugates mostly showed a slightly lower buffering ability, more pronounced for highly substituted conjugates such as bPEI10-PA60. The data point out that chemical grafting of hydrophobic PA residues plays only a marginal role on the buffering capacity of the bPEI moiety of the conjugate.

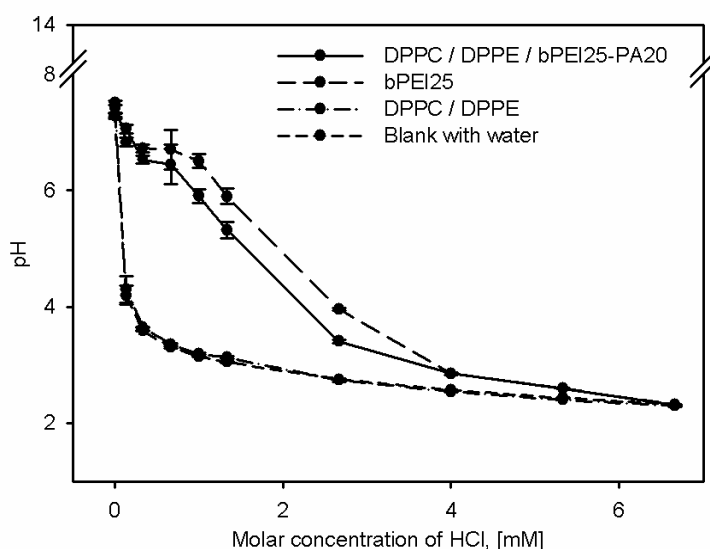


Figure 55: Buffering capacity of polycationic liposomes comprising bPEI25-PA20 compared to bPEI25 and zwitterionic DPPC / DPPE liposomes. Blank measurement was carried out with water. The buffering capacity of bPEI25-PA20 was close to that of bPEI25.

The persisting acid buffering capacity in the pH range from 6 to about 4 of bPEI-PA suggests that it will be able to leverage the acidic conditions in endolysosome, where the pH approaches 5, and to mediate their osmotic rupture.

4.3.5. Zeta potential of polycationic liposomes with bPEI-PA

The Zeta potential of bPEI-PA comprising PCL was significantly influenced by the substitution rate of bPEI with PA, showing a non-linear dependency (Figure 56). At lower substitution rates such as 10, 20, and 30 PA grafts per bPEI molecule the Zeta potential declined by about 3 mV and fell by further 7 mV with increasing the substitution to 100 PA grafts per molecule. At further increase of the substitution rate from 100 to 300 PA grafts per molecule bPEI there was no major change in the PCL Zeta potential.

It is possible to hypothesize that increasing the ratio between PA grafts per bPEI molecule causes a stronger interaction with the phospholipids. Therefore, the bPEI residue is denser enveloped with phospholipids shielding the outwards Zeta potential. Another explanation for this effect could be the consumption of protonable primary and secondary amine groups which are converted to amide moieties through the grafting with PA.

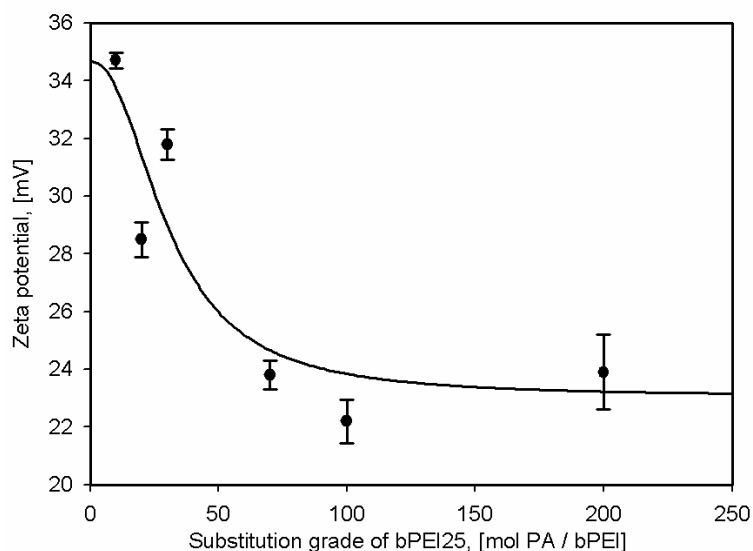


Figure 56: Effect of bPEI25 substitution with PA on the Zeta potential of polycationic liposomes at pH 7.4. At lower substitution rates of 10 to 100 PA grafts per bPEI molecule, the Zeta potential sloped steeply down from about 35 mV to about 23 mV. Further increase of the substitution rate to 300 PA grafts per molecule produced no significant changes in the Zeta potential ($n = 3$, $p < 0.05$).

The effect of increased bPEI-PA concentration on the Zeta potential of polycationic liposomes was non-linear, resulting in a rapid increase from 5-6 mV, if no polycation is present, to about 35 mV at a nitrogen concentration of 20 mM. Further increase of the bPEI-PA concentration to 40 mM nitrogen raised the Zeta potential only moderately to 40-43 mV, while no significant further increase followed at higher polycation amounts of up to 100 mM nitrogen. Nevertheless, the increasing concentration of bPEI25-PA20 significantly increased the viscosity of the formulations and made them inapplicable for the production of MBs.

The behavior of polycationic liposomes Zeta potential during acid titrations in the pH range from 6 to about 4 was studied simultaneously with the buffering capacity of bPEI-PA (Figure 57). The Zeta potential of polycationic liposomes showed no proportionality to the protonation rate of the bPEI residue during the pH titration (see Figure 55). Similarly to bPEI25, the amphiphilic conjugate bPEI25-PA20 effectively buffered the pH range from 6 to

about 4. However, the pH interval of buffering the Zeta potential of PCL initially increased from 70 mV (at a pH of 6.53) to about 88 mV (at a pH of 5.3). A similar behavior was observed with non-substituted bPEI25, where the Zeta potential rose from 73 mV (at a pH of 6.7) to about 86 mV (at a pH of 3.96).

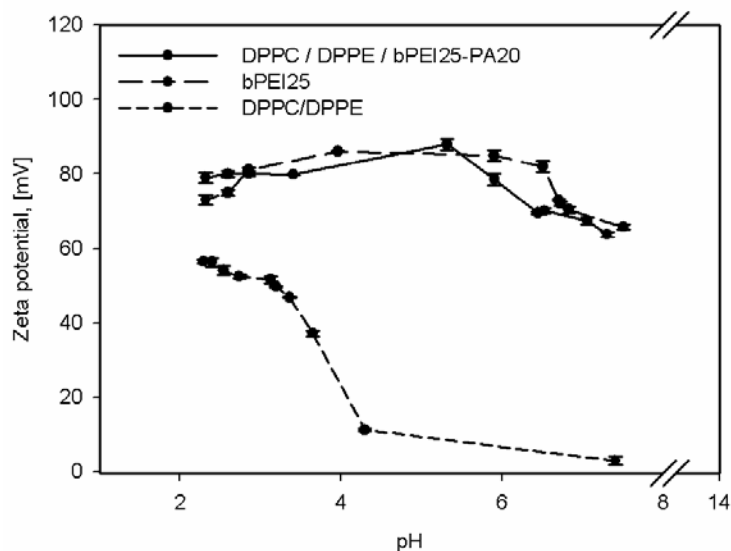


Figure 57: Effect of pH change on the Zeta potential of bPEI25-PA20 liposomes, compared to bPEI25 and DPPC / DPPE liposomes. At lower pH values the Zeta potential was depressed by the increasing conductivity of the sample medium ($n = 3$).

The negative control sample, comprising DPPC / DPPE liposomes, demonstrated a pH dependent shift of Zeta potential, too. In the pH interval from about 4.3 to 2.3, the Zeta potential rapidly increased from 11 mV to 56.5 mV. This could be contributed to the protonation of the phosphate group of DPPE, having in bilayers a transition in the protonation state at a pH of approximately 3 [293].

4.4. Studies on the loading of bPEI-PA liposomes with pDNA

In following formulation studies, the loading capacity of PCL was examined with regard to their size, Zeta potential and capacity to produce MBs upon mechanical agitation.

The pDNA loading studies were aimed at the formulation of small polyplexes, sized in the lower nanometer range which after loading possess a residual net positive Zeta potential, and produce appropriate yields of MBs upon agitation.

4.4.1. Complexation capacity of bPEI-PA liposomes for pDNA

The ability of PCL to bind pDNA was scrutinized using the ethidium bromide exclusion assay [265]. The fluorescent dye ethidium bromide intercalates between the base pairs of DNA. The degree of access to the binding sites is mainly dependent on the condensation state of DNA. The fluorescence quantum yield of ethidium bromide is also significantly enhanced by intercalation between nucleotide pairs. When a polycation binds to the nucleic acid, intercalated ethidium bromide is displaced and a fluorescence intensity drop can be noticed. The maximum curve slope (first derivative) indicates the N/P-ratio, at which maximum DNA binding occurs and the polycation affinity to DNA.

Experimental data revealed a general trend of decreasing of the bPEI-PA capacity to bind and condense pDNA with increasing rate of chemical substitution with PA (Figure 58). This effect was clearly observed in the case of bPEI1.8 and its conjugates.

For non-substituted bPEIs further binding of pDNA was no more possible beyond N/P ratios of between 1.2 and 2. Substituted bPEI-PA conjugates showed less complexation ability and had higher saturation N/P ratios of about 3.0-3.4 for bPEI1.8-PA2, bPEI10-PA12, bPEI10-PA30, bPEI25-PA10, and bPEI25-PA20. Even lower binding capacities of N/P 4.5-5.0 were observed in the cases of bPEI1.8-PA2 and bPEI25-PA30. Phospholipid liposomes, comprising no polycation, did not bind and condense pDNA.

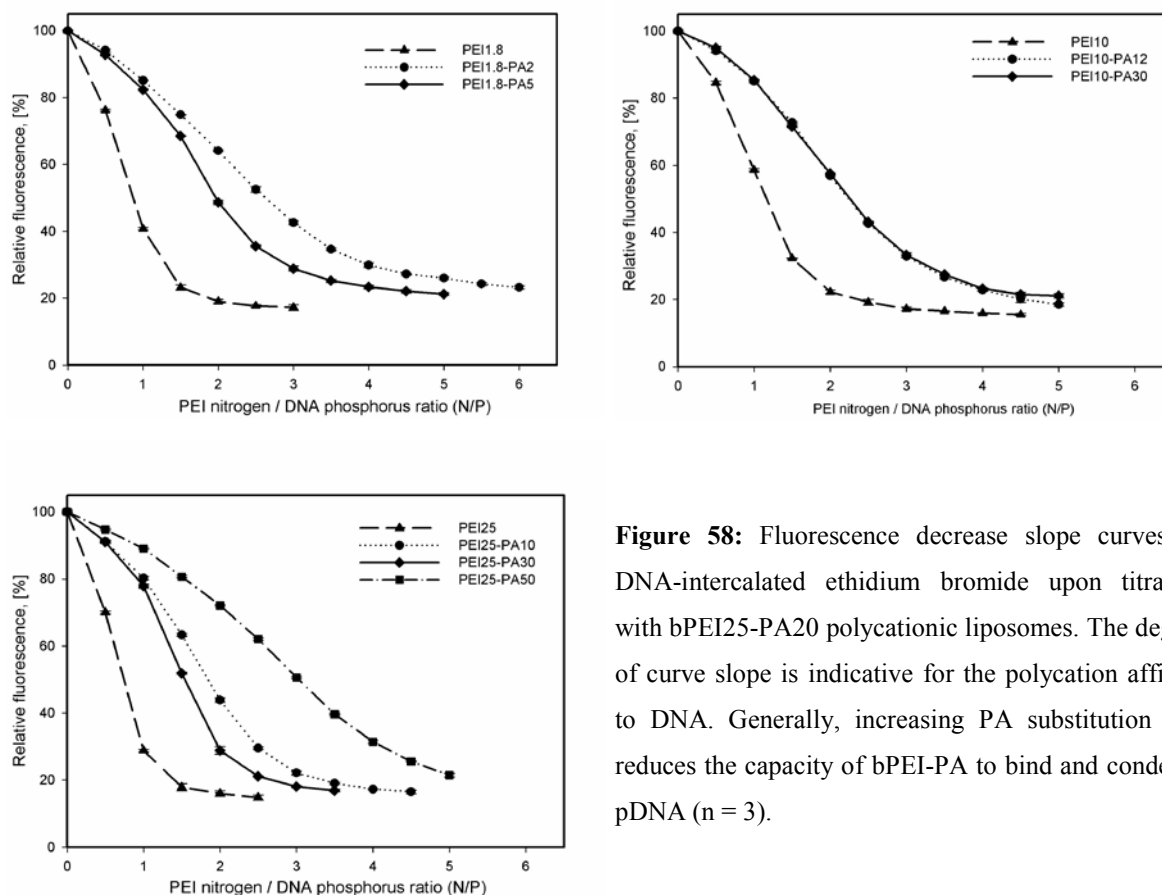


Figure 58: Fluorescence decrease slope curves of DNA-intercalated ethidium bromide upon titration with bPEI25-PA20 polycationic liposomes. The degree of curve slope is indicative for the polycation affinity to DNA. Generally, increasing PA substitution rate reduces the capacity of bPEI-PA to bind and condense pDNA ($n = 3$).

The decreasing complexation ability of amphiphilic conjugates compared to the non-substituted bPEI species can be attributed to their interaction with the phospholipid phase. Provided the hydrated bPEI moieties build a hydrophilic core, where the hydrophobic PA rests are directed outwards, they can interact with phospholipid molecules and build liposome- and micelle-like structures. Similar to the structures, proposed by Ko et al. (2009) [294], in the so formed core-shell associates the bPEI-PA could be enveloped in phospholipid molecules rather than exposed at the liposome surface, as suggested by Oku et al. (2001) [230].

Further hypotheses can be considered with regard to conformational changes of bPEI and the occurring of steric tension after the lipopolymer molecule has been deformed by the hydrophobic association with other bPEI-PA molecules and phospholipids. It is also probable that the consumption of primary amino groups by the chemical grafting plays a role, too.

4.4.2. Effect of pH on the polycationic liposome size

In aqueous dispersions polyplexes of pDNA and bPEI-PA do not exist as distinct structures, but are associated by phospholipid into polycationic liposomes or other lyotropic structures.

On the other hand, polycationic liposomes are dissipated during the production of polyplex-associated MBs while the polyplexes presumably retain their size. For this reason, particle size measurements in dispersions of polycationic liposomes do not represent the real size of the secondary-carrier particles, but a higher value. Although one of the important aims of the current formulation research was to obtain smaller polyplex liposomes as an indirect sign for smaller polyplexes.

The size of polyplex liposomes and their polydispersity could be successfully influenced by changes of the pH prior to the complexation with pDNA (Figure 59).

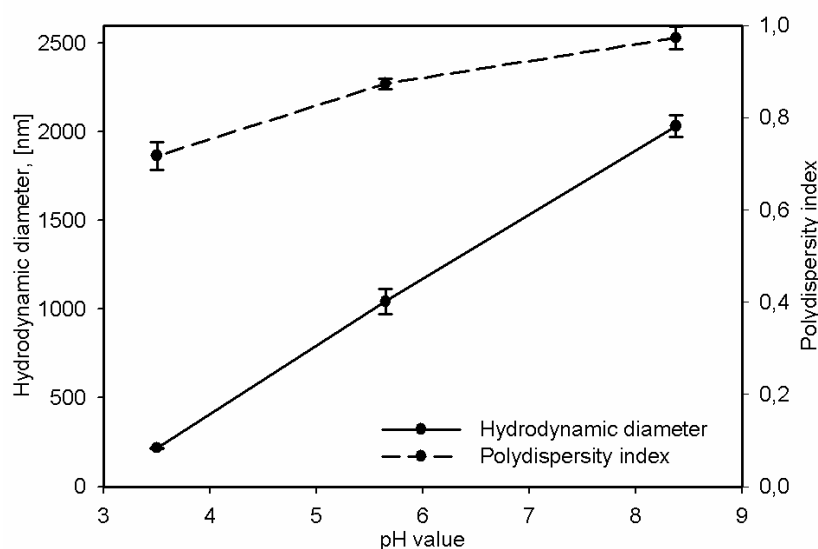


Figure 59: Effect of the pH value on the diameter of polycationic liposomes comprising bPEI25-PA20 at a nitrogen concentration of 20 mM and an N/P loading ratio of 15. A decrease of both particle size and polydispersity was achieved by reducing the pH value. After lowering the pH from 8.3 to 3.5 the liposome hydrodynamic diameter decreased from about 1,900 nm to about 300 nm, while the polydispersity index declined by about 0.2 units.

The size of DNA-loaded polyplex liposomes was successfully reduced by lowering the pH value. A pH decrease from 8.3 to 3.5 led to a 6.3-times decrease from 1,900 nm to about 300 nm of the hydrodynamic diameter. The polydispersity index decreased by approximately 2.4-fold from about 8.3 to 3.5. As the pH range below 4 approaches extreme acidic conditions, a pH span of 4.5 to 4.0 was selected as best suitable for formulations.

The observed effect of particle size decrease can be explained with electrostatic effects caused by the protonation of bPEI-PA and DPPE. As depicted in the titration curves on Figure 55 on p.176 and on Figure 57 on p.178, with decreasing pH bPEI is progressively protonated and

the positive charge density per molecule grows. Up to a pH of about 3.5 the negative charge number of pDNA is not affected, hence each bPEI molecule provides more binding sites for pDNA and thus, less molecules polycation are necessary to condense a single plasmid.

4.4.3. Polycationic liposome size according to bPEI molecular weight, PA substitution, and loading with pDNA

In the following study, a more extensive comparison will be made between the particle size and polydispersity of polycationic liposomes, comprising bPEI with various molecular weights and bPEI-PA conjugates with different substitution rates. Following, the bPEI-PA will be compared according to their particle size growth after loading with pDNA at an N/P ratio of 15.

Generally, unloaded polycationic liposomes had hydrodynamic diameters of 100-160 nm with no apparent influence caused by bPEI different molecular weights. Comparing particle sizes in aqueous dispersions of bPEI-PA conjugates in absence of phospholipid (Figure 48, p.165), and the corresponding polycationic liposomes (Figure 60) it is obvious that the complexation of bPEI-PA with phospholipid has contributed to decreasing particle size. Under equal conditions, phospholipid-free dispersions of bPEI-PA have particle sizes of 200-230 nm, whereby the particle size and polydispersity are dependent on the bPEI molecular weight and substitution rate with PA.

The particle size of polycationic liposomes after loading with pDNA was influenced by the molecular weight of the bPEI used. Neu et al. (2005) [218] demonstrated that low-molecular weight bPEI in the order of 1.8 kDa provides only over a limited capacity to condense pDNA and to form small polyplexes. In the current study these findings were confirmed since in absence of phospholipid polyplexes, formed with bPEI1.8 were sized about 9,000 nm, compared to about 500 nm sized polyplexes, produced from bPEI25. The extensive discrepancy between polyplex size can be explained with the inability of small bPEI to complex all neutral charges of the plasmid molecule. For this reason, one plasmid can be bound to two or more polyplexes at the same time and act as a inter-particle cross-bridge [295].

In the presence of phospholipid the size of polyplexes with bPEI1.8 was stabilized at about 500 nm. However, in average polyplexes and DNA-loaded polycationic liposomes comprising bPEI1.8-PA were still bigger sized than formulations with bPEI10 and bPEI225 and their conjugates.

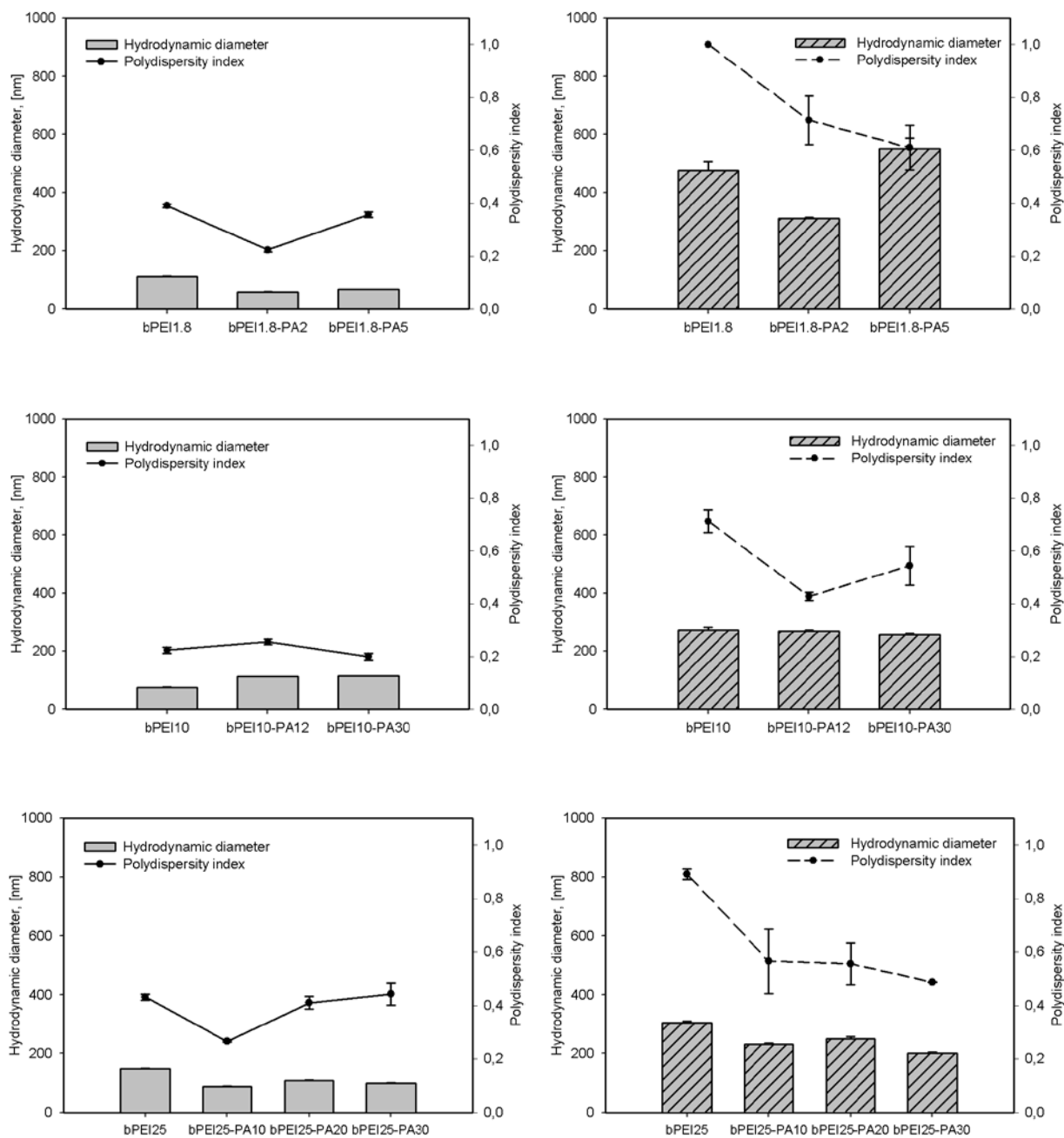


Figure 60: Hydrodynamic diameter and polydispersity index of polycationic liposomes, comprising phospholipids and bPEI with various molecular weights and their amphiphilic conjugates with various amounts of PA in water prior to (on the left side) and after their loading with DNA (on the right side), $n = 3$.

There was no significant difference between polyplexes, comprising bPEI10 and its conjugates which were all about 300 nm sized. DNA-loaded polycationic liposomes with bPEI25-PA conjugates had somewhat lower sizes of around 200 nm, independently from the rate of PA grafting.

As expected, when loading of increasing amounts of DNA the Zeta potential of polycationic liposomes was turned more negative with decreasing N/P ratio, and reached highly negative values of about -40 mV at an N/P of about 7 (Figure 61, solid line). Simultaneously the particle size distribution of polycationic liposomes (dashed line) reached a maximum when the Zeta potential approached zero and the electrostatic repulsing forces between particles were practically neutralized. Under these conditions, polyplexes tend to aggregate [296] due to the prevalence of attractive such as hydrophobic interactions and van-der-Waals forces [297].

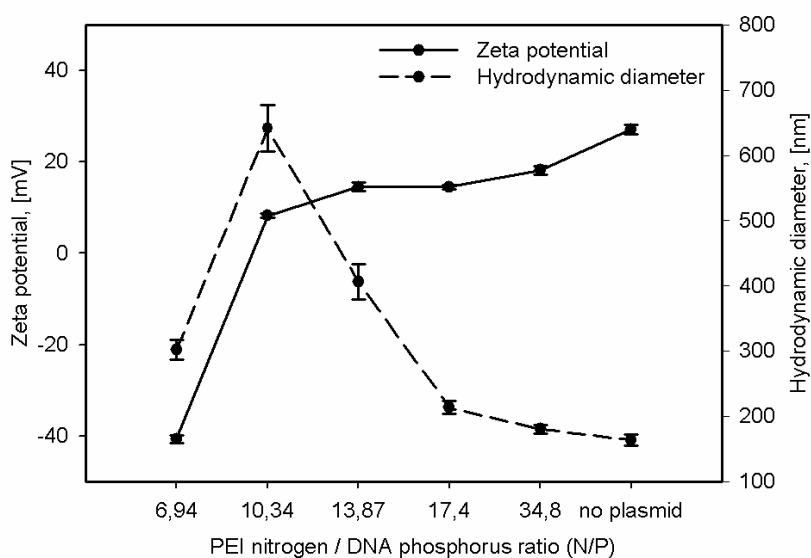


Figure 61: Zeta potential of polycationic liposomes with bPEI25-PA30 at various N/P DNA loading ratios.

Interestingly, the cationic bPEI charges were shielded by DNA at an N/P ratio of about 10. However, according to Figure 58 on p.180 the saturation of bPEI25-PA30 lies much lower between N/P ratio values of 3.0-3.5. Though the higher protonation of bPEI25-PA30 during the current loading study its loading capacity was limited not by the rate of DNA condensation, but by the depression of Zeta potential and the particle size growth. Therefore, according to the above data, the binding ability of bPEI seems to be higher than its loading capacity, determined by its Zeta potential. Indeed, the binding of DNA is thought to be driven by entropic forces arising from the release of counter ions or hydrating water, rather than by electrostatic interactions [218, 298]. However, the observed progress of particle size and Zeta potential was not typical for all bPEI-PA conjugates tested. Accordingly, loading with pDNA with N/P ratios of down to 10 was achieved in later studies.

A comparison of the Zeta potential shift of polyplexes, comprising various bPEI conjugates, and loaded at a constant N/P ratio of 15 is given in Figure 62. The shift of Zeta potential upon loading with DNA was dependent from the molecular weight and from the degree of substitution with PA. Generally, the Zeta potential was stronger influenced in polycationic liposomes comprising bPEI1.8 and bPEI10 than in the case of bPEI25. On average the Zeta potential of loaded polyplexes approached values of about 30 mV.

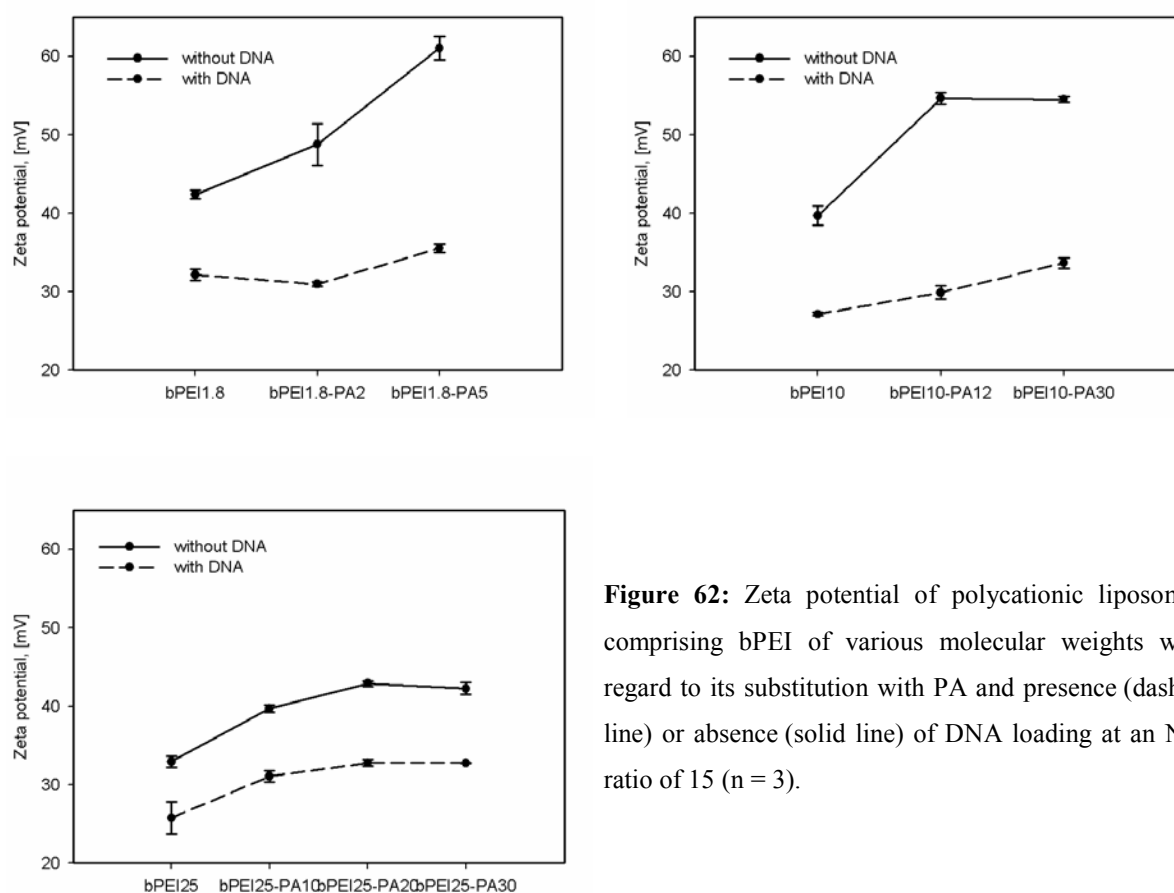


Figure 62: Zeta potential of polycationic liposomes comprising bPEI of various molecular weights with regard to its substitution with PA and presence (dashed line) or absence (solid line) of DNA loading at an N/P ratio of 15 ($n = 3$).

Comparing the particle size data in Figure 60 on p.183 with findings about the Zeta potential of polycationic liposomes, the degree of polyplex aggregation was again corresponding to the reduction of Zeta potential.

In summary, polycationic liposomes are explicitly prone to aggregation owing to features of the lyotropic state, hydrophobicity, *etc.* Repulsing electrostatic interactions seem to play an important role for their colloidal stability, particularly with regard to loading with DNA. Colloidal stability of DNA-loaded polycationic liposomes can be successfully influenced by adjustments of the pH, dispersant viscosity and polarity, phospholipid hydration state, as well

as by selection of appropriate molecular weight of bPEI and a suitable rate of substitution with PA.

4.5. Formulation and characterization of polyplex-associated MBs, loaded with pDNA

Beyond the colloidal stability and DNA complexing capacity, polycationic liposomes, loaded with DNA must possess the ability to produce MBs with an appropriate size distribution and an acceptable particle yield upon mechanical agitation.

4.5.1. Effect of electrolytes on the MB production and liposome aggregation

One major problem, solved during the formulation studies, was the extremely limited “foamability” of polycationic liposomes, leading to low particle yields of 10^3 - 10^5 MB/ml. For the first time Borden et al. (2007) [113] identified the issue about the balance between surface charge and MB stability. They observed a monotonously declining stability of positively charged MBs when the concentration of cationic phospholipid increased. Furthermore, the authors successfully overcame the shell monolayer instability by employing the ionic strength as a formulation lever. The apparent reason for the MB instability was the lateral electrostatic repulsions between cationic charges in the bubble shell. Beyond a certain concentration limit of cationic charges per unit of area, the Coulomb repulsions between phospholipid headgroups exceed the hydrophobic attractions between acyl chains. This can lead to reduction of the co-lateral adhesion between phospholipid molecules, alter the lyotropic state, increase of the surface tension, and finally impair the MB structure.

In the above mentioned paper the increasing electrolyte concentration was exploited as a formulation tool to prevent MB shell instability. According to the Debye length equation (Equation 12, p.107), when the ion concentration is increased the electrostatic repulsions are shielded and the tension in the shell monolayer is relaxed.

There is also another direct effect of the electrolyte concentration on the collateral adhesion between zwitterionic phospholipid molecules in the shell monolayer. According to the study of Oncins et al. [299] sodium chloride in the concentration range of 10 mM to 100 mM increases the collateral cohesion between phosphatidylcholine molecules and raises the layer compactness. This effect is owing to the shielding of the electrostatic repulsions between phosphate groups as well as between quaternary ammonium groups which increase the distances between neighboring molecules.

Increasing the electrolyte concentration was successfully employed in the present work to reduce the electrostatic repulsions between polyplexes. However in this case the electrolyte conditions had to be very precisely selected since too high ion concentrations lead to aggregation of the polycationic liposomes. For this reason, the Coulomb interactions were only partially screened by adjusting with electrolyte, while trying to increase the MB yield causing a minimum increase of liposome size.

Briefly, experimental data revealed an increasing tendency of polycationic liposomes to agglomerate upon increasing electrolyte concentration (Figure 63). This effect was more pronounced for triple-charged anions such as citrate compared to simple anions such as chloride. In the case of addition of triple-charged anions, the average hydrodynamic diameter of polyplex liposomes grew steeply from about 300 nm to about 7,600 nm after addition of 30 mM electrolyte. This rapid size increase did not permit the particle size to be adjusted by means of citrate.

On the other hand, a much more moderate effect was obtained by the use of single-charged anions such as the chloride. The ion concentration range between 0 mM and 50 mM provides opportunities to optimize the MB production without increasing the size of liposome precursors over 1,000 nm.

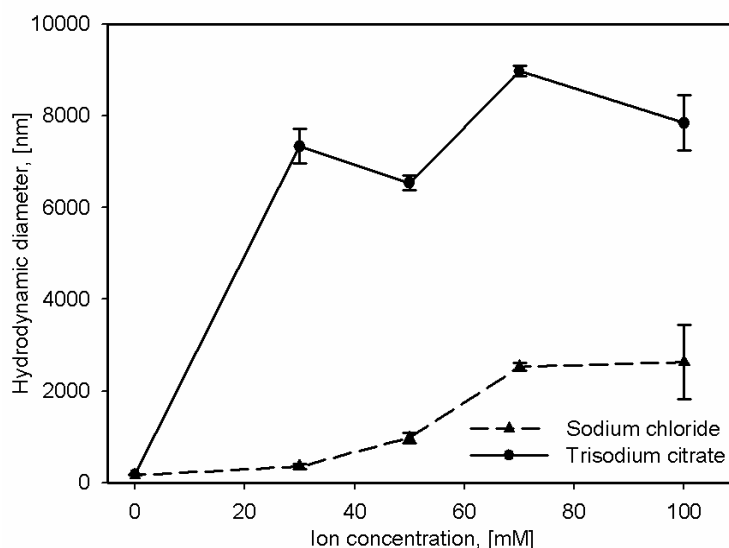


Figure 63: Effect of electrolyte concentration and anion charge on the diameter of polycationic liposomes, comprising bPEI25-PA20. The ion concentration was varied from 0, 30, 50, 70, and 100 mM.

Apparently the size increase of polycationic liposomes upon electrolyte shielding is governed by electrostatic Coulomb interactions. This is substantiated by the relation between particle

growth events and the shift of Zeta potential (Figure 64). While single-charged chloride anions caused a moderate decrease of positive Zeta potential of polycation liposomes, triple-charged citrate neutralized the polyplex cationic charges much faster.

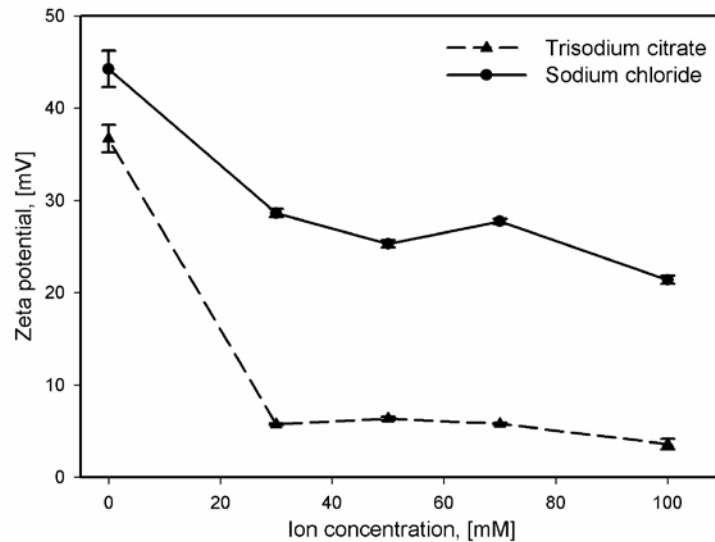


Figure 64: Effect of electrolyte concentration and anion charge on the PCL Zeta potential.

In the concentration range from 0 mM to 50 mM chloride anions shielded the Zeta potential from about 44 mV to about 25 mV, while liposomes shielded by citrate had only about 5 mV cationic Zeta charge.

The concentration of MBs did not linearly increase together with the ion concentration, as was expected according to the findings of Borden et al. Both, for citrate and chloride anions there was a maximum in the MB yield at 30 mM to 70 mM (Figure 65), while at higher ionic concentrations the MB concentration decreased again.

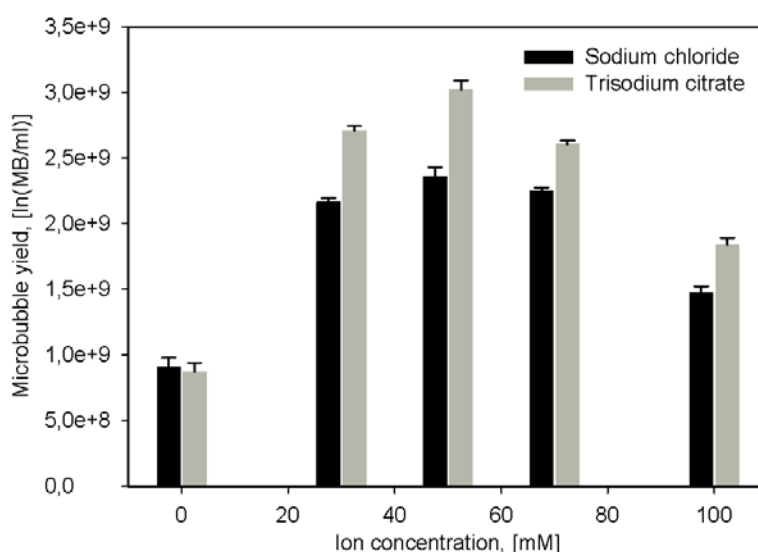


Figure 65: Effect of electrolyte concentration and anion charge on the MB yield (n = 6).

Generally, at equal ion concentrations sodium citrate produced a higher MB yield than sodium chloride. This corresponds well to the higher ability of citrate anions to shield Zeta potential (Figure 64) due to their triple charge. However, these positive features were connected with the greater liposome aggregation, caused by citrate (Figure 63).

For this reason, sodium chloride was preferred to adjust the ionic strength in a controllable manner and was included in the formulation in amounts of 10-20 mM for the production of pDNA-loaded MBs. Because DNA additionally compensates positive charges on the MB surface, it also contributed to increase the MB concentration. In contrast to pDNA-loaded formulations, unloaded liposomes produced about 10^5 -fold less bubbles.

4.5.2. Optimal formulation for polyplex-associated MBs for *in-vivo* studies

Following the research development of polyplex-associated MBs several important formulation factors were optimized and summarized into a standard formulation setup, described here. In Table 22 the amounts of pDNA and excipients in the final formulation are represented.

| Component | Molar concentration, [mM] | Mass concentration, [mg/ml] |
|--|---------------------------|-----------------------------|
| DPPC | 2.40 | 2.94 |
| DPPE | 0.60 | 0.70 |
| bPEI25-PA30 (20 mM nitrogen) | Approx. 0.03442 | Approx. 0.86 |
| HEPES | 30 | 7.15 |
| Sodium chloride | 15 | 0.875 |
| EDTA | 1 | 0.292 |
| Hydrochloric acid (for adjusting of pH) | Approx. 25 μ l | |
| Glycerol, water-free | 50 vol% | |
| Water, electrolyte-free | 50 vol% | |
| DNA (N/P = 10) | 0.40 mg/ml | |

Table 22: Optimal constitution of final formulations of polyplex-associated MBs. The concentration of bPEI nitrogen can vary from 10 mM to 20 mM. Approx. – approximately. The represented concentration result from the mixing of polycationic liposomes and pDNA solutions.

The total phospholipid concentration in final MB preparations was 3 mM, comprising 20 mol% DPPE and 80 mol% DPPC. At an N/P loading ratio of 10 and 20 mM bPEI nitrogen one single dosage unit of polyplex-associated MBs contains 160 μ g pDNA and about 4×10^9 MBs. Control pH measurements revealed moderate deviations of $\pm 4.6\%$ ($n = 12$) prior to and after the equilibration of polycationic liposomes.

Successful loading of polycationic liposomes was observed from Zeta potential measurements, while the loading of polyplexes on the MBs was demonstrated through fluorescence confocal microscopic imaging below.

4.5.3. Structure analysis of polyplex-associated MBs

The fluorescent micrographs of unloaded MBs revealed equally stained spherical structures, possessing dark interiors and a fluorescent shell (Figure 66).

Clearly the amphiphilic bPEI-PA remains associated to the phospholipid shell and does not penetrate the gas core, as confirmed by 3D-microscopic images. In unloaded MBs bPEI-PA appears equally distributed throughout the MB shell without obvious signs of lateral segregation. The conjugate is apparently incorporated mainly in the MB shell as little red fluorescence due to TexasRed[®] labeled bPEI25-PA30 was found in the background of Figure 66 A.

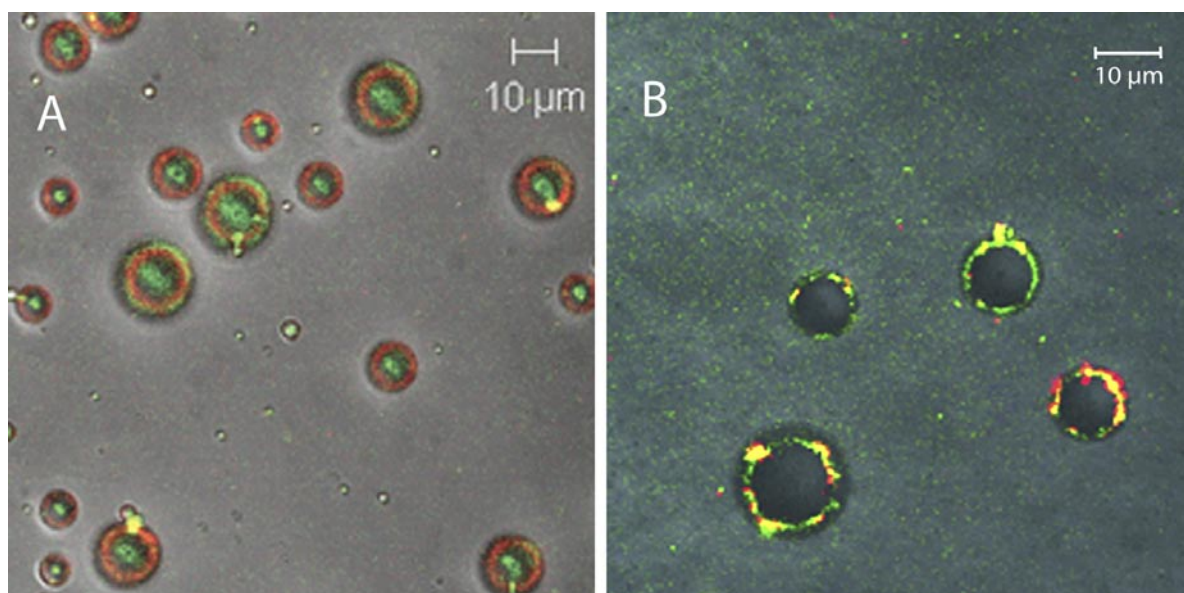


Figure 66: Confocal fluorescence microscopy image of perfluoropropane microbubbles stabilized by a Coumarine-6[®] labeled phospholipid monolayer (in green) containing the amphiphilic bPEI25-PA30. The microbubbles are either unloaded (A) or loaded with pDNA (B). On image A (left) the bPEI25-PA30 is covalently labeled with TexasRed[®] (red), while on image B (right) the red staining indicates the partition of pDNA, labeled by propidium iodide. Depending on the position of the confocal plane the MBs appear either as filled circles (confocal plane at the top or bottom of the MB) or as fluorescent rings (confocal plane in the middle of the MB).

In the case of polyplex-associated MBs loaded with pDNA (Figure 66 B) there was an condensation of phospholipid, bPEI-PA, and pDNA. Thereby, nanoparticles were spontaneously formed on the MB surface via condensation of pDNA by bPEI-PA. Between the bubbles some green (phospholipid) and red fluorescence (plasmid) is still detected indicating the presence of a residual amount of pDNA-bearing liposomes which was not transformed to MBs during the agitation.

4.5.4. Protection of pDNA against enzymatic degradation

The polyplex-loaded MBs were challenged with 200 U/l DNase I which amount is about 45-fold higher than the DNase activity in human blood [300] and allows reliable conclusions about the protection capacity of the bPEI-PA polyplex secondary carriers.

Figure 67 represents the gel electrophoresis results on polyplex-associated MBs loaded with pDNA at N/P ratios ranging from 15 to 5. As shown, the unchallenged plasmid produces two bands in the gel (lane 1 on the left) according to the coil state of the DNA strain. In lane 2, the pDNA was successfully protected by inhibition of DNase through EDTA.3Na, while the

plasmid was fragmented when fully exposed to the enzyme (lane 3). Unloaded MBs did not exhibit any intrinsic fluorescence as shown in lane 4. Furthermore, DPPE / DPPC phospholipid MBs without bPEI-PA failed to protect pDNA from degradation by DNase (data not shown).

In lanes 5, 6, and 7 on the right, no fragment bands were observed, demonstrating that in this loading range pDNA was mostly protected from enzymatic digestion by the condensation with bPEI-PA. Only trace amounts in the order of 1.0-1.5% from the total lane fluorescence were found using ImageJ software v.1.41o (National Institute of Health, USA) beyond the main plasmid band.

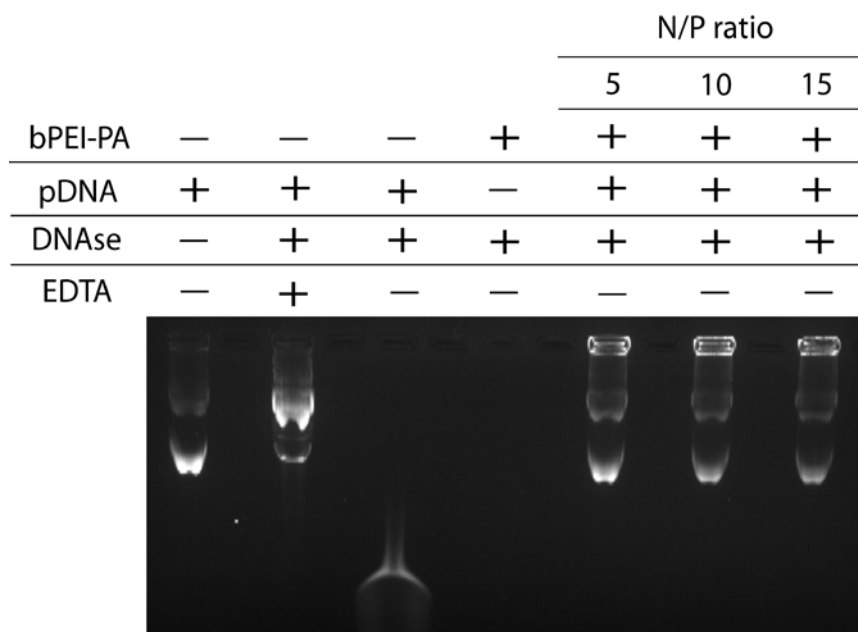


Figure 67: Agarose-gel electrophoresis of polyplex-associated MBs, loaded with pDNA at various N/P ratios after DNase challenge assay. In the N/P loading range from 15 to 5 the bPEI-PA conjugates were able to protect pDNA against enzymatic degradation, while naked plasmid was fragmented.

Clearly the pDNA was not thoroughly detached from the complex with bPEI-PA and was retained in the slots of the agarose gel which makes further quantitative assumptions unreliable. Furthermore, comparing the mean band height of free untreated pDNA and of the plasmid, released from the polyplex-associated MBs, apparently no conformational change of pDNA was caused by the condensation in polyplexes.

4.5.5. Effective encapsulation of pDNA in polycationic liposomes and in polyplex-associated MBs

According to the gel retention assay data the plasmid DNA was completely bound to polyplex-associated MBs at an N/P loading ratio of 15 (Figure 68). At higher loading amounts between N/P 13 and 5, a moderate pDNA leakage of between 3.00% and 7.84% (according to the total fluorescence of free pDNA) was observed.

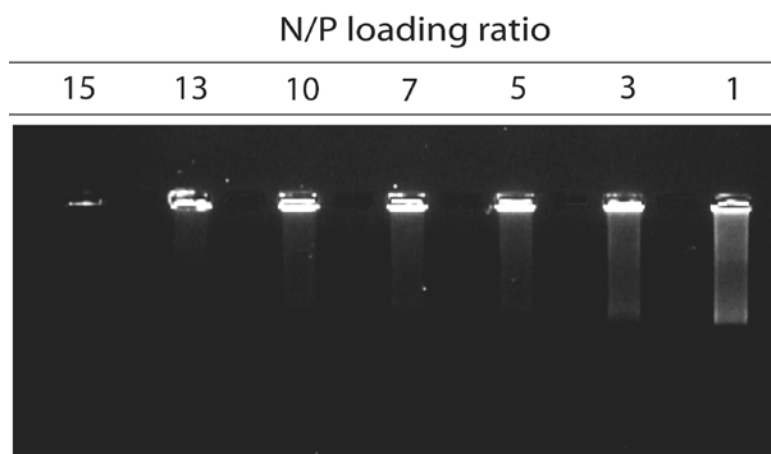


Figure 68: Gel retention assay of pDNA-loaded polycationic liposomes at various N/P ratios. Plasmid DNA remains fully bound to liposomes until an N/P of about 10 to 7, where the earliest smear is viewable. At higher pDNA amounts, particle leakage continuously aggravates.

At high loading ratios of N/P 3 and 1 practically no pDNA was bound and the loss increased exponentially correspondingly to 15.81% and 31.54% from the total plasmid fluorescence.

Further on, the effectiveness of DNA-encapsulation in polyplex-associated MBs was evaluated. MB formulations comprising bPEI25-PA20 were studied at an N/P-loading ratio of 15. From the total amount of 160 μg pDNA about 76.68% were effectively encapsulated in the MB fraction (Table 23). This results in an effective amount of about 122.69 μg pDNA encapsulated in polyplex-associated MBs.

| | Mass amount, [μg] | Percent amount, [%] |
|---------------------------------|--------------------------------|---------------------|
| Polyplex-associated MBs | 122.69 \pm 5.89 | 76.68 \pm 3.68 |
| Residual polycationic liposomes | 37.31 \pm 5.89 | 23.32 \pm 3.68 |
| Free pDNA | Trace amount | Trace amount |
| Total pDNA input amount | 160 | 100 |

Table 23: Phase partition of pDNA in polyplex-associated MB formulations comprising bPEI25-PA20 in concentrations, corresponding to 20 mM nitrogen and loaded with pDNA at an N/P molar ratio of 10.

4.6. Comparative *in-vitro* transfection / cell viability studies with pDNA-loaded polycationic liposomes and polyplex-associated microbubbles

4.6.1. The effect of bPEI molecular weight

Gene transfection efficacy and cell viability after treatment with polyplexes comprising bPEI with molecular weight of 1.8 kDa, 10 kDa, and 25 kDa prepared without addition of phospholipid were compared below. Low-molecular weight bPEI 1.8 kDa produced rather low transfection rates of $3.6 \times 10^3 \pm 2.1 \times 10^3$ RLU (Figure 69). The low transfection activity of such polyplexes could be attributed to their large size of several micrometers in absence of phospholipid.

In contrast, bPEI with a molecular weight of 10 kDa achieved about 10^3 -fold higher transfection rates than bPEI 1.8 kDa.

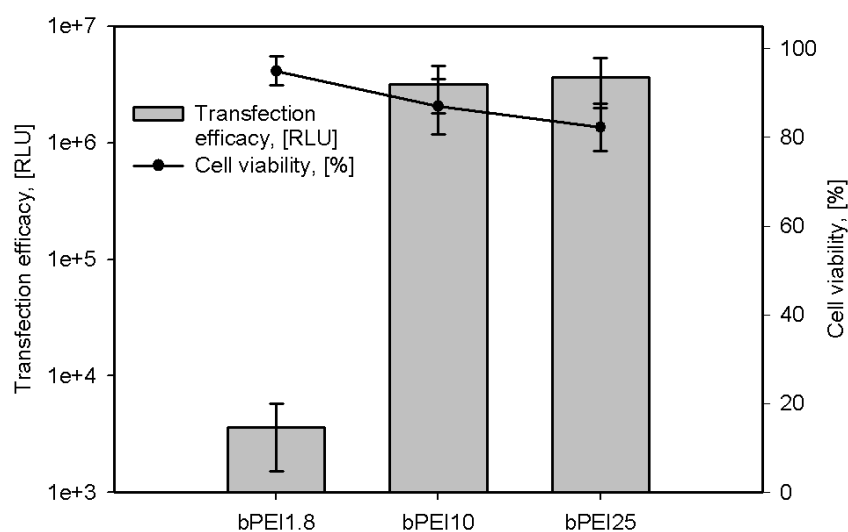


Figure 69: Transfection efficiency of unmodified bPEI with molecular weights of 1.8, 10, and 25 kDa, demonstrated by luciferase assay (n = 15, RLU – relative luminescence units). Cell viability is expressed in percents regarding untreated cells.

Transfection efficacy of bPEI 10 kDa revealed no statistically significant difference to the transfection rates achieved with the positive standard bPEI 25 kDa (p = 0.9753).

Polyplex toxicity of all polyplexes was moderate and generally increased with increasing bPEI molecular weight (Figure 69, solid line). There was no statistically significant difference

between the toxicity of bPEI 10 kDa and that of the positive standard bPEI 25 kDa ($p = 0.7981$).

4.6.2. The effect of conjugation with PA

In the following study, nanoparticles from amphiphilic conjugates of bPEI and PA without addition of phospholipids were examined. This was done in order to scrutinize the intrinsic transfection efficacy and the toxicity of the bPEI-PA conjugates. These were compared to unsubstituted bPEIs and the effect of grafting with PA was assessed.

Chemical grafting of PA to bPEI delivered no uniform trend in cell cultures treated with different molecular weights of bPEI. In the case of bPEI 1.8 kDa and its conjugates low-grade substitution led to a small, but significant increase of transfection rates (Figure 70). Conjugates of bPEI 10 kDa demonstrated continuous decreasing transfection activity with increasing substitution grade. On the other hand, loss of transfection efficacy in bPEI 25 kDa and its conjugates was observed only between ungrafted and grafted polycations, while there was no significant difference between the particular conjugates.

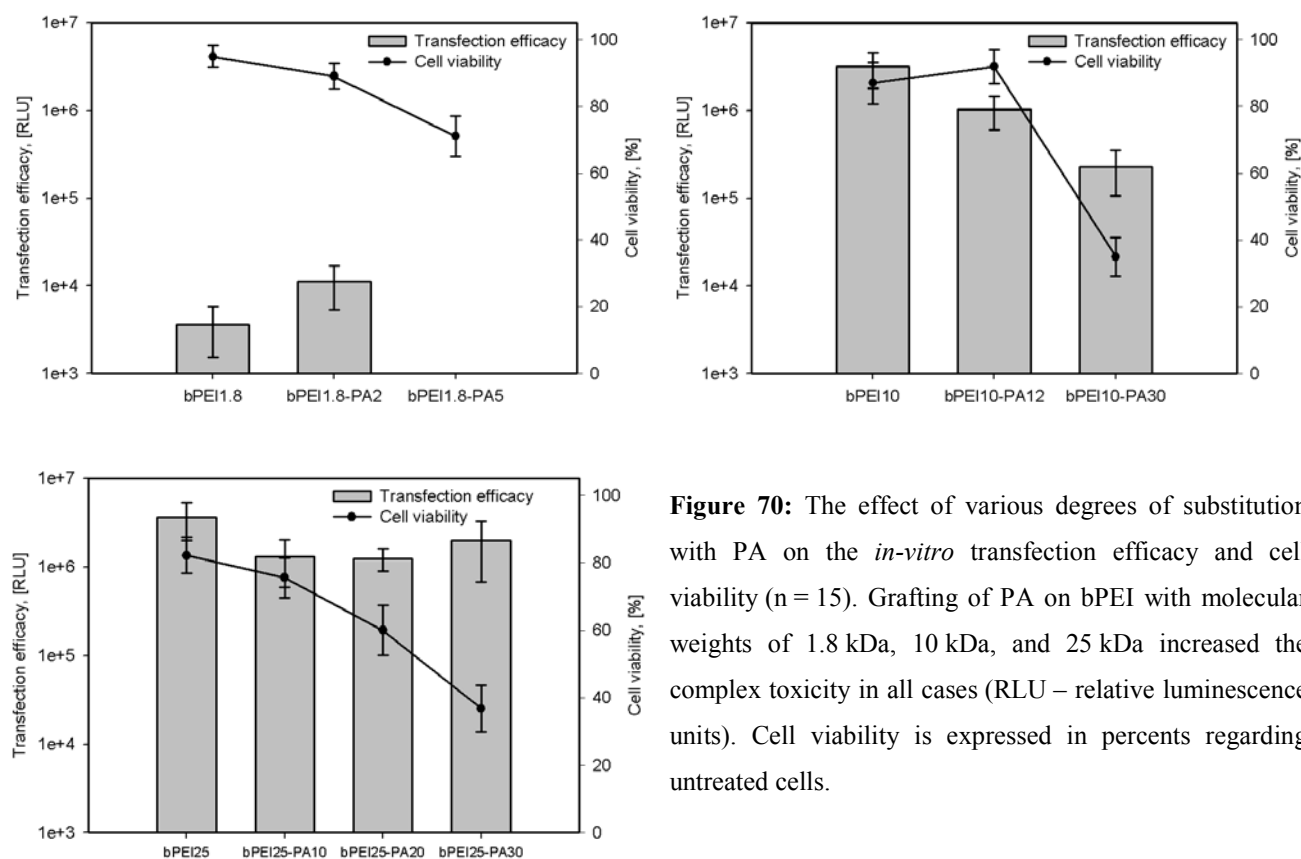


Figure 70: The effect of various degrees of substitution with PA on the *in-vitro* transfection efficacy and cell viability ($n = 15$). Grafting of PA on bPEI with molecular weights of 1.8 kDa, 10 kDa, and 25 kDa increased the complex toxicity in all cases (RLU – relative luminescence units). Cell viability is expressed in percents regarding untreated cells.

4.6.3. The effect of phospholipid

In the next step of the study, polycationic liposomes were formed out of phospholipids (DPPC and DPPE) and amphiphilic bPEI-PA conjugates with various molecular weight and substitution grade. Their transfection activity and toxicity was then compared to that in absence of phospholipids (Figure 70).

In all cases, addition of phospholipids to either unmodified bPEI or bPEI-PA resulted in a significant loss of transfection efficacy. This effect was most pronounced with conjugates of bPEI 25 kDa, where the activity was depleted by up to 300-fold. Interestingly, while bPEI 10 kDa was almost completely inhibited by the presence of phospholipid, its amphiphilic conjugate bPEI10-PA12 was only moderately influenced and retained about 65% of its intrinsic activity. At last, the addition of phospholipid to bPEI 1.8 kDa and its conjugates resulted in complete loss of transfection activity.

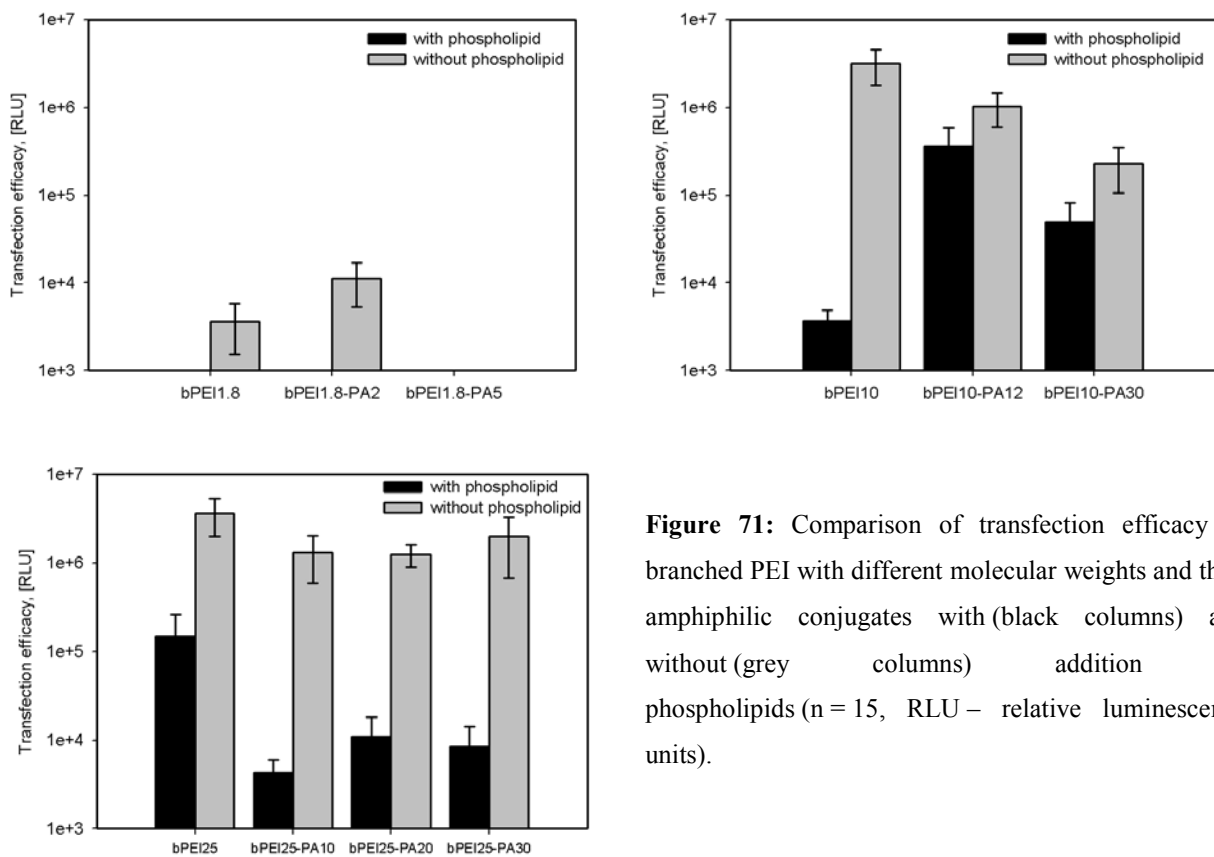


Figure 71: Comparison of transfection efficacy of branched PEI with different molecular weights and their amphiphilic conjugates with (black columns) and without (grey columns) addition of phospholipids (n = 15, RLU – relative luminescence units).

The lower transfection rates were not accordant with the data on cell viability. In several cases the addition of phospholipid did not affect the toxicity of bPEI-PA polyplexes *e.g.* bPEI10-PA12, bPEI10-PA30, and bPEI25-PA30 (Figure 72). In others, polyplex toxicity was strongly increased by phospholipid as in the cases of bPEI1.8-PA2, bPEI1.8-PA5, and bPEI25-PA10.

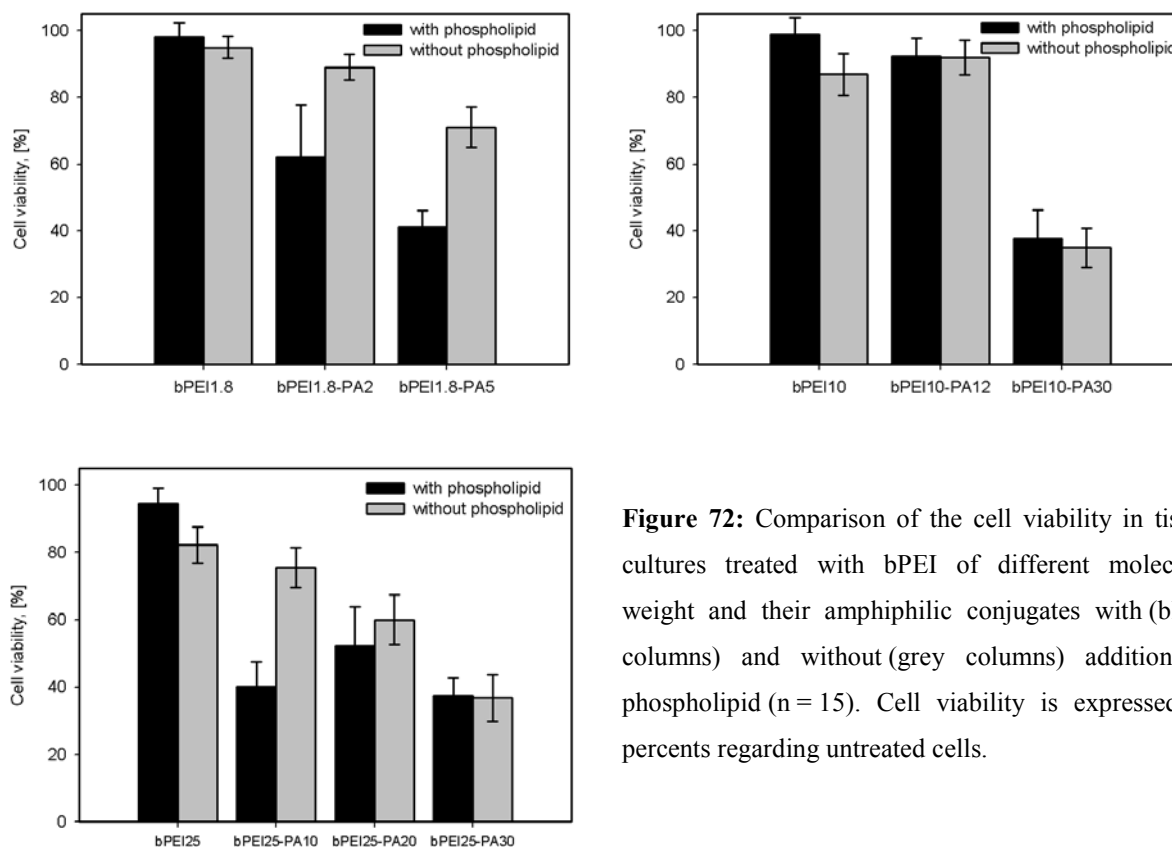


Figure 72: Comparison of the cell viability in tissue cultures treated with bPEI of different molecular weight and their amphiphilic conjugates with (black columns) and without (grey columns) addition of phospholipid (n = 15). Cell viability is expressed in percents regarding untreated cells.

Because of the complex interplay of bPEI molecular weight, substitution grade with PA, and the presence or absence of phospholipids the selection of a suitable candidate for *in-vivo* studies affords thorough monitoring. The bPEI-PA candidates were ranked after two selection criteria – high transfection efficacy and low cell toxicity, obtained in presence of phospholipid. Accordingly, they were compared to the positive standard – bPEI 25 kDa in absence of phospholipid (Figure 73).

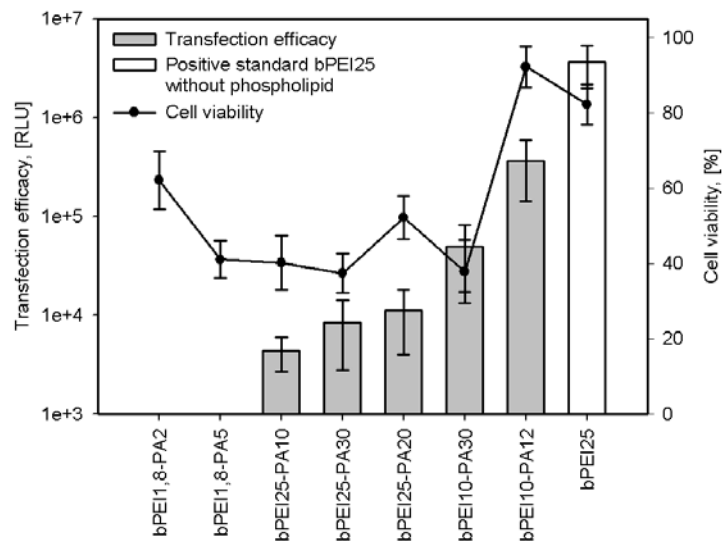


Figure 73: Comparison of the transfection efficacy and toxicity of bPEI-PA conjugates in presence of phospholipid with the positive control – bPEI 25 kDa in absence of phospholipid (n = 15, RLU – relative luminescence units). Cell viability is expressed in percents regarding untreated cells.

Amongst all tested bPEI-PA conjugates, bPEI10-PA12 provided the highest transfection rates. Its transfection efficacy in presence of phospholipid approached the transfection achieved by the positive control bPEI 25 kDa without phospholipid. Even more, the cell toxicity of bPEI10-PA12 was significantly lower than that of bPEI25. Therefore, bPEI10-PA12 has been selected as a suitable transfection agent for further studies.

4.6.4. The effect of US-mediated destruction of MBs

Cell cultures were further treated with pDNA-loaded polyplex-associated MBs in combination with US. The obtained data revealed that cavitation effects caused by US-mediated destruction of MBs did not significantly improve the transfection efficacy of pDNA-loaded polycationic liposomes (Figure 74). Transfection rates of $3.67 \times 10^5 \pm 2.25 \times 10^5$ RLU / 6×10^4 cells and a cell viability of $92.25\% \pm 5.47\%$ were achieved by incubation of 200 ng pDNA, 430 ng bPEI10-PA12, and 1.82 μ g phospholipid for 24 hours. Under the same experimental conditions, but treating cells with MBs, instead of polycationic liposomes, transfection rates of $4.11 \times 10^5 \pm 2.43 \times 10^5$ RLU / 6×10^4 cells at a cell viability of $78.79\% \pm 6.14\%$ were reached with no statistically significant difference of the transfection rates ($p = 0.9801$).

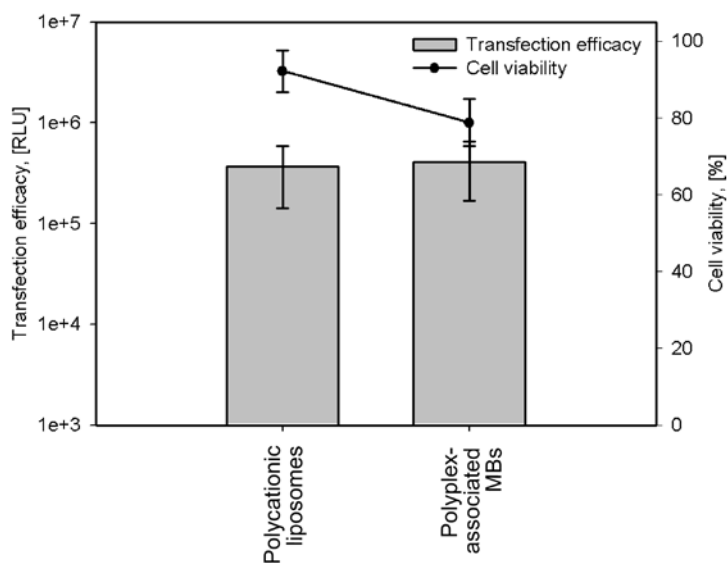


Figure 74: Comparison between the *in-vitro* transfection activity of pDNA-loaded polycationic liposomes and polyplex-associated MBs in combination with US, both comprising bPEI10-PA12 (n = 10, RLU – relative luminescence units). Cell viability is expressed in percents regarding untreated cells.

The obtained results confirmed the suggestion that cellular uptake by means of cell membrane poration is size-limited to macromolecules in the range of proteins or plasmids [33, 56, 58, 245]. However, shell fragments, resulting from the *in-vitro* destruction of polyplex-associated MBs, are sized $151.15 \text{ nm} \pm 13.06 \text{ nm}$ and are apparently too large to pass through the sonopores. Therefore, after the fragmentation of MBs the pDNA-bearing shell fragments can be only taken up by the cells via the endosomal pathway.

Nonetheless, under *in-vivo* conditions MBs are supposed to fulfill a different function than enhancing the cellular uptake of pDNA. When exposed to diagnostic US on the target site, MB oscillation enhance the permeability of capillary endothelium for colloidal particles. This allows the DNA-bearing shell fragments (secondary carriers) to leave the capillary bed, to reach the target cells, and to be taken up by phagocytosis. Further *in-vivo* clinical studies are still necessary to prove this concept.

5. Summary and outlook

Recently, microbubble ultrasound contrast agents (MBs) have become a promising tool for targeted drug and gene delivery. This is because MB drug carriers provide several distinctive advantages. On the one hand, they aid the visualization of the target site by diagnostic ultrasound (US) by acting as contrast agents. On the other hand, drug-loaded MBs can deliver their load specifically to the site of disease after they are fragmented by subsequently increasing the US intensity. At last, MBs in combination with US can increase the permeability of many physiological membranes such as the blood-brain barrier, capillary endothelium, or the cell membrane for macromolecules or even colloidal particles.

Because of their potential as carriers for targeted gene therapy MBs, loaded with plasmid DNA [56, 233], antisense oligonucleotides [301], or siRNA [243, 302], have been newly intensively investigated on a laboratory and clinical scale. Although numerous promising therapeutic outcomes have been acquired [118, 241] the clinically relevant application of MB-mediated gene therapies is still posed to several challenges. On the first place, the carrier capacity of MBs is limited based on their structure, comprising over 95% gas. Furthermore, current gene-loaded MBs do not provide protection of gene material from degradation by serum nucleases.

In the present research project a new type of secondary-carrier associated MBs was developed and characterized. The MBs comprised a gas core of perfluoropropane, surrounded by a soft phospholipid monolayer shell. The active gene load of plasmid DNA, encoding for luciferase, was encapsulated into polyplexes comprising properly synthesized amphiphilic conjugates of branched polyethylenimine (bPEI) and palmitic acid (PA). The DNA-bearing polyplexes were anchored by hydrophobic interactions to the MB shell monolayer.

Amphiphilic polycationic conjugates (bPEI-PA) were synthesized by pyridine-catalyzed nucleophilic substitution between branched PEI and PA after chemical activation of the fatty acid. After extensive purification the successful covalent conjugation was proven by ^1H and ^{13}C NMR. Initially, twelve bPEI-PA conjugates were synthesized from bPEI with molecular weights of 1.8 kDa, 10 kDa, and 25 kDa with various substitution degrees with PA, ranging from 2 mol% to 50 mol% according to the bPEI monomer units. In following development conjugates were assessed in their applicability for MB formulation and in their transfection efficacy and cell toxicity. Five highly-saturated candidates were excluded during the early development owing to solubility problems. Totally seven candidates were launched into later development studies and *in-vitro* biological studies (refer to Table 21, p.161).

The development and production of polyplex-associated MBs have been carried out according to the properly established *liposomal-controlled microbubble production* (LCMP) approach. MBs were produced by mechanical agitation of DNA-loaded polycationic liposome precursors together with the MB core gas octafluoropropane. The polycationic liposomes comprised amphiphilic polycation (bPEI-PA), and the saturated C16 zwitterionic phospholipids DPPC and DPPE.

In following studies the pH buffering capacity of bPEI-PA conjugates in the pH region between 4 and 6 was demonstrated. Their ability to complex DNA was either demonstrated with the conclusion that chemical grafting of PA lowers the binding potential of bPEI-PA especially at higher substitution rates.

The relationship between polyplex size and N/P loading ratio was governed by the shift of Zeta potential, as the highest degree of agglomeration was observed at Zeta potential approaching zero. Additionally, several trends of polycationic liposome particle size were observed at various bPEI molecular weights and PA substitution rates. Briefly, particle size of unloaded polycationic liposomes was independent from these two parameters as the liposomes were significantly smaller than the bPEI-PA nanoparticles formed by self-association in aqueous medium in absence of phospholipids.

After loading with pDNA the particle size decreased with increasing molecular weight of the bPEI moieties. There was no consistent trend according to the substitution grade with PA.

Another intensive influence on the polycationic liposome size after loading with pDNA was observed at decreasing pH in the range from 8 to 3.5 resulting in about 8-fold smaller particles. This effect could be explained with the increasing charge density of bPEI-PA which allows the complexation of a greater number of negative charges per plasmid molecule.

An intriguing effect of electrolyte concentration on the MB yield and stability was observed too. Because of the high positive charge density due to the presence of bPEI-PA the MB shell was destabilized by lateral repulsions leading to extremely low MB yields. However, when the electrostatic repulsions were shielded by electrolytes the shell integrity was recovered by the prevalence of attractive lateral hydrophobic forces. However, beyond a certain concentration limit the downgrading of electrostatic repulsions led to colloidal instability of polycationic liposomes and aggregation. Therefore, a narrow interval of electrolyte concentration was selected, where both conditions of MB shell stability and liposome colloidal stability are fulfilled.

In comparison to conventional cationic phospholipid MBs [117] the newly developed polyplex-associated MBs reached a 5-fold higher plasmid loading of about $0.01 \text{ pg}/\mu\text{m}^2$,

comparable to albumin-shelled MBs [56] (refer to Table 18, p.136), but providing much higher echogenicity and acoustic destructibility [15]. Furthermore, as shown in experimental studies polyplex-associated MBs are able to protect the active gene load from enzymatic degradation in serum due to its condensation with bPEI (refer to “4.5.4, *Protection of pDNA against enzymatic degradation*”, p.191).

In-vitro transfection studies revealed the biological activity of the seven amphiphilic bPEI-PA candidates in terms of their transfection ability and cell toxicity. On the first place, the transfection efficacy of bPEI-PA was determined by the molecular weight of the bPEI moiety. Conjugates of low-molecular weight bPEI of 1.8 kDa reached marginal transfection rates, while transfection with conjugates of bPEI 10 kDa approached the efficacy of the positive control bPEI 25 kDa. The degree of substitution played a negative role both for the transfection efficacy and for the toxicity of bPEI-PA.

The most intensive negative influence was exerted by the addition of phospholipids – 20 mol% DPPE and 80 mol% DPPC, in order to form polycationic liposomes. Although the phospholipids had a positive effect of decreasing particle size compared to bPEI-PA self-associates, their influence on the transfection efficiency was strongly inhibiting. However, the transfection activity loss was not as pronounced with every bPEI-PA candidates, but was greatest in the case of bPEI25-PA. The addition of phospholipid affected in some cases the cell viability, but did not allow drawing a consistent tendency.

As a final outcome of the *in-vitro* cell culture studies one candidate – bPEI10-PA12, was selected for launching into *in-vivo* studies based on its superior transfection efficacy, approaching this of bPEI 25 kDa. Polycationic liposomes comprising bPEI10-PA12 also demonstrated very low cell toxicity expressed as $92.2\% \pm 5.5\%$ remaining cell viability compared to untreated cells.

In perspective, the targeting and transfection efficacies of polyplex-associated MBs comprising the selected candidate bPEI10-PA12 need to be demonstrated under *in-vivo* conditions as a final proof of concept. Thereby, the optimal dosage regimen and US parameters should be discriminated. A further aspect which deserves attention is the transfection interference in particle clearing organs such as the liver, the lungs, the spleen, and the kidneys. As a first step in this direction the acute toxicity of the newly developed MBs was already characterized in rat models, giving a promising outlook for further clinical studies.

VI. Chapter: General summary of the thesis

In the past decades microbubbles (MBs) have gained wide clinical applications as well tolerated contrast agents for the ultrasound (US) diagnostics. Recently, their potential as specific drug and gene-carriers for targeted therapy has been discovered and many therapeutic applications have been established on clinical scale. These encompass thrombolysis [303], delivery of plasmid DNA [56, 212], siRNA [266, 323], protein delivery [58, 59], as well as the delivery of small drug molecules [134].

Because they are US contrast agents and drug carriers at the same time, MBs provide the unique ability to outline the site of disease and to achieve highly specific drug targeting in a single needle prick. MBs can be intravenously administered to the patient by either bolus injection or infusion and reach even distant tissues and organs. On the target site they can be visualized by well tolerated diagnostic US and aid the localization of *e.g.* solid tumors. Accordingly, the drug can be released from the MBs by increasing the US intensity and “bursting” them. Beyond the targeting effect, the combination of MBs and US can turn biological barriers such as the blood-brain barrier, capillary endothelium, and the cell membrane permeable for polar drugs, macromolecules, and even colloidal particles [23, 24, 36].

The above dissertation work focused on the pharmaceutical formulation of phospholipid-shelled drug and gene-loaded MBs by mechanical high speed agitation. Thereby, a pre-filled sterile vial containing a liquid phase and a gas phase was agitated on its length-axis with definite duration and frequency using a mechanical device. In the context of the above work, the precursor vial comprised an aqueous phospholipid dispersion and octafluoropropane gas, in which form it can be stored for long terms. Immediately prior to the drug administration the vial was activated by agitation and the produced concentrated MB dispersion was diluted with physiological medium.

A novel approach for formulation of drug-loaded MBs – the *liposomal-controlled microbubble production* (LCMP) was established here and implemented to develop MBs, loaded with doxorubicin and with plasmid-bearing nanoparticles. According to the LCMP approach, the pharmaceutical properties of drug-loaded MBs such as particle size, particle yield, and encapsulation efficacy, could be controlled by tuning the properties of the precursor liposomal formulations, *e.g.* ionic strength, pH, particle size, *etc.* This new strategy brought the advantage of having all formulation components – MB core gas, shell phospholipids, and drug, in a single ready-to-use vial, providing MBs with definite quality upon activation.

Several dependences and trends have been observed in the formulation development of phospholipid MBs which allowed hypothesizing about the physico-chemical aspects in their background. At the beginning of the thesis the exothermic character of high-speed agitation has been revealed. Based on the gradual temperature increase during the agitation on the one hand and on the melting transition temperature of the MB shell phospholipids on the other, the connection has been established between the time of agitation and the MB yield. Thereby, MBs were formed and downsized by high-shear forces, caused by the agitation, as long as the shell phospholipids persist in condensed gel phase state. As soon as the temperature in the tube reached the phospholipid melting temperature, a rapid process of MB degradation took place. Apparently, the gel-to-liquid crystalline phase transition attenuated the lateral hydrophobic cohesion between phospholipid molecules, impaired the monolayer integrity, and shifted the equilibrium from formation of MBs back to the formation of liposomes.

A further intriguing correlation between the thermotropic phase behavior of phospholipids and their ability to form MBs upon agitation has been observed in several studies of this work. Apparently, the MB yield is reverse proportional to the peak sharpness and broadness, expressed as the ratio between peak width at half peak height ($W_{0.5}$) and peak height (H). Pure phospholipids such as DPPC and DPPG, having sharp peaks and low $W_{0.5}/H$ ratios, failed to form MBs despite of their high ability to produce stable liposomes. On the contrary, their mixtures with up to 15-times higher $W_{0.5}/H$ ratios provided high MB yields. The same phenomenon was observed also in the cases of DPPC / DPPE mixtures (see Figure 50, p.169) and in complexes of DPPC / DPPG anionic bilayers with doxorubicin.

A possible explanation for that relationship can be the large cooperative unit in DPPC bilayers, involving from 125 molecules [276] to 400-600 molecules [304]. Blending DPPC at equimolar ratios with DPPE increases the bilayer fluidity by diminishing the cooperative unit to only 15 phospholipid molecules [276]. The cooperation unit represents the number of lipid molecules in a membrane domain which simultaneously undergo a temperature phase transition. In highly cooperative phospholipid systems these domain units are extremely large and the transition shows a sharp peak in the thermogram. The size of cooperative unit can be reduced, leading to membrane fluidizing [274], *e.g.* through the absorption of small molecules such as doxorubicin. In such cases the transition usually starts at lower temperature and shows broadening and lowering of the thermogram peak.

More detailed studies are needed to substantiate the relation between liposome membrane fluidity and MB production. Nonetheless, in the past research work phase transition behavior

and membrane fluidity were in several cases successfully exerted in order to predict the MB particle yield.

In summary, two major factors appear to be decisive for the stability of the MB shell monolayer. On the one hand, the high lateral monolayer fluidity renders the shell flexible and plastic, as suggested by other authors too [86]. On the other hand, the equilibrium between lateral hydrophobic cohesions and electrostatic repulsions either promote or impair the monolayer stability. A characteristic example therefore is the occurring instability of cationic monolayers at high charge densities [113].

At the begin of this research thesis, several early pre-formulation studies on unloaded phospholipid MBs were carried out in order to give the basics for further development of drug and gene-loaded MBs. Accordingly, available instrumental methods were compared in order to chose appropriate approaches for MB sizing, concentration measurements, measurements of the Zeta potential, and structure analysis. The laser diffraction in combination with a properly established optical model for MBs has been selected as the most reliable method for particle sizing. MB concentration was determined by light blockage with some approximation due to size range limitations. Determination of MB Zeta potential was abandoned due to setup complications and the Zeta potential of liposomes was measured instead. MB structure was reliably characterized by fluorescence confocal laser scanning microscopy.

Two major formulation projects were described in the present thesis work. The aim of the first project was to establish doxorubicin-loaded carriers for targeted tumor therapy. Two constructs were developed and compared – thin-shelled phospholipid MBs and acoustically active lipospheres (AALs), comprising an additional oil layer. Within the phospholipid monolayer-shelled MBs, the cationic doxorubicin (DOX) was complexed by electrostatic interactions to an anionic phospholipid – dipalmitoyl phosphatidylglycerol (DPPG). Furthermore, the complex was stabilized by additional hydrophobic attractions. On this manner DOX was incorporated in a few nanometer thick soft phospholipid-monolayer MB shell.

In the case of DOX-loaded AALs the drug was included in an oil layer of glycerol triacetate (triacetin) which was located between the innermost gas core and the outermost phospholipid monolayer. In order to make the drug loading more efficient, DOX was turned more lipophilic by transforming its hydrochloride salt into free base.

Both candidates – DOX-loaded MBs and DOX-loaded AALs, were compared under *in-vitro* and *in-vivo* conditions and the more appropriate of them – the phospholipid MBs, was launched into clinical studies. DOX-loaded MBs were preferred rather than the triacetin

AALs mainly for their much better echogenicity and acoustic destructibility, demonstrated *in-vitro* as well *in-vivo*.

DOX-loaded MBs possessed a superior loading ability for DOX, reaching almost 90% of the input drug amount. Furthermore, the excipient burden of MBs, calculated on the basis of the mass concentrations of DOX and total phospholipid, was found to be 6.49 which value approximates that of the commercially available DOX-loaded liposome product (Doxil[®], Ortho Biotech, Bridgewater, USA). The *in-vivo* US contrasting efficacy of DOX-loaded MBs was close to that of the commercial US contrast agent SonoVue[®] (Bracco International, B.V., The Netherlands) while their acoustic destructibility even surpassed the positive control by 175%.

In-vitro studies on the therapeutic efficacy of DOX-loaded MBs in tissue cultures revealed a 3.2-fold increase of therapeutic activity compared to free DOX and DOX liposomes (n = 10). *In-vivo* studies in subcutaneous xenograft tumor models in rat demonstrated an about 12-fold accumulation of DOX in US-treated tumors, compared to tumors which became no US (n = 6, p < 0.005). Further *in-vivo* studies in rat tumor models are foreseen in order to assess the therapeutic potential of DOX-loaded MBs by monitoring the pace of tumor growth. As a step forward, DOX-loaded MBs will be tested in their therapeutic efficacy *i.e.* the ability to inhibit tumor growth. Furthermore, they will be applied in large animal models in order to determine the optimal setting conditions for diagnostic US and to achieve the most effective therapeutic treatment.

In summary, DOX-loaded MBs brought at least three important advantages in comparison to current administration forms for this anti-tumor agent. Firstly, because of their backscattering properties DOX-loaded MBs can act as contrast agents and aid tumor visualization. Furthermore, DOX-loaded MBs provide specific drug targeting which can be externally controlled by the clinician. Moreover, the released energy of MB “bursting” enhances the permeability of capillary endothelium and cell membrane for DOX and enhances its therapeutic effect. The combination of DOX, MBs and US demonstrated a synergistic augmentation of the therapeutic efficacy *in-vitro*. At last, MBs are generally considered blood-pool agents because of their size. Therefore, similarly to liposomes they obviously can reduce the distribution volume of DOX to that of blood plasma.

Besides targeted tumor therapy, another key application of MB agents is the gene therapy. One conventional approach for formulation of gene-loaded MBs is by electrostatic bounding of the negatively charged nucleotides to the surface of the cationic MB phospholipid shell.

However, this approach is limited in the amount of loaded gene material since the MB surface becomes saturated at about $0.002 \text{ pg}/\mu\text{m}^2$ plasmid DNA [113, 117]. Furthermore, the active gene load, attached to the MB surface, is liable to degradation by serum nucleases.

The second research project in the above thesis addressed the above depicted problems about enhancing the active load amount and protection the gene load from enzymatic degradation. Therefore, micron-sized MBs were loaded with nanometer-sized particles – *secondary carriers*, encapsulating the gene material (see Figure 66, p.191). After such secondary-carrier associated MBs have been “burst” by US on the target site their destruction causes perforations in the capillary wall and turns it permeable for the nanoparticulate secondary carriers which are released from the MBs at the same moment. Thereupon the gene-loaded nanoparticles may leave the capillary bed and penetrate the interstitium where they are actively taken up by the cells via endocytosis.

In the present work, novel MB carriers were established comprising a gas core and a phospholipid monolayer shell, decorated with polyplex nanoparticles, The nanoparticles were anchored apparently by hydrophobic interactions to the phospholipid monolayer (Figure 2 D, p.19).

Polyplex nanoparticles comprised properly synthesized amphiphilic conjugates of branched polyethylenimine (bPEI) and palmitic acid (PA) linked by covalent amine bridges. Conjugates were synthesized using bPEI of different molecular weight (1.8 kDa, 10 kDa, and 25 kDa) and at various substitution degrees with PA by activating PA with N,N-dicyclohexylcarbodiimide. The substitution was further catalyzed by pyridine. The chemical structure and stoichiometric substitution degree with PA were confirmed by ^1H and ^{13}C NMR. As demonstrated in following characterization studies the amphiphilic bPEI-PA conjugates were able to complex pDNA. The conjugate binding capacity for pDNA mainly decreased with increasing substitution degrees with PA. Generally, maximum N/P binding ratios for bPEI-PA conjugates lied between 4 and 6. Phospholipid liposomes, comprising only DPPC and DPPE but no polycation did not complex pDNA. Similarly, gel retention assay studies revealed that complete complexation of pDNA is possible at N/P ratios of 5-7. However, in later studies loading was possible at N/P ratios of up to 10 because of colloidal instability, occurring at higher loading ratios.

Amphiphilic bPEI-PA conjugates were able to buffer the pH range between 4 and 6, as revealed in pH titration studies. This finding was accepted as a proof of concept that the chemically modified conjugates retain their proton buffering capacity and can fulfill the mechanism of osmotic endosome degradation.

Furthermore, polyplex-associated MBs were able to protect their gene load from degradation by serum nucleases in DNase challenge assay studies in the N/P range from 5 to 15.

Exhaustive pre-formulation research has been dedicated to attaining control over the particle size of pDNA-loaded polyplex-liposomes and over the MB yield. Higher protonation degrees of bPEI-PA at lower pH values strongly improved the colloidal stability of polycationic liposomes upon loading with pDNA and lowered the liposome size. Apparently, at lower pH the higher density of cationic charges in bPEI-PA can compensate more negative charges in the pDNA molecule. Therefore, less bPEI-PA molecules are necessary to condense a single plasmid which reduces the particle size of the final polyplex particle.

Accordingly, the synthesized amphiphilic bPEI-PA candidates were subjected to *in-vitro* studies on their transfection efficacy and cell toxicity in human melanoma cell cultures. The conjugates were compared and the candidate with the highest transfection ability and lowest toxicity was selected for further *in-vivo* clinical studies. As a positive control polyplexes of pDNA with bPEI 25 kDa were applied.

The new polyplex-associated MBs allowed increasing the effective load amount of pDNA about 5-fold compared to conventional cationic phospholipid MBs. Although the transfection efficiency of pDNA-loaded polycationic liposomes was inhibited by the chemical grafting of PA and by the presence of shell phospholipids, the finally selected conjugate bPEI10-PA12 retained 84.8% of the activity of the positive control bPEI 25 kDa.

Further *in-vivo* studies are still necessary to demonstrate the proof of concept for US targeted delivery of pDNA by the newly established polyplex-associated MBs.

References:

1. de Jong, N., Frinking, PJ, Bouakaz, A, Cate, FJ, *Detection procedures of ultrasound contrast agents*. Ultrasonics, 2000. **38**: p. 87-92.
2. Gramiak, R., Shah, PM, *Echocardiography of the aortic root*. Invest Radiol, 1968. **3**(5): p. 356-366.
3. Pitt, W., Hussein, GA, Staples, BJ, *Expert opinion on ultrasound drug delivery – a general review*. Expert Opin Drug Deliv 2004. **1**(1): p. 37-56.
4. Porter, T., *Perfluorobutane ultrasound contrast agent and methods for its manufacture and use.*, B.o.R.o.t.U.o. Nebraska, Editor. 1997: USA.
5. Chi, D., Liu, YL, Wang, P, Chen, XL, Liu, J, Xie, ZB, Li, Q, Ou, WC, Xiu, JC, Zha, DG, Wu, PS, Xu, DL, *Value of echocardiography for observing left ventricular hypertrophy in the diagnosis of myocardial microvascular damage in hypertensives*. Di Yi Jun Yi Da Xue Xue Bao 2003. **23**(7): p. 702-705.
6. Blomley, M., Claudon, M, Cosgrove, D, *World Federation for Ultrasound in Medicine and Biology (WFUMB) Safety Symposium on ultrasound contrast agents: clinical applications and safety concerns*. Ultrasound Med Biol, 2007. **33**(2): p. 180-186.
7. Krestan, C., *Ultraschallkontrastmittel: Substanzklassen, Pharmakokinetik, klinische Anwendungen, Sicherheitsaspekte*. Radiologe, 2005. **45**: p. 513-519.
8. *Ultrasound technology information portal, ultrasound database*. 2008 [cited 2008 December 10th]; Available from: <http://www.us-tip.com>.
9. Stolz, E., Kaps, M, *Ultrasound contrast agents and imaging of cerebrovascular disease*. Semin Cerebrovasc Dis Stroke, 2005. **5**: p. 111-131.
10. Wells, P., *Ultrasonic imaging of the body*. Rep Prog Phys, 1999. **62**: p. 671-722.
11. Soldner, R., *Physikalische Grundlagen sonographischer Bildgebung, Ultraschall-Gewebe-Interaktion und Sicherheitsaspekte*. Echosignalverstärker und transkraniale Farbduplex-Sonographie, ed. U. Bogdahn, Becker, G, Schlachetzki, F. 1998, Berlin, Wien: Blackwell Wiss-Verlag.
12. Nanda, N., Carstensen, EL, *Echo-enhancing agents: Safety*. In Nanda NC, Schlieff R, Goldberg BB, editors. Advances in echo imaging using contrast enhancers. Dordrecht, the Netherlands: Kluwer, 1997: p. 115-131.
13. Albrecht, T., Blomley, M, Bolondi, L, Claudon, M, Correas, JM, Cosgrove, D, Greiner, L, Jäger, K, de Jong, N, Leen, E, Lencioni, R, Lindsell, D, Martegani, A, Solbiati, L, Thorelius, L, Tranquart, F, Weskott, HP, Whittingham, T, *European Federation of Societies for Ultrasound in Medicine and Biology Study Group (EFSUMB) guidelines for the use of contrast agents in ultrasound*. Ultraschall in der Medizin 2004. **25**: p. 249-256.
14. Borden, M., Dayton, P, Zhao, S, Ferrara, KW, *Physico-chemical properties of the microbubble lipid shell*. IEEE Trans Ultrason Ferroelectr Freq Control Proc, 2004.
15. Mehier-Humbert, S., Yan, F, Frinking, P, Schneider, M, Guy, RH, Bettinger, T, *Ultrasound-mediated gene delivery: Influence of contrast agent on transfection*. Bioconjugate Chem, 2007. **18**: p. 652-662.
16. Bloch, S., Wan, M, Dayton, PA, Ferrara, KW, *Optical observation of lipid- and polymer-shelled ultrasound microbubble contrast agents*. Appl Phys Lett, 2004. **84**(4): p. 631-633.
17. May, D., Allen, J, Gut, J, Ferrara, KW, *Acoustic fragmentation of therapeutic contrast agents designed for localized drug delivery*. IEEE Ultras Symp Proc, 2001.

18. Mukherjee, D., Wong, J, Griffin, B, Ellis, SG, Porter, T, Sen, S, Thomas, JD, *Ten-fold augmentation of endothelial uptake of vascular endothelial growth factor with ultrasound after systemic administration*. J Am Coll Cardiol, 2000. **35**: p. 1678-1686.
19. Zderic, V., Vaezy, S, Martin, RW, Clark, JI, *Ocular drug delivery using 20-kHz ultrasound*. Ultrasound Med Biol, 2002. **28**: p. 823-829.
20. O'Brien, W., *Ultrasound - biophysics mechanisms*. Progr Biophys Mol Biol, 2007. **93**: p. 212-255.
21. United States Food and Drug Administration, F., *Information for manufacturers seeking marketing clearance of diagnostic ultrasound systems and transducers*. 1997.
22. Miller, D., Quddus, J, *Sonoporation of monolayer cells by diagnostic ultrasound activation of contrast-agent gas bodies*. Ultrasound Med Biol, 2000. **26**(4): p. 661-667.
23. Miller, D., Pislaru, SV, Greenleaf, JF, *Sonoporation: mechanical DNA delivery by ultrasonic cavitation*. Som Cell Mol Genet, 2002. **27**(1/6): p. 115-134.
24. Yang, F., Gu, N, Chen, D, Xi, X, Zhang, D, Li, Y, Wu, J, *Experimental study on cell self-sealing during sonoporation*. J Contr Release, 2008. **131**: p. 205-210.
25. Marmottant, P., Hilgenfeldt, S, Versluis, M, Gardeniers, H, van den Berg, A, Lohse, D, *Cell permeabilisation and transport focused around oscillating microbubbles*. XXI ICTAM, 15th–21st August 2004, Warsaw, Poland, 2004.
26. Marmottant, P., Hilgenfeldt, S, *Controlled vesicle deformation and lysis by single oscillating bubbles*. Nature 2003. **423**: p. 152-156.
27. Barnett, S., *Nonthermal issues: cavitation—its nature, detection and measurement*. Ultrasound Med Biol, 1998. **24**(11-21).
28. Guzman, H., McNamara, AJ, Nguyen, DX, Prausnitz, MR *Bioeffects caused by changes in acoustic cavitation bubble density and cell concentration: a unified explanation based on cell-to-bubble ratio and blast radius*. Ultrasound Med Biol 2003. **29**(8): p. 1211-1222.
29. Wang, Z., Pecha, R, Gompf, B, Eisenmenger, W, *Single bubble sonoluminescence: investigations of the emitted pressure wave with a fiber optic probe hydrophone*. Phys Rev 1999. **E 59**: p. 1777–1780.
30. Lawrie, A., Brisken, AF, Francis, SE, Cumberland, DC, Crossman, DC, Newman, CM, *Microbubble-enhanced ultrasound for vascular gene delivery*. Gene Ther 2000. **7**: p. 2023-2027.
31. Lawrie, A., Brisken, AF, Francis, SE, Wyllie, D, Kiss-Toth, E, Qwarnstrom, EE, Dower, SK, Crossman, DC, Newman, CM, *Ultrasound-enhanced transgene expression in vascular cells is not dependent upon cavitation-induced free radicals*. Ultrasound Med Biol 2003. **29**: p. 1453-1461.
32. Bouakaz, A., Tran, TA, Roger, S, Leguennec, JY, Tranquart, F, *On the mechanisms of cell membrane permeabilization with ultrasound and microbubbles*. Ultrasound Med Biol 2006. **32**(5): p. 90.
33. Schlicher, R., Radhakrishna, H, Tolentino, TP, Apkarian, RP, Zarnitsyn, V, Prausnitz, MR, *Mechanism of intracellular delivery by acoustic cavitation*. Ultrasound Med Biol 2006. **32**: p. 915-924.
34. Deng, C., Sieling, F, Pan, H, Cui, J *Ultrasound-induced cell membrane porosity*. Ultrasound Med Biol, 2004. **30**: p. 519–526.
35. McNeil, P., Terasaki, M *Coping with the inevitable: How cells repair a torn surface membrane*. Nat Cell Biol 2001. **3**: p. 124-129.
36. Pan, H., Zhou, Y, Izadnegahdar, O, Cui, J, Deng, CX, *Study of sonoporation dynamics affected by ultrasound duty cycle*. Ultrasound Med Biol 2005. **31**: p. 849–856.

37. Kudo, K., Yamamoto, K. *Behavior of microbubbles exposed to pulsed ultrasound and their mechanical effect on a cell.* in *4th National Symposium on Therapeutic Ultrasound.* 2005: American Institute of Physics.
38. Liu, Y., Miyoshi, H, Nakamura, M, *Encapsulated ultrasound microbubbles: Therapeutic application in drug/gene delivery.* J Control Release 2006. **114**: p. 89-99.
39. Duvshani-Eshet, M., Baruch, L, Kesselman, E, Shimoni, E, Machluf, M, *Therapeutic ultrasound-mediated DNA to cell and nucleus: Bioeffects revealed by confocal and atomic-force microscopy.* Gene Ther, 2006. **13**: p. 163-172.
40. Duvshani-Eshet, M., Adam, D, Machluf, M, *The effects of albumin-coated microbubbles in DNA delivery mediated by therapeutic ultrasound.* J Contr Release, 2006. **112**: p. 156-166.
41. Stieger, S., Caskey, CF, Adamson, RH, Qin, S, Curry, FR, Wisner, ER, Ferrara, KW, *Enhancement of vascular permeability with low-frequency contrast-enhanced ultrasound in the chorioallantoic membrane model.* Radiology, 2007. **243**(1): p. 112-121.
42. Howard, C., Forsberg, F, Minimo, C, Liu, JB, Merton, DA, Claudio, PP, *Ultrasound guided site specific gene delivery system using adenoviral vectors and commercial ultrasound contrast agents.* J Cell Physiol 2006. **209**: p. 413-421.
43. Skyba, D., Price, R, Linka, A, Skalak, T, Kaul, S, *Direct in-vivo visualization of intravascular destruction of microbubbles by ultrasound and its local effects on tissue.* Circulation 1998. **98**: p. 290-293.
44. Li, P., Cao, LQ, Dou, CY, Armstrong, WF, Miller, D, *Impact of Myocardial Contrast Echocardiography on Vascular Permeability: An in-vivo dose response study of delivery mode, pressure amplitude and contrast dose.* Ultrasound Med Biol, 2003. **29**(9): p. 1341-1349.
45. Song, J., Chappell, JC, Qi, M, VanGieson, EJ, Kaul, S, Price, RJ, *Influence of injection site, microvascular pressure and ultrasound variables on microbubble-mediated delivery of microspheres in muscle.* J Am Coll Cardiol, 2002. **39**(4): p. 726-731.
46. Price, R., Skyba, DM, Kaul, S, Skalak, TC, *Delivery of colloidal particles and red blood cells to tissue through microvessel ruptures created by targeted microbubble destruction with ultrasound.* Circulation, 1998. **98**: p. 1264-1267.
47. Imada, T., Tatsumi, T, Mori, Y, Nishiue, T, Yoshida, M, Masaki, H, Okigaki, M, Kojima, H, Nozawa, Y, Nishiwaki, Y, Nitta, N, Iwasaka, T, Matsubara, H, *Targeted delivery of bone marrow mononuclear cells by ultrasound destruction of microbubbles induces both angiogenesis and arteriogenesis response.* Arterioscler Thromb Vasc Biol, 2005. **25**: p. 2128-2134.
48. Sheikov, N., McDannold, N, Vykhodtseva, N, Jolesz, F, Hynynen, K, *Cellular mechanisms of the blood-brain barrier opening induced by ultrasound in presence of microbubbles.* Ultrasound Med Biol, 2004. **30**: p. 979-989.
49. Shimamura, M., Sato, N, Taniyama, Y, Yamamoto, S, Endoh, M, Kurinami, H, Aoki, M, Ogihara, T, Kaneda, Y, Morishita, R, *Development of efficient plasmid DNA transfer into adult rat central nervous system using microbubble-enhanced ultrasound.* Gene Ther, 2004. **11**: p. 1532-1539.
50. Treat, L., McDannold, N, Vykhodtseva, N, Zhang, Y, Tam, K, Hynynen, K, *Targeted delivery of doxorubicin to the rat brain at therapeutic levels using MRI-guided focused ultrasound.* Int J Cancer, 2007. **121**: p. 901-907.
51. Jacobsen, J., Oyen, R, Thomsen, HS, Morcos, SK, *Safety of ultrasound contrast agents.* Eur Radiol, 2005. **15**: p. 941-945.
52. Tranquart, F., Claudon, M, Correas, JM, *Guidelines for the use of contrast agents in ultrasound.* J Radiol, 2005. **86**: p. 1047-1054.

53. Dufrene, Y., Barger, W, Green, J, Lee, G, *Nanometerscale surface properties of mixed phospholipid monolayers and bilayers*. Langmuir, 1997. **13**: p. 4779-4784.
54. Molecular Imaging and Contrast Agent Database. *Air-filled, cross-linked, human serum albumin microcapsules*. 2007 [cited; Available from: <http://www.ncbi.nlm.nih.gov/books/bookres.fcgi/micad/Quantison.pdf>].
55. Unger, E., McCreery, T, Sweitzer, R, Vielhauer, G, Guan-Li, W, Shen, D, Yellowhair, D, *MRX 501: A novel ultrasound contrast agent with therapeutic properties*. Acad Radiol, 1998. **5**(1): p. 247-249.
56. Bekeredjian, R., Chen, S, Frenkel, P, Grayburn, P, Shohet, R, *Ultrasound-targeted microbubble destruction can repeatedly direct highly specific plasmid expression to the heart*. Circulation 2003. **108**: p. 1022-1026.
57. Vannan, M., McCreery, T, Li, P, Han, Z, Unger, E, Kuersten, B, Nabel, E, Rajagopalan, S, *Ultrasound-mediated transfection of canine myocardium by intravenous administration of cationic microbubble-linked plasmid DNA*. J Am Soc Echocardiogr, 2002. **15**: p. 214-218.
58. Bekeredjian, R., Chen, S, Grayburn, P, Shohet, R, *Augmentation of cardiac protein delivery using ultrasound targeted microbubble destruction*. Ultrasound Med Biol, 2005. **31**(5): p. 687-691.
59. Bekeredjian, R., Kuecherer, HF, Kroll, RD, Katus, HA, Hardt, SE, *Ultrasound-targeted microbubble destruction augments protein delivery into testes*. Urology 2007. **69**: p. 386-389.
60. Fang, J., Hung, CF, Liao, MH, Chien, CC *A study of the formulation design of acoustically active lipospheres as carriers for drug delivery*. Eur J Pharm Biopharm, 2007. **67**(1): p. 67-75.
61. Hauff, P., Seemann, S, Reszka, R, Schultze-Mosgau, M, Reinhardt, M, Buzasi, T, Plath, T, Rosewicz, S, Schirner, M, *Evaluation of gas-filled microparticles and sonoporation as gene delivery system: Feasibility study in rodent tumor models*. Radiology 2005. **236**: p. 572-578.
62. Burstein, O., Wheatley, MA, *Drug loaded contrast agents for cancer tumors: A combination of imaging and therapy*. Biomedical Technology Showcase, School of Biomedical Engineering, Science & Health Systems, Drexel University, PA, 2006. **0**(0): p. 0.
63. Kheirloom, A., Dayton, P, Lum, A, Little, E, Paoli, E, Zheng, H, Ferrara, K, *Acoustically-active microbubbles conjugated to liposomes: Characterization of a proposed drug delivery vehicle*. J Contr Release, 2007. **118**: p. 275-284.
64. Lum, A., Borden, M, Dayton, M, Kruse, D, Simon, S, Ferrara, K, *Ultrasound radiation force enables targeted deposition of model drug carriers loaded on microbubbles*. J Contr Release, 2006. **111**(1-2): p. 128-134.
65. Taylor, S., Rahim, AA, Bush, NL, Bamber, JC, Poter, CD, *Targeted retroviral gene delivery using ultrasound*. J Gene Med 2007. **9**: p. 77-87.
66. Lentacker, I., de Geest, BG, Vandenbroucke, RE, Peeters, L, Demeester, J, de Smedt, SC, Sanders, NN, *Ultrasound-responsive polymer-coated microbubbles that bind and protect DNA*. Langmuir, 2006. **22**: p. 7273-7278.
67. Borden, M., Little, E, Gillies, R, Ferrara, K, *DNA and polylysine adsorption and multilayer construction onto cationic lipid-coated microbubbles*. Langmuir, 2007. **23**(18): p. 9401 - 9408.
68. Rapoport, N., Gao, Z, Kennedy, A, *Multifunctional nanoparticles for combining ultrasonic tumor imaging and targeted chemotherapy*. J Natl Cancer Inst, 2007. **99**: p. 1095-1106.

69. Chomas, J., Dayton, P, Allen, J, Morgan, K, Ferrara, KW, *Mechanisms of contrast agent destruction*. IEEE Trans Ultrason Ferroelectr Freq Control, 2001. **48**(1): p. 232-248.
70. de Laplace, P., *Mechanique Celeste*. Supplement to Book 10. 1806, Paris: Durat.
71. Epstein, P., Plesset, MS *On the stability of gas bubbles in liquid-gas solutions*. J Chem Phys 1950. **18**: p. 1505-1509.
72. Borden, M., Longo, ML, *Dissolution behavior of lipid monolayer-coated, air-filled microbubbles: effect of lipid hydrophobic chain length*. Langmuir, 2002. **18**: p. 9225–9233.
73. Kabalnov, A., Klein, D, Pelura, T, Schutt, E, Weers, J, *Dissolution of multicomponent microbubbles in the bloodstream: 1. Theory*. Ultrasound Med Biol, 1998. **24**: p. 739–749.
74. Kabalnov, A., Bradley, J, Flaim, S, Klein, D, Pelura, T, Peters, B, Otto, S, Reynolds, J, Schutt, E, Weers, J, *Dissolution of multicomponent microbubbles in the bloodstream: 2. Experiment*. Ultrasound Med Biol, 1998. **24**(751-760).
75. Schutt, E., Klein, DH, Mattrey, RM, Riess, JG, *Injectable microbubbles as contrast agents for diagnostic ultrasound imaging: The key role of perfluorochemicals*. Angew Chem Int Ed, 2003. **42**: p. 3218-3235.
76. Duncan, P., Needham, D, *Test of the Epstein-Plesset model for gas microparticle dissolution in aqueous media: effect of surface tension and gas undersaturation in solution*. Langmuir, 2004. **20**: p. 2567-2578.
77. Ferrara, K., Pollard, R, Borden, M, *Ultrasound microbubble contrast agents: Fundamentals and application to gene and drug delivery*. Annu Rev Biomed Eng, 2007. **9**: p. 415-447.
78. Langmuir, I., Schaefer, VJ, *Rates of evaporation of water through compressed monolayers on water*. J Franklin Inst, 1943. **235**(119): p. 126-128.
79. Möhwald, H., *Phospholipid Monolayers*. Handbook of Biological Physics, ed. R. Lipowski, Sackmann, E. Vol. 1. 1995, Amsterdam: Elsevier.
80. Kabalnov, A., Weers, J., Arlauskas, R., Tarara, T., *Phospholipids as emulsion stabilizers. I: Interfacial tensions*. Langmuir, 1995. **11**(8): p. 2966-2974.
81. Obladen, M., Brendlein, F, Krempien, B, *Surfactant substitution*. Eur J Pediatr, 1979. **131**: p. 219-228.
82. Vines, R. Retardation of evaporation by monolayers: Transport processes, ed. V. la Mer. 1962, New York: Academic Press.
83. Barnes, G., *Permeation through monolayers*. Colloids Surf A, 1997. **126**: p. 149-158.
84. Israelachvili, J. 2 ed. Intermolecular and Surface Forces, ed. A. Press. 1992, San Diego.
85. Kim, D., Costello, MJ, Duncan, PB, Needham, D *Mechanical properties and microstructure of polycrystalline phospholipid monolayer shells: Novel solid microparticles*. Langmuir 2003. **19**: p. 8455-8466.
86. Borden, M., Martinez, GV, Ricker, J, Tsvetkova, N, Longo, M, Gillies, RJ, Dayton, PA, Ferrara, KW *Lateral phase separation in lipid-coated microbubbles*. Langmuir, 2006. **22**: p. 4291-4297.
87. van Dijck, P., Kaper, AJ, Oonk, HAJ, de Gier, J, *Miscibility properties of binary phosphatidylcholine mixtures*. Biochim Biophys Acta, 1977. **470**: p. 58-69.
88. Vaz, W., Melo, EC, Thompson, TE, *Translational diffusion and fluid domain connectivity in a two-component, two-phase phospholipid bilayer*. Biophys J, 1989. **56**: p. 869-876.
89. Massari, S., *Phospholipid miscibility in ternary mixtures*. Biochim Biophys Acta, 1982. **688**: p. 23-28.

90. Mansour, H., Wang, D.S., Chen, C.S., Zograf, G., *Comparison of bilayer and monolayer properties of phospholipid systems containing dipalmitoylphosphatidylglycerol and dipalmitoylphosphatidylinositol*. Langmuir, 2001. **17**: p. 6622-6632.
91. Seddon, J., *Structure of the inverted hexagonal (HII) phase, and non-lamellar transitions of lipids*. Biochim Biophys Acta, 1990. **1031**: p. 1-69.
92. Karlovská, J., Williams, A, Macri, R, Gandour, R, Funari, S, Uhríková, D, Balgavý P, *Synchrotron SAX and WAX diffraction study of a hydrated very long-chain, dendritic amphiphile + DPPC mixture* Colloids Surf B, 2006. **54**(2): p. 160-164.
93. Anton, N., Patrick, S, Boury, F, Foussard, F, Benoit, JP, Proust, JE, *The influence of headgroup structure and fatty acyl chain saturation of phospholipids on monolayer behavior: a comparative rheological study*. Chem. Phys. Lipids, 2007. **150**: p. 167-175.
94. Dyck, M., Kruger, P, Losche, M, *Headgroup organization and hydration of methylated phosphatidylethanolamines in Langmuir monolayers*. Phys Chem Chem Phys, 2005. **7**: p. 150-156.
95. Lakhdar-Ghazal, F., Tichadou, JL, Tocanne, JF, *Effect of pH and monovalent cations on the ionization state of phosphatidylglycerol in monolayers*. Eur J Biochem, 1983. **134**: p. 531-537.
96. Ranck, J., Tocanne, JF, *Polymyxin B induces interdigitation in dipalmitoylphosphatidylglycerol lamellar phase with stiff hydrocarbon chains*. FEBS Lett, 1982. **143**: p. 171-174.
97. van der Net, A., Drenckhan, W, Weaire, D, Hutzler, S, *The crystal structure of bubbles in the wet foam limit*. Soft matter, 2006. **2**: p. 129-134.
98. van der Net, A., Delaney, GW, Drenckhan, W, Weaire, D, Hutzler, S, *Crystalline arrangements of microbubbles in monodisperse foams*. Colloids and Surfaces A: Physicochemical and Engineering Aspects, 2007. **309**(1-3): p. 117-124.
99. Shortencarier, M., Dayton, PA, Bloch, SH, Schumann, PA, Matsunaga, TO, Ferrara, KW, *A method for radiation-force localized drug delivery using gas-filled lipospheres*. IEEE Trans Ultrason Ferroelectr Freq Control, 2004. **51**(7): p. 822-831.
100. Meltzer, R., Tickner, EG, Popp, RL, *Why do the lungs clear ultrasonic contrast?* Ultrasound Med Biol, 1980. **6**: p. 263-269.
101. Fisher, N., Christiansen, JP, Klibanov, A, Taylor, RP, Kaul, S, Lindner, JR, *Influence of microbubble surface charge on capillary transit and myocardial contrast enhancement*. J Am Coll Cardiol, 2002. **40**(4): p. 811-819.
102. Mie, G., *Beiträge zur Optik trüber Medien, speziell kolloidaler Metallösungen*. Ann Phys, 1908. **330**(3): p. 377-445.
103. Kokhanovsky, A., *Single light scattering: Bubbles versus droplets*. Am J Phys 2004. **72**(2): p. 258-263.
104. Qiu, H., Hsu, CT, *The impact of high order refraction on optical microbubble sizing in multiphase flows*. Exp Fluids, 2004. **36**: p. 100-107.
105. Zhang, X., Lewis, M, Johnson, B, *Influence of bubbles on scattering of light in the ocean*. Appl Optics, 1998. **37**(27): p. 6525-6536.
106. Clift, R., Grace, JR, Weber, ME, *Bubbles, drops and particles*. 1978, New York: Academic Press.
107. Schneider, C., Neumann, R, Souza, AS, *Determination of the distribution of size of irregularly shaped particles from laser diffractometer measurements*. Int J Miner Process, 2007. **82**(1): p. 30-40.
108. Aden, A., Kerker, M, *Scattering of electromagnetic waves from two concentric spheres*. J Appl Phys, 1951. **22**(10): p. 1242-1246.

109. Marston, P., *Colors observed when sunlight is scattered by bubble clouds in seawater*. Appl Opt, 1991. **30**(24): p. 3479-3484.
110. Guan, J., Matula, TJ, *Using light scattering to measure the response of individual ultrasound contrast microbubbles subjected to pulsed ultrasound in vitro*. J Acoust Soc Am, 2004. **116**(5): p. 2832-2842.
111. Kelsall, G., Tang, S, Smith, AL, Yurdakul, S, *Measurement of rise and electrophoretic velocities of gas bubbles*. J Chem Soc Faraday Trans, 1996. **92**: p. 3879 - 3885.
112. Kinoshita, T., *The method to determine the optimum refractive index parameter in the laser diffraction and scattering method*. Adv Powder Tech, 2001. **12**(4): p. 589-602.
113. Borden, M., Caskey, CF, Little, E, Gillies, RJ, Ferrara, KW, *DNA and polylysine adsorption and multilayer construction onto cationic lipid-coated microbubbles*. Langmuir, 2007. **23**(18): p. 9401-9408.
114. Cavalieri, F., Hamassi, AE, Chiessi, E, Paradossi, G, *Stable polymeric microbubbles as multifunctional device for biomedical uses: Synthesis and characterization*. Langmuir, 2005. **21**: p. 8758-8764.
115. Cavalieri, F., Hamassi, AE, Chiessi, E, Paradossi, G, Villa, R, Zaffaroni, N, *Ligands tethering to biocompatible ultrasound active polymeric microbubble surface*. Macromol Symp, 2006. **234**(94-101).
116. Feshitan, J., Chen, CC, Kwan, JJ, Borden, MA, *Microbubble size isolation by differential centrifugation*. J Colloid Interface Sci, 2009. **329**(2): p. 316-324.
117. Christiansen, J., French, BA, Klibanov, AL, Kaul, S, Lindner, JR, *Targeted tissue transfection with ultrasound destruction of plasmid-bearing cationic microbubbles*. Ultrasound Med Biol, 2003. **29**: p. 1759-1767.
118. Leong-Poi, H., Kuliszewski, MA, Lekas, M, Sibbald, M, Teichert-Kuliszewska, K, Klibanov, AL, Stewart, DJ, Lindner, JR, *Therapeutic arteriogenesis by ultrasound-mediated VEGF165 plasmid gene delivery to chronically ischemic skeletal muscle*. Circ Res 2007. **101**: p. 295-303.
119. Lentacker, I., de Smedt, SC, Demeester, J, Sanders, NN, *Microbubbles which bind and protect DNA against nucleases*. J Contr Release 2006. **116**(2): p. e73-e75.
120. Li, M., Folger, HS, *Acoustic emulsification part 1. On the instability of the oil water interface to form the initial droplets*. J Fluid Mech, 1978. **88**: p. 499.
121. Li, M., Folger, HS, *Acoustic emulsification part 2. Breakup of the large primary oil droplets in a water medium*. J Fluid Mech, 1978. **88**: p. 513.
122. Unger, E., McCreery, TP, Sweitzer, RH, Caldwell, VE, Wu, Y, *Acoustically active lipospheres containing paclitaxel: a new therapeutic ultrasound contrast agent*. Invest Radiol, 1998. **33**(12): p. 886-892.
123. Moran, C., Anderson, T, Pye, SD, Sboros, V, McDicken, WN, *Quantification of microbubble destruction of three fluorocarbon-filled ultrasonic contrast agents*. Ultrasound Med Biol, 2000. **26**(4): p. 629-639.
124. Lazewatsky, J., Kagan, M, Barrett, J, *The effect of dilution medium on the measurement of in-vitro properties of ultrasound contrast agents*. IEEE Ultras Symp Proc, 1999.
125. Marsh, J., Hall, CS, Scott, MJ, Fuhrhop, RW, Gaffney, PJ, Wickline, SA, Lanza, GM, *Improvements in the ultrasonic contrast of targeted perfluorocarbon nanoparticles using an acoustic transmission line model*. IEEE Trans Ultrason Ferroelectr Freq Control, 2002. **49**(1): p. 29-38.
126. Hoff, L., *Acoustic characterization of Nycomed's NC100100 contrast agent*. IEEE Ultras Symp Proc, 1998: p. 1799-1802.

127. Caskey, C., Stieger, SM, Qin, S, Dayton, PA, Ferrara, KW, *Microbubble oscillations in gel phantom and ex vivo preparation validate proposed mechanisms for contrast-based drug delivery*. IEEE Ultras Symp Proc, 2007: p. 769-772.
128. Caskey, C., Kruse, DE, Dayton, PA, *Microbubble oscillation in tubes with diameters of 12, 25, and 195 microns*. Appl Phys Lett, 2006. **88**(033902): p. 1-3.
129. Apfel, R., Holland, CK, *Gauging the likelihood of cavitation from short-pulse, low-duty cycle diagnostic ultrasound*. Ultrasound Med Biol, 1991. **17**: p. 179-185.
130. Holland, C., Apfel, RE, *An improved theory for the prediction of microcavitation thresholds*. IEEE Trans Ultrason Ferroelectr Freq Control Proc, 1989. **36**(2): p. 204-208.
131. Marsh, J., Hall, CS, Wickline, SA, Lanza, GM, *Temperature dependence of acoustic impedance for specific fluorocarbon liquids*. J Acoust Soc Am, 2002. **112**(6): p. 2858-2862.
132. Greis, C., *Technology overview: Sonovue (Bracco, Milan)*. Eur Radiol Suppl, 2004. **14**(Suppl 8): p. 11-15.
133. Shortencarier Tartis, M., McCallan, J, Lum, AF, LaBell, R, Stieger, SM, Matsunaga, TO, Ferrara, KW, *Therapeutic effects of paclitaxel-containing ultrasound contrast agents*. Ultrasound Med Biol, 2006. **32**(11): p. 1771-1780.
134. Shortencarier, M., Dayton, PA, Ferrara, KW, Matsunaga, T, LaBell, R, Schumann, P. *Targeted chemotherapy delivery with ultrasound*. in *IEEE Ultras Symp Proc*. 2005.
135. Shi, W., Böhmer, M, van Wamel, A, Celebi, M, Klivanov, AL, Chin, CT, Chlon, C, Emmer, M, Kooiman, K, de Jong, N, Hall, CS, *Ultrasound therapy with drug loaded microcapsules*. IEEE Ultras Symp Proc, 2007: p. 773-776.
136. Haanen, C., Hillen, G, *Combination chemotherapy with doxorubicin in "bad risk" leukemia patients*. Adriamycin review, ed. M. Stagnet. 1975, Ghent, Belgium: European Press Medicon.
137. Frederick, C., Williams, DL, Ughetto, G, van der Marel, GA, van Boom, JH, Rich, A, Wang, HJ, *Structural comparison of anticancer drug-DNA complexes: Adriamycin and Daunomycin*. Biochemistry, 1990. **29**: p. 2538-2549.
138. d'Arpa, P., Liu, LF, *Topoisomerase-targeting antitumor drugs*. Biochim Biophys Acta, 1989. **989**(2): p. 163-177.
139. Tritton, T., Yee, G, *The anticancer agent adriamycin can be actively cytotoxic without entering cells*. Science, 1982. **217**: p. 248-250.
140. Zwelling, L., Kerrigan, D, Michaels, S, *Cytotoxicity and DNA strand breaks by 5-iminodaunorubicin in mouse leukemia L1210 cells: Comparison with adriamycin and 4'-(9-acridinylamino)methanesulfon-m-anisidide*. Cancer res, 1982. **42**: p. 2687-2691.
141. Siegfried, J., Sartorelli, AC, Tritton, TR, *Evidence for the lack of relationship between inhibition of nucleic acid synthesis and cytotoxicity of adriamycin*. Cancer Biochem Biophys, 1983. **6**(3): p. 137-142.
142. Murphree, S., Tritton, TR, Smith, PL, Sartorelli, AC, *Adriamycin-induced changes in the surface membrane of sarcoma 180 ascites cells*. Biochim Biophys Acta, 1981. **649**(2): p. 317-324.
143. Arancia, G., Molinari, A, Crateri, P, Calcabrini, A, Silvestri, L, Isacchi, G, *Adriamycin-plasma membrane interaction in human erythrocytes*. Eur J Cell Biol, 1988. **47**(2): p. 379-387.
144. Nicolay, K., de Kruijff, B *Effects of adriamycin on respiratory chain activities in mitochondria from rat liver, rat heart and bovine heart. Evidence for a preferential inhibition of complex III and IV*. Biochim Biophys Acta, 1987. **892**: p. 320-330.
145. Paradies, G., Ruggiero, FM, *The effect of doxorubicin on the transport of pyruvate in rat-heart mitochondria*. Biochem Biophys Res Commun, 1988. **156**: p. 1302-1307.

146. Eksborg, S., Ehrsson, H, Ekqvist, B, *Protein binding of anthraquinone glycosides with special reference to adriamycin*. Cancer Chemother Pharmacol, 1982. **10**: p. 7-10.
147. DiFrancesco, R., Griggs, J, Donnelly, DiCenzo, R, *Simultaneous analysis of cyclophosphamide, doxorubicin and doxorubicinol by liquid chromatography coupled to tandem mass spectrometry*. J Chromatogr B, 2007. **852**: p. 545-553.
148. Rahman, A., Carmichael, D, Harris, M, Roh, JK, *Comparative pharmacokinetics of free doxorubicin and doxorubicin entrapped in cardiolipin liposomes*. Cancer Res, 1986. **46**: p. 2295-2299.
149. Yadav, A., Mishra, P, Mishra, AK, Mishra, P, Jain, S, Agrawal, GP, *Development and characterization of hyaluronic acid-anchored PLGA nanoparticulate carriers of doxorubicin*. Nanomedicine, 2007. **3**(4): p. 246-257.
150. Tewes, F., Munnier, E, Antoon, B, Ngaboni Okassa, L, Cohen-Jonathan, S, Marchais, H, Douziech-Eyrolles, L, Souce, M, Dubois, P, Chourpa, I, *Comparative study of doxorubicin-loaded poly(lactide-co-glycolide) nanoparticles prepared by single and double emulsion methods*. Eur J Pharm Biopharm, 2007. **66**(3): p. 488-492.
151. Lee, Y., Park, SY, Mok, H, Park, TG, *Synthesis, characterization, antitumor activity of pluronic mimicking copolymer micelles conjugated with doxorubicin via acid-cleavable linkage*. Bioconjugate Chem, 2008. **19**(2): p. 525-531.
152. Gabizon, A., Shmeeda, H, Barenholz, Y, *Pharmacokinetics of PEGylated liposomal doxorubicin: Review of animal and human studies*. Clin Pharmacokin, 2003. **42**(5): p. 419-436.
153. Verma, S., Dent, S, Chow, B, Rayson, D, Safra, T, *Metastatic breast cancer: The role of pegylated liposomal doxorubicin after conventional anthracyclines*. Cancer Treatment Reviews, 2008. **34**(5): p. 391-406.
154. Gabizon, A., Goren, D, Horowitz, A, Tzemach, D, Lossos, A, Siegal, T, *Long-circulating liposomes for drug delivery in cancer therapy: A review of biodistribution studies in tumor-bearing animals*. Adv drug deliv rev, 1997. **24**: p. 337-344.
155. Carrion, C., M.A. de Madariaga, and J.C. Domingo, *In vitro cytotoxic study of immunoliposomal doxorubicin targeted to human CD34+ leukemic cells*. Life Sciences, 2004. **75**(3): p. 313-328.
156. Maruyama, K., Ishida, O, Takizawa, T, Moribe, K, *Possibility of active targeting to tumor tissues with liposomes*. Adv drug deliv rev, 1999. **40**: p. 89-102.
157. Oh, K., Lee, ES, Kim, D, Bae, YH, *Histidine-based pH-sensitive anticancer drug carrier micelle: Reconstitution and brief evaluation of its systemic toxicity*. Int J Pharm, 2008. **358**(1-2): p. 177-183.
158. Mills, J., Needham, D, *Temperature-triggered nanotechnology for chemotherapy: Rapid release from lysolipid temperature-sensitive liposomes*, in 2006 NSTI Nanotechnology Conference and Trade Show - Nanotech 2006 - 9th Annual. 2006: Boston, USA.
159. Mykhaylyk, O., Dudchenko, N, Dudchenko, A, *Doxorubicin magnetic conjugate targeting upon intravenous injection into mice: High gradient magnetic field inhibits the clearance of nanoparticles from the blood*. Journal of Magnetism and Magnetic Materials, 2005. **293**(1): p. 473-482.
160. Burstein OM, W.M., *Drug loaded contrast agents for cancer tumors: A combination of imaging and therapy*, in Biomedical Technology Showcase. 2006, School of Biomedical Engineering, Science & Health Systems: Drexel University, PA.
161. Mickisch, G., Rahman, A, Pastan, I, Gottesman, MM, *Increased effectiveness of liposome-encapsulated doxorubicin in multidrug-resistant-transgenic mice compared with free doxorubicin*. J Natl Cancer Inst, 1992. **84**(10): p. 804-805.
162. Nicolay, K., Aue, WP, Seelig, J, van Echteld, CJ, Ruigrok, TJ, de Kruijff, B, *Effects of the anticancer drug adriamycin on the energy metabolism of rat heart as measured by*

- in vivo phosphorous-31 NMR and implications for adriamycin-induced cardiotoxicity.* Biochim Biophys Acta, 1987. **929**(1): p. 5-13.
163. Goormaghtigh, E., Brasseur, R, Ruyschaert, JM, *Adriamycin inactivates cytochrome c oxidase by exclusion of the enzyme from its cardiolipin essential environment.* Biochem Biophys Res Commun, 1982. **104**(1): p. 314-320.
 164. Herman, E., Rahman, A, Ferrans, V, Vick, J, Schein, P, *Prevention of chronic doxorubicin cardiotoxicity in beagles by liposomal encapsulation.* Cancer res, 1983. **43**: p. 5427-5432.
 165. Goormaghtigh, E., Chatelain, P, Caspers, J, Ruyschaert, JM, *Evidence of a specific complex between adriamycin and negatively-charged phospholipids.* Biochim Biophys Acta, 1980. **597**: p. 1-14.
 166. de Wolf, F., Maliepaard, M, van Dorsten, F, Berghuis, I, Nicolay, K, de Kruijff, B, *Comparable interaction of doxorubicin with various acidic phospholipids results in changes of lipid order and dynamics.* Biochim. et Biophys. Acta, 1991. **1096**: p. 67-80.
 167. Dupou-Cezanne, L., Sautereau, AM, Tocanne, JF, *Localization of adriamycin in model and natural membranes.* Eur J Biochem, 1989. **181**: p. 695-702.
 168. Gallois, L., Fiallo, M, Laigle, A, Priebe, W, Garnier-Suillerot, A, *The overall partitioning of anthracyclines into phosphatidyl-containing model membranes depends neither on the drug charge nor the presence of anionic phospholipids.* Eur J Biochem, 1996. **241**: p. 879-887.
 169. Speelmans, G., Staffhorst, RW, de Kruijff, B, *The anionic phospholipid-mediated membrane interaction of the anti-cancer drug doxorubicin is enhanced by phosphatidylethanolamine compared to other zwitterionic phospholipids.* Biochemistry, 1997. **36**: p. 8657-8662.
 170. Heywang, C., Saint-Pierre Chazalet, M, Masson, M, Bolard, J, *Orientation of anthracyclines in lipid monolayers and planar asymmetrical bilayers: A Surface-Enhanced Resonance Raman Scattering study.* Biophys J, 1998. **75**: p. 2368-2381.
 171. Tinkov, S., Bekeredjian, R, Winter, G, Coester, C, *Characterization of ultrasound-mediated destruction of drug-loaded microbubbles using an improved in vitro model.* Appl Acoust, 2008.
 172. Ardhammar, M., Lincoln, P, Norden, B, *Invisible liposomes: Refractive index matching with sucrose enables flow dichroism assessment of peptide orientation in lipid vesicle membrane.* Proc Natl Acad Sci USA, 2002. **99**(24): p. 15313–15317.
 173. European Pharmacopoeia 5.00, *Allgemeine Vorschriften, Doxorubicini hydrochloridum.* 2005. p. 2009-2010.
 174. Food and Drug Administration, F., *International Conference of Harmonization; Guidelines for the Photostability Testing of New Drug Substances and Products; Availability; Notice,* D.o.H.a.H. Services, Editor. 1997. p. 27115-27122.
 175. Raghunand, N., Mahoney, BP, Gillies, RJ, *Tumor acidity, ion trapping and chemotherapeutics. II. pH dependent partition coefficients predict importance of ion trapping on pharmacokinetics of weakly basic chemotherapeutic agents.* Biochem Pharmacol, 2003. **66**: p. 1219-1229.
 176. Elbayoumi, T., Torchilin, V, *Enhanced cytotoxicity of monoclonal anticancer antibody 2C5-modified doxorubicin-loaded PEGylated liposomes against various tumor cell lines.* Eur J Pharm Sci, 2007. **32**(3): p. 159-168.
 177. Mosmann, T., *Rapid colorimetric assay for cellular growth and survival: Application to proliferation and cytotoxicity assays.* Journal of Immunological Methods, 1983. **65**(1-2): p. 55-63.
 178. Tamura-Lis, W., Lis, LJ, Quinn, PJ, *Structures and mechanisms of lipid phase transitions in nonaqueous media.* Biophys J, 1988. **53**: p. 489-492.

179. Constantinides, P., Inouchi, N, Tritton, TR, Sartorelli, AC, Sturtevant, JM, *A scanning calorimetric study of the interaction of anthracyclines with neutral and acidic phospholipids alone and in binary mixtures.* J Biol Chem, 1986. **261**(22): p. 10196-10203.
180. McIntosh, T., *Differences in hydrocarbon chain tilt between hydrated phosphatidylethanolamine and phosphatidylcholine bilayers. A molecular packing model.* Biophysical Journal, 1980. **29**(2): p. 237-245.
181. Goormaghtigh, E., Brasseur, R, Huart, P, Ruyschaert, JM, *Study of the adriamycin-cardiolipin complex structure using attenuated total reflection infrared spectroscopy.* Biochemistry, 1987. **26**: p. 1789-1794.
182. Goldman, R., Facchinetti, T, Bach, D, Raz, A, Shinitzky, M, *A differential interaction of daunomycin, adriamycin and their derivatives with human erythrocytes and phospholipid bilayers* Biochim Biophys Acta, 1978. **512**: p. 254-269.
183. Findlay, E., Barton, PG, *Phase behavior of synthetic phosphatidylglycerols and binary mixtures with phosphatidylcholines in the presence and absence of calcium ions.* Biochemistry, 1978. **17**(12): p. 2400–2405.
184. McIntosh, T., McDaniel, RV, Simon, SA, *Induction of an interdigitated gel phase in fully hydrated lecithin bilayers.* Biochim Biophys Acta, 1983. **731**: p. 109-114.
185. Belsito, S., Bartucci, R, Montesano, G, Marsh, D, Sportelli, L, *Molecular and mesoscopic properties of hydrophilic polymer-grafted phospholipids mixed with phosphatidylcholine in aqueous dispersion: Interaction of dipalmitoyl N-poly(ethylene glycol)phosphatidylethanolamine with dipalmitoylphosphatidylcholine studied by spectrophotometry and spin-label electron spin resonance.* Biophys J, 2000. **78**: p. 1420–1430.
186. Szleifer, I., Gerasimov, O, Thompson, D, *Spontaneous liposome formation induced by grafted poly(ethylene oxide) layers: Theoretical prediction and experimental verification.* Proc Natl Acad Sci USA, 1998. **95**: p. 1032–1037.
187. Malvern Instruments Limited, A.n. *The use of Zeta potential measurements to study sterically stabilized liposomes.* **Volume**,
188. Vautrin, C., Dubois, M, Zemb, T, Schmölzer, S, Hoffmann, H, Gradzielski, M, *Chain melting in swollen catanionic bilayers.* Colloids and Surfaces A: Physicochemical and Engineering Aspects, 2003. **217**(1-3): p. 165-170.
189. Zemb, T., Carrière, D, Glinel, K, Hartman, M, Meister, A, Vautrin, C, Delorme, N, Fery, A, Dubois, M, *Catanionic bilayers as micro-crystals with in-plane ordered alternated charges.* Colloids and Surfaces A: Physicochemical and Engineering Aspects, 2007. **303**(1-2): p. 37-45.
190. Kegel, W., van der Schoot, P, *Competing hydrophobic and screened-coulomb interactions in hepatitis B virus capsid assembly.* Biophys J, 2004. **86**: p. 3905-3913.
191. Toko, K., Yamafuji, K, *Influence of monovalent and divalent cations on the surface area of phosphatidylglycerol monolayers* Chem Phys Lipids, 1980. **26**: p. 79-99.
192. Burke, T., Tritton, TR, *Structural basis of anthracycline selectivity for unilamellar phosphatidylcholine vesicles: an equilibrium binding study.* Biochemistry, 1985. **24**: p. 1768 -1776.
193. Heywang, C., Saint-Pierre Chazalet, M, Masson, M, Garnier-Suillerot, A, Bolard, J, *Incorporation of exogenous molecules inside mono- and bilayers of phospholipids: Influence of the mode of preparation revealed by SERRS and surface pressure studies.* Langmuir, 1996. **12**: p. 6459-6467.
194. May, D., Allen, JS, Ferrara, KW, *Dynamics and fragmentation of thick-shelled microbubbles.* IEEE Trans Ultrason Ferroelectr Freq Control, 2002. **49**(10): p. 1400-1410.

195. Unger, E., *Acoustically active drug delivery systems*, U. Patent, Editor. 2002, Bristol-Myers Squibb Medical Imaging, Inc., Princeton, NJ: USA. p. 62.
196. Li, X., Hirsh, DJ, Cabral-Lilly, D, Zirkel, A, Gruner, SM, Janoff, AS, Perkins, WR, *Doxorubicin physical state in solution and inside liposomes loaded via a pH gradient* Biochem Biophys Acta Biomembr, 1998. **1415**(1): p. 23-40.
197. *Dielectric constant of glycerine-water solutions at 25°C (77°F)*. 2008 [cited February, 22nd 2009]; Available from: <http://www.dow.com/glycerine/resources/table5.htm>.
198. Mhawi, A., Fernandes, AB, Ottensmeyer, FP, *Low-energy-loss electron microscopy of doxorubicin in human breast cancer MCF-7 cells: Localization by color*. J Struct Biol, 2007. **158**(1): p. 80-92.
199. Tartis, M., Kruse, DE, Zheng, H, Zhang, H, Kheirloom, A, Marik, J, Ferrara, KW, *Dynamic microPET imaging of ultrasound contrast agents and lipid delivery*. J Contr Release, 2008. **131**: p. 160-166.
200. Yanagisawa, K., Moriyasu, F, Miyahara, T, Yuki, M, Iijima, H, *Phagocytosis of ultrasound contrast agent microbubbles by Kupffer cells*. Ultrasound Med Biol, 2007. **33**(2): p. 318-325.
201. Moghimi, S., Hunter, AC, Murray, JC, *Long-circulating and target-specific nanoparticles: theory to practice*. Pharmacol Rev, 2001. **53**(2): p. 283-318.
202. Oku, N., *Delivery of contrast agents for positron emission tomography imaging by liposomes*. Adv Drug Deliv Rev, 1999. **37**(1-3): p. 53-61.
203. Rahman, A., Fumagalli, A, Barbieri, B, Schein, PS, Casazza AM, *Antitumor and toxicity evaluation of free doxorubicin and doxorubicin entrapped in cardiolipin liposomes*. Cancer Chemother Pharmacol, 1986. **16**: p. 22-27.
204. Crystal, R., *Transfer of genes to humans: Early lessons and obstacles to success*. Science 1995. **270**: p. 404-410.
205. *Gene Therapy Database*. 2009 [cited 2009 january, 10th]; Available from: <http://wiley.co.uk/genetherapy/clinical/>.
206. Raper, S., Yudkoff, M, Chirmule, N, Gao, GP, Nunes, F, Haskal, ZJ, Furth, EE, Propert, KJ, Robinson, MB, Magosin, S, Simoes, H, Speicher, L, Hughes, J, Tazelaar, J, Wivel, NA, Wilson, JM, Batshaw, ML, *A pilot study of in-vivo liver-directed gene transfer with an adenoviral vector in partial ornithine transcarbamylase deficiency*. Hum Gene Ther, 2002. **13**: p. 163-175.
207. Sun, L., Li, J, Xiao, X, *Overcoming adeno-associated virus vector size limitation through viral DNA heterodimerization*. Nature Med, 2000. **6**(5): p. 599-602.
208. Boulaiz, H., Marchal, JA, Prados, J, Melguizo, C, Aranega, A, *Non-viral and viral vectors for gene therapy*. Cell Mol Biol, 2005. **51**: p. 3-22.
209. Shohet, R., Chen, S, Zhou, YT, Wang, Z, Meidell, RS, Unger, RH, Grayburn, PA, *Echocardiographic destruction of albumin microbubbles directs gene delivery to the myocardium*. Circulation, 2000. **101**: p. 2554-2556.
210. Frenkel, P., Chen, S, Thai, T, Shohet, RV, Grayburn, PA, *DNA-loaded albumin microbubbles enhance ultrasound-mediated transfection in-vitro*. Ultrasound Med Biol, 2002. **28**(6): p. 817-822.
211. Chen, S., Shohet, RV, Bekeredjian, R, Frenkel, P, Grayburn, PA, *Optimization of ultrasound parameters for cardiac gene delivery of adenoviral or plasmid deoxyribonucleic acid by ultrasound-targeted microbubble destruction*. J Am Coll Cardiol, 2003. **42**: p. 301-308.
212. Chen, S., Ding, JH, Bekeredjian, R, Yang, BZ, Shohet, RV, Johnston, SA, Hohmeier, HE, Newgard, CB, Grayburn, PA, *Efficient gene delivery to pancreatic islets with ultrasonic microbubble destruction technology*. Proc Natl Acad Sci USA, 2006. **103**(22): p. 8469-8474.

213. Boussif, O., Lezoualc'h, F, Zanta, MA, Mergny, MD, Scherman, D, Demeneix, B, Behr, JP, *A versatile vector for gene and oligonucleotide transfer into cells in culture and in vivo: Polyethylenimine*. Proc Natl Acad Sci USA, 1995. **92**(16): p. 7297-7301.
214. Mislick, K., Baldeschwieler, JD *Evidence for the role of proteoglycans in cation-mediated gene transfer*. Proc Natl Acad Sci USA, 1996. **93**: p. 12349-12354.
215. Mounkes, L., Zhong, W, Cipres-Palacin, G, Heath, TD, Debs, RJ *Proteoglycans mediate cationic liposome-DNA complex-based gene delivery in vitro and in vivo*. J Biol Chem, 1998. **273**: p. 26164-26170.
216. Eliyahu, H., Serivel, N, Domb, AJ, Barenholz, Y, *Lipoplex-induced hemagglutination: potential involvement in intravenous gene delivery*. Gene Ther, 2002. **9**: p. 850-858.
217. Ogris, M., Brunner, S, Schuller, S, Kircheis, R, Wagner, E, *PEGylated DNA/transferrin-PEI complexes: reduced interaction with blood components, extended circulation in blood and potential for systemic gene delivery*. Gene Ther, 1999. **6**: p. 595-605.
218. Neu, M., Fischer, D, Kissel, T, *Recent advances in rational gene transfer vector design based on poly(ethylene imine) and its derivatives*. The Journal of Gene Medicine, 2005. **7**(8): p. 992-1009.
219. Bragonzi, A., Boletta, A, Biffi, A, Muggia, A, Sersale, G, Cheng, SH, Bordignon, C, Assael, BM, Conese, M, *Comparison between cationic polymers and lipids in mediating systemic gene delivery to the lungs*. Gene Ther, 1999. **6**: p. 1995-2004.
220. Neu, M., *Modified Poly(ethylene imines) for plasmid delivery: Physico chemical and in-vitro / in-vivo investigations*, in *Pharmacy*. 2006, Philips-University - Marburg: Marburg.
221. Wen, Y., Pan, S, Luo, X, Zhang, X, Zhang, W, Feng, M, *A Biodegradable low molecular weight polyethylenimine derivative as low toxicity and efficient gene vector*. Bioconjug Chem, 2009. **20**(2): p. 322-332.
222. Fischer, D., Li, Y, Ahlemeyer, B, Krieglstein, J, Kissel, T, *In-vitro cytotoxicity testing of polycations: Influence of polymer structure on cell viability and hemolysis*. Biomaterials, 2003. **24**(7): p. 1121-1131.
223. Fischer, D., Bieber, T, Li, Y, Elsasser, HP, Kissel, T, *A novel non-viral vector for DNA delivery based on low molecular weight, branched polyethylenimine: Effect of molecular weight on transfection efficiency and cytotoxicity*. Pharmaceut Res, 1999. **16**(8): p. 1273-1279.
224. Godbey, W., Barry, MA, Saggau, P, Wu, KK, Mikos, AG, 2000. *J Biomed Mater Res, Poly(ethylenimine)-mediated transfection: a new paradigm for gene delivery*. **51**(3): p. 321-328.
225. Kim, Y., Park, JH, Lee, M, Kim, YH, Park, TG, Kim, SW, *Polyethylenimine with acid-labile linkages as a biodegradable gene carrier*. J Contr Release, 2005. **103**(1): p. 209-219.
226. Yamazaki, Y., Nango, M, Matsuura, M, Hasegawa, Y, Hasegawa, M, Oku, N, *Polycation liposomes, a novel nonviral gene transfer system, constructed from cetylated polyethylenimine*. Gene Ther, 2000. **7**: p. 1148-1155.
227. Brownlie, A., Uchegbu, IF, Schätzlein, AG, *PEI-based vesicle-polymer hybrid gene delivery system with improved biocompatibility*. Int J Pharm, 2003. **274**: p. 41-52.
228. Kim, S., Choi, JS, Jang, HS, Suh, H, Park, J, *Hydrophobic modification of polyethyleneimine for gene transfectants*. Bulletin of the Korean Chemical Society, 2001. **22**(10): p. 1069-1075.
229. Thomas, M., Klivanov, AM, *Enhancing polyethylenimine's delivery of plasmid DNA into mammalian cells*. Proc Natl Acad Sci USA, 2002. **99**(23): p. 14640-14645.

230. Oku, N., Yamazaki, Y, Matsuura, M, Sugiyama, M, Hasegawa, M, Nango, M, *A novel non-viral gene transfer system, polycation liposomes*. Adv drug deliv rev, 2001. **52**(3): p. 209-218.
231. Brownlie, A., Uchegbu, IF, Schätzlein, AG, *PEI-based vesicle-polymer hybrid gene delivery system with improved biocompatibility*. Int J Pharm, 2004. **274**: p. 41-52.
232. Newman, C., Bettinger, T *Gene therapy progress and prospects: Ultrasound for gene transfer*. Gene Ther 2007. **14**: p. 465-475.
233. Akowuah, E., Gray, C, Lawrie, A, Sheridan, PJ, Su, CH, Bettinger, T, Brisken, AF, Gunn, J, Crossman, DC, Francis, SE, Baker, AH, Newman, CM, *Ultrasound-mediated delivery of TIMP-3 plasmid DNA into saphenous vein leads to increased lumen size in a porcine interposition graft model*. Gene Ther 2005. **12**: p. 1154-1157.
234. Endoh, M., Koibuchi, N, Sato, M, Morishita, R, Kanzaki, T, Murata, Y, Kaneda, Y, *Fetal gene transfer by intrauterine injection with microbubble-enhanced ultrasound*. Mol Ther 2002. **5**(5): p. 501-508.
235. Koike, H., Tomita, N, Azuma, H, Taniyama, Y, Yamasaki, K, Kunugiza, Y, Tachibana, K, Ogihara, T, Morishita, R, *An efficient gene transfer method mediated by ultrasound and microbubbles into the kidney*. J Gene Med, 2005. **7**: p. 108-116.
236. Lan, H., Mu, W, Tomita, N, Huang, XR, Li, JH, Zhu, HJ, Morishita, R, Johnson, RJ, *Inhibition of renal fibrosis by gene transfer of inducible smad7 using ultrasound-microbubble system in rat UUO model*. J Am Soc Nephrol, 2003. **14**: p. 1535-1548.
237. Sakakima, Y., Hayashi, S, Yagi, Y, Hayakawa, A, Tachibana, K, Nakao, A, *Gene therapy for hepatocellular carcinoma using sonoporation enhanced by contrast agents*. Canc Gene Ther 2005. **12**: p. 884-889.
238. Miao, C., Brayman, AA, Loeb, KR, Ye, P, Zhou, L, Mourad, P, *Ultrasound enhances gene delivery of human factor IX plasmid*. Hum Gene Ther, 2005. **16**: p. 893-905.
239. Miller, D., Song, J *Tumor growth reduction and DNA transfer by cavitation-enhanced high-intensity focused ultrasound in-vivo*. Ultrasound Med Biol, 2003. **29**: p. 887-893.
240. Porter, T., Hiser, WL, Kricsfeld, D, Deligonul, U, Xie, F, Iversen, P, Radio, S, *Inhibition of carotid artery neointimal formation with intravenous microbubbles*. Ultrasound Med Biol, 2001. **27**(2): p. 259-265.
241. Korpany, G., Chen, S, Shohet, RV, Ding, J, Yang, B, Frenkel, PA, Grayburn, PA, *Targeting of VEGF-mediated angiogenesis to rat myocardium using ultrasonic destruction of microbubbles*. Gene Ther, 2005. **12**: p. 1305-1312.
242. Zhigang, W., Zhiyu, L, Haitao, R, Hong, R, Qunxia, Z, Ailong, H, Qi, L, Chunjing, Z, Hailin, T, Lin, G, *Ultrasound-mediated microbubble destruction enhances VEGF gene delivery to the infarcted myocardium in rats*. Clin Imaging, 2004. **28**: p. 395-398.
243. Negishi, Y., Endo, Y, Fukuyama, T, Suzuki, R, Takizawa, T, Omata, D, Maruyama, K, Aramaki, Y, *Delivery of siRNA into the cytoplasm by liposomal bubbles and ultrasound*. J Contr Release, 2008. **132**(2): p. 124-130.
244. Tinkov, S., Bekeredjian, R, Winter, G, Coester, C, *Microbubbles as ultrasound triggered drug carriers*. J Pharm Sci, 2008.
245. Mayer, C., Geis, NA, Katus, HA, Bekeredjian, R, *Ultrasound targeted microbubble destruction for drug and gene delivery*. Expert Opin Drug Deliv, 2008. **5**(10): p. 1121-1138.
246. Kheirulomoom, A., Dayton, P, Lum, A, Little, E, Paoli, E, Zheng, H, Ferrara, K, *Acoustically-active microbubbles conjugated to liposomes: Characterization of a proposed drug delivery vehicle*. J Contr Release, 2007. **118**(3): p. 275-284.
247. Bayer, E., Wilchek, M, *The Use of the avidin-biotin complex as a tool in molecular biology*, in *Methods of Biochemical Analysis*, G. David, Editor. 2006. p. 1-45.

248. Schneider, M., Bussat, P, Yan, F, Senete, A, *Assembly of gas-filled microvesicle with active component for contrast imaging*, U.S.P.a.T. Office, Editor. 2007, Bracco Research S.A.: USA. p. 32.
249. Lentacker, I., de Smedt, SC, Demeester, J, Sanders, NN, *Microbubbles which bind and protect DNA against nucleases*. J Contr Release, 2006. **116**(2): p. e73-e75.
250. Lentacker, I., de Geest, BG, Vandenbroucke, RE, Peeters, L, Demeester, J, de Smedt, SC, Sanders, NN, *Ultrasound-responsive polymer-coated microbubbles that bind and protect DNA*. Langmuir, 2006. **22**(17): p. 7273-7278.
251. Lentacker, I., De Smedt, SC, Demeester, J, Van Marck, V, Bracke, M, Sanders, NN, *Lipoplex-loaded microbubbles for gene delivery: A trojan horse controlled by ultrasound*. Adv Funct Mater, 2007. **17**(12): p. 1910-1916.
252. Sugiyama, M., Matsuura, M, Takeuchi, Y, Kosaka, J, Nango, M, Oku, N, *Possible mechanism of polycation liposome (PCL)-mediated gene transfer*. Biochim Biophys Acta, 2004. **1660**: p. 24-30.
253. Xu, Y., Szoka, FC, *Mechanism of DNA release from cationic liposome / DNA complexes used in cell transfection*. Biochemistry, 1996. **35**(18): p. 5616-5623.
254. Cho, Y., Kim, JD, Park, K, *Polycation gene delivery systems: Escape from endosomes to cytosol*. J Pharm Pharmacol, 2003. **55**: p. 721-734.
255. Wrobell, I., Collins, D, *Fusion of cationic liposomes with mammalian cells occurs after endocytosis*. Biochim Biophys Acta, 1995. **1235**: p. 296-304.
256. Murphy, R.F., S. Powers, and C.R. Cantor, *Endosome pH measured in single cells by dual fluorescence flow cytometry: rapid acidification of insulin to pH 6*. J. Cell Biol., 1984. **98**(5): p. 1757-1762.
257. Suh, J., Paik, HJ, Hwang, BK, *Ionization of poly(ethylenimine) and poly(allylamine) at various pH*. Bioorg Chem, 1994. **22**(318-327).
258. Boussif, O., Zanta, MA, Behr, JP, *Optimized galenics improve in vitro gene transfer with cationic molecules up to 1000-fold*. Gene Ther, 1996. **3**: p. 1074-1080.
259. Godbey, W., Wu, KK, Mikos, AG, *Tracking the intracellular path of poly(ethylenimine)/DNA complexes for gene delivery*. Proc Natl Acad Sci USA, 1999. **96**: p. 5177-5181.
260. Mortimer, I., Tam, P, MacLachlan, I, Graham, RW, Saravolac, EG, Joshi, PB., *Cationic lipid-mediated transfection of cells in culture requires mitotic activity*. Gene Ther, 1999. **6**: p. 403-411.
261. Zauner, W., Brunner, S, Buschle, M, Ogris, M, Wagner, E, *Differential behaviour of lipid based and polycation based gene transfer systems in transfecting primary human fibroblasts: a potential role of polylysine in nuclear transport*. Biochim Biophys Acta, 1999. **1428**: p. 57-67.
262. Mo, Y., Wang, C, Beck, WT., *A novel nuclear localization signal in human DNA topoisomerase I*. J Biol Chem, 2000. **275**: p. 41107-41113.
263. von Harpe, A., Petersen, H, Li, Y, Kissel, T, *Characterization of commercially available and synthesized polyethylenimines for gene delivery*. J Contr Release, 2000. **69**(2): p. 309-322.
264. Griffin, W., *Calculation of HLB Values of Non-Ionic Surfactants*. J Soc Cosm Chem, 1954. **5**: p. 259.
265. Meyer, M., Philipp, A, Oskuee, R, Schmidt, C, Wagner, E, *Breathing life into polycations: Functionalization with pH-responsive endosomolytic peptides and polyethylene glycol enables siRNA delivery*. J Am Chem Soc, 2008. **130**(11): p. 3272-3273.
266. Horiuchi, S., Aoyama, Y, *Systematic lactose-functionalization of amphiphilic octaamine macrocycle as a gene carrier. Optimization of the charge, size, toxicity,*

- and receptor factors for hepatocyte targeting.* J Contr Release, 2006. **116**(2): p. 107-114.
267. Jones II, G., Jackson, WR, Choi, CY, Bergmark, WR, *Solvent effects on emission yield and lifetime for coumarin laser dyes. Requirements for a rotatory decay mechanism.* J Phys Chem, 1985. **89**(2): p. 294-300.
268. Thomas, M., Lu, J, Ge, Q, Zhang, C, Chen, J, Klibanov, A, *Full deacylation of polyethylenimine dramatically boosts its gene delivery efficiency and specificity to mouse lung.* Proc Natl Acad Sci USA, 2005. **102**(16): p. 5679-5684.
269. Sochanik, A., Cichon, T, Makselon, M, Strozyk, M, Smolarczyk, R, Jazowiecka-Rakus, J, Szala, S, *In vivo gene transfer using cetylated polyethylenimine.* Acta Biochim Pol, 2004. **51**(3): p. 693-702.
270. Saito, T., Hayamizu, K, Yanagisawa, M, Yamamoto, O. *Spectral Database for Organic Compounds, SDBS.* 2009 [cited 2008 April, 23rd]; Available from: http://riodb01.ibase.aist.go.jp/sdbs/cgi-bin/direct_frame_top.cgi.
271. Naumann, C., Brooks, CF, Fuller, GG, Lehmann, T, Ruhe, J, Knoll, W, Kuhn, P, Nuyken, O, Frank, CW, *Two-dimensional physical networks of lipopolymers at the air/water interface: Correlation of molecular structure and surface rheological behavior.* Langmuir, 2001. **17**(9): p. 2801-2806.
272. Naumann, C., Brooks, CF, Wiyatno, W, Knoll, W, Fuller, GG, Frank, CW, *Rheological properties of lipopolymer-phospholipid mixtures at the air-water interface: A novel form of two-dimensional physical gelation.* Macromolecules, 2001. **34**(9): p. 3024-3032.
273. Foreman, M., Coffman, JP, Murcia, MJ, Cesana, S, Jordan, R, Smith, GS, Naumann, CA, *Gelation of amphiphilic lipopolymers at the air-water interface: 2D analogue to 3D gelation of colloidal systems with grafted polymer chains?* Langmuir, 2003. **19**(2): p. 326-332.
274. Han, S., Kim, NH, Lee, YS, *Effect of phenothiazine derivatives on the thermotropic phase transition of liposomal phospholipid membrane.* Arch Pharm Res, 1986. **9**(2): p. 75-79.
275. Caetano, W., Ferreira, M, Tabak, M, Mosquera Sanchez, MI, Oliveira, ON, Krüger, P, Schalke, M, Lösche, M, *Cooperativity of phospholipid reorganization upon interaction of dipyrindamole with surface monolayers on water.* Biophysical Chemistry, 2001. **91**(1): p. 21-35.
276. Blume, A., Ackermann, T, *A calorimetric study of the lipid phase transitions in aqueous dispersions of phosphorylcholine-phosphorylethanolamine mixtures.* FEBS Lett, 1974. **43**(1): p. 71-74.
277. Stidder, B., Fragneto, G, Roser, SJ, *Structure and stability of DPPE planar bilayers.* Soft matter, 2007. **3**: p. 214-222.
278. Hamai, C., Yang, T, Kataoka, S, Cremer, PS, Musser, S, *Effect of average phospholipid curvature on supported bilayer formation on glass by vesicle formation.* Biophys J, 2006. **90**: p. 1241-1248.
279. Leekumjorn, S., Sum, AK, *Molecular simulation study of structural and dynamic properties of mixed DPPC/DPPE bilayers.* Biophys J, 2006. **90**: p. 3951-3965.
280. Boggs, J., Rangaraj, G, Koshy, KM, *Effect of hydrogen-bonding and non-hydrogen-bonding long chain compounds on the phase transition temperatures of phospholipids.* Chem Phys Lipids, 1986. **40**: p. 23-34.
281. McDaniel, R., McIntosh, TJ, Simon, SA, *Nonelectrolyte substitution for water in phosphatidylcholine bilayers.* Biochim Biophys Acta, 1983. **731**: p. 97-108.
282. Bateman, J., Gabriel, C, *Dielectric properties of aqueous glycerol and a model relating these to the properties of water.* J Chem Soc Faraday Trans, 1987. **83**: p. 355-369.

283. Aggarwal, V., Gupta, AK, *Ultrasonic absorption and velocity measurements in a critical mixture of water and phenol*. J Phys D Appl Phys, 1975. **8**: p. 1206-1210.
284. The Dow Chemical Company, M., MI, USA. *Dielectric Constant, ϵ , of Glycerine-Water Solutions at 25°C (77°F)*. 2008 [cited; Available from: <http://www.dow.com/glycerine/resources/table5.htm>].
285. *Handbook of chemistry and physics*, ed. R. Weast. 1974, Cleveland: CRC Press.
286. Nagle, J., Wilkinson DA, *Lecithin bilayers. Density measurement and molecular interactions*. Biophys J, 1978. **23**: p. 159-175.
287. Boon, J., McClain, RL, Breen, JJ, Smith, BD, *Inhibited phospholipid translocation across interdigitated phosphatidylglycerol vesicle membranes*. J Supramolec Chem, 2001. **1**(1): p. 17-21.
288. Swamy, M., Marsh, D, *Thermodynamics of interdigitated phases of phosphatidylcholine in glycerol*. Biophys J, 1995. **69**(4): p. 1402-1408.
289. Frank, C., Naumann, CA, Knoll, W, Brooks, CF, Fuller, GG *Two-dimensional physical networks of lipopolymers at the air / water interface*. Macromol Symp, 2001. **166**: p. 1-12.
290. Masotti, A., Moretti, F, Mancini, F, Russo, G, Di Lauro, N, Checchia, P, Marianecchi, C, Carafa, M, Santucci, E, Ortaggi, G, *Physicochemical and biological study of selected hydrophobic polyethylenimine-based polycationic liposomes and their complexes with DNA*. Bioorg Med Chem, 2007. **15**(3): p. 1504-1515.
291. Lee, M., Rentz, J, Han, SO, Bull, DA, Kim, SW, *Water-soluble lipopolymer as an efficient carrier for gene delivery to myocardium*. Gene Ther, 2003. **10**(7): p. 585-593.
292. Wang, D., Narang, AS, Kotb, M, Gaber, AO, Miller, DD, Kim, SW, Mahato, RI, *Novel branched poly(ethylenimine)-cholesterol water-soluble lipopolymers for gene delivery*. Biomacromolecules, 2002. **3**(6): p. 1197-1207.
293. Hauser, H., Phillips, MC. *Progress in Surface and Membrane Science*, ed. D. Cadenhead. Vol. 13. 1979, New York: Academic Press.
294. Ko, Y., Kale, A, Hartner, WC, Papahadjopoulos-Sternberg, B, Torchilin, VP, *Self-assembling micelle-like nanoparticles based on phospholipid-polyethyleneimine conjugates for systemic gene delivery*. J Contr Release, 2009. **133**(2): p. 132-138.
295. Trubetskoy, V., Loomis, A, Slattum, PM, Hagstrom, JE, Budker, VG, Wolff, JA, *Caged DNA does not aggregate in high ionic strength solutions* Bioconjug Chem, 1999. **10**: p. 624-628.
296. Erbacher, P., Bettinger, T, Belguise-Valladier, P, Zou, S, Coll, JL, Behr, JP, Remy, JS, *Transfection and physical properties of various saccharide, poly(ethyleneglycol), and antibody-derivatized polyethylenimines (PEI)*. J Gene Med, 1999. **1**(3): p. 210-222.
297. Ogris, M., Steinlein, P, Kursa, M, Mechtler, K, Kircheis, R, Wagner, E, *The size of DNA/transferrin-PEI complexes is an important factor for gene expression in cultured cells*. Gene Ther, 1998. **5**(10): p. 1425-1433.
298. Bronich T, K.A., Marky L, *A thermodynamic characterization of the interaction of a cationic copolymer with DNA*. J Phys Chem B, 2001. **105**: p. 6041-6050.
299. Oncins, G., Garcia-Manyes, S, Sanz, F, *Study of frictional properties of a phospholipid bilayer in a liquid environment with lateral force microscopy as a function of NaCl concentration*. Langmuir, 2005. **21**(16): p. 7373-7379.
300. Nadano, D., Yasuda, T, Kishi, K, *Measurement of deoxyribonuclease I activity in human tissues and body fluids by a single radial enzyme-diffusion method*. Clin Chem, 1993. **39**(3): p. 448-452.
301. Erikson, J., Freeman, GL, Chandrasekar, B, *Ultrasound-targeted antisense oligonucleotide attenuates ischemia / reperfusion-induced myocardial tumor necrosis factor-alpha*. J Mol Cell Cardiol, 2003. **35**: p. 119-130.

302. Otani, K., Yamahara, K, Ohnishi, S, Obata, H, Kitamura, S, Nagaya, N, *Nonviral delivery of siRNA into mesenchymal stem cells by a combination of ultrasound and microbubbles*. J Contr Release, 2009. **133**(2): p. 146-153.
303. Slikkerveer, J., Dijkmans, PA, Sieswerda, GT, Doevendans, PA, van Dijk, AP, Verheugt, FW, Porter, TR, Otto Kamp, O, *Ultrasound enhanced prehospital thrombolysis using microbubbles infusion in patients with acute ST elevation myocardial infarction: Rationale and design of the Sonolysis study*. Trials, 2008. **9**(72).
304. Lewis, R., McElhaney, RN *The structure of biological membranes*, ed. P. Yeagle. 1992: CRC Press, Boca Raton, USA. 73.

Curriculum Vitae

Steliyan Stanimirov Tinkov

EDUCATION

| | |
|----------------------------|---|
| Oct. 2005 – est. Apr. 2009 | Ludwig-Maximilians-University – Munich, Germany Ph.D. study in Pharmaceutical Technology and Biopharmaceutics |
| Sept. 1998 – Jan. 2004 | Medical University – Sofia, Bulgaria, Faculty of Pharmacy Master study in Pharmacy |
| May 1994 – Sept. 1998 | Secondary school of Natural Sciences and Mathematics – Lovech, Bulgaria |

PROFESSIONAL EXPERIENCE

| | |
|-------------------------|-------------------------------|
| March 2005 – Sept. 2005 | Pharmacist |
| Nov. 2004 – Feb. 2005 | Pharmaceutical representative |
| Apr. 2004 – Oct. 2004 | Military service |
| Oct. 2003 – March 2004 | Pharmacist under supervision |

LANGUAGE SKILLS

| | |
|-----------|----------------|
| Bulgarian | First language |
| German | Fluently |
| English | Fluently |
| Russian | Intermediate |

PUBLICATIONS**S. Tinkov, G. Winter, C. Coester, R. Bekeredjian**

New doxorubicin-loaded phospholipid microbubbles for targeted tumor therapy: Part I - Formulation development and in-vitro characterization, Journal of Controlled Release (submitted)

S. Tinkov, R. Bekeredjian, G. Winter, C. Coester

Microbubbles as Ultrasound Triggered Drug Carriers (review article), Journal of Pharmaceutical Sciences, 98(6):1935-61, 2009

S. Tinkov, R. Bekeredjian, G. Winter, C. Coester

Characterization of Ultrasound-mediated Destruction of Drug-loaded Microbubbles Using an Improved In-vitro Model, Applied Acoustics, 70(10): 1323-1329, 2009

R. Bekeredjian, R. Kroll, E. Fein, S. Tinkov, C. Coester, G. Winter, H. Katus, H.**Kulaksiz**

Ultrasound Targeted Microbubble Destruction Increases Capillary Permeability in Hepatomas, Ultrasound in Med. & Biol., 33(10): 1592-1598, 2007

Heun, G. Tinkov, S.

Sterilization of Parenterals with Microwaves as an Alternative to Autoclavation, Pharmazeutische Industrie, 65(9A): 977-983, 2003

PATENTS**S. Tinkov, R. Bekeredjian, G. Winter, C. Coester**

Pharmaceutical Composition Comprising Microbubbles for Targeted Drug Therapy, submission number: 581806, application number: EP09160913.1, May 22nd 2009

CONGRESS PRESENTATIONS**S. Tinkov, R. Bekeredjian, G. Winter, C. Coester**

In-vitro/ In-vivo Correlation Model of Ultrasound Mediated Destruction of Microbubbles

Using an Improved Acoustic Transmission Line, 5th International Workshop on Drug Delivery Systems, May, 16th- 18th, 2007, Trest Castle, Czech Republic

S. Tinkov, R. Bekeredjian, G. Winter, C. Coester

Polyplex-conjugated microbubbles for enhanced ultrasound targeted gene therapy, 2008 AAPS Annual Meeting and Exposition, November 16th-20th 2008, Georgia World Congress Center, Atlanta, GA, USA

S. Tinkov, R. Bekeredjian, G. Winter, C. Coester

Acoustic destructibility and in-vitro efficacy of a new microbubble delivery system for targeted tumor therapy, 6th World Meeting on Pharmaceutics, Biopharmaceutics, and Pharmaceutical Technology, April 6th-10th 2008, Barcelona, Spain

S. Tinkov, R. Bekeredjian, G. Winter, C. Coester

Kinetics of Ultrasound Mediated Microbubble Destruction Using an Improved In-Vitro Acoustic Transmission Line Model, Controlled Release Society German Chapter Annual Meeting, March 22nd-23rd, 2007, Freiburg, Germany